University of Strathclyde

Department of Electronic and Electrical Engineering

3D Tumour-Stroma Microfluidic Cultures for the Assessment of Anti-Cancer Therapies

Karla Anna Findlay Paterson

A thesis submitted in partial fulfilment of the requirements for the degree of Doctor of Philosophy

2022

Declaration of Authorship

This thesis is the result of the author's original research. It has been composed by the author and has not been previously submitted for examination which has led to the award of a degree at the University of Strathclyde in 2022.

The copyright of this thesis belongs to the author under the terms of the United Kingdom Copyright Acts as qualified by University of Strathclyde Regulation 3.50. Due acknowledgement must always be made of the use of any material contained in, or derived from, this thesis.

Signed:

Date: 4th April 2022

Abstract

Cancer is a highly complex disease composed of a heterogeneous range of cell types within the tumour microenvironment (TME). Despite advances in cancer treatment, there exists a lack of pre-clinical screening systems that represent the true complexity of *in vivo* tumours. The solid TME plays a crucial role in tumour development and therapy resistance. Established analytical *in vitro* methods are often too simplistic in their depiction of solid tumours and are primarily based on 2D cultures of immortalised cancer cell lines. Current preclinical assays commonly lack features of the TME and fail to represent the plethora of cell types present in native human tumours. There exists a need for the development of preclinical platforms that provide greater levels of physiological relevance and predictive value to rapidly determine the efficacy of novel anti-tumour agents and their consequential effects on the various cell types present in the TME. Furthermore, personalised *in vitro* models could be used for assessing patient tissue to increase accuracy of the predictions of treatment outcomes for patients. Immunotherapy is a promising form of cancer treatment that has not yet been widely harnessed towards the treatment of solid tumours and requires improved methods of *in vitro* assessment. Microfluidic technologies can provide a cost-effective solution through the advantages of miniaturisation where much smaller volumes of reagents and cell numbers are required in comparison to traditional *in vitro* assays. Many microfluidic models have been developed featuring tumour spheroids and vascular network structures to study tumour angiogenesis and to assess the performance of anti-cancer agents targeting tumour cells and tumour vasculature. Microfluidic assays have also been established for the study of immunotherapies targeting liquid tumours. However, there is a gap in the development of equivalent models for assessing the efficacy of immunotherapeutics targeting solid tumours.

Therefore, elements of the TME were identified to integrate into and increase the complexity of current *in vitro* models and microfluidic technology utilised to achieve the development of novel microfluidic protocols for miniaturized assays that could be utilized for personalised immunotherapy applications. The aims of this work included achieving the assessment of both the cytotoxicity and target specificity of CAR-T cells in 3D TME relevant models and the validation of the *in vitro* assessment of CAR-T therapy in combination with chemotherapy and checkpoint blockade. Proof-of-concept applications of assays and protocols for nanoparticle drug delivery, tumour stroma interaction and immune-oncology were demonstrated. Specifically, a viable solid tumour-stromal microenvironment was established using a primary breast cancer cell line and characterisation of co-cultures performed via time-lapse imaging and quantification of fluorescence and protein expression. Adaptable protocols were validated

2

and have potential for use in the analysis of various types of immunotherapy with the potential for incorporation of various cancer and TME associated cell types. This thesis also contains the first report of microfluidic technology combined with SERS to assess targeted nanoparticle binding to and penetration of 3D tumour spheroids. In addition, novel ACT methodology and data analysis protocols were developed to present the first report of the assessment of EGFR specific CAR-T cell cytotoxicity and target specificity in a 3D solid tumour-stromal microfluidic model as a monotherapy and in combination with carboplatin chemotherapy and anti-PD-L1 treatment. These miniaturized proof-of-concept systems using small cell numbers and volumes are highly suited for the analysis of patient biopsy tissue and for determining the efficacy of expensive immunotherapy agents to obtain the maximum data output possible. These assays, due to their sample-saving properties, are amenable for precision medicine applications using patient biopsy tissue, as well as providing a general platform for studying TME interactions. Preliminary assays using primary murine gamma delta T cells demonstrated the potential for human biopsy tissue to be used in microfluidic studies for assessing immunotherapy efficacy and present possible future applications in ACT therapy development.

Acknowledgements

Contents

List of Figures

14

Abbreviations

ACLY	ATP citrate synthase
ALL	Acute lymphoblastic leukaemia
AML	Acute myeloid leukaemia
BSA	Bovine serum albumin
CAF	Cancer associated fibroblasts
CAR-T	Chimeric antigen receptor T cell
CTC	Circulating tumour cells
CTLA-4	Cytotoxic T-lymphocyte-associated antigen 4
ECM	Extracellular matrix
ERα	Oestrogen receptor alpha
EGFR	Epidermal growth factor
EpCAM	Epithelial cell adhesion molecule
FAP	Fibroblast activation protein
FBS	Foetal bovine serum
FDA	Fluorescein diacetate
GFP	Green fluorescent protein
GM-CSF	Granulocyte-macrophage colony-stimulating factor
HNC	Head and neck cancer
HUVEC	Human umbilical vein endothelial cells
ICI	Immune checkpoint inhibitors
ICD	Immunogenic cell death
IFN	Interferon
IL	Interleukin

IRF	Interferon regulatory factor
mAbs	Monoclonal antibodies
MSCs	Mesenchymal stem cells
NSCLC	Non-small cell lung cancer
P300	Histone acetyltransferase
PBS	Phosphate buffered saline
PBMC	Peripheral blood mononuclear cell
PD-1	Programmed cell death protein 1
PDH	Pyruvate dehydrogenase
PD-L1	Programmed death ligand 1
PDMS	Polydimethylsiloxane
PDX	Patient derived xenografts
PI	Propidium iodide
PYCR1	Pyrroline-5-carboxylate reductase 1
SERD	Selective oestrogen receptor down-regulator
SERS	Surface-enhanced Raman spectroscopy
SMA	Smooth muscle actin
TGFβ	Transforming growth factor β
TILs	Tumour-infiltrating lymphocytes
TME	Tumour microenvironment
VEGF	Vascular endothelial growth factor

Thesis Overview

In this introductory chapter, the key aims and novelty of the project are presented, together with a brief summary of the thesis structure, project contributions and publications that have stemmed from this work.

Motivation

One of the major challenges in the management of all cancers is identifying the efficacy of anticancer drugs. Stratified or genetic-based approaches can be used to select the course of treatment for a patient, but these methods do not account for the extent of possible variation of tumour biology leading to significant variability in patient response to therapy.[1, 2] Cancer cell lines have been relied upon to establish drug efficacy at the preclinical level, but these 2D models are often too simplistic to recapitulate the complexity of the native tumour microenvironment and patient to patient heterogeneity.[3] The use of human tumour tissue for preclinical drug efficacy studies can provide greater physiological relevance and will, hopefully, lead to better clinical outcomes in future.[4, 5] However, the techniques involved in assays using primary human tissue demand a great deal of manual labour, as well as the use of expensive animal-based procedures for *in vivo* experiments or to expand the tumour tissue.[6, 7] This is of particular importance in the development of immunotherapies for solid tumours, where the immunocompromised host system and differences between animal and human immune systems present challenges for immunoassays.[7, 8, 9] Cancer immunotherapy has seen significant success in recent years against liquid tumours but tackling solid tumours has proven more challenging.[10, 11] A major obstacle for this therapy against solid tumours is the immunosuppressive tumour microenvironment (TME).[12, 13] The solid TME has recently been the focus of investigations due to its role in protecting cancer cells and promoting resistance to therapy.[14]

Current *in vitro* models are commonly lacking in sufficient 3D TME structures to adequately mimic the immunosuppressive solid tumour milieu. Microfluidic technology enables analysis of novel immunotherapies in a 3D environment where various TME characteristics can be modelled. The miniaturization possible with microfluidics means that far smaller quantities of cells and reagents are required, particularly useful when dealing with small volumes of biopsy tissue and expensive immunotherapeutic drugs.[2, 15] Such an approach has great potential to identify the optimum therapeutic strategy for each individual based on screening human biopsy tissue. A Venn diagram depicting the fields of research involved in this project are depicted below (**Figure A**).
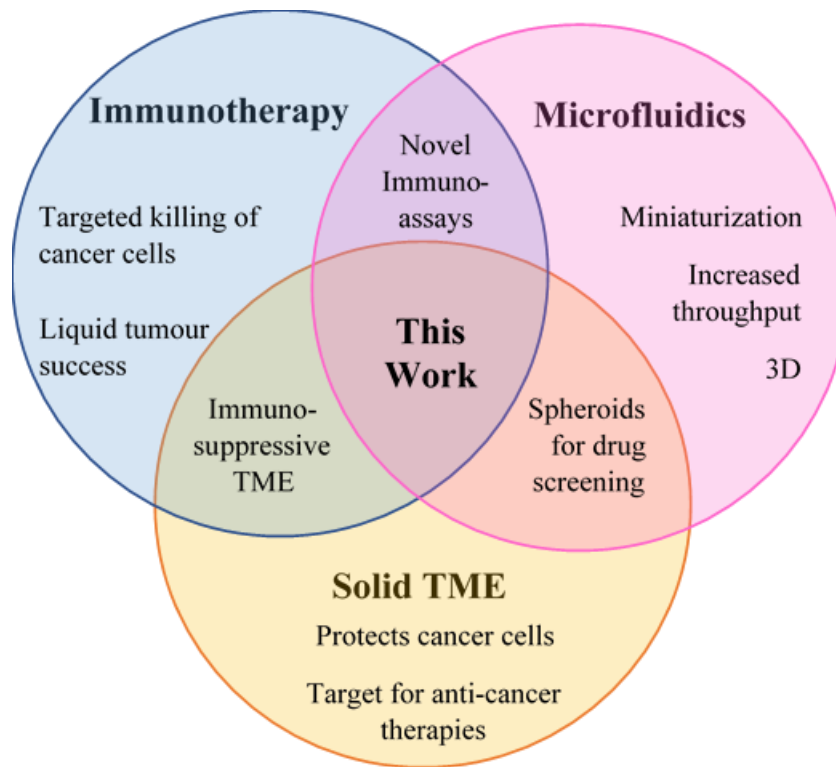
Figure A. Venn diagram of the interdisciplinary research areas involved in this project. TME = Tumour microenvironment, CAF = cancer associated fibroblasts.

Immunotherapy offers a targeted and potentially longstanding approach to cancer treatment in comparison to traditional treatment regimes.[16] The human TME is not effectively represented in current preclinical models which often give inaccurate predictions of clinical outcomes of immunotherapy treatments.[17] Microfluidic technology offers an opportunity to facilitate the investigation of the solid TME in 3D *in vitro* models and in the context of various stromal and immune cell interactions. The immune system is highly complex and new methodologies comprising more physiologically relevant assays are required for establishing the efficacy of novel immunotherapies and their potential side effects.

Aims and Novelty of Research

The overall aim of this PhD studentship was to develop novel microfluidic protocols to deliver miniaturised assays as a proof of concept system that could be utilized for personalised immunotherapy applications. The objectives included identifying the optimum culture conditions to deliver a more physiologically-relevant model of the *in vivo* solid TME for anticancer drug testing and immunoassays with the smallest possible amount of starting material. Such microfluidic protocols would be of use in the development and screening of

therapeutic agents through co-culture of tumour spheroids, stromal tissue and immune cells to mimic TME interactions.

This work has resulted in the development of novel, miniaturised 3D assays that could be readily used in R&D industrial and academic laboratories for a variety of immune-oncology and cancer therapeutic applications. Benefits from this approach would include a more cost effective and biologically relevant alternative in comparison to current preclinical models. In addition, this work demonstrates the ability to perform novel immunotherapy tests *in vitro* to determine the potential value and side effects of a novel compound prior to animal studies to considerably reduce the use of animals in drug efficacy studies.

Thesis outline

Chapter 1 describes the complexity of the TME and explains the need for the development of more physiologically relevant *in vitro* models for anti-cancer drug screening. Background concepts are described to provide context and justification of this research. Comparisons are made between current *in vitro* models featured in recent literature and the value of microfluidic technology and 3D cell culture in this field are discussed.

Chapter 2 details the materials and methodology required for all experimental work, including cell culture and the production of microfluidic devices. Also included is a description of the anti-tumour agents used and the data analysis developed and performed.

Chapter 3 describes preliminary work involving investigation into creating a more physiologically relevant system through incorporation of a vascular network and the development of microfluidic protocols for 3D tumour spheroid formation. Collaborative work investigating the efficacy of receptor-targeting nanoparticles was conducted and assays developed for nanoparticle-mediated therapy studies. The results from this work were included in a journal publication.[18]

Chapter 4 describes the incorporation of stromal cells into the spheroid forming devices and the study of their characteristics in 3D. The role of various enzyme inhibitors in inhibiting CAF function was investigated and various factors assessed including spheroid viability, size, proliferation and collagen deposition. The data within this chapter was presented as a poster presentation at the BioMedEng 2019 conference and included in a journal paper currently under review.[19]

Chapter 5 discusses the use of microfluidic TME models for evaluating the therapeutic potential of specific receptor targeting CAR-T cells as a monotherapy and in combination with chemotherapy and checkpoint blockade. Findings from this research were prepared in a journal

paper currently under review and an oral presentation given at the BioMedEng 21 conference.[20]

Chapter 6 provides an overall evaluation and discusses the outcomes and challenges of this project. Furthermore, potential future directions from the research are highlighted within this chapter.

Project contributions

For this project, the author carried out all experimental work and data analysis unless specified otherwise. The author independently developed and optimized experimental protocols and assays using pre-existing microfluidic platforms. Cell culture training was provided by Dr Theresa Mullholland and teaching relating to photolithography and soft lithography given by Dr Michele Zagnoni.

Publications

Sections of this work have been published and presented in peer reviewed journal publications and conference proceedings.

Peer Reviewed Journals:

Kapara A, Findlay Paterson KA, Brunton VG, Graham D, Zagnoni M, Faulds K. "*Detection of Estrogen Receptor Alpha and Assessment of Fulvestrant Activity in MCF-7 Tumor Spheroids Using Microfluidics and SERS.*" Analytical Chemistry. 2021;93(14):5862-71.

Paterson K, Zanivan S, Glasspool R, Coffelt SB, Zagnoni M. "*Microfluidic technologies for immunotherapy studies on solid tumours.*" Lab on a Chip. 2021;21(12):2306-29.

Kay E, Paterson K, Domingo C, Sumpton D, Daebritz H, Tardito S, Boldrini C, Hernandez-Fernaud C, Dhayade S, Stepanova E, Gjerga E, Shaw R, Neilson L, Lilla S, Hedley A, Koulouras G, McGregor G, Jamieson C, Johnson R, Park M, Kirschner K, Miller C, Kamphorst J, Loayza-Puch F, Saez-Rodriguez J, Mazzone M, Blyth K, Zagnoni M, Zanivan S. "*PYCR1-dependent proline synthesis in cancer-associated fibroblasts is required for the deposition of pro-tumorigenic extracellular matrix*", bioRxiv, 2021:2020.05.30.125237, accepted by Nature Metabolism.

Paterson K, Paterson S, Mulholland T, Coffelt SB, Zagnoni M. "*Assessment of CAR-T mediated and targeted cytotoxicity in 3D microfluidic TBNC co-culture models for combination therapy.*" bioRxiv. 2021:2021.09.14.458168, under consideration by IEEE Open Journal of Engineering in Medicine and Biology.

Conference Presentations:

Paterson KAF, Kay E, Zanivan S, Zagnoni M. *"Microfluidic Primary Spheroid Co-culture for Studying CAF-Mediated Tumour Progression"*, BioMedEng19 Conference, 5th-6th September, 2019, London, United Kingdom (poster presentation)

Paterson KAF, Paterson S, Mulholland T, Zagnoni M, *"Targeted CAR-T Killing in 3D Microfluidic Cancer-Stromal Co-cultures"*, BioMedEng19 Conference, 6th-7th September, 2021, Sheffield, United Kingdom (oral presentation)

Chapter 1: Background

1.1 Cancer Overview

Despite great advances in cancer treatment and improvements in survival rates, cancer still remains a leading cause of death globally.[21] More than 200 different forms of cancer exist with incident rates rising year on year in the UK.[22,23] By 2040, 27.5 million new diagnoses will be made globally each year.[24,2] Cancer is defined as the abnormal division of cells in an uncontrolled manner with the potential to spread to other bodily tissues.[25] The hallmarks of cancer were first described by Hanahan and Weinberg in a landmark paper in 2000, where the authors outlined 6 biological features thought to be possessed by all cancer cells at some stage of their transition from normal to cancerous cells.[26] These abilities consisted of sustaining proliferative signalling, evading growth suppressors, resisting cell death, enabling replicative immortality, inducing angiogenesis, and activating invasion and metastasis.[26] Later, additional hallmarks were included to account for the impact of the TME on tumorigenesis, including mutation and genome instability, reprogramming of energy metabolism, tumour-promoting inflammation and evading immune destruction.[27]

1.2 Tumour Microenvironment

Tumours are complex and evolving structures. Within the hypoxic core and surrounding extracellular matrix (ECM) exists a heterogeneous repertoire of cancer cells, cancer stem cells, fibroblasts, pericytes, endothelial cells, adipocytes, healthy tissue and immune cells[14, 28] (**Figure 1.1**)[28].

Hyaluronan-rich extracellular matrix

Tumor microenvironment

Adipocytes	Fibroblasts		Macrophages, Tumor Associated Macrophages
Collagens	Granulocytes (Eosinophils, Basophils, Neutrophils)		Mesenchymal stem/stromal cells
Dendritic cells	Hyaluronan backbone, Proteoglycan filaments		Tumor cells
Endothelial cells	Lymphocytes (T cells, B cells, and NK cells)	CAF	Cancer Associated Fibroblasts

Figure 1.1: Components of the inflammatory tumour microenvironment. Schematic depiction of the solid tumour microenvironment and the role of cancerous and non-cancerous cells involved. Adapted with permission from Sevic et al., 2019, Hepatocellular Carcinoma, https://creativecommons.org/licenses/by-nc/4.0/. (CAF= cancer-associated fibroblasts, CSC= cancer stem cells, ECM= extracellular matrix, HA= hyaluron, MSC= mesenchymal stem/stromal cells, TAM= tumour-associated macrophages, TME= tumour microenvironment)

This heterogeneous assortment of cells, defined as the TME, plays a role in cancer resistance, progression and metastasis, as well as influencing the action of anti-cancer drug mechanisms.[14] However, the TME as a target for anticancer agents is a relatively new concept and many traditional cancer treatments have only targeted cancer cells and their enhanced replicative ability.[29, 30] More recently, greater numbers of preclinical and clinical investigations regarding TME targeting therapies have been conducted with some approved as part of standard course of treatment against certain cancers.[31] Immune checkpoint therapy, in particular, has seen recent success and has spawned investigation into alternative immune checkpoint inhibitors, those targeting lymphocyte activation gene 3 protein (LAG-3) and T cell immunoglobulin and mucin domain-containing protein 3 (TIM-3) for example.[32, 33] However, several studies have reported that acquired resistance to immune checkpoint targeting drugs in patients remains an issue.[32] Variation between cells within the tumour arises through differences in the proximity of cells to the blood supply, which can be derived from the host's own vasculature or through tumour angiogenesis.[29] Angiogenesis can be specified as the generation of new blood vessels concerning the movement, development and differentiation of endothelial cells which line the inner surface of blood vessels.[34] This process is of critical importance in cancer progression as

enlarging tumours require extensive vasculature in order to provide oxygen and nutrients to cancer cells, as well as to remove their waste.[34] In normal tissues, angiogenesis is moderated through the balance of stimulating and inhibiting chemical signals.[34] Tumours have the means to emit stimulating chemical signals and downregulate inhibitors in order to elicit angiogenesis.[34]

Due to the speed at which a tumour mass can enlarge, regions exist in the tumour which are not able to be sufficiently perfused by vasculature.[35] This leads to the formation of leaky blood vessels which are helpful to the intravasation and metastasis of tumour cells and impair the delivery of immune cells and anti-tumour agents.[35] Over time, cells in the centre of the tumour are subject to more restricted access to the vasculature and an increasingly limited oxygen supply.[36] This is in comparison to externally located cells, which receive sufficient nutrients and oxygen to be able to proliferate rapidly.[36] The result of which is the development of a hypoxic core and/or necrosis.[36, 37] Hypoxia can result in tumours developing therapy resistance to some anti-cancer drugs and radiation that require oxygen to be fully cytotoxic.[38, 39] Furthermore, hypoxic conditions also assist tumour cells by enhancing their ability to detoxify drug compounds and promoting genetic instability, accelerating the development of drug resistant cancer cells.[38, 39] Abnormalities in the vascular architecture of tumours, in contrast to that of normal blood vessel development, is responsible for the degree of heterogeneity that arises in tumours and which impacts flow rates and perfusion of oxygen and nutrients.[40]

Vascular endothelial cells are responsible for the regulation of transvascular transport, vasodilation and the creation and deterioration of blood vessels.[41] Irregular blood flow or vessel blockage enables disease progression and development.[42] Tumour vasculature differs from the architecture of healthy blood vessels, causing the delivery of blood borne molecules, nanoparticles and therapeutic agents to be more challenging.[43] Tumour vessel diameter can be up to 10 times greater than that of normal vessels which creates unsteady blood flow and greater fragility of the vessels, affecting their functionality.[44] Furthermore, the highly heterogeneous shear stress on tumour vasculature impedes the ability of lymphocytes to reach tissues.[44] Once tumour cells have intravasated into the blood vessel, they must travel through the peripheral circulatory system and adhere to a point on the vascular endothelium to begin the process of extravasation.[45, 46] Mechanical forces experienced by tumour cells during this time are crucial to the success of their adhesion and consequential extravasation into neighbouring tissue.[45] It has been suggested that the likelihood of survival of cancer patients can be significantly increased with the use of vascular endothelial growth factor (VEGF) inhibitor to provoke hypertension.[45, 47, 48] This creates a more inhospitable mechanical

environment for metastasising cancer cells that is detrimental to their survival and provides an explanation for the low numbers of tumour cells present in the circulatory system of cancer patients.[45] In addition, this theory suggests that patients undertaking physical activity and, therefore, increasing the circulation of blood can aid in lessening the prevalence of tumour metastases.[45]

Proteins incorporated into the ECM, such as collagen, elastin, laminin and fibronectin, are packed into gaps between cells and aid in a variety of ECM functions.[49] This crucial component for cells functions as a scaffold, barrier, anchorage point and motion path and is of great importance to the stages involved in cancer progression.[49] Hyaluron is an abundant feature of tumour ECM known to stimulate stromal cells to trigger cell proliferation, metastasis, differentiation, angiogenesis and resistance to anti-cancer agents.[28] Tumour cells can degrade and remodel adjacent ECM causing variations in the density and network structure.[50, 51] These mechanisms have implications for cancer progression and therapeutic response.[50, 51] For example, perpendicular alignment of collagen I fibres to tumours has been related to cancer relapse after surgical removal of the tumour, as well as in guiding metastatic cancer cells in the direction of fibre alignment.[50] Mesenchymal stem cells (MSCs) are attracted to the inflammatory tumour site to secrete growth factors, cytokines and ECM components and play a role in tissue repair and immunomodulation.[28]

Biochemical effects, for example the release of cytokines and growth factors, can cause tumour cells to exhibit greater viability and motility with less incidence of apoptosis.[52] The biophysical consequences of the presence of fibroblasts are a primary contributor to cancer malignancy through reorganization and increasing the stiffness of the ECM.[52] Out of the vast array of cells present in the TME, cancer associated fibroblasts (CAF) have become of recent interest as targets for complementary cancer therapies.[35] CAF are produced through stimulation of resident fibroblasts or other precursor cells by environmental or cancer-cell derived stimuli.[35] Once activated, CAF release a variety of growth factors, cytokines and ECM components.[53] This aids them in fulfilling their role in protecting cancer cells against apoptosis via collagen deposition whilst encouraging tumour cell proliferation and intravasation via remodelling of ECM components.[52,54] Despite this, studies regarding CAF metabolism have been limited to reports on CAF secretion of tumour-promoting metabolites, rather than regarding the pathways supporting ECM deposition by CAF.[19] Enzymes of importance include ATP citrate synthase (ACLY) and pyruvate dehydrogenase (PDH) which are involved in the conversion of citrate and pyruvate, respectively, to acetyl CoA.[55, 56] Also of relevance is histone acetyltransferase (p300), a transcriptional co-activator essential for many cellular

processes, and pyrroline-5-carboxylate reductase 1 (PYCR1)[57], an enzyme responsible for catalysing the conversion of pyrroline-5-carboxylate to proline.[58]

1.3   The Role of the Immune System in Cancer Progression

The immune system is the body's defence mechanism against foreign pathogens and unhealthy cells and is divided into two parts: innate and adaptive. Innate immunity involves cells such as macrophages, natural killer (NK) cells and dendritic cells that provide a non-specific and immediate reaction to all foreign bodies.[35, 59] Macrophages are phagocytic cells, responsible for engulfing and digesting cell debris and foreign pathogens.[60] NK cells do not require prior sensitization and are able to destroy a range of abnormal cells.[61] Dendritic cells provide the link between the innate and adaptive immune system by capturing, processing and presenting antigens to adaptive immune cells and inducing protective immune responses.[62] They operate by establishing immune synapses with target cells and then secreting cytolytic granules, such as perforin and granzymes, to trigger the lysis of the target cell.[61] Adaptive immune cells consist of a variety of B and T lymphocytes which provide a specific defence towards cells expressing a particular antigen.[35] Critically, adaptive immune cells develop immunological memory so they can recognize and respond quicker to foreign antigens that they have previously encountered.[15] The immune system is highly regulated by an assortment of activating and inhibiting agents and can function to help, hinder or be tolerant to cancer growth and metastasis depending on the factors it releases, such as those to trigger tumour-promoting inflammation or anti-tumour inflammation.[2, 63] The tumour itself can release signals, triggering cytokine production or the expression of proteins specific to normal tissue as a means of disguising itself to evade immunosurveillance.[35]

The immune system is typically activated by antigens the body doesn't recognise as its own. However, as cancerous cells originate from the body's own material, the immune cells must recognise specific antigens present on the surface of cancer cells to be able to establish that they are harmful and eliminate them.[15] Through the dynamic process of immune-editing, cancer cells develop ingenious ways to evade this immunosurveillance.[15] Immune-editing is characterised by three phases: *elimination*, where the successful detection and elimination of cancerous cells by the innate and adaptive immune system takes place;[64] *equilibrium*, where a portion of cancer cells that have not been eliminated by the immune system remain dormant;[59] and *escape*, where the remaining cancer cells are able to overcome the immune system sufficiently to proliferate and metastasize.[59]

In summary, the interplay between tumours and their complex and dynamic environment influences their development. Their growth, invasion and metastatic behaviour can be

impacted by components of their surroundings, as well as by the host's immune system which can play a dual role in cancer progression and prevention. The complexity of the disease requires skilled clinical decision making regarding treatment selection and which takes into account these influencing factors.

1.4 Traditional Cancer Therapies

Cancer patients are commonly treated with multi-modality therapies. The five pillars of cancer treatment are *surgery*, *radiotherapy*, *chemotherapy*, *targeted therapy* and *immunotherapy*. These can be administered individually or in conjunction with each other to increase their probability of success. Through technological advances, surgical removal of cancer has become less invasive and more conservative over the years in an attempt to preserve as much healthy tissue and organ functionality as possible.[65] Radiotherapy can be applied before or after surgery and entails the administration of high doses of radiation to eliminate or lessen the proliferation of cancer cells by damaging their DNA to a point where they are no longer functioning and can be eradicated from the body.[66] Radiotherapy is a cost-effective treatment that is able to provide a cure for a variety of localised cancers and a successful pain reliever for incurable cancers.[67] Chemotherapy can be used alongside radiotherapy to increase its efficacy and to target metastasized cancer cells that could not be eliminated by surgery or radiotherapy alone.[68] Chemotherapy is delivered intravenously or orally and affects rapidly dividing cells by stopping or slowing their growth.[69] Targeted cancer therapies instead use drugs or antibodies to specifically inhibit proteins involved in cancer cell proliferation and metastasis.[70] This form of therapy treats cancer in a variety of ways, including by halting growth and angiogenesis, initiating a specific cancer cell targeting immune response, triggering cancer cell death and direct delivery of cytotoxic agents to cancer cells.[70] Drug loaded nanoparticles have shown a great deal of promise in their role in treating cancer, as a result of their selectivity and efficiency.[71] However, the task of transitioning their use to clinics has been challenging.[71] This being partly due to a lack of complexity in the representation of the *in vivo* environment in current *in vitro* models.[71, 72] Whilst improvements to cancer treatments are continuously ongoing, inconsistencies in treatment success, relapse and severe side effects for patients remain commonly reported issues for anti-cancer treatment development.

1.5 Anti-Cancer Treatment Development

The drug discovery process currently requires compounds to be investigated using 2D *in vitro* assays, followed by preclinical *in vivo* models and then finally human clinical trials[2, 3, 73] (**Figure 1.2**)[74].
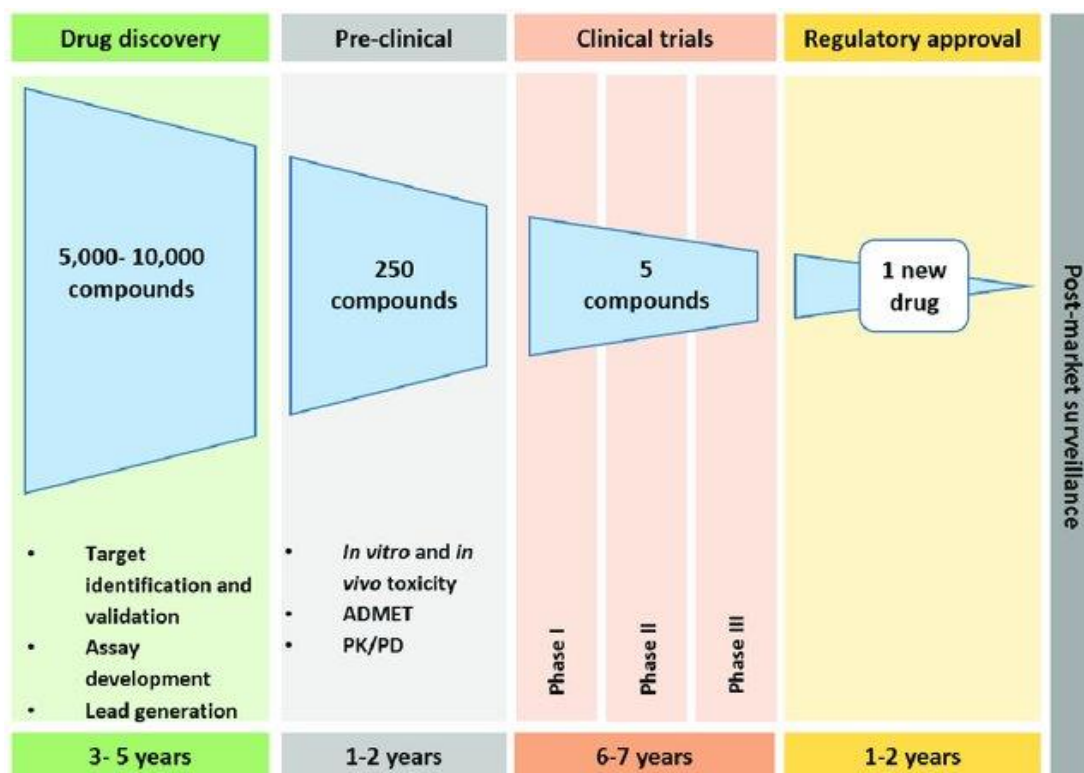
Figure 1.2: Timeline of drug discovery and development. Preclinical studies include assessment of pharmacokinetic and pharmacodynamic (PK/PD) relationships and absorption, distribution, metabolism, excretion and toxicology (ADMET) properties. Adapted with permission from Matthews et al., Proteomes, 2016, https://creativecommons.org/licenses/by-nc/4.0/.

If drug candidates are effective in preliminary phases, evaluation of their safety, efficacy and dosing in comparison to current treatment regimens is undertaken through clinical trials. High attrition rates in clinical trial phases is a major contributor towards the slow pace and cost of drug development.[75, 76] Only a minor fraction of anticancer drugs subjected to phase I trials are approved by the Food and Drug Administration (FDA) as they are shown to be either unsafe or ineffective in later human studies, despite having promising results from preclinical assays.[2, 77] Unreliable disease and drug screening models that fail to mimic *in vivo* TME conditions to accurately predict the efficacy of a drug in patients are amongst the reasons for these poor clinical translation rates.[2, 77]

Enhanced methods of quickly and accurately identifying potentially beneficial drug candidates and disregarding those which are ineffective would accelerate drug development and the rate at which effective compounds could be available to patients.[2, 77] Currently, chemotherapeutic compounds are tested using randomized clinical trials where a therapy regime is allocated to patients by chance.[2] Due to the uniqueness of each patient's tumour biology, response to therapy can vary significantly.[2] Therefore, there is a drive towards precision or personalized medicine to provide patient-specific selection of the optimum therapeutic regime.[2] Pre-clinical

models that can carry out drug screening on established cancer cell lines, as well as patient biopsy tissue are needed.[2]

In particular, there is a need for the development of pre-clinical immunoassays that can provide more accurate predictions than current pre-clinical models. Immunotherapy is an up-and-coming method of anti-cancer treatment that requires pre-clinical assays that take into account the complexity of the immune system and its potential role in cancer treatment.

1.6 Immunotherapy

Immuno-oncology is defined as the study and development of therapies that exploit the immune system to fight cancer.[68] Dating back to ancient Egypt, anecdotal reports can be found of tumours regressing after infection.[78] William Coley, now known as the father of immunotherapy, reported in the 1890's the ability to take advantage of the body's immune system to treat cancer through injecting patients with *Streptococcus pyogenes* and *Serratia marcescens* to cause partial or complete tumour regression.[79] The theory behind this is that the infection triggers a systemic immune response which, in addition to fighting the infection, also targets cancer cells.[79]

Immunotherapy has become the latest and most promising form of cancer treatment. It utilises the intrinsic capabilities of the immune system to identify, target and eradicate cancer cells regardless of the tissues they affect, meaning it has the potential to be a universal solution for all cancer types. It can be administered in combination with other forms of therapy and could be a possible solution to cancers that have been unresponsive to previous treatments when administered individually. This said, the efficacy of immunotherapeutics can be impeded or enhanced by previous anti-cancer treatment and so the sequence of different treatment modalities requires careful planning and investigation.[80, 81] Various methods of immunotherapy exist which improve the capability of the immune system to eradicate tumour cells and thwart their escape from immunosurveillance, in addition to targeting immune cells to avoid them aiding in tumour progression.[72] Immune cells can additionally be targeted to stop them delivering assistance to cancer cells.[72] Immunotherapy has the advantage over conventional cancer treatments of being both a targeted and systemic therapy, allowing the treatment of the local tumour bulk and distant metastases.[82] Immunotherapy offers specific cancer cell killing, in contrast to traditional radiotherapy and chemotherapy which do not distinguish between healthy and cancerous cells. Furthermore, this method of treatment offers the potential for long-standing cancer treatment and prevention against recurrence due to the memory capabilities of the immune system.[16]

Immunotherapy to date has seen more success in treating haematological malignancies in comparison to solid tumours. A reason for this is considered to be largely due to the hostile and immunosuppressive TME associated with solid cancers. The TME is a multicellular organization within the ECM that interacts with cancer cells to promote tumorigenesis.[83] Secretions from the variety of cells within the TME, such as the chemokines and cytokines expressed from immunosuppressive tumour-associated macrophages, encourage the development of chronic inflammation, hypoxia, angiogenesis and immunosuprression.[83] In particular, CAF which construct and remodel the ECM have become known for their regulation of anti-tumour immune responses.[83] The dense fibrotic tissue that can encompass solid tumours creates a physical barrier for immunotherapeutic agents attempting to reach cancer cells.[84] Furthermore, the abnormal and compressed vasculature associated with tumour development additionally impedes delivery of immunotherapeutics.[85] Immunosuppressive checkpoints are responsible for preventing immune cells from attacking harmless cells in normal physiological conditions but can also inhibit immune cell killing of tumour cells.[86] Moreover, a lack of suitable cancer specific antigens is a major limitation in the progress of the use of immunotherapies for treating solid tumours and has resulted in low efficacy and off-target toxicity in clinical trials.[82] Another major difficulty for intratumoural immunotherapy is tumour accessibility and is the reason a great deal of clinical studies focus on breast and skin carcinomas.[87]

In 1986, the FDA approved the first commercially available cancer immunotherapy agent, the cytokine interferon (IFN)-α, to treat hairy cell leukaemia.[88] In subsequent years, anti-PD therapy received FDA approval for a variety of malignancies and has been proven to be an effective treatment in more than 25 types of solid cancers and multiples liquid malignancies, including Hodgkin's lymphoma, Merkel cell carcinoma, large B cell lymphoma, metastatic melanoma, lung cancer, head and neck cancer (HNC), renal cell carcinoma, urothelial carcinoma, liver cancer, gastric cancer, cervical cancer and microsatellite instable positive tumours.[89] In 2017, the first gene-modified T cell therapy received FDA approval after recording cancer remission for 83% of the 63 B-cell acute lymphoblastic leukaemia (ALL) patients treated in the study.[90] The rise of adoptive cell transfer (ACT) therapies, primarily CAR-T (chimeric antigen receptor-T cell technology), has been a major development in tackling haematological cancers with more recent translation to bring benefit to solid tumours.[10] Numerous CAR-T regimens have been trialled against triple negative breast cancer (TNBC) including ROR1+CAR-T cells, anti-MUC1 CAR-T cells and NKG2D CAR-T cells.[91, 92] Another TNBC clinical trial using c-Met-CAR T-cells showed targeting of c-Met-positive tumours without resulting in cytokine release syndrome (CRS).[93] This is another promising

target for CAR-T therapy against TNBC with 52% of TNBC tumours showing c-Met overexpression.[93] Clinically, trials applying immunotherapies to paediatric solid tumours have been conducted as an alternative to radiotherapy and chemotherapy, due to their frequent failure to control disease progression.[84] These immunotherapy studies have delivered promising outcomes but with concerns remaining over safety and anti-tumour efficacy.[84] This said, clinical trials using dendritic vaccines to treat paediatric solid tumours have been successful in reducing tumour volume without causing significant toxicity.[84]

Delivering immunotherapy systematically can result in severe side-effects and hinder the development of combination therapy regimes due to the side effects of the immunotherapy treatment so further treatment is not possible .[87] General challenges facing immunotherapy treatments include on-target off-tumour toxicity, CRS, the development of resistance, autoimmune reactions and vascular leak syndrome.[88] Even though immunotherapy has been applied to a variety of cancer types, benefits to survival have only been seen for a proportion of patients due to the complexity and regulation of the immune system.[7] Challenges for the further development of immunotherapies include enhancing the effectiveness of T cell-based therapy for solid tumours and identifying the critical influences that stimulate immune cell infiltration to the tumour site.[94] Despite the promising results of T cell-based immunotherapies, side effects on the performance of vital organs resulting from T cell-driven inflammation remains a concern.[90] Another important question to be answered is why some patients respond to immunotherapy and others do not. These individual differences emphasize the need for better prediction of clinical outcomes to provide guidance on personalized treatment.[17] More investigation is needed into the causes of and procedures to mitigate the unwanted and potentially lethal side effects that can occur as a consequence of immunotherapy treatment, such as CRS and central nervous system -related and immune-related adverse events.[95]

Targeting solid tumours with immunotherapies is a field in development. The TME plays a major role in immunosuppression, not only in regard to the dense ECM, but a barrier between the tumour and immune cells is also established by immunosuppressive regulatory T cells that can thwart T cell attempts to reach the tumour site. Other challenges for immunotherapies targeting solid tumours include immunosuppressive agents, such as transforming growth factor β (TGF-β) and Interleukin (IL)-10, hypoxia and immune checkpoints.[13] Even if T cells are able to overcome these challenges to ultimately engage with cancer cells, their stimulation and activation can still be interrupted through CTLA-4 binding.[89] Furthermore, infiltrating monocytes, dendritic cells, macrophages and tumour cells express PD-L1 that binds to T cells to prevent their attack of tumours.[13]

1.7 Types of Immunotherapy

Some of the most common immunotherapy types include non-specific immunostimulation, small molecules, vaccines, monoclonal antibodies and ACT (**Figure 1.3**)[11].
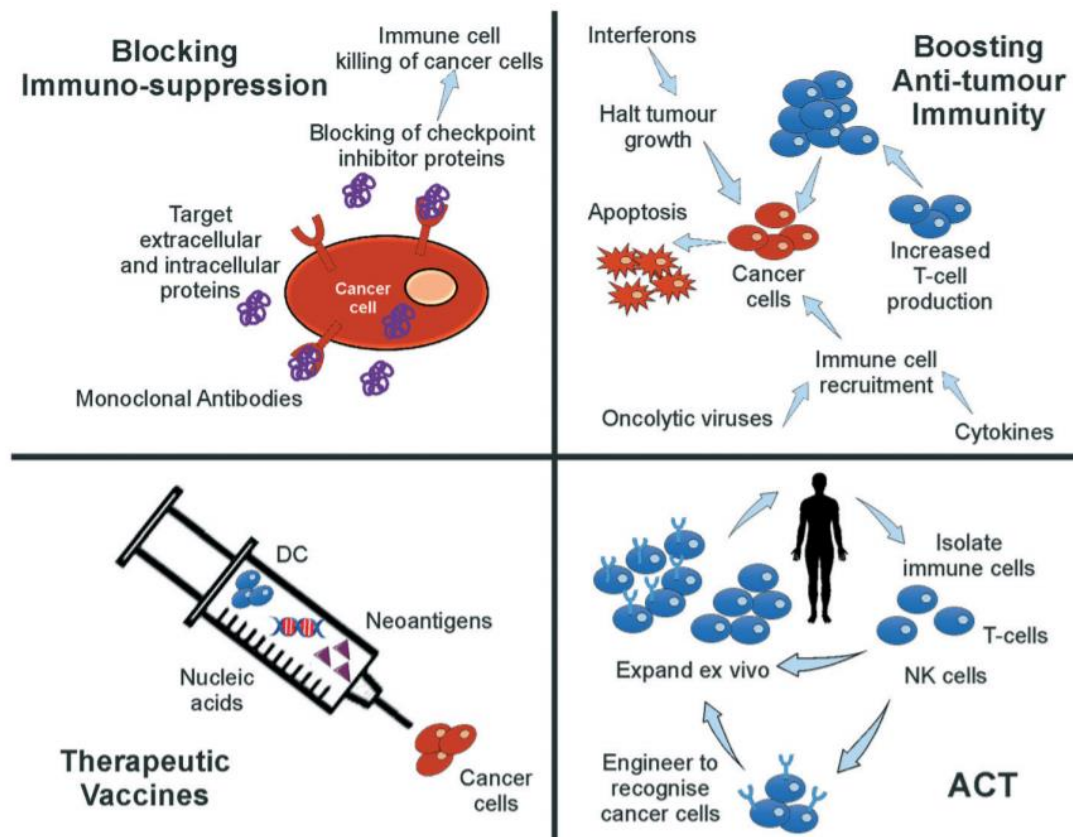
***Figure 1.3** Immunotherapy treatment types. Schematic diagram of the most common immunotherapies and their mode of action. The top left quadrant depicts the blocking of immunosuppressive proteins using monoclonal antibodies, resulting in cancer cells being able to be killed by immune cells. The top right quadrant shows a schematic of how anti-tumour immunity can be generally enhanced through cytokines, oncolytic viruses and interferons. The bottom left quadrant depicts the components of therapeutic vaccines which can be directly injected into tumours. These vaccines can include nucleic acids to enhance immune system recognition and destruction of cancer cells. Vaccine components can also include dendritic cells and neoantigens to induce specific immune responses targeted towards cancer cells. The bottom right quadrant shows the processes involved in adoptive cell transfer therapy. (DC= dendritic cells, ACT= adoptive cell transfer). Adapted with permission from Paterson et al., Lab on a chip, 2021, https://creativecommons.org/licenses/by/3.0/.*

1.7.1 Non-Specific Immunostimulation

A number of immunotherapies instigate non-specific immunostimulation without exclusively targeting tumour cells. The 3 main cytokines for this form of immunotherapy are interleukins, IFNs, and granulocyte-macrophage colony-stimulating factor (GM-CSF).[88] Interleukins are a group of messenger molecules that regulate cell behaviour and immune responses and can stimulate other immune cells to augment an anti-tumour immune reaction.[96] IFNs regulate cell functions and can act to have an apoptotic and anti-angiogenic effect on tumours, thus decelerating or halting tumour growth.[96] IFNα and IL-2 treatments have experienced success

in treating a range of solid and liquid malignancies despite mixed results for paediatric solid tumour trials.[84, 88] GM-CSF stimulates the production of white blood cells to enhance the immune response and has been shown to increase the sensitivity of acute myeloid leukaemia (AML) cells to enhance chemotherapy efficacy.[84] GM-CSF therapy supports T cell homeostasis and survival and encourages dendritic cell differentiation, enabling their expression of tumour specific antigens.[88] A downside to the use of cytokines, however, is their short half-life, meaning that treatment needs to be delivered at a high dose which can result in serious side effects, such as CRS, vascular leak syndrome and autoimmune attacks.[88]

1.7.2 Small Molecules

Small molecules are also used in immunotherapy and have the benefit of being able to target proteins both intracellularly and extracellularly. These are administered in combination with other immunotherapies to restrict tumour growth and alter the TME.[97,89] CB-1158 and epacadostat are examples of inhibitors of immunosuppressive enzymes that promote regulatory T cell proliferation, MDSC recruitment and TCR signalling impairment.[97] While epacodostat has shown promise in treating advanced solid tumours in clinical trials, it has not provided an improvement to the anti-tumour response when combined with checkpoint inhibitors.[97] The small molecule immune modulator, ADU-S100, has, however, been shown to be of benefit in treating TNBC and melanoma when given in combination with spartalizumab, a checkpoint inhibitor.[87]

1.7.3 Vaccines

Therapeutic vaccines are administered to patients with the aim of enhancing their immune system response towards cancer cells.[89, 98] These vaccines can include immune cells, dead cancer cells, recombinant viral, bacterial and yeast vectors and proteins[88, 89, 98, 99, 100], with the main types involving nucleic acids, dendritic cells and neoantigens.[88] Cancer vaccines have been proven to regulate DC function and increase their immunostimulatory activity in murine models, thus delaying tumour growth.[88] mRNA vaccines can cause protein expression without having to pass the nuclear barrier, are non-infectious and are not integrated into the genome.[88] Cancer vaccines have seen minimal clinical success to date when administered as a monotherapy, thought to be due to the immunosuppressive TME.[101] However, results have been more promising for combination treatment with checkpoint inhibition.

The Bacillus Calmette–Guérin (BCG) vaccine was the first FDA approved immunotherapy in 1990 for the treatment of bladder cancer and continues to be the only intravesical therapy for the prevention of non-muscle invasive bladder cancer progression.[102] Neoantigen vaccines have been proven effective against several solid tumour types with the TG01 mutant K-Ras

peptide vaccine approved for the treatment of pancreatic cancer.[101] DC vaccines have been studied the most thoroughly out of all immunotherapeutic vaccine types.[88] The sipuleucel-T vaccine was found to enhance overall patient survival against prostate cancer and was approved in 2010.[88, 89] However, this therapy was only shown to have moderate efficacy and has a complex manufacturing process.[88, 89] DC vaccines are one of the safest forms of immunotherapy but their manufacture is labour and resource intensive and they have shown mixed outcomes in clinical trials.[88] Oncolytic viral therapy uses the ability of a virus to destroy tumour cells with the potential for triggering an anti-tumour response and has been shown beneficial against some solid tumour types.[84, 101] Oncolytic viruses specifically replicate inside and kill tumour cells without damage to normal cells.[101] Once the cancer cell has been lysed, antigens are released and recognised, resulting in an anti-tumour immune response.[101] Specifically, variants of the oncolytic Herpes virus have demonstrated benefit for various solid malignancies.[84] Intratumoural injection is suited to directly kill cancer cells in a solid tumour mass without harmful systemic effects or hepatic virus degradation.[84] However, this form of treatment is not always possible due to the surrounding solid TME which can act as a barrier.[84, 101] Other issues include complete viral clearance and acquired specific immunity against the virus.[84]

1.7.4 Monoclonal Antibodies

Monoclonal antibodies (mAbs) are another form of immunotherapy, of which immune checkpoint inhibitors (ICI) are the most widely used. ICI are the most investigated form of cancer immunotherapy with programmed cell death protein 1 (PD-1)/ programmed death ligand 1 (PD-L1) blockade and cytotoxic T-lymphocyte-associated antigen 4 (CTLA-4) blockade being the most common area of study.[88] ICI bring about a therapeutic effect by blocking proteins between the surface of immune and tumour cells that would inhibit the attack of cancer cells by the immune system. Normally, these checkpoints prevent the immune system attacking healthy cells unnecessarily during infection and are critical to the maintenance of homeostasis.[103] However, this mechanism can be manipulated by tumour cells as a means of avoiding destruction by the immune system.[103] CTLA-4 blocking allows the restoration of T cell function and the recognition and killing of tumour cells, whilst mAbs targeting PD-1/PD-L1 prevents T cell inactivation.[88] TNBC has the largest population of tumour-infiltrating lymphocytes (TILs) amongst all breast cancer subtypes, making this form of cancer highly suited for the incorporation of immune-checkpoint blockade into treatment regimes.[104] Combination anti-PD-L1 and chemotherapy treatment for TNBC has been shown more efficacious than the individual monotherapies in both pre-clinical and clinical studies.[104, 105] Carboplatin chemotherapy is often incorporated into treatment regimens against TNBC[105],

with several clinical investigations of carboplatin and PD-1/PD-L1 inhibitor combinations.[106, 107] A crucial aspect of ICI systemic administration is the potential to negatively impact many vital organs.[88] Furthermore, reports of only a small proportion of patients receiving benefit from ICI treatment have been made, potentially due to the range of immunosuppressive systems in the TME.[88] Notably, it has been observed that ICI elicit a greater response and provide longer progression free survival for tumours that have metastasized to lymph nodes rather than the liver, a more challenging tissue for T cells to infiltrate.[7] Ipilimumab was the first CTLA-4 ICI to be discovered and approved for metastatic melanoma treatment, showing success in improving overall survival rate, yet with a range of side effects and 5 deaths recorded during clinical trials.[81, 82, 101] The first two PD-1 ICIs to be approved were pembrolizumab and nivolumab which show similar efficacy to CTLA-4 ICI but without as severe side effects.[101, 82] Pembrolizumab and nivolumab have been proven effective for more than 25 types of solid cancers and multiple liquid malignancies as monotherapies and in combination treatments.[7, 81, 82, 101]

Other mAbs that have received FDA approval for solid tumours include Rituximab, a CD20 targeted treatment, Cetuximab, an antibody specific to EGFR, and trastuzumab, a HER2 inhibitor targeted therapy.[108] Clinical trials for lexatumumab and anti-B7-H1 mAbs have demonstrated anti-tumour activity against multiple solid tumour types.[84, 89] Denosumab is a RANKL antibody that has been shown to impede the resorption of bone in clinical trials for metastatic breast and prostate cancer.[84] FDA-approved dinutuximab and naxitamab have been administered alongside GM-CSF and activated NK to enhance immune responses in both PDX studies and clinical trials.[84]

1.7.5 Adoptive Cell Transfer

The next category to be discussed is ACT therapy. This form of treatment involves the administration of immune cells to a patient, including allogenic cells taken from a donor or the patient's own immune cells that have been isolated and subsequently modified and expanded *ex vivo*, before being returned to the patient's system[109, 85] (**Figure 1.4**)[110].
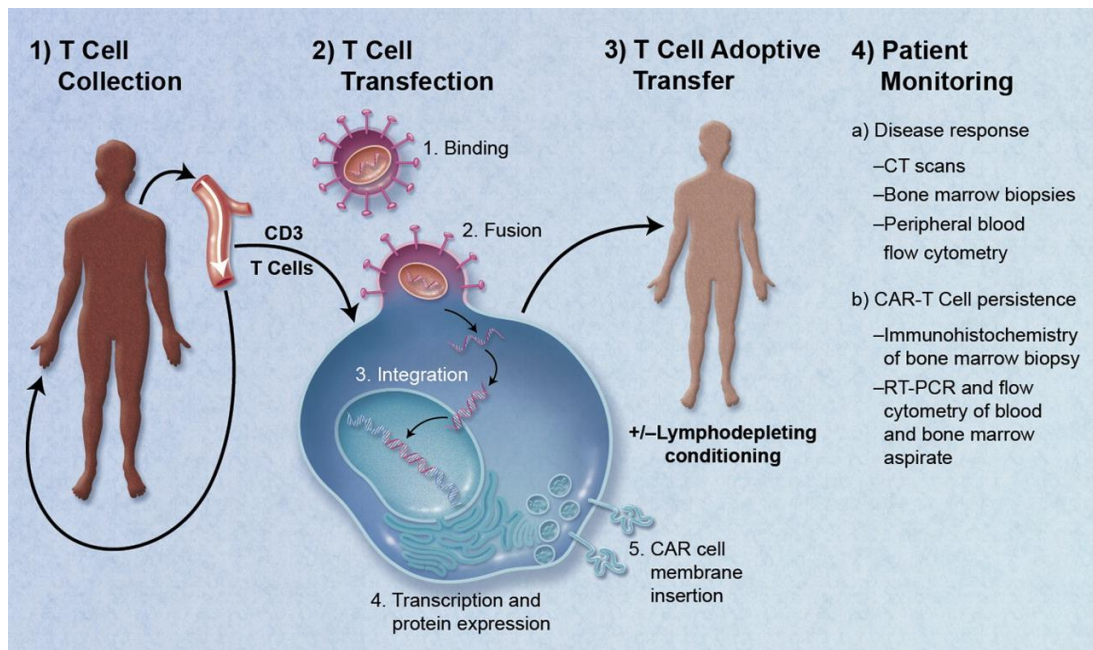
Figure 1.4: Schematic of CAR-T cell production and patient treatment. Adapted with permission from Jacobson et al, Blood, 2011, http://creativecommons.org/licenses/by/4.0.

ACT normally involves the transfer of T-cells, CAR-T cells, NK cells and CAR-NK cells and has been successful in treating melanoma, HNC, renal cancers and gynaecological cancers.[101] NK cell based immunotherapy has been mostly investigated for haematological malignancies, such as AML and ALL. [101] Clinical trials have demonstrated ACT to be well tolerated by patients but with limited success in multiple solid malignancies due to a lack of sufficient NK infiltration and proliferation.[101] While the immunosuppressive TME plays a role limiting immune cell infiltration, several approaches have been reported of mechanisms acquired by tumour cells to escape NK cell attack and inhibit NK activity and function.[84]

T-cell immunotherapy is an up-and-coming approach to cancer treatment, particularly when applied to haematological forms. This therapy involves the isolation of a patient's T cells which are engineered to express a receptor specific to the proteins expressed on the surface of their cancer cells.[85] CARs allow T cells to bind specifically to tumour cells and eliminate them.[85] CAR-T cells are highly efficient at identifying and killing target tumour cells and can stay active for up to a decade once injected, potentially being a one-time therapy.[88] Tisagenlecleucel and axicabtagene-ciloleucel were the first to be approved for ALL and certain types of large B-cell lymphoma.[82] For solid tumours, CAR-T cells have been demonstrated to be safe in clinical trials regarding a variety of cancers, including non-small cell lung cancer (NSCLC), neurological malignancies, breast, pancreatic, sarcoma and metastatic colon cancer.[101] Anti-tumour effects of CAR-T have also been shown to be enhanced with combinatory use with ICI in melanoma, NSCLC and Hodgkin's lymphoma.[101]

To enhance CAR-T tumour infiltration, tumours could first be exposed to localised chemotherapy or radiotherapy that cause tumour cells to undergo immunogenic cell death (ICD).[111] Damage-associated molecular patterns are secreted as a consequence of ICD and subsequently trigger the release of chemokines and tumour antigens from dendritic cells. This stimulates a T cell response and establishes a more hospitable environment for T cells.[111] However, it is important to consider that CAR-T cell therapy is only suitable for patients who have an intact immune system.[92] Due to the immunosuppression caused by cytotoxic chemotherapy, T-cells would first need to be obtained from the patient for *in vitro* expansion.[92] However, the presence of CAR-T cells in the TME alone does not guarantee the elimination of the tumour.[111] The inhospitable TME conditions also affecting CAR-T function include low pH, hypoxia and a lack of essential cell nutrients.[111] Other issues associated with CAR-T therapy include CRS, neurotoxicity and agammaglobulinemia, a type of toxicity caused by a lack of gamma globulin in blood plasma resulting in immune deficiency.[84][111]

Worldwide, many research groups are advancing CAR-T cell therapies for targeting solid tumours, but limited success has been achieved thus far. For T cells entering the solid TME, they are faced with a high degree of immunosuppressive factors, a challenge not present when treating haematological malignancies and one that inhibits their accumulation and proliferation at the tumour site.[12, 13, 112] CAR-T cells must circumvent immunosuppressive molecules and cells in order to exert a cytotoxic effect upon solid tumours.[111] Immune checkpoints include inhibitory PD-L1 ligands that tumour cells can express to mute CAR-T cell function.[111] Immunosuppressive cells present in the TME include CAF which have high fibroblast activation protein (FAP) expression and collagen deposition that inhibits T cell access to tumour cells.[19, 35, 111] CAR-T targeted towards FAP or CAR-T that have been engineered to release enzymes that degrade the ECM could enhance their infiltration of the TME killing of tumour cells.[111] Whilst combination treatment of CAR-T cells targeting FAP has been shown to improve anti-tumour immunity in immunodeficient murine models, FAP CAR-T cells have also been reported to recognize and kill normal cells expressing FAP resulting in lethal toxicity and cachexia.[83]

Tumour antigen loss is thought to be an effective method for tumours to avoid CAR-T mediated killing and has been associated with poor responses in haematological clinical trials with CD19 CAR-T cells.[7] Clinical trials using CAR-T cells have been conducted against many types of solid cancers.[113] In many cases, the target antigen is expressed by multiple organs, such as epidermal growth factor receptor (EGFR), natural killer group 2D (NKG2D)-ligands and human epidermal growth factor receptor 2 (HER2).[113] These are amongst the most targeted

antigens for CAR-T clinical trials for solid tumours.[113] The widespread application of CAR-T therapy for solid tumours has been hindered by a lack of reliable tumour-specific target antigens that are consistently expressed throughout the tumour tissue and are absent from normal cells to avoid low efficacy, off-target toxicity and serious or even life-threatening toxicities.[82, 111, 112, 114] CAR-T therapy is limited in this way as approved methods for the prediction of such toxicities are not yet available.[115] Improving CAR-T design to prevent unintended targeting of normal cells with low target antigen expression is required.[116] The further development of CAR-T cells to better distinguish between cancerous and normal cells expressing the same antigen offers a solution to the absence of entirely tumour cell exclusive targets.[111] Thus, enhancing tumour cell targeting, efficacy of treatment and patient safety.[111]

Other challenges for CAR-T therapy include the laborious, expensive and time-consuming production.[88] The procedures involved in acquiring patient cells for CAR-T manufacture are costly.[117] Leukapheresis is used to isolate T cells from patients which can then be activated and genetically manipulated *ex vivo*.[117] Cells are subsequently expanded and re-administered to the patient.[117] Quality control measures and cryopreservation can then be carried out to enable shipping from the centralised manufacturing site to a clinical facility for infusion into the patient.[117, 118] Commercially sustainable manufacturing processes and facilities are needed to enable broader use of this technology.[117]

Due to the vast mechanisms of immunosuppression by tumour cells, there are an infinite combination of treatments and genetic variations of T cells that could be trialled.[111, 114] 3D spheroid models offer enhanced mimicking of intercellular interactions.[5] To enhance the recapitulation of tumour characteristics, models using human or murine cell lines could be replaced with primary or patient biopsy tissue for use in precision medicine.[5] Better models are needed for screening treatment variations and to enhance the speed of clinical translation of effective therapeutics for patients.[111] Investigating the ways in which treatment resistance arises and changes after therapy by studying post-treatment biopsies would allow the development of future combinations.[111]

In vitro CAR-T assays are typically conducted in 2D using 96-well plates, such as by Zhuo *et al.* in 2019 who performed MTT assays using MUC287 CAR-T cells in a 2:1 effector: target (E:T) ratio against TNBC tumour cell lines.[119] Dillard *et al.* formed spheroids using a colorectal cell line in 96-well plates and used live imaging to track spheroid growth, effector cell cytotoxicity and target cell apoptosis.[120] More recently in 2021, Li *et al.* also used 96-well plates for cytokine release assays with CD-16 CAR-T cells against various kidney and lung tumour cell lines in 10:1 or 5:1 E:T ratios.[121] In 2020, Liu *et al.* assessed CXCR2-expressing

CAR-T cells against hepatocellular carcinoma tumour tissues and cell lines using transwell assays for *in vitro* studies and xenograft models.[122] Recently in 2021, Ronteix *et al.* formed spheroids using droplets with B16 murine melanoma cells and matrigel. Droplets containing cytotoxic T lymphocytes (CTLs) were merged with spheroids and time-lapse imaging performed to measure spheroid disaggregation, contact time and accumulation.[123] Herter *et al.* formed spheroids by the hanging drop method and incorporated LS174T human colon adenocarcinoma cells, MRC-5 normal fetal lung fibroblast cells and CCD-18Co a normal colon fibroblast cell line into the model.[124] Cultures were treated with immunocytokines and T cell bispecific antibodies targeted towards tumour cells or fibroblasts. As of yet, high throughput immunoassays that incorporate tumour spheroid and stromal cultures are not widely used.

EGFR is a common receptor that is over-expressed on many types of solid tumour.[125] Previous investigations into EGFR-CAR-T include that by Bergeron *et al.* in 2017 who carried out 2D monolayer and 3D spheroid assays using 384-well Corning spheroid microplates.[126] The target cells were lung tumour cell lines with E:T ratios varying from 40:1 to as low as 0.04:1. Wallstabe *et al.* used a basement membrane scaffold and formed 3D spheroids using the non–small cell lung cancer cell line A459 and the TNBC MDA-MB-231 cell line.[127] Tumour cells were exposed to ROR1-CAR T with expression of truncated epidermal growth factor receptor (EGFRt) transduction marker for more than 72h with subsequent analysis of PD-1 T cell expression. EGFR specific CAR-T cells were also used by Liu *et al.* in 2019 for *in vitro* cytokine release and cytotoxicity assays and tumour growth assays in TNBC cell lines and patient-derived xenograft murine models.[128]

In summary, having described the complexity of the disease and the impact of the TME and immune system on the effectiveness of anti-cancer treatment, the pre-clinical models used to assess these treatments will now be discussed. This is with particular focus on immunotherapy, as the newest and most promising form of anti-cancer treatment. The need for enhanced methods to further our understanding of ACT therapy specifically will be further discussed and the value of microfluidic technology for this role presented.

1.8 *In vivo* Models

The clinical implementation of immunotherapies has been challenging, mainly due to shortcomings in the representation of the native *in vivo* environment in current preclinical models. [129] A variety of factors have to be considered when studying combinations of different

treatment modalities, such as the sequence of therapies, dosage and toxicity assessment. There exists a variety of preclinical models used to study immune responses (**Figure 1.5**)[130].

	2D cell culture	**In-vivo model**	**3D cell culture model**	**Microfluidic Device**
Advantages	• Low Cost • Ease of use • Highly reproducible • Can be used for high-throughput drug screening	• Living organism • Heterogeneity present	• High throughput • Co-culture possible • Cell-ECM interactions • More physiologically relevant than 2D models	• Can be humanized • Physiologically relevant • Cell-cell and cell-ECM can be analysed in real time • Can incorporate a vascular like component
Disadvantages	• Not representative of in-vivo interactions • No TME/ECM • Often not clinically relevant	• Not human • High Cost • Require skilled individuals • Ethical limitations • Large scale experiments not possible	• Not highly reproducible • Long term culture is complex/ lacks stability • Optimisation required for different cell types	• Can have high cost • Low throughput • Optimisation required for different cell types

Figure 1.5: Schematic diagram showing the advantages and disadvantages of current pre-clinical models. Adapted with permission from Reidy et al., Cancers, 2021, https://creativecommons.org/licenses/by/4.0/

Despite animal models providing a higher level of complexity and being able to represent human physiological response more faithfully than traditional 2D monolayer cell culture, these methods are limited in their clinical translational value to patients.[2] Animal studies are needed for investigating drug efficacy and side effects systemically and over time. Yet differences between human and animal physiology can be significant and can put clinical trial volunteers at risk when translating *in vivo* data.[75] Various types of murine models are commonly employed and frequently involve implanting tumours derived from cancer cell lines, known as xenografts, or cancer patient tumour tissue into immunodeficient or immunocompetent mice.[7] Syngeneic models are one of the oldest and most commonly used murine models.[131, 132] These models involve implanting a murine cancer cell line into immunocompetent mice and are useful tools in providing the ability to study the effects of immunotherapies in the context of a functional immune system.[131, 132] This is particularly beneficial for cancer immunotherapy studies which are developed to operate in conjunction with patient immune systems to enhance native immune responses targeting tumour cells.[131] However, these models can have low tumour heterogeneity and fail to represent the complexity of the TME.[131] Patient derived xenografts (PDX) models were established to improve the accuracy of predictive response for humans.[2] However, these do not provide the contextual or tumour/organ-specific features that can determine tumour development and the immune system's response, as is seen in human tumours.[7] Many studies have reported issues with successful engrafting of human cells and their long-term survival in the host.[6] While cytokines can be administered in an attempt to

prolong human cell survival in these models, this has the potential to skew the immune response and could lead to data that cannot be associated with the actual human immune response.[6] PDX models could not be considered suitable for high throughput precision medicine assays as they can take months to establish, are costly and are limited by the quantity of assays that could be carried out.[2] Genetically engineered models are considered the most reliable of murine model for depicting human disease and allow for evaluation of immune responses in regard to specific oncogenes or driver mutations, but provide limited information as the cancer cells mutate, the host's TME can overtake the human TME and the immune response evolves.[7]

Experiments involving animals are prone to predictability issues due to the immune system of the animal being compromised, in addition to general differences in comparison to the human immune system. [7, 8, 9] Less than 8% of *in vivo* assays are able to be successfully translated into clinical cancer trials.[9] These methods are also unfavourable in relation to ethical issues, including the 3Rs policy, as well as being associated with high costs and in the procurement of misleading or misrepresentative data corresponding to the human *in vivo* condition.[3,133]

1.9 *In vitro* Models

In vitro models are far less costly than *in vivo* in both monetary and labour terms and can provide higher throughput assays.[2, 3] Commonly used *in vitro* methods to study tumour-immune cell interactions include identifying tumour associated antigens with Cr release assays, while quantitative PCR and flow-cytometry can provide information on the expression of cytokine genes and factors in 2D assays.[134] As acquiring a sufficient quantity of human primary tumour and immune cells for *in vitro* studies is difficult, cytotoxicity studies of immune cells often rely on cancer cell line monolayers.[134] Transwell assays are a simple and commonly used *in vitro* technique in drug screening and cancer cell migration and invasion studies.[2] These involve using porous membranes that allow migration from one side to another and can include ECM layers.[2] However, this method only provides data on individual cell migration and does not account for 3D tumour *in vitro* structure within the TME.[2] Many simplistic and low cost 2D and 3D *in vitro* models have been established to investigate the effects of therapeutic agents on cell proliferation, communication, migration and protein and gene expression. Yet, their ability to capture the complexity of the *in vivo* TME is limited and they are not equipped for investigations into intricate cell spatial organizations and interactions.[135] 3D scaffolds and hydrogels have been used as a more physiological means of investigating interactions between immune and cancer cells. An advantage of these models is that their mechanical properties can be modified to be comparable to that of tumour ECM.[136]

A hurdle in evaluating immunotherapy is that of establishing *in vitro* models that provide sufficient clinical translation. *In vitro* models, have often been considered too simplistic in their depiction of the TME. This is due to the reliance on 2D cell monolayers which artificially alters cell proliferation and differentiation to what is seen *in vivo*.[3] The low success rate for drugs receiving market approval can be blamed on the lack of accuracy and relevance of 2D predictions of drug efficacy with respect to the true tumour environment.[3] It is of great value to consider the 3D TME when designing *in vitro* models to more accurately recapitulate the physiology of native tumours.[15] 2D cell culture enables cells to grow in homogenous monolayers along a surface where they are exposed to an equal supply of oxygen and nutrients.[137] Whereas, cells cultured in a 3D environment experience culture conditions that more closely reflect the real *in vivo* scenario with varying availability of nutritional and oxygen resources.[137] Differences between cell-cell interactions crucial to cell proliferation, differentiation, function and drug metabolism between cells in 2D and 3D have also been reported. [2, 137] Immune cells have been shown to be unable to kill cancer cells in a 3D environment, despite being able to do so in 2D assays, due to the nature of their mechanisms to evade immune cell killing.[13] Immune cell function has been validated in various spheroid models with findings showing that the anti-tumour effects of T cells is significantly reduced in 3D cultures.[134] This could be explained by the increase in lactic acid production that occurs in 3D cultures in comparison to 2D assays which has been shown to impede the efficacy antigen specific CTL.[134] 3D cell culture is a useful tool in bridging the gap between *in vivo* and traditional monolayer cell culture.[137] Therefore, it is necessary to establish a more physiologically relevant method of determining anti-cancer drug efficacy that combines the physiological relevance of *in vivo* models with the reduced cost and workload of *in vitro* models.

One of the reasons for the low success rate for anti-cancer drugs receiving market approval can also be attributed to the lack of physiological relevance in preclinical models used to assess drug efficacy, often based on the use of immortalized cells lines rather than on patient-derived tissues.[138] *In vivo* conditions can be recreated through control of pressure, flow and nutrient levels.[2] *In vitro* 3D models, using ex-vivo human tumour tissue, such as spheroids and organoids, are increasingly being used.[4] Organoids can offer a faithful recapitulation of *in vitro* characteristics over longer time frames in comparison to spheroids formed from tumour cell lines.[139] However, the immune component of such models is often neglected.[4] Organoids have been recently shown to offer a degree of clinical predictive value in some cancers.[140] They have been shown to provide an *in vivo* like morphology of real patient tumours, as well as providing faithful genetic and phenotypic recapitulations.[140] Yet, they lack TME

characteristics and their production can be cost and time-intensive, as a result of the expensive cell culture reagents and low-throughput technology used.[141] While anti-cancer drug testing can be conducted using tumour organoids composed of only epithelial cells to establish drug efficacy, immunotherapy testing requires a more complex system that includes immune cells.[142]

Alternatively, spheroids provide a simple and easy to use platform for drug discovery applications, without the price-tag and complexities of *in vivo* studies.[143] Multicellular tumour spheroids were first discovered by Holtfreder and Moscona in the 1940's.[144] The first stage of spheroid formation involves the aggregation of cells to form a stable mass and can take a varying length of time depending on cell type and the dynamics of the culture conditions.[14] The second stage sees an increase in cell proliferation and biomass production before the final phase.[14] This is characterised by a decrease in proliferation and growth of the spheroid until it steadies at a constant diameter and achieves homeostasis.[14] Traditional spheroid formation mechanisms include the use of magnetic levitation, bioprinting, bioreactor flasks and liquid overlay.[14] Many of the conventional methods are time-consuming, low throughput and do not permit control over cell numbers in each spheroid, producing spheroids with differing diameters which are laborious to separate and group.[14] Current 3D spheroid models can experience limitations that include their low throughput, time consuming protocols and lack of homogenous spheroid formation.[42] Spheroids have been formed from many types of tumour cell lines for use in a variety of assays, including investigations into tumour growth, cell function and interactions, metastasis and drug screening.[3, 145] Multiple cell types can be used in spheroid generation and their size can be easily controlled.[146-148] High-throughput and efficient methodologies that allow for rapid homogenous spheroid generation are required to accelerate anti-cancer drug development. Some commercially available assays include the GravityPLUS™ hanging drop system and GravityTRAP™ ultra-low adhesion plate from InSphero. The GravityPLUS™ hanging drop system is a lower throughput assay that involves more processing steps than the GravityTRAP™ plate and so is better suited for culturing primary cells and complex multi-cellular spheroids.[149, 150] The GravityTRAP™ assay is a cost effective and high throughput system suited to the culture of cancer cell lines.[150, 151] The bottom of wells in the GravityTRAP™ plate are composed of a thin transparent plastic that allows easy visualization and imaging of spheroids.[150] The Nunclon™ Sphera™ ultra-low attachment liquid overlay system is another commercially available assay which has been extensively validated for use in the formation of tumour spheroids using various cancer cell lines.[152] Microfluidic technology can offer advantages in comparison to these systems such as

being able to create more complex multicellular assays with reduced cell and reagent quantities.

Inadequacies in current *in vitro* models occur as a result of culturing conditions which do not recreate *in vivo* conditions effectively enough.[153] This can have consequences for cell behaviour and analysis and lead to insufficient predictability of the efficacy of anti-cancer drugs.[153] A mere 3.4% of anticancer drugs currently succeed through Phase I testing to receive eventual approval.[154] More reliable and physiologically relevant *in vitro* models are required that more closely mimic *in vivo* conditions to assess both fundamental biological questions and drug efficacy to ensure confident pre-clinical validation of immunotherapeutic agents. Microfluidic technology can provide a solution by allowing greater control of fluid volumes, culture conditions, surface chemistry, channel dimensions and stimuli exposure.[155] Whilst microfluidic technology has been broadly applied to cancer studies of drug efficacy, cell interactions and metastasis, there have been comparatively few relating to the impact of 3D tumour culture on cancer cell sensitivity to immune cell activity.[134]

1.10 Microfluidic Technology

Microfluidic technologies provide large throughput yet miniaturised methods to assess the phenotypic response and drug effects on human tumour models in 3D with a high degree of physiological relevance.[15] Microfluidic technology was first developed in the 1980s and is the study of fluid behaviour, control and manipulation in microscale channel systems.[156] Microfluidics is a promising technology that offers solutions for a wide range of subjects.[156] It offers the advantages of using reduced volumes of samples and reagents, decreased expenses, high-throughput potential and more precise control over experimental constraints.[156] Microfluidic devices have been used to establish physical and chemical gradients, manipulate cell distribution and perform high resolution time lapse imaging.[72] As the magnitude of dimensions in a system reduces, there is an increase in the surface area to volume ratio.[157] This creates a more favourable environment for microscale channels to trap targets, for example cells and nanoparticles.[158] Microfluidic devices, also known as lab-on-a-chip devices, are fabricated using various polymer materials as a replica of a master created by photolithography (**Figure 1.6**)[159].
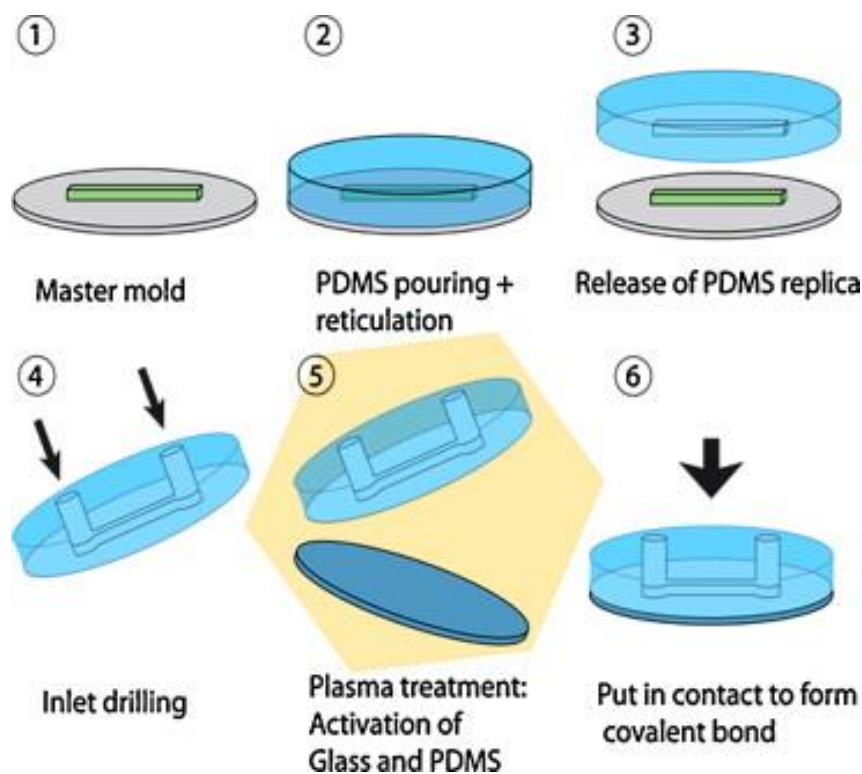
Figure 1.6: Schematic diagram of the typical fabrication procedure for a single layer microfluidic device. The silicon master mould is produced by photolithography and photoresist patterning to create the microfluidic channel structures. After the application of an adhesive, the wafer can be used to cast PDMS onto the wafer which is then cured in an oven at for 3 hours. Holes are created in PDMS layers using biopsy punches or syringe needles. These PDMS layers can then be plasma treated and bonded to glass slides or other PDMS layers to form complete devices. Adapted with permission from Velve-Casquillas et al., Nano Today, 2010, https://creativecommons.org/licenses/by/4.0/.

This method allows the fabrication of intricate shapes down to 1μm lateral resolution and with a maximum thickness of 200μm.[44] The most popular material option being polydimethylsiloxane (PDMS) due to its favourable bio-chemical behaviour and lower cost compared to alternative options for microfluidic chip materials.[160] Its optical transparency allows easy visualisation of micro-channels and the fluid within them, while its gas permeability allows sufficient gas exchange for cell culture.[160] The flexibility of PDMS also allows for easy manipulation of the material for use in a wide range of applications.[161] This can be easily adjusted to obtain the desired degree of elasticity, using cross-linking agents.[161] While PDMS is a low cost material to manufacture microfluidic devices from, estimated at approximately £0.20/gram, the thermal cost and time required to cure and bond PDMS devices increases the overall cost of device manufacture.[162]

Pumps, including pneumatic, syringe and peristaltic devices can be employed to provide a controlled continuous delivery of nutrients to cells.[163] Limitations exist for these pumps, however, due to fluctuations in flow rate or the generation of excessive shear stress which can negatively impact cells in devices.[163, 164] Whilst the use of external instrumentation is useful in

sustaining liquid velocity and pressure, this can be cumbersome and could prove difficult to adapt to a high throughput setting. Less complex and low-cost device set-ups are, thus, more convenient for larger throughput applications.

Microfluidic devices are frequently utilized in a variety of research, diagnostic and pharmaceutical applications, such as drug development and administration, chemical gradient generation and point-of-care treatment.[163] By allowing greater control of fluid volumes, culture conditions, surface chemistry and stimuli exposure, microfluidic technologies can provide a solution to some of the challenges faced by conventional *in vitro* or *in vivo* models.[156] This is in addition to offering large throughput yet miniaturised methods to assess the phenotypic response and drug effects on complex human tumour models in 3D, with a high degree of physiological relevance.[15] Combining ACT and microfluidics can provide novel insights into ACT mechanisms and the efficiency of tumour cell killing in a miniaturized 3D environment.

1.10.1 Microfluidic 3D Cell Culture

Microfluidic technology has advanced spheroid formation and enabled their widespread use in testing novel anti-cancer agents and investigations into 3D cell interactions and expression.[165] Miniaturization allows tissue taken from one animal to be used in hundreds of assays rather than conducting one test in hundreds of animals.[2] Equally, the use of microfluidics maximizes the potential number of assays that can be performed when using scarce resources of patient biopsy tissue.

Microfluidic approaches have been increasingly employed in recent years for testing anti-cancer therapies on spheroids, organoids[166] as well as tumour tissue slices.[167] These methods have highlighted the importance of using primary and patient-derived tissue when analysing cell death and proliferation markers as a predictive tool of treatment efficacy. Examples of which include studies evaluating chemotherapy agents through miniaturised large-throughput screening of tumoroids established from biopsy tissue,[15] investigation of the synergistic effects of radiotherapy and chemotherapy on primary cell lines[168] and assessing responses of biopsy-derived cultures from local and distant tumour sites to radiotherapy.[169] The Chen spheroid model was one of the first to combine drug cytotoxicity testing with signalling pathway analysis in a 3D microfluidic environment (**Figure 1.7**).[170]
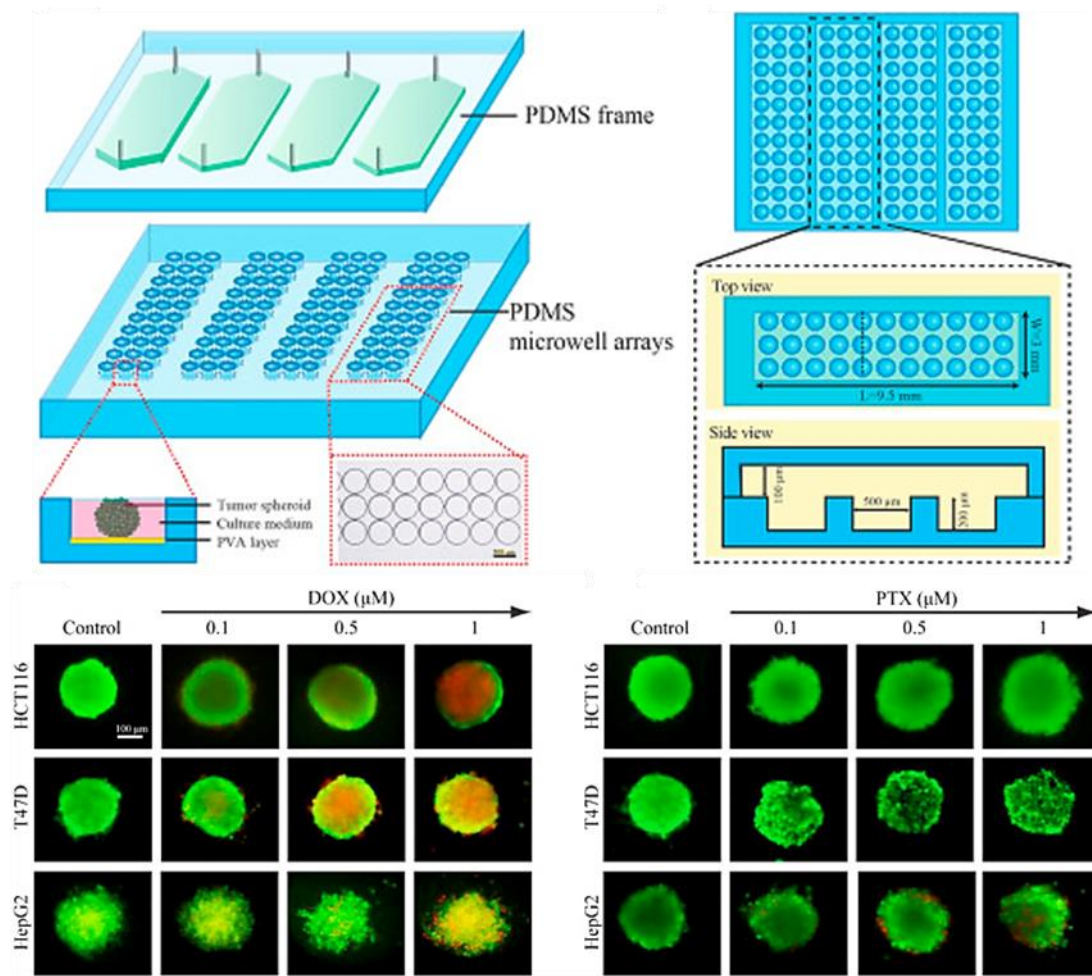
Figure 1.7 *Microfluidic device for cytotoxicity studies on tumour spheroids of a range of sizes. Spheroids were treated with doxorubicin and paclitaxel chemotherapy with viability staining performed on day 10 of culture with calcein AM (live cells, green) and ethidium homodimer-1 (dead cells, red). Spheroids were formed from human colon (HCT166), breast (T47D) and hepatocellular (HepG2) cancer cell lines in circular microwells, 500μm in diameter and 200μm in depth. Scale bar = 100μm. Adapted with permission from Chen et al., 2015, Copyright 2015, Analytica Chimica Acta. (DOX= doxorubicin, PTX= paclitaxel)*

Spheroids were established from human colon, breast and hepatocellular cancer cell lines in circular microwells and treated with a range of chemotherapy agents. Spheroids showed increased cytotoxicity with increasing chemotherapeutic doses. The device design is compatible with a microplate reader with potential for high throughput applications. Some groups have avoided the use of PDMS in device fabrication due to certain material limitations. For example, the hydrophobic nature of the PDMS surface could be restrictive when scaling up production for commercial applications.[171, 172] Ko *et al.* instead used injection moulding to create a polystyrene platform for spheroid culture in a standardized 96-well plate format.[172] The device incorporates a simplistic design with a central tapered cavity that allows patterning of a spheroid with 3D ECM and an assortment of cell types.[172] While this design permits greater control over spheroid properties, spheroids may be too large for certain applications. In 2013, Patra *et al.*, developed a microfluidic system to generate 5,000 uniform spheroids

using the HepG2 liver cancer cell line.[173] Spheroids were formed using low-adhesion square micro-wells and could be extracted from the device for further analysis. Later in 2016 the same set-up was used to assess spheroid response to three anti-cancer drugs administered individually and in combination.[174] Distinct differences in cell viability after drug treatment was reported between the 3D spheroid cultures and 2D cultures, as well as between spheroids of differing size. Cells were more viable after resveratrol and tirapazamine treatment in spheroids that in 2D, whilst cisplatin treatment was shown to result in greater cell death for smaller spheroids in comparison to 2D cultures. Mulholland *et al.* developed a device for the high throughput screening of human tumour biopsy derived spheroids.[15] The device contained a central grid of spheroids in which a drug concentration gradient could be established for up to 16 hours without the requirement for external fluid actuation equipment. The UVW human glioma cell line and LNCap prostate cancer cell line, as well as patient prostate cancer biopsy tissue, were cultured in devices and treated with the chemotherapy agents, cisplatin and docetaxel. Spheroids of varying sizes were generated in the device, allowing detection of size-dependent drug effects. To increase the complexity and predictive accuracy of tumour-on-chip devices, TME components can be incorporated into models, as well as oxygen and cytokine gradients.[2] In 2021, Berger Fridman *et al.* developed a high throughput microfluidic device with an oxygen gradient to study the cytotoxic effects of two chemotherapeutic agents, doxorubicin and tirapazamine, against MCF7 breast cancer spheroids in varying oxygen conditions.[175] The device was designed so water-in-oil droplets containing spheroid embedded hydrogel could be cultured in an array containing 1000 docking sites of 200µm diameter. Despite the high number of docking sites, occupancy rates ranged from 50% to 70% of which between 100 and 500 uniform spheroids were selected for analysis. Results showed that at low oxygen levels tirapazamine efficacy was significantly lower than had been reported in the literature and demonstrates the requirement for 3D models in hypoxia targeting drug development.

1.10.2 Microfluidic Vascular Network Models

Microfluidics have been used to mimic the *in vivo* vascular network with models of varying complexity using various cell types, hydrogel compositions and device geometries. In 2006, Chrobak *et al.* developed a system to form endothelial tubules and to investigate the optimal conditions for collagen gel preparation for endothelial cells to invade and contract the gel as little as possible.[176] Both human umbilical vein endothelial cells (HUVEC) and human dermal microvascular endothelial cells (HDMEC) were used to create vascular structures. HDMEC have a greater resemblance to *in vivo* microvessels but contain a significant proportion of cells of lymphatic origin.[176] In comparison, HUVEC are known to not express any lymphatic

markers. Both endothelial cell types became confluent after 2 to 3 days and underwent permeability and leukocyte adhesion testing. One of the first successful examples was that produced by Kim *et al.* in 2013 (**Figure 1.8**).[41]
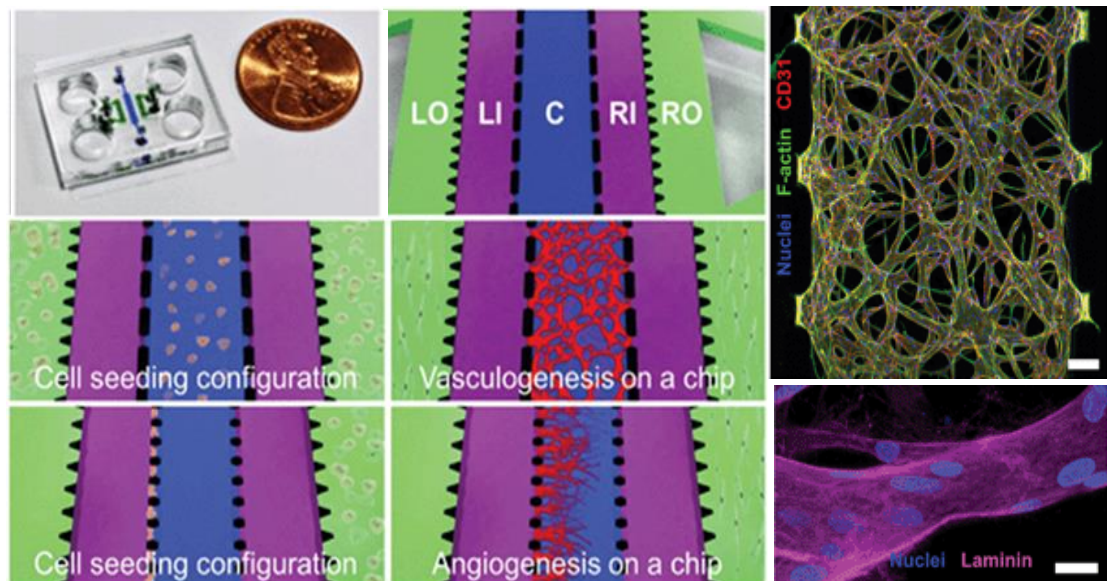
Figure 1.8 *Microfluidic device for the formation of a vascular network. Endothelial cells, fibroblasts, pericytes, cancer cells and leukocytes were seeded in different configurations in the five interconnected parallel channels to model vasculogenesis or angiogenesis. Confocal imaging was performed on mature vessels and used to quantify vessel diameter. LO = left outside channel, LI = left inside channel, C = central channel, RI = right inside channel and RO = right outside channel. Scale bars = 100µm. Adapted with permission from Kim et al., 2013, Copyright 2013, Lab on a chip.*

This five-channel device allowed combined culture of endothelial, tumour and stromal cells suspended in a fibrinogen gel. Only when HUVEC were co-cultured alongside lung fibroblasts could a perfusable vascular network be established. More interconnected vasculature was observed when using an open network, with lung fibroblasts in their own separate channels, in comparison to culturing both cell types in the central channel. This model has been used as a basis for many other microfluidic designs, such as by Lee *et al.* in 2014.[177] This device mimicked angiogenesis and the intravasation of circulating tumour cells (CTC). Quantification of angiogenic sprouts demonstrated that microvessels in the presence of cancer cells possess a greater number and coverage area of angiogenic sprouts in contrast to those without. Intravasating MDA-MB-231 breast cancer cells were also observed in the lumens of vessels after 3 days of culture. Oh *et al.* reported a device with a similar channel configuration to the Kim model.[178] Here, an increased number of endothelial cells were observed to have migrated underneath micropores where spheroids were present in the upper region, forming complex microvascular networks, as well as increased microvessel thickness in the presence of tumour spheroids. Zervantonakis *et al.* demonstrated the ability of macrophages to create leakier microvessels, as well as a greater loss of endothelial barrier integrity through tumour necrosis

factor (TNF)-α exposure, and, thus, enabling easier intravasation of cancer cells.[179] Phan *et al.* combined a microfluidic system with a bottomless 96-well plate to create vascularised microtissues for large-scale anti-cancer drug screening.[180] A pressure regulator was used to retain fibrin gel inside the tissue chambers. However, issues arose regarding the maintenance of the hydrostatic pressure and flow velocity due to the small volumes used. It was also observed that connections between vascular networks were not as tight as those present *in vivo*. Further work from this group saw the development of a vascularized spheroid forming device used to test various anti-angiogenic drugs.[181] Various breast, colorectal and melanoma cancer cell lines were seeded into devices alongside human endothelial colony forming cell-derived endothelial cells and normal human lung fibroblasts (NHLF). Vascularized spheroids formed in the system with network perfusion confirmed using fluorescently labelled dextran. Another recent study examined the relationship between interstitial flow and VEGF concentration on the integrity of vascular network formation.[182] The media volume of a pair of plastic reservoirs connected to two microchannels was manipulated. This allowed for the creation of a pressure difference between the two microchannels and, thus, interstitial flow across a central gel area. Varying magnitudes of interstitial flow caused HUVEC cells to produce vascular sprouts on day 1 of culture. This was in comparison to static conditions which formed a limited number of sprouts by day 3 that subsequently degenerated after a further 2 days of culture. While greater levels of interstitial flow were advantageous for network formation, significant collagen degradation could be observed. This was thought by the authors to occur as a result of the greater interstitial flow causing increased matrix metalloproteinase activity by endothelial cells, resulting in collagen degradation.[182] This was in addition to the separation of cells from network structures, likely as a result of mechanical stress.

1.10.3 Vascular-Tumour Microfluidic Models

2D models are commonly used to investigate barrier function, endothelial mechanosensitive responses and trans endothelial migration of blood-borne cells, such as leukocytes and CTCs.[41] However, these systems do not reflect the true complexity of native biological structures or provide the 3D context that is crucial to blood vessel functioning and architecture.[41] Chemokine gradients can play an important role in instigating the migration of cancer cells, a feature that has been absent from many previous models.[183,184] Developments in microfluidic technology have enabled the manufacture of devices that can provide varying features, such as cytokine gradients, fluid flow across assorted tumour components and communications and exchanges between different varieties of cells.[184] The use of porous membranes allows the exchange of material between microfluidic channels and for precise control over biochemical gradients to mimic pathological occurrences, such as cancer cell intravasation.[44] Tissue

specific tumour cell extravasation was modelled by Jeon *et al.* using a microfluidic bone-mimicking microenvironment and vascular network.[185] Endothelial cells formed a vascular network while MSCs and osteoblast-differentiated cells developed the organ-mimicking gel. Tumour cells were then introduced into the vasculature and extravasated into the bone mimicking channel. In 2018, Lee *et al.* produced a microfluidic device that incorporated cancer, stromal, fibroblast and endothelial cells encased in a 3D collagen matrix.[52] Collagen type I coating was maintained at a pH of between 7.4 to 8.0 to represent the *in vivo* condition. A micropump provided a continuous supply of oxygen and nutrients to cells, mimicking the flow of blood in the capillary, and ensuring interaction between tumour and stromal sections of the device. NIH3T3 murine fibroblasts were used in the model as they were found to express CAF-specific markers when treated with TGFβ. mRNA analysis was performed and showed that fibroblast cells contribute to tumour formation and survival by upregulating the cancer cell gene expression of genes relating to metastasis and angiogenesis, as well as downregulating genes relating to apoptosis. TGFβ, known to be an angiogenic stimuli was found, to induce the cell migration and alignment of stromal cells. The group reported an increase in resistance of A549 lung cancer cells when in co-culture with fibroblasts to chemotherapy treatment for paclitaxel monotherapy and combination paclitaxel and gemcitabine therapy. It was also noted that fibroblasts caused the formation of vessel-like structures between adjacent tumoroids. Nashimoto *et al.* established a device that integrated a vascular network and tumour spheroid (**Figure 1.9**).[186]
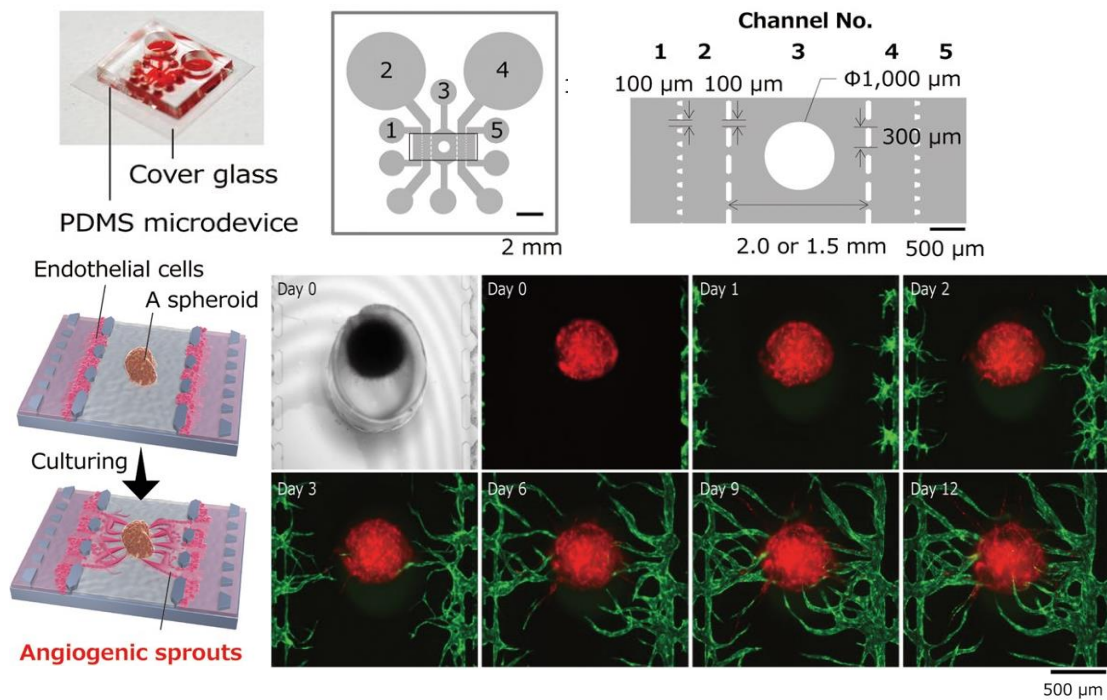
Figure 1.9 *Microfluidic device combining spheroid and vascular network formation. Spheroids were cultured in 96-well plates prior to insertion into devices containing five interconnected parallel channels. Angiogenic sprouts grew towards the spheroid from HUVEC seeded in adjacent channels. Adapted with permission from Nashimoto et al., 2017, Copyright 2017, Integrative Biology.*

While the Kim model depicted a one—dimensional vascular network, the five channel device structure was advanced for a 3D model. Spheroids were cultured in 96-well plates and collected and suspended in a collagen gel. These were then included in the central device channel prior to the addition of HUVEC into adjacent side channels. A perfusable vascular network was formed after 8-19 days of culture and was shown to be able to deliver biological material to the spheroid interior. The device could be used to form spheroids with or without a necrotic core, depending on the desired study, through establishment of the vascular network. High concentrations of VEGF were shown to diminish HUVEC migration and impact their role in anastomosing angiogenic sprouts. This is thought to be as a result of the high levels of VEGF decreasing the sensitivity of HUVEC to human lung fibroblasts, which encourage the growth of the vasculature towards the cancer spheroid. In 2018, Du *et al.* designed a multi-layered device to culture cancerous cells and normal vascular endothelial cells together.[187] By manipulating cancer cell density, their invasion could be studied using models with varying tumour growth rates. This model was also used to study the effect of co-culture on IL-6 expression, a cytokine known to control the morphology and migration of cells. Results demonstrated increased IL-6 expression for breast cancer and epithelial cells when co-cultured in comparison to monocultures. Co-culturing was also shown to result in greater cancer cell migration, potentially promoted by the greater levels of IL-6.

Having described the microfluidic technology developed so far for anti-cancer agent testing, models specific to immunotherapy investigations will now be discussed. A range of microfluidic immunoassays will be presented, as well as the suitability of the application of microfluidic technology towards *in vitro* immunoassay development.

1.11 Microfluidic Immunoassays

The precise control offered by microfluidic technology over intricate cell interactions, local environmental factors and acquisition of real-time information makes microfluidics an ideal platform for testing immunotherapeutic agents.[17, 188] Microfluidic platforms have been used to model both solid and liquid tumours. Specific to immune oncology, microfluidic technologies have been employed for the study of immune cell behaviour, communication and migration, but have not been extensively used for cancer immunotherapy efficacy studies. Microfluidic approaches for liquid tumours are available[189,190] with more limited work done regarding the use of the technology applied to immune-oncology for solid tumours.[11] However, recent investigation has focused on adoptive T cell therapy.[11] Microphysiological systems have been employed for the study of immune cell behaviour, communication and migration but have not been extensively used for investigation into cancer immunotherapy. Crosstalk between cancer and immune cells can elicit a powerful anti-cancer response, the dynamic interactions of which can be investigated using microfluidics.
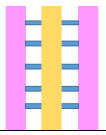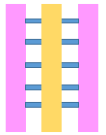
Compared to standard 2D and 3D cell culture techniques based on well-plate or trans-well platforms, microfluidic technologies hold specific advantages for *in vitro* immunotherapy testing, allowing precise control over cellular and biochemical features of the TME, including culture of multiple cell types in defined spatial and temporal configurations and real-time monitoring for time-lapse studies.[135] Microfluidic devices allow for the formation of more complex *in vitro* models that are simple to analyse with a variety of spectroscopy techniques.[95, 135] They offer a cost-effective platform in comparison to *in vivo* models and allow manipulation of specific experimental variables for mechanistic studies, as well as increasing the number of experiment repetitions possible from limited quantities of patient samples.[95, 135] Importantly, the use of cancer biopsy-derived tissue in miniaturised assays could allow for rapid screening of immunotherapeutics in a physiologically relevant manner that could give an indication of the best treatment option to apply to individuals. As patients can also develop resistance to immunotherapy through genetic predisposition or acquired mutations, it is of value to be able to assess *ex vivo* specific patient responses using human clinical samples rather than relying on immortalized cancer cells or animal models.[94] Additionally, microfluidics offers the potential for large-throughput screening of existing immunotherapies and facilitates
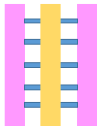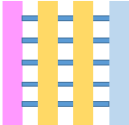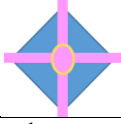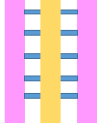
investigation of anti-tumour effects of novel agents as part of a combinatorial regime,[191, 134] and are suitable *in vitro* tools for investigating both solid and liquid malignancies in a range of experimental settings.[17] Despite the technology having been applied to develop liquid tumour immunoassays, its application towards solid tumours have been relatively limited.[188]
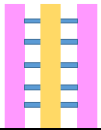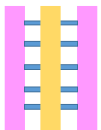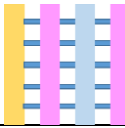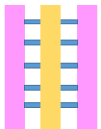
1.11.1 Cell interaction/migration Immunoassays

A large proportion of the solid tumour microfluidic immunoassays that have been conducted have focused on the study of cancer and immune cell interactions (**Table 1**).

Table 1: Summary of microfluidic devices involved in immune-oncology cell interaction/migration studies. Ab: Antibody, BCG: Bacillus Calmette–Guérin, CAR-T: Chimeric Antigen Receptor T cells, DC: Dendritic Cell, FPR1: Frizzled-related protein, EMT: Epithelial-Mesenchymal Transition, ICB: Immune Checkpoint Blockade, IT: Immunotherapy, NK: Natural Killer Cells, NP: Nanoparticle, PBMC: Peripheral Blood Mononuclear Cells, PDMS: Polydimethylsiloxane, TCR: T Cell Receptor. Adapted with permission from Paterson et al., Lab on a chip, 2021, https://creativecommons.org/licenses/by/3.0/.[11]

Author	Topic	IT type	Model	Chip material	2D /3D	Static/Perfusion	Chip Layout
Hsu *et al.*, 2012[192]	Interactions between human lung cancer cells, macrophages and myofibroblasts.	General cell interactions /migration	Cell lines	PDMS	2D	Pneumatic conduits and microvalves allowed control over conditioned medium available to each cell type	Three cell culture chambers connected by y-shaped channel designed so all angles were at 120° to allow for symmetrical distribution of conditioned media.
Businaro *et al.*, 2013[193]	Role of IRF-8 in communications between cancer and immune cells.	General cell interactions /migration	Mixed	PDMS	3D	Static - Manual pipetting	Three cell culture chambers connected by an array of microchannels to permit chemical and physical contact amongst the two cell types.
Agliari *et al.*, 2014[194]	Benefit of integrating microfluidics with mathematical models to fully quantify experimental image data of real-time interactions between cells.	General cell interactions /migration	Mixed	PDMS	3D	Static - Manual pipetting	Three cell culture chambers connected by an array of microchannels to permit chemical and physical contact amongst the two cell types.

Mattei *et al.*, 2014[195]	Role of IRF-8 in communications between cancer and immune cells.	General cell interactions /migration	Mixed	PDMS	3D	Static - Manual pipetting	Three cell culture chambers connected by an array of microchannels to permit chemical and physical contact amongst the two cell types.
Bai *et al.*, 2015[196]	Effect of different macrophage subtypes on tumour aggregate dispersion (mimicking EMT).	General cell interactions /migration	Mixed	PDMS	3D	Static - Manual pipetting	Four cell culture chambers connected by an array of microchannels to permit chemical and physical contact amongst multiple cell types and allowing hydrogel formation.
Zhao *et al.*, 2015[197]	Role of lactate on macrophage recruitment by and cytotoxicity against cancer cells (relevant to BCG vaccine immunotherapy).	General cell interactions /migration	Cell lines	PDMS	3D	Static - Manual pipetting	Four culture chambers with one media channel, each of which could house a different cell type. One matrigel channel and seven migration channels lay between each adjacent culture chamber with each chamber having its own media channel.
Liu *et al.*, 2015[198]	Sensitivity of cancer cells to six different chemotherapy regimes.	General cell interactions /migration	Cell lines	PDMS	3D	Microscale vacuum suction apparatus	Culture channels interconnected by microchannels to allow exchange of soluble biological factors and metabolites between cell types. Four cell culture areas connected to a central pool through microchannels which functioned to provide a pressure balance during matrigel perfusion.
Vacchelli *et al.*, 2015[199]	Effect of FPR1 expression on DC response to cancer cells after chemothera	General cell interactions /migration	Mixed	PDMS	3D	Static - Manual pipetting	Three cell culture chambers connected by an array of microchannels to permit chemical and

							physical contact amongst the two cell types.
	py treatment.						
Biselli *et al.*, 2017[200]	Interactions between human breast and colon cancer cells and human PBMC.	General cell interactions /migration	Mixed	PDMS	3D	Static - Manual pipetting	Three cell culture chambers connected by an array of microchannels to permit chemical and physical contact amongst the two cell types.
Lucarini *et al.*, 2017[201]	Effect of the drug decitabine (DAC) in enhancing anti-tumour effects of IFN through immune cell recruitment to the tumour site.	General cell interactions /migration	Mixed	PDMS	3D	Static - Manual pipetting	Three cell culture chambers connected by an array of microchannels to permit chemical and physical contact amongst the two cell types.
Chen *et al.*, 2018[202]	Role of inflamed neutrophils in promoting cancer cell metastasis under perfusion conditions.	General cell interactions /migration	Mixed	PDMS	3D	Perfusion of vascular network - Manual pipetting	Formation of 8 independent vascular beds with a single gel injection port connected by a branching network. Each sub-unit consisted of 4 parallel channels.
Boussommier-Calleja *et al.*, 2019[203]	Migration and development of various subsets of monocytes and monocyte-derived macrophages as targets for anti-metastatic immunotherapies and their effect on cancer cell extravasation.	General cell interactions /migration	Cell lines	PDMS	3D	Perfusion of vascular network - Manual pipetting	Three parallel channels where monocytes can be observed over a 5 day period migrating through an endothelial barrier to interact with fibroblasts in a central hydrogel channel.

Lei et al., 2020[204]	Interactions between cancer and immune cells involved in tumour escape from immune surveillance.	General cell interactions /migration	Mixed	Paper layer on top of PMMA layer	3D	Static - Manual pipetting	Paper layer containing 5 microreactors on top of a PMMA layer with hydrogel diffusion channels.

Layered microreactor device

Y-shaped interconnected cell culture chambers

Interconnected cell culture chambers with central pool

Parallel microchannels showing cell culture (yellow), hydrogel (blue) and media channels (pink)

Mattei *et al.* established a microfluidic system to investigate the function of IFN regulatory factor 8 (IRF-8) transcription factor on communications between murine melanoma cells and splenocytes that results in the secretion of soluble factors and immune cell recruitment.[195] The set-up consisted of interconnected microfluidic chambers that allowed chemical and physical contact between non-adherent splenocytes and adherent tumour cells. This system demonstrated the increasingly invasive behaviour of melanoma cells when in the presence of splenocytes from mice deficient of IRF-8, referred to as knock out (KO), in comparison to wild type (WT) splenocytes. Findings from microfluidic assays were shown to be in agreement with *in vivo* results and demonstrated the value of IRF-8 expression in tumour-immune cell communications. Businaro *et al.* previously used this device to demonstrate an upregulation of the CD69 leukocyte activation marker expression for WT splenocytes in comparison to IRF-8 KO (**Figure 1.10**).[193]
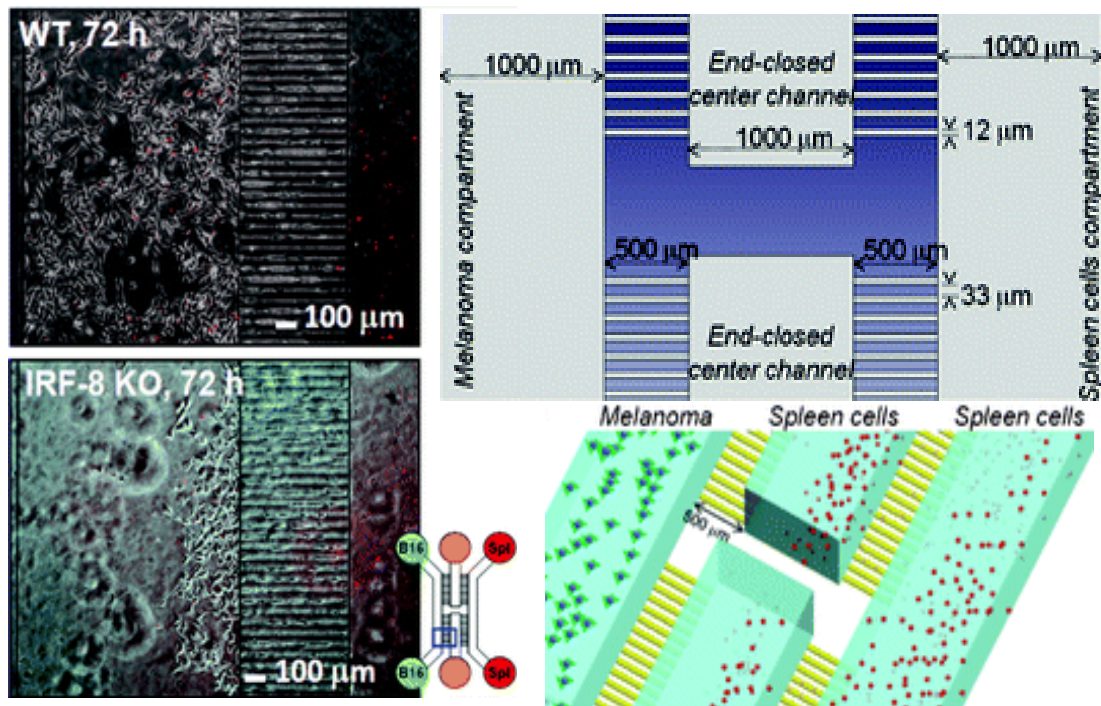
Figure 1.10 *Microfluidic device for the co-culture of tumour and immune cells. The chip is composed of two cell culture compartments for culture of cancer and immune cells connected by four sets of microchannels. Phase contrast images show the extent of cancer cell migration after 72h when IRF-8 KO splenocytes are cultured in the immune cell compartment but not with WT splenocytes. Adapted with permission from Businaro et al., 2013, Copyright 2013, Lab on a chip. (KO= knock out, WT= wild type).*

Agliari *et al.* then went on to develop mathematical models and analysed the dynamics of WT and IRF-8 splenocyte motion when in contact with murine melanoma cells.[194] This work revealed a distinct migration of WT immune cells in the direction of tumour cells to form immune cell clusters and demonstrated the value of combining microfluidic assays and mathematical modelling to obtain quantifiable data on real-time cell interactions. The system was also used by Biselli *et al.* in 2017 to investigate contact between human peripheral blood mononuclear cells (PBMC) with varying expression of the FPR1 gene and human colon and breast cancer cells.[200] MDA-MB-231 breast cancer cells were pre-treated with doxorubicin, triggering the release of chemo-attract signals. This resulted in immune cell migration from the neighbouring microfluidic compartment which could be tracked with time-lapse imaging. WT PBMCs were found to be recruited to cancer cells but not mutated FPR1 variants, representing clinical reports of patients with WT FPR1 expression having better prognoses. Similarly, the impact of FPR1 expression on DC migration towards chemotherapy pre-treated tumour cells has also been investigated.[199] The model was later adapted by Lucarini *et al.* in 2017 to culture PBMC in a central compartment surrounded by matrigel containing tumour cells.[201] The function of this configuration was to determine the beneficial effect of the drug decitabine in enhancing immune cell recruitment to the tumour site and, thus, the anti-tumour effects of IFN treatment. Untreated tumour cells could be cultured in one of the compartments

parallel to the central PBMC channel while decitabine and IFN treated cells could be cultured in the channel on the opposite side as a competitive assay to show the preferential migration of PBMC towards the treated cells. Enhanced PBMC infiltration towards cancer cells treated with both decitabine and IFN was recorded in contrast to administration of one agent only and untreated cells.

Bai *et al.* established a multi-channel device to depict epithelial-mesenchymal transition.[196] The influence of macrophage subtypes on the breakup of tumour aggregates was investigated. Depending on experimental conditions (contact or non-contact), macrophages were injected into the same channel hosting the tumour aggregates or into the adjacent hydrogel channel. The microfluidic device used allowed acquisition of real-time images and quantification of cell-cell distances. Chen *et al.* later developed a device with 8 interconnected vascular networks formed from one gel injection port.[202] This study focused on inflamed neutrophils as potential targets for immunotherapies and preventing their promotion of tumour cell metastasis. Neutrophils were stimulated with lipopolysaccharide to mimic inflammation and formed clusters with tumour cells under perfusion conditions. Greater extravasation of tumour cells proximal to neutrophils was observed and highlights neutrophil proximity as an indicator of cancer cell migration. Subsequently, Boussommier-Calleja established a device to investigate the use of monocytes and monocyte-derived macrophages as part of an anti-metastatic immunotherapy regime.[203] Monocytes have substantial potential to be used in immunotherapy due to their heterogeneity and plasticity which allows them to adapt to their environment and be prompted to support or suppress inflammation. Monocyte migration and their role in cancer cell extravasation was investigated. This was the first example of high resolution imaging in microfluidics of the evolution of monocytes as they move through human vasculature. Inflammatory monocytes were shown to be much more prone to extravasate than patrolling monocytes, matching *in vivo* findings. Notably, patrolling monocytes moved faster in devices than *in vivo*, potentially due to a lack of flow or adhesion molecules on HUVEC.

Microfluidic technology has also been applied to the study of interactions between human lung cancer cells, macrophages and myofibroblasts using a multi-layered microfluidic device made up of three interconnected cell culture compartments.[192] Inter-chamber connections were operated using three sets of pneumatic microvalves that allowed control over the conditioned medium available to each cell type. The three chambers were connected by a Y-shaped channel with all angles set to 120° to provide a homogeneous flow of conditioned media. TNF-α was shown to encourage tumour cell migration when administered directly to cancer cells but could

conversely restrict the ability of myofibroblasts to enhance cancer cell migration. This system allowed for the transfer of conditioned media without exposure to external air and at 37°C, which maximised the conservation of cytokine functional activity. Time-lapse recordings revealed that exposing cancer cells to a mix of conditioned media from macrophages and myofibroblasts promoted their migration. However, pre-treatment of myofibroblasts with macrophage conditioned media reduced their capability to increase cancer cell migration. Likely due to TNF-α secretion by macrophages, decreasing myofibroblast α- smooth muscle actin (SMA) expression and secretion of TGF-β.

Work by Zhao *et al.* in 2015, relevant to BCG vaccine immunotherapy, investigated the influence of lactate on macrophage recruitment and tumour cell cytotoxicity.[197] After lactate treatment, M1 macrophages showed reduced nitric oxide expression, an anti-tumour agent, and an increased expression of Arg-1, a marker for M2 macrophages. Results showed that lactate was able to reprogram M1 macrophages into M2 macrophages, to reduce cancer cell viability when in co-culture with macrophages and to increase macrophage recruitment. Furthermore, this process was demonstrated to be interrupted and halted by the lactate inhibitor, quercetin. A reduction in migration of cancer cells when in co-culture with M1 macrophages but not M2, suggested that M1 macrophages have an anti-metastatic action on tumour cells. This is in agreement with clinical reports of BCG-induced M1 polarization of tumour associated macrophages that impeded the development and spread of transitional cell carcinoma of the bladder. Traditional tube formation assays or transwell migration assays would not have been able to allow the quantification of the dynamics of macrophage migration and behaviour possible with microfluidics. The bladder cancer microenvironment was also modelled in a comparable device using perfusion instrumentation to supply a continuous flow of nutrients.[198] The device had a U-shaped configuration of interconnected ECM infused media and cell culture channels that allowed for the exchange of various metabolites and soluble factors between the four different cell types. The four cell culture areas were connected to a central pool in the middle of the device through microchannels which functioned to provide a pressure balance during perfusion. Tumour cells were exposed to six different chemotherapy regimens where, after 12h, macrophages could be observed migrating through microchannels in the gel towards cancer cells, mimicking *in vivo* macrophage recruitment to the tumour site.

The potential for the use of nanoparticles in immunotherapeutic cell communication was also investigated in work by Wimalachandra *et al.*[205]. Specifically, chemokine-loaded folic-acid conjugated nanoparticles were developed to target folic-acid receptor expressing tumour cells and to attract immune cells towards the target cells. The device was configured to allow
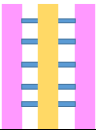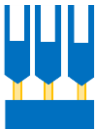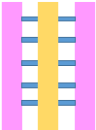
chemokine-loaded nanoparticles to elicit the migration of DC and T cells through an endothelial barrier towards cancer cells. Nanoparticles were added to one of the lateral channels for 24h, then DC or Jurkat, an immortalized T cell line, was injected into the same channel. Migration of the immune cells was then observed after 6 hours. After 24h, signal from folic-acid nanoparticles was detected at cancer cells at the interface of the endothelial and tumour compartments and within the central channel. This was in comparison to nanoparticles without folic-acid which would also have crossed the endothelial barrier but not been taken up by folic-acid receptor expressing cancer cells. A higher number of DC and T cells were observed after exposure to chemokine-loaded folic-acid nanoparticles but not folic-acid nanoparticles only.
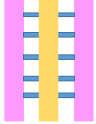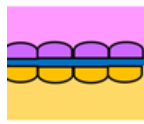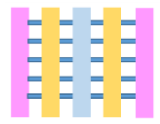
Non-traditional materials have also been used to fabricate microfluidic devices for immunotherapy studies. One device from Lei *et al.* was composed of a paper layer housing five microreactors above a PMMA layer with hydrogel diffusion channels.[206] The system was produced to obtain a better understanding of the cancer-immune cell communications associated with cancer cell escape from immune surveillance. A central circular microreactor was encompassed by four square microreactors containing various cell types. Different configurations of cells and agents were added to the various microreactors and the effects on cell proliferation measured using a colorimetric assay. Scanning electron microscopy was used to assess cell morphology and showed that cells do not attach to the paper substrate with cell proliferation quantified by a conventional water-soluble tetrazolium salt assay. The device enabled investigation into cross-talk between different cell types that would not have been as straightforward using conventional methods, such as well-plates or petri-dishes. Paper-based microfluidics offers a low-cost solution to performing neutralizing and competitive assays and can sustain nutrient and oxygen gradients mimicking organ-level functions. Reduced claudin, integrin and laminin expression and increased CXCL2, IL-8 and ANGPTL4 expression for paper culture in comparison to tissue culture polystyrene was observed and is consistent for cells cultured in a 3D environment. A cell proliferation assay showed that cells could proliferate in the device until the third day, when they reached a plateau. This was thought to be due to the hydrogel not being replaced, resulting in a lack of nutrients for the cells.

1.11.2 Immunoassays for Mechanistic Studies

Various microfluidic platforms have also been utilised for immunotherapy related mechanistic and mode of action studies (**Table 2**).

Author	Topic	IT type	Model	Chip material	2D/3D	Static/ Perfusion	Chip Layout
Zervant onakis et al., 2012[179]	Examining the mode of action by which macrophages influence tumour cells via TNF release.	Ab	Mixed	PDMS	3D	Static - Manual pipetting	Three cell culture chambers connected by an array of microchannels to permit chemical and physical contact amongst the two cell types.
Lu et al., 2015[207]	DC/tumour fusions to elicit anti-tumour immunity.	DC Vaccine	Cell lines	PDMS	3D	Perfusion - syringe pump, electrodes	960 pairs of trapping channels. Cell electrofusion device that can pair and fuse homogeneous and heterogeneous cells.
Jenkins et al., 2017[208]	Novel TBK1/IKKε inhibitor mechanisms.	ICB	Primary	PDMS	3D	Static - Manual pipetting	Three cell culture chambers connected by an array of microchannels to permit chemical and physical contact amongst the two cell types.
Kulasin ghe et al., 2017[209]	Non-invasive method to identify candidates for anti-PD-L1 therapy. Involved blood sample from a SCC patient to determine the PD-L1 expression of CTCs.	ICB	Mixed	PDMS	3D	Perfusion - Syringe pump	Spiral microfluidic channel.
Parlato et al., 2017[210]	Effect of biochemical stimuli on DC migration. IFNα-conditioned dendritic cells for use as a therapeutic vaccine in combinations	DC Vaccine	Cell lines	PDMS	3D	Static - Manual pipetting	Five cell culture chambers connected by an array of microchannels to permit chemical and physical contact amongst the two cell types.

	with romidepsin.					
Aref et al., 2018[211]	ICB in conjunction with small hydrophobic molecules.	ICB	Primary	COP Plastic device from AIM BIOTECH	3D - MDOTS viability affected by PD-1 blockade in 3D microfluidic culture but not in 2D culture using 384-well plates	Static - Manual pipetting	Three cell culture chambers connected by an array of microchannels to permit chemical and physical contact amongst the two cell types.
Huh et al., 2018[212]	Mimicking the drug toxicity-induced pulmonary oedema seen in cancer patients after IL-2 treatment.	Cytokines -IL-2	Cell lines	PDMS	2D	Perfusion - Syringe pump, vacuum pump	Two parallel microchannels separated by a thin and porous ECM coated membrane, permitting perfusion and cyclic stretching of the cell layers attached to a flexible membrane, mimicking physiological breathing motions.
Moore et al., 2018[213]	Study of the mechanisms by which anti-PD-1 antibodies augment the cytotoxicity of TILs.	ICB	Primary	COC Plastic EVIDENT device	3D	Perfusion-Pressure-pump driven system	Tumour fragment trapped in V-designed channels.
Nguyen et al., 2018[214]	Effects of Trastuzumab and CAF on cancer cell proliferation, cell death and motility. Effects of co-culture with CAF and immune cells in 3D.	Ab	Mixed	PDMS	3D - The drug decreased mitosis, tumour growth and apoptosis. In 2D experiments the drug did not inhibit the growth of	Perfusion - Syringe pump	Five cell culture chambers connected by an array of microchannels to permit chemical and physical contact amongst the two cell types.

					cancer cells.		
Yin *et al.*, 2018[215]	Antibodies for the identification of the stage of cancer progression and determination of the optimum course of treatment.	Ab	Mixed	PDMS and patterned nickel micropillar substrate	3D	Syringe pump and magnets used to immobilize antibodies onto micropillars of device	Chaotic mixer with a patterned nickel micropillar substrate.
Wimala chandra *et al.*, 2019[205]	Chemokine-loaded folic-acid conjugated NPs for targeting folic-acid receptor expressing cancer cells and attracting immune cells towards the target cells.	Chemokine-loaded NPs	Mixed	PDMS	3D	Static-Manual pipetting	Three cell culture chambers connected by an array of microchannels to permit chemical and physical contact amongst the two cell types.
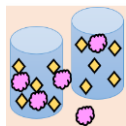
 Patterned micropillars

 Tumour-trapping V-channel

 Spiral microchannels

 Cell trapping channels
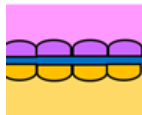
 Parallel microchannels with flexible membrane
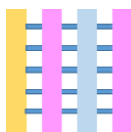
 Parallel microchannels showing cell culture (yellow), hydrogel (blue) and media channels (pink)

Alternative microfluidic-based immunotherapy work has included a microfluidic device for examining the function of macrophages in tumour cell intravasation.[216] A Y-junction was used to control an EGF concentration gradient in the device while the 3D matrix enabled paracrine and juxtacrine signalling to take place between tumour and endothelial cells. Cancer cell intravasation and endothelial permeability was increased for tumour cell-macrophage co-cultures and which could be lessened through exposure to anti-TNF antibodies. Jenkins *et al.*

utilised a device, initially designed to investigate angiogenic growth, to study the efficacy of a novel TBK1/IKKε inhibitor on murine- and patient-derived tumour spheroids.[217] Assessment of patient anti-tumour immune response to ICB therapy is currently limited to whole blood/plasma measurements and static biopsy evaluation. Whereas, this more physiologically relevant system could allow for the identification of biomarkers and agents to tackle resistance to treatment. MC38 murine derived organotypic tumour spheroids (MDOTS) showed significantly more cell death after anti-PD-1 treatment, which was greater with increasing dose and exposure time.

Plastic microfluidic devices have also been used for immunoassays. Plastic devices exhibit different material characteristics in comparison to PDMS, potentially being more suitable for testing of ICB in conjunction with small hydrophobic molecules, as these can be adsorbed by PDMS.[218] Aref *et al.* developed a device using cyclic olefin polymer to culture murine- and patient-derived organotypic small intestinal neuroendocrine tumour spheroids (**Figure 1.11**).[211]
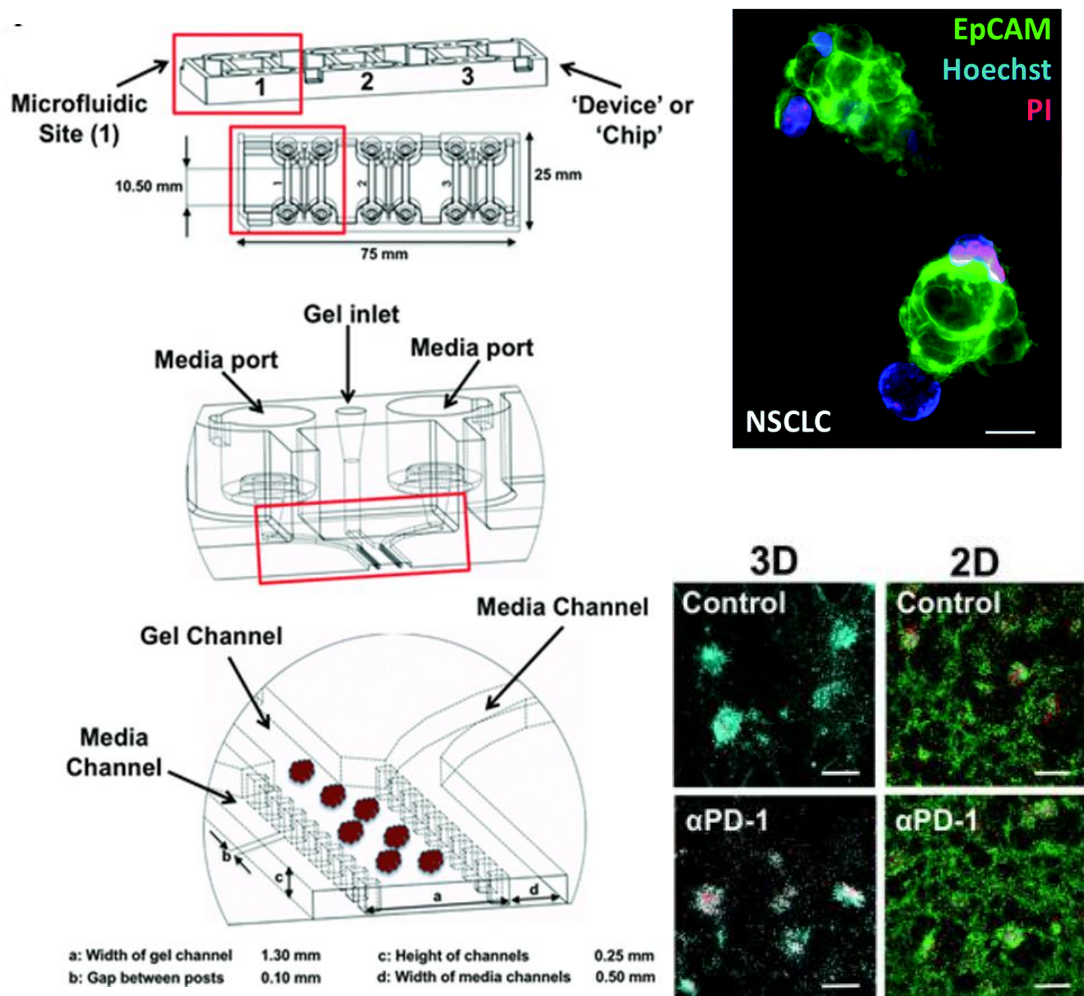
Figure 1.11 Microfluidic device (AIM Biotech) for culture of murine and patient derived tumour tissue as spheroids for identification of sensitivity to immune checkpoint blockade. This device was made from cyclic olefin polymer (COP) and was composed of a central gel channel with two adjacent media channels. Fluorescent images show live/dead staining of 3D spheroids cultured in microfluidic devices compared to 2D cultures in 384 well plates with and without PD-1 blockade. 3D cultures showed sensitivity to PD-1 blockade in comparison to controls. In contrast, 2D cultures showed no statistically significant differences between live and dead cell areas amongst control and treatment conditions. Adapted with permission from Aref et al, 2018, Copyright 2018, Lab on a chip.

The efficacy of ICB treatment using anti-PD-1 and anti-CTLA-4 was assessed as individual monotherapies and in combination. As seen with previous studies, results varied between 2D and 3D conditions. MDOTS viability was affected by PD-1 blockade in 3D microfluidic culture but not in 2D culture using 384-well plates. In comparison to control conditions and single therapy treatment, combination ICB therapy demonstrated enhanced immune-mediated killing of PDOTS and relative expansion of CD8 T cells and M0 macrophages. Limitations of this set-up include tumour, stromal, and immune changes throughout the culture period, challenges associated with using biopsy tissue in devices and the need for greater understanding on the effect of device dimensions, biophysical parameters, interstitial flow, hypoxia, and metabolic changes that occur as a result of culturing cells in microfluidic devices

on tumour–immune interactions, especially cytokine production. Patient tissue has also been utilized in microfluidic *ex vivo* ICB studies.[213] The device used provided a dynamic environment using a pressure-pump-driven system to culture up to 12 individual tumour biopsy fragments under a continuous flow of tumour-infiltrating lymphocytes (TIL). Greater cancer cell killing was observed in channels with anti-PD-1 treated TILs, despite reports of bubble formation and a build-up of cell debris resulting in fluid obstruction. This is a proof of concept system with the potential to be scaled up for more high-throughput applications.

Other microfluidic studies include those investigating the use of DC, such as that established by Parlato *et al.* who investigated IFNα-conditioned DC as a therapeutic vaccine in conjunction with the chemotherapy agent, romidepsin.[210] This system mimicked *in vitro* DC crossing of the endothelial barrier and allowed study of the effect of biochemical stimuli on DC migration by seeding treated/non-treated SW620 colon cancer cells in only one tumour channel. While DC moved toward both treated and untreated cancer cells, migration was faster, interaction time was longer and there was a greater number of DC present in the tumour chamber for treated cells. This proof of concept work showed the potential for tracking interactions between cancer and immune cells. Lu *et al.* developed a cell electrofusion device that functions to pair and fuse cells together using 960 pairs of trapping channels.[207] The system demonstrated 68% pairing and 64% fusion efficiency and is a significant development for the manufacture of DC-tumour vaccines that can be used to provoke anti-tumour immune responses. Once cells have been fused, they can be readily removed from the device, unlike alternative electrofusion equipment.[207] These systems can be cumbersome and not easily transportable, in addition to their uniform electric field resulting in multiple cell fusion. Microfluidic cell fusion can deliver enhanced cell viability, precise cell pairing, improved fusion efficiency and minimise the risk of sample contamination and effects from Joule heating.

Immunotherapeutic antibody investigations have also been carried out using microfluidic technology. Trastuzumab (Herceptin) is a monoclonal antibody against the HER2 receptor and was assessed in a device in various co-culture conditions.[214] A collagen hydrogel-based device architecture was developed, comprising 5 parallel compartments with a variety of cells from the TME and a central endothelial channel connected by microchannels. Proliferation, cell death and migration could be observed directly and quantified. Control over cell density, ratio of cell types, ECM components and vascular perfusion was possible, as well as the ability to study the effect of CAF and immune cells in 3D. Trastuzumab reduced tumour growth and increased apoptosis to varying degrees depending on the proportion of cells in culture. 2D

assays, however, reported no growth inhibition of tumour cells. Cancer cells had a slower doubling time when cultured in the device in comparison to 2D. This is thought to be due to their culture within the gel and is considered more reflective of their proliferation *in vivo*. The proportion of cell types present also reflected that *in vivo*: a median 2.3:1 ratio for immune to cancer cells and a median 1:5.8 ratio for CAF to cancer cells. However, a limitation of this device is the short PBMC viability with 50% death after 4 days of culture.

Microfluidic technology has also been applied to investigations into potential side effects of immunotherapy treatments. A device from Huh *et al.* was developed to simulate drug toxicity-induced pulmonary oedema that can be experienced by cancer patients after receiving IL-2 treatment.[212] The device was constructed from an optically transparent silicone elastomer and composed of two parallel microchannels separated by a thin and porous ECM coated membrane. The upper channel contained alveolar epithelial cells exposed to air flow and the lower channel hosted the endothelial cell compartment where culture medium and IL-2 were perfused. Side channels allowed a cyclic vacuum to be applied for cyclic stretching of the cell layers attached to the flexible membrane, mimicking physiological breathing motions. Two agents to combat IL-2 induced toxicity were tested, Angiopoietin-1 (Ang-1) and a novel transient receptor potential vanilloid 4 ion channel inhibitor (GSK2193874). This set-up provides a better representation of the *in vivo* condition in comparison to conventional stationery assays and allows complexity to be added to the system as is required, which would not be possible with animal models. Air volume was reduced over time by fluid leaking into the alveolar chamber and permeability of the alveolar-capillary barrier assessed using FITC-conjugated insulin. Quantification of intracellular gaps confirmed a significant loss of barrier integrity with IL-2 and strain, with Ang-1 and GSK negating the increased barrier permeability and gap formation caused by IL-2. Another device has also been produced by Kulasinghe *et al.* as a non-invasive means for identifying patients that could potentially benefit from anti-PD-L1 treatment.[209] A spiral microfluidic device was perfused with a syringe pump to allow flow of patient squamous cell carcinoma (SCC) blood samples. Five head and neck cancer cell lines were tested to ascertain a series of PD-L1 expression. The device was connected to a phase contrast microscope and staining carried out to detect CTCs and their PD-L1 expression. It is important to determine the PD-L1 expression of CTC as primary tumour PD-L1 expression differs from that at metastatic tumour sites and, therefore, it is not possible to predict patients who could potentially benefit from PD-L1 therapy by examining primary tumour biopsies alone. A dual-antibody-functionalised microfluidic device was developed by Yin *et al.* using anti-epithelial cell adhesion molecule (EpCAM) and anti-prostate specific membrane antigen (PSMA) antibodies.[215] The device was made up of a PDMS chaotic mixer
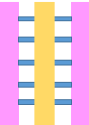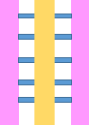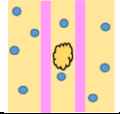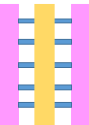
with a patterned nickel micropillar substrate. A syringe pump and magnets were used to immobilize antibodies onto micropillars of the device. Cell suspensions were then injected into the device where cells captured on the micropillars could be fixed and stained for analysis. Different subsets of CTC can express EpCAM or PSMA. Therefore, a combination of anti-EpCAM and anti-PSMA Ab would enhance the capture of CTC with different expressions for analysis. This is in contrast to conventional CTC capture methods that only capture epithelial or mesenchymal CTC. These antibodies are required to identify cancer stage of progression and the optimal therapy regime. CTCs positive and negative for EpCAM can be captured in the device and would be sufficient to detect CTC for the majority of patients tested. Higher numbers of CTC were detected in the dual-antibody device in comparison to when only EpCAM antibodies were used. Furthermore, captured CTCs can be recovered from the device for analysis and could be used for personalized therapy.
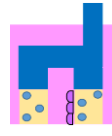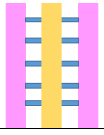
1.12 Microfluidic models for ACT Therapy
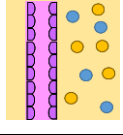
More recently, microfluidic technology has been employed for immunoassays but their use is still limited in relation to CAR-T studies (**Table 3**).

Table 3: Summary of microfluidic devices applied to immune cell mediated cytotoxicity studies. Ab: Antibody, ADCC: antibody-dependent cellular cytotoxicity, BCG: Bacillus Calmette–Guérin, CACI-IMPACT: Cytotoxicity Assay for Cancer Immunotherapy, CAR-T: Chimeric Antigen Receptor T cells, CTL: Cytotoxic T Lymphocytes, DC: Dendritic Cell, FPR1: Frizzled-related protein, EMT: Epithelial-Mesenchymal Transition, HBV: hepatitis B virus, HUVEC: Human Umbilical Vein Endothelial Cells, ICB: Immune Checkpoint Blockade, IDES: Interdigitated electrode structures, ITO: Indium Tin Oxide, IT: Immunotherapy, OET: Optoelectronic Tweezers, OPD: organic photodiode, NK: Natural Killer Cells, NP: Nanoparticle, PBMC: Peripheral Blood Mononuclear Cells, PC: Polycarbonate, PEG-DA: Poly(ethylene glycol) diacrylate, PDMS: Polydimethylsiloxane, TCR: T Cell Receptor, TiOPC: titanium oxide phthalocyanine, ZA: Zoledronic Acid. Adapted with permission from Paterson et al., Lab on a chip, 2021, https://creativecommons.org/licenses/by/3.0/.[11]

Author	Topic	IT type	Model	Chip material	2D/3D	Static/ Perfusion	Chip Layout
Charwat *et al.*, 2013[219]	Simultaneous study of tumour cell invasion and escape of immune surveillance. Effect of a nonlethal cytotoxic agent (urine) on adherent cells in relation to the use of urine analysis for non-invasive biomarker detection in diagnoses.	T cells	Mixed	PDMS	3D	Perfusion - syringe pump, impedance sensors, notch filter, light scattering sensors, external valves, injection ports	IDES and integrated fully spray-coated organic photodiode OPD arrays for electrical and optical light scattering measurements under perfusion conditions. PDMS layer sandwiched between electronics and upper interface.

Reference	Aim	Cells	Type	Material	Dimension	Flow	Device description
Layer *et al.*, 2017[220]	T cell chemotaxis studied via tracking migration and speed of T cells through a chemokine gradient.	T cells	Mixed	μ–Slide III 3in1 Ibidi plastic	3D	Perfusion - syringe pump	Three cell culture chambers connected by an array of microchannels to permit chemical and physical contact amongst the two cell types.
Pavesi *et al.*, 2017[221]	Evaluation of T cell function against single tumour cells and aggregates.	TCR-engineered T cells	Mixed	PDMS	3D - Compared 3D microfluidic with 2D results. 2D assays significantly overestimated T cell killing abilities and could not determine an effect of hypoxia on T cell killing.	Static - Manual pipetting	Three cell culture chambers connected by an array of microchannels to permit chemical and physical contact amongst the two cell types.
Ayuso *et al.*, 2018[222]	NK cell cytotoxicity and ADCC.	NK and Abs (anti-EpCam)	Cell lines	PDMS	3D	Static - Manual pipetting	Multi-compartments containing spheroids in ECM with an endothelial lined channel on either side to represent vasculature. NK cells either embedded in the gel or perfused through the endothelial channels.
Ke *et al.*, 2018[223]	NK cell activity and their interaction with cancer cells.	NK	Cell lines	TiOPC coated ITO glass with PEG-DA microwells	2D - TiOPc-based OET	Perfusion - syringe pump	OET cell manipulation into PEG-DA hydrogel within four-leaf-clover-shaped microwells. The electric-field distribution in the device is controlled by a dynamic light pattern, which created the OET non-contact force to guide cell movement.
Lee *et al.*, 2018[224]	To determine monocytes inhibition of the function of HBV TCR T cells and their dependence on the method of cell engineering to produce the T cells.	TCR-engineered T cells	Mixed	PDMS	3D - In comparison, the 2D equivalent culture showed no effect of the monocytes on either cell type.	Static - Manual pipetting	Three cell culture chambers connected by an array of microchannels to permit chemical and physical contact amongst the two cell types.

Ando et al., 2019[225]	Effect of oxygen availability on the cytotoxicity of CAR T cells.	CAR T	Cell lines	PDMS	3D	Static - Manual pipetting	PDMS plasma-bonded to a glass slide with a milled PC cap.
Di Mascolo et al., 2019[226]	T cells exposed to ZA containing nanoparticles (ZA-SPNs) to determine their promotion of T cell extravasation and migration towards cancer cells through a vascular structure.	T cells	Mixed	PDMS	3D	Perfusion - syringe pump	Two cell culture chambers connected by an array of microchannels to permit chemical and physical contact amongst the two cell types .
Park et al., 2019[227]	Cytotoxic capabilities of lymphocytes.	NK	Cell lines	Polystyrene, mass produced from injection moulding.	3D - 3D experiments showed significantly less NK cell cytotoxicity compared to 2D.	Perfusion of vascular network - Manual pipetting	Rail-based microstructures with hydrophilic surfaces for gel patterning.
Wu et al., 2019[228]	Droplets solidified in CaCl2 solution to form porous microspheres that could be used as a vehicle to house NK-92MI cells for immunotherapeutic applications.	NK	Cell lines	Microfluidic electrospray forming PEO/ALG droplets	3D - Precursor solution of alginate solution and PEO injected through an electrospray microfluidic device under an electric field to form droplets.	Microfluidic electrospray	Microfluidic electrospray.
Chen et al., 2020[229]	Migration characteristics and anti-cancer response of CTLs.	T cells	Cell lines	PDMS	3D	Perfusion - Syringe pump	Three cell culture chambers connected by an array of microchannels to permit chemical and physical contact amongst the two cell types.

| Ayuso et al. 2021[230] | NK cell cytotoxicity and ADCC. | NK, small molecule inhibitors and antiPD-L1 Ab | Mixed | PDMS | 3D | Static - Manual pipetting | Collagen hydrogel containing tumour cells injected. Endothelial lined channel representing vasculature for NK cells, antibodies and inhibitors to be perfused through. |

 PDMS-IDES sandwich
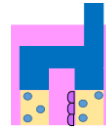
 Rail-based microstructure

 Microfluidic electrospray

 PDMS-Glass sandwich

 Four-leaf-clover design
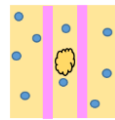
 Endothelial channel in tumour cell hydrogel

 Parallel microchannels showing cell culture (yellow), hydrogel (blue) and media channels (pink)
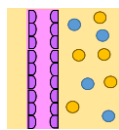
 Parallel microchannels with spheroid culture

T cell based immunotherapy is an up-and-coming treatment approach to cancer, specifically haematological forms. This therapy involves the isolation of a patient's T cells which are engineered to express a receptor specific to the proteins expressed on the surface of their cancer cells. These specific receptors are known as CARs which allow T cells to bind specifically to tumour cells, killing them.[72] Microfluidic devices can be used to determine the efficacy of these manipulated T cells on a patient specific basis prior to administration and also to study their effect on the tumour in the context of other immune cell types, such as macrophages and natural killer cells.

Microfluidic technology has also been applied to studies investigating the effects of hypoxia and cytokines on the effectiveness of ACT therapy. One device was designed to assess the killing ability of engineered primary human T cells against single HepG2-Env human hepatoma cancer cells and aggregates in a 3D matrix.[221] In this study, the impact of diminished oxygen levels in a hypoxic environment and the influence of inflammatory cytokines on T cell

function was investigated with optimal killing of cancer cells in high O_2 conditions with the presence of IFN-γ and TNF-α. This device provided a means to replicate an *in vivo* hypoxic and inflammatory tumour environment that would not have been possible with traditional cell culture methods. Comparison of 3D and 2D monolayer results showed a significant overestimation of T cell cytotoxicity for 2D assays. 2D cultures were also not capable of detecting the impact of hypoxia on T cell function, further demonstrating the usefulness of 3D models in pre-clinical assays. Decreased killing of tumour cells at 2% O_2 was reported in comparison to 20% O_2. Increased killing was recorded when inflammatory cytokines were present, specifically with high O_2 conditions. These findings are relevant for anti-cancer studies where the native TME is hypoxic and hosts a variety of inflammatory molecules. The Pavesi device was adapted by Lee *et al.* in 2018 with the addition of human primary monocytes to imitate the hepatitis B virus (HBV)-related hepatocellular carcinoma TME.[224] This assay was used to investigate monocyte inhibition of HBV T cell receptor-redirected T cells (TCR T cells). Inhibition can, as occurs with natural T cells via checkpoint inhibition. Also studied was the incident of inhibition in relation to the cell engineering method. T cell cytotoxic killing of cancer cells was found to be impaired by monocytes for retrovirally transduced TCR T cells but not mRNA electroporated TCR T cells. Blocking PD-L1/PD-1 was found to restore the killing abilities of Tdx TCR T cells.

ACT therapy has been by far the most investigated immunotherapy type using microfluidics. In 2013, a novel approach for continuous and non-invasive monitoring of behaviour among tumour, adherent stromal cells and non-adherent immune cells was reported.[219] Electrical and optical light scattering measurements were obtained using interdigitated electrode structures and integrated fully spray-coated organic photodiode arrays under perfusion conditions. Cell surface interactions were recorded by cellular impedance sensing and the number and morphology of cells quantified using light scatter data. This was possible as rounded cells give higher scatter values, in contrast to elongated cells. This device allowed cancer cell invasion and immune escape to be investigated simultaneously. In metastatic invasion assays, light scatter measurements showed that DU-145 prostate cancer cells did not cross a HUVEC monolayer, in contrast to prior reports. A T cell cytotoxicity assay using OCM-1 ocular melanoma cells found that activated primary T cells caused a significant impedance reduction, as tumour cells were removed from the sensor surface, in comparison to when non-active T cells and culture media were introduced. Also in this work, researchers investigated the effect of a nonlethal cytotoxic agent (urine) on adherent cells in relation to the use of urine analysis for non-invasive biomarker detection in diagnoses. In other work, a device was established with a controlled chemokine gradient and used to track the movement and velocity of T

cells.[220] This work found that T cell infiltration could be improved through inhibition of the MYCN proto-oncogene. Although not demonstrated in this paper, a future application of this approach could be in identifying patients suitable for checkpoint blockade immunotherapy treatment. As this form of therapy is more suitable for patients with good TME immune cell infiltration, suitable patients without MYCN amplification and, thus, greater immune cell presence in the TME could be identified using the microfluidics for ICB. Whilst patients with poor TME immune cell penetration, such as those with MYCN-amplified neuroblastomas, could receive alternative treatment. Aminobisphosphonates, such as zoledronic acid (ZA), have also been investigated as promoters of anti-tumour Vδ2 T cell proliferation.[226] Nanoparticles smaller than 200nm are suitable vehicles to take advantage of the enhanced permeability and retention effect to provide enhanced deposition of the drug in the tumour tissue in comparison to free drugs. Such nanoparticles would also conserve the pharmacological properties and improve the circulation half-life of the agent. The dynamics of T cell movement through a vascular network and endothelial monolayer to reach cancer cells contained within hydrogel could be observed. T cells were exposed to ZA containing nanoparticles to determine their promotion of T cell extravasation and migration towards cancer cells through a vascular structure. A model by Chen *et al.* in 2020 had also studied migration times and cell numbers using murine hepatic cancer cells and cytotoxic T lymphocytes (CTLs).[229] This set-up involved the use of a syringe pump for media perfusion and hydrostatic pressure with the device made up of parallel interconnected tumour and T cell channels. However, limitations of this method included the manual quantification, limited throughput and insufficient mimicking of the *in vivo* fibrotic tissue due to the collagen gel being too soft. In comparison to alternative CAR-T 3D *in vitro* assays and CAR-T assays performed in well-plates, microfluidic technology can be effective in miniaturising screening for CAR-T therapeutic strategies whilst decreasing cost and time expenditure for optimising CAR-T and other immune cell therapies. In 2019, Ando *et al.* compared CAR-T cell behaviour on normoxic and hypoxic conditions using a device with an oxygen gradient (**Figure 1.12**).[225]
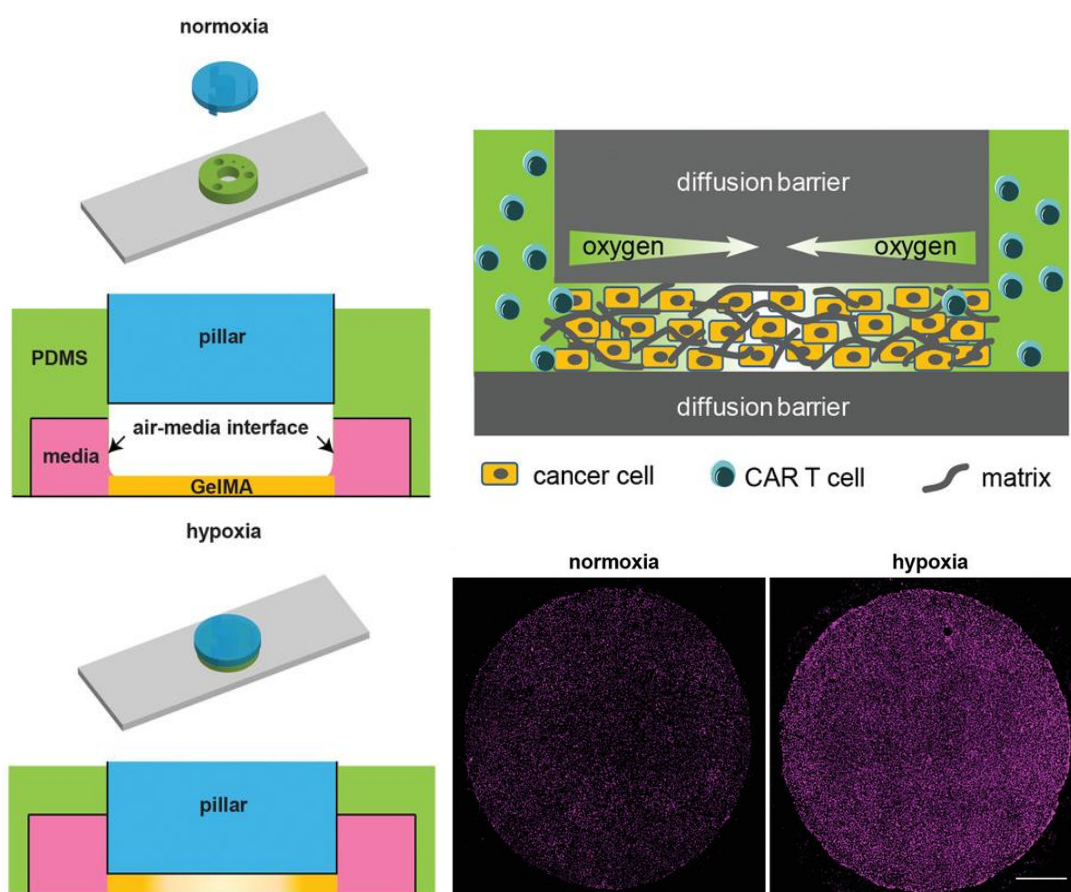
Figure 1.12 Microfluidic device for evaluating CAR-T cell function in varying conditions of oxygen availability. The PDMS device is bonded to a glass slide with a milled polycarbonate cap and gel layer containing SKOV3 human epithelial ovarian cancer cells. Fluorescence images showed upregulation of PD-L1 expression in hypoxic conditions in the device in comparison to normoxic conditions. Adapted with permission from Ando et al., 2019, Copyright 2019, Advanced Healthcare Materials.

The device consisted of a PDMS layer plasma-bonded to a glass slide with a milled polycarbonate cap. This design offered the advantage of being able to be adapted for studying the effect of different oxygen conditions on the cytotoxicity of CAR T cells. The device allowed the generation and control over the oxygen gradient and demonstrated that the highest cytotoxicity occurs in normoxic conditions with greater E:T ratios (10:1 and 20:1) with negligible infiltration of CAR-T cells within the tumour body after 24h. PD-L1 surface expression of T cells increased after 24h in hypoxia. Whilst after 72h, there was extensive CAR-T cell-induced cytotoxicity at the periphery of hypoxic samples and uniform cytotoxicity across normoxic samples. Total cell death in normoxic and hypoxic conditions was found to be comparable after 72h. Other microfluidic T cell models include that from Lee *et al.* in 2021, who established a multi-layered blood vessel-tumour tissue chip and used time-lapse imaging to observe T cell migration.[231] NK cells are another form of ACT therapy that have been studied in recent years with microfluidics. In 2018, Ayuso *et al.* looked at NK cell cytotoxicity

and antibody-dependent cellular cytotoxicity using a microfluidic chip.[232] Vesicles containing antibodies were detected in some spheroids, meaning that the antibodies could have been endocytosed by the spheroids as a way of escaping immunosurveillance. NK cells could detect cancer cell spheroids from hundreds of microns in the distance to which they could migrate towards, penetrate and exert a cytotoxic effect on peripheral and interior cancer cells. Other studies on tumour and immune cell interactions include a device produced using titanium oxide phthalocyanine based optoelectronic tweezers (OET).[223] This device is able to regulate cell-cell contacts by directing cells into four-leaf-clover-shaped microwells, enabling direct cell contact. The design of the microwells meant that there existed a slower flow velocity in the centre region which created a setting for the OET force to direct cell interactions. The electric-field distribution in the device was controlled by a dynamic light pattern which generated the OET non-contact force to guide cell movement. Shrinking and blebbing could be observed, indicating apoptosis of cancer cells upon contact with NK cells. Significantly, greater NK killing of target cells was recorded in the device compared to conventional analysis, flow cytometry in a 96 well-plate and eppendorf tube. This suggests that traditional methods can cause cells to interact randomly with each other without the direct cell-to-cell contact as seen with this system. However, a potential limitation of this system for higher throughput applications is that it requires the use of several equipment components, including a charge-coupled device, projector, function generator, syringe pump, optical lens and microscope. A more straightforward setup was developed by Park *et al.* in 2019 who proposed a 3D cytotoxicity assay to determine the cytotoxic capabilities of lymphocytes.[227] Devices were mass produced from injection moulding of polystyrene to form plastic culture arrays and rail-based microstructures with hydrophilic surfaces used to pattern collagen gel embedded with tumour cells. The multi-well format allowed multiple assays to be conducted in one device simultaneously. 3D experiments showed significantly less NK cell cytotoxicity compared to 2D experiments, likely due to the dense 3D matrix present restricting migration. In agreeance with previous reports, significantly greater tumour cell killing was also seen with the higher effector: target ratios, specifically 20:1 compared to 5:1. Another means by which microfluidics has been used in NK studies was by Wu *et al.* who established a system to fabricate microspheres for shielding NK cells from the inhospitable tumour environment and avoid attack by the host's immune system.[228] A precursor solution was administered through an electrospray microfluidic device under an electric field. Droplets were produced and used to form porous microspheres that could be used as a vehicle to house NK cells for immunotherapeutic applications. The morphology of the porous microspheres could be tuned as desired. Microspheres can be produced on a large scale and were shown to maintain 85%

cell viability after 72h, with cells continuing to be viable for up to 2 weeks. NK cells secreted cytotoxic factors, perforin, granzyme and IFN-ɣ over 7 days with encapsulated NK cells demonstrating increased *in vivo* killing when compared to free NK cells. No adverse events were recorded after microspheres were administered *in vivo.*

In conclusion, microfluidic devices are powerful tools suited for cancer immunotherapy applications and offer alternative methods of studying the mechanisms of action and efficacy of novel immunotherapeutic agents. Whilst microfluidic technology has been limited to proof-of-concept solid tumour immunotherapy studies so far, this work has demonstrated the great potential of the technology to aid in the approval of novel anti-cancer agents in future. Furthermore, microfluidic assays that incorporate the various immune cells could provide enhanced representation of the solid TME and greater understanding of the anti-cancer treatment efficacy in the context of cancer associated cell types.

1.13 Summary of Literature

In summary, the literature review discussed in this chapter highlighted the following principal points:

- The TME is a critical feature of tumour development and resistance to therapy.
- Current preclinical assays are too simplistic in their depiction of solid tumours. They commonly lack TME representation and do not account for the plethora of cell types present in *in vivo* human tumours.
- There is a drive for the development of more physiologically relevant and personalised preclinical platforms that could be used for assessing patient tissue to increase accuracy of the predictions of treatment outcomes for patients.
- Immunotherapy is a promising field of treatment that has yet to be broadly applied to solid tumours and requires more physiologically relevant methods of *in vitro* evaluation.

Therefore, having identified features of the TME to incorporate into and enhance current *in vitro* models and recognised the potential of microfluidics, this thesis describes the development of novel protocols to achieve the following:

- Formation of a viable solid tumour-stromal microenvironment using a primary breast cancer cell line and characterisation of co-culture models through time-lapse imaging, fluorescence and protein expression analysis.

- Development of adaptable protocols for the analysis of a wide range of immunotherapeutic compounds with the potential for incorporation of multiple cancer and TME associated cell types.

- Establishment of a miniaturized proof-of-concept system using small cell numbers and volumes, beneficial for patient biopsy tissue and when assessing the efficacy of expensive immunotherapeutic compounds to achieve the maximum experimental data possible.

- Development of novel ACT methodology to assess cytotoxicity and specificity in a 3D solid tumour-stromal microfluidic environment incorporating normal and cancerous cells to identify potential off-target toxicity.

Chapter 2: Materials and Methods

2.1 Device Fabrication

All of the multi-layered microfluidic devices used in this work were fabricated using the same standard soft lithography techniques and used to culture spheroids, in accordance with established protocols.[26] In brief, a 10:1 ratio of PDMS prepolymer (Sylgard 184, Dow Corning) and curing agent were mixed and dispensed onto patterned silicon wafers. Wafers were degassed and incubated at 85°C for a minimum of 3 hours to allow curing of the PDMS solution. Wafers were then removed from the oven and allowed to cool for 30 minutes. PDMS layers were subsequently cut from the wafers and wells cut using a 4mm surgical biopsy punch (Miltex). PDMS layers were cleaned and exposed to oxygen plasma treatment (Pico plasma cleaner, Diener electronic) to permanently bond layers together, forming a microfluidic device. Devices were then stored overnight at 85°C to strengthen bonding and kept dry until ready for experiments at ambient temperature.

2.2 Preparation of Spheroid Devices

Devices were exposed a second time to oxygen plasma at 100% for 2 minutes before injecting a 1% Synperonic F108 (Sigma-Aldrich) solution, creating ultra-low adhesion conditions. After storage of devices for a 24-hour period in an incubator at 37°C and 5% CO_2, they were then washed using phosphate buffered saline (PBS, Fisher Scientific) and Roswell Park Memorial Institute 1640 culture medium (RPMI, ThermoFisher). Cell culture media was then added to channels to maintain moisture and devices kept in an incubator prior to cell seeding. All microfluidic devices are single-use and are disposed of upon completion of experiments.

2.3 Preparation of Hydrogel Solutions for Injection into Vascular Network Devices

All devices and gel aliquots containing pH 9 collagen I (2.3mg/ml, ThermoFisher), fibrinogen type I from bovine plasma (5mg/ml, ThermoFisher) and aprotinin bovine recombinant (0.045mg/ml, ThermoFisher) were prepared and stored at 4ºC prior to gel injection. Immediately before gel administration into devices, thrombin from bovine plasma (0.5U/ml, ThermoFisher) was added and gently pipetted up and down with the gel solution. It is necessary to do this individually for each device to avoid premature solidification of thrombin.

2.4 Preparation of Vascular Network Devices for Cell Seeding

Devices were composed of a PDMS layer bonded to a glass slide (1.2mm thick, Fisher Scientific) and were made up of three interconnected parallel channels. Devices were exposed to oxygen plasma for sterilisation (100% for 2 minutes) and stored at 85°C overnight to

strengthen bonding. Vascular network devices were then kept dry at an ambient temperature until use in experiments. 35μl of the hydrogel solution was pipetted into one well of the central channel. Using a 5ml sterile disposable syringe (ThermoFisher), sufficient pressure was applied to this well to push the hydrogel through the central channel but not to the extent to cause entry into the side channels. 40μl of the hydrogel was then added to the opposite well in the central channel and 5μl of PBS pipetted on top of the gel solution in the wells. Devices were then incubated for 60 minutes for gelation to occur and a phase microscope used to check for the presence of fibrils. 35μl of media was then added to one well of a side channel and the syringe again used to create negative pressure in the opposing well of the same side channel until media flow was established. Both wells were then topped up with media and the process repeated for the other side channel.

2.5 Cell Culture

All cells were incubated at 37 °C and 5% CO_2 in a humidified incubator. MCF-7 cells were obtained from American Type Culture Collection (ATCC, Queens Road, Teddington, Middlesex, TW11 0LY, UK) and cultured in Rosewell Park Memorial Institute medium (RPMI 1640 Medium, ThermoFisher) supplemented with 1% penicillin/streptomycin (10000 units/ mL, ThermoFisher) and 10% heat-inactivated FBS (ThermoFisher). MDA-MB-468 and SKBR-3 cell lines were obtained from E. Piletska (Department of Chemistry, University of Leicester, LE1 7RH, UK) and cultured in DMEM (ThermoFisher) with 1% penicillin/streptomycin (10000 units/ mL, ThermoFisher) and 10% heat-inactivated FBS (ThermoFisher). The Cellaria Wood Primary Breast Cancer cell line were purchased from AMS Biotechnology (Europe) Limited (184 Park Drive, Milton Park, Abingdon OX14 4SE, UK.) and cultured in Renaissance Essential Tumor Medium (RETM, Cellariabio) supplemented with RETM Supplement (15 mL, thawed briefly in a 37°C water bath), 25 ng/mL cholera toxin (Sigma), 5% FBS and 1% penicillin/streptomycin (10000 units/ mL). CAF were isolated by S. Zanivan (Institute of Cancer Sciences, University of Glasgow, Glasgow, UK, Cancer Research UK Beatson Institute, Glasgow, UK) and cultured in DMEM (ThermoFisher) supplemented with 1% penicillin/streptomycin (10000 units/ mL) and 10% heat-inactivated FBS. Normal human lung fibroblasts (NHLF) were purchased from Lonza and cultured in ready to use PrimaPure™ Fibroblast Growth Medium (AMS Biotechnology (Europe) Limited). HUVEC (ATCC) were cultured in either EGM-2 Endothelial Cell Growth Medium-2 BulletKit (Lonza) or F-12K Medium (ThermoFisher) supplemented with Endothelium Progenitor Outgrowth Cell (EPOC) supplement, 1% penicillin/streptomycin (10000 units/ mL) and 10% heat-inactivated FBS. EGFR-TM28-GITR-CD3z CAR-T cells and CAR-T cell media containing FBS were both obtained from AMS Biotechnology (Europe)

Limited. Upon thawing, CAR-T cells were centrifuged and their supernatant discarded. They were resuspended in pre-warmed media and incubated overnight for a minimum duration of 8 hours prior to use in assays. KP and KB1P murine breast cancer cell lines were obtained from S. Coffelt (Institute of Cancer Sciences, University of Glasgow, Glasgow, UK, Cancer Research UK Beatson Institute, Glasgow, UK) and cultured in DMEM (ThermoFisher) supplemented with 1% penicillin/streptomycin (10000 units/ mL), L-glutamine (2mM, ThermoFisher) and 10% heat-inactivated FBS. Primary murine gamma-delta T cells were isolated by Robert Wiesheu (Cancer Research UK Beatson Institute, Glasgow, UK).

2.6 Cell Seeding and Culture in Vascular Network Devices

A HUVEC solution of 10×10^6 cells/ml was prepared. Inside a sterile glass petri dish, inverted weigh boats were used to hold devices in a tilted position to allow for injection of 10μl of cell suspension into one of the side channel wells (**Figure 2.1**.). Tilted devices were then incubated for 45 minutes at 37°C. After incubation, weigh boats were removed and 30μl of media added to each of the 4 side channel wells. Media was refreshed every 48 hours, with media added to the side channel opposite to that which had been seeded with endothelial cells containing 50ng/ml VEGF (ThermoFisher) to encourage cell growth.
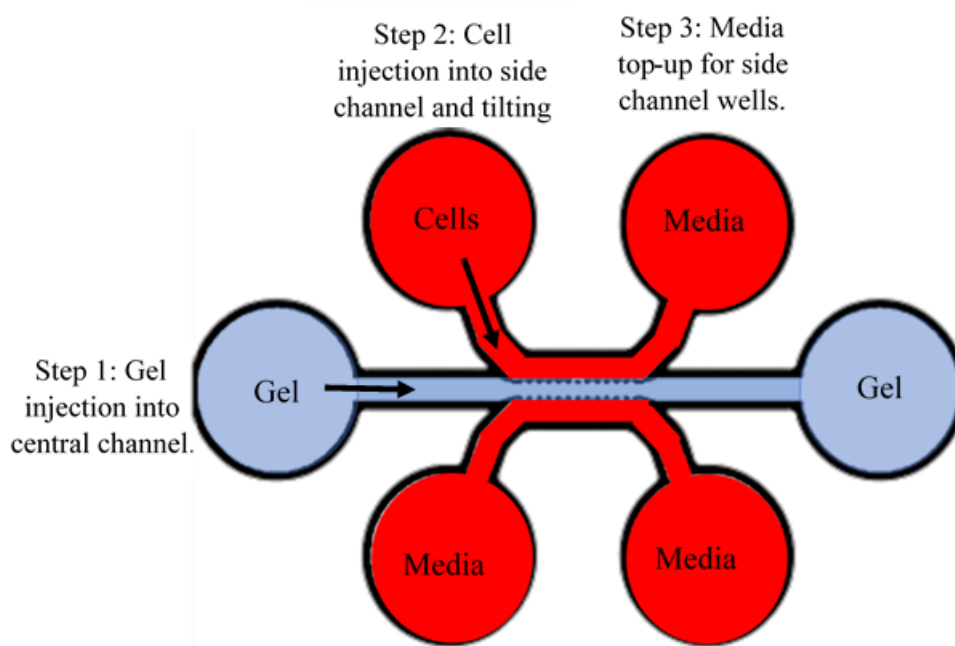
Figure 2.1 *Schematic diagram of vascular network device showing gel injection (blue) and cell seeding (red).*

2.7 Cell Seeding and Culture in Spheroid Devices

Multi-layered PDMS devices contained an array of microwells in each channel connecting two open wells. Two variations of spheroid-forming devices were used in experiments that consisted of either 7 channel devices[15], with 8x8 arrays of square traps of dimension

150×150×150μm^3, or 24 channel *OC^{3D} Single* microfluidic devices (ScreenIn3D Ltd, UK) channel devices, with 5x5 arrays of square traps of dimension 250×250×200μm^3. For 7 channel devices, cells were seeded into devices at a concentration of 5×10^6 cells/mL to form spheroids, with each microfluidic channel containing at least 32 spheroids of similar dimension (~80 μm diameter) for analysis. The cell suspension was injected into alternating open wells on each channel side to create a hydrostatic pressure that would permit cells to flow through the microfluidic channels. Cells passed over arrays of microwells in the channels where they aggregated and formed spheroids by the second day of culture, as previously described.[15] After each injection, flow through channels was confirmed by observing the cells under a brightfield microscope. A 5 minute period between injections allowed for the cessation of flow prior to the subsequent injection on the alternate channel side. On the second day of cell culture in devices, a 10μl pipette tip was used to dislodge any cell aggregates that had formed at the bottom of channel wells as a result of the seeding process. Media was then removed and replenished with equal volumes on both channel sides. Media was exchanged every 48 hours. For 24 channel devices, cell seeding was as described above with the exception that cells were seeded at higher concentration of 7×10^6 cells/mL with a single injection of 5μL into one channel well (**Figure 2.2**).
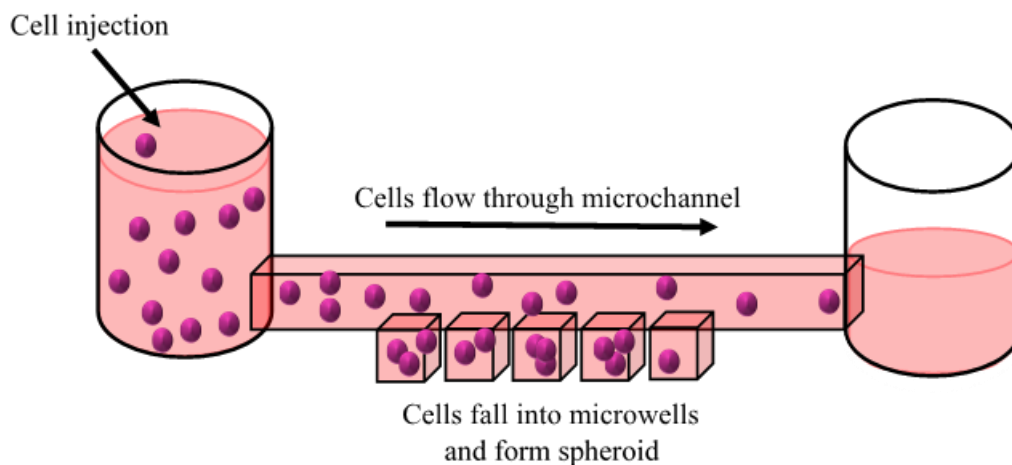
Figure 2.2 Schematic diagram of spheroid device cell seeding.

For fluorescent cell labelling, freshly prepared far red, blue or CSFE CellTrace™ dyes (Thermofisher) were used prior to cell injection into devices. 20uL of DMSO (Sigma) was added to a CellTrace stock vial. Cells in suspension were centrifuged and resuspended in pre-warmed PBS buffer (PBS/2%FBS) to a maximum concentration of 1x10^6 cells/ml. 1μL of CellTrace dye per ml of cell suspension was then added and cells incubated for 20 minutes at 37°C. Ice-cold quenching solution at 5 times the volume of the cell-CellTrace staining solution

was then added. Cells were centrifuged and the supernatant removed. Labelled cells were then resuspended in the desired volume of cell culture media for use in experiments.

2.8 Enzyme Inhibitor Treatment in Spheroid Devices

Two human cell types were co-cultured in the 7 channel spheroid device. These consisted of immortalised CAF and Cellaria Wood primary breast cell line. Spheroids were formed at a 1:1 ratio of cancer-CAF cells and cultured in a 1:1 mix of the supplier recommended complete culture media for the two cell types: RETM for the primary breast cells and DMEM for the CAF.

Spheroids were treated with either ACLY inhibitor (Concentrations: 25μM, 50μM and 100μM), p300 inhibitor (Concentrations: 12.5μM, 25μM, 50μM and 100μM), PYCR1 inhibitor (Concentrations: 25μM, 50μM, 100μM and 150μM) or PDH inhibitor (Concentrations: 50μM, 100μM and 200μM) beginning on either the first or third day of culture, depending on the experimental setup. Inhibitor action on cells was then reversed with administration of either acetate (Concentrations: 1mM and 2mM) or proline as rescue agents in combination with drug treatment. Inhibitor treatment commenced 24 hours after cell seeding and was carried out on every second day of culture for one week. Control experiments were performed for each set of experiments.

2.9 Fulvestrant Treatment and SERS Nanoparticle Loading in Microfluidic Devices

Fulvestrant stock was dissolved in DMSO at a concentration of 1640μM and the solution stored at 4 °C. Fulvestrant solution was diluted in RPMI media to obtain the desired concentration, immediately prior to injection into devices. Fulvestrant solution (1μM and 10μM) was added to devices on the third day of culture and incubated with spheroids for 24 hours at 37 °C and 5% CO_2. Subsequently, the drug was pipetted out and replaced with media containing nanoparticles. Preparation of ER-α (60pM), HER2 (60pM) or a mixture of ER-α/HER2 (60pM) nanoparticles for injection into the microfluidic devices was carried out the day prior to administration. Nanoparticles were gently pipetted up and down prior to injection into devices to avoid aggregation and blocking of the microfluidic channels. Pipetting was performed at an angle to ensure flow of the nanoparticles through the entirety of the microfluidic channel. Nanoparticles were incubated for 2 hours before being removed, with channels washed twice with PBS to remove any unbound nanoparticles. Control experiments were performed for each set of experiments where spheroids were cultured in the absence of fulvestrant or nanoparticles treatment.

2.10 Combination Immunotherapy Assays

MDA-MB-468 and stromal cells, CAF or NHLF, were seeded into spheroid devices as mono and co-cultures. Carboplatin stock solution was diluted in cell culture media to the desired concentration for experiments (12.5-200μM) and added for 24h to devices once cells had aggregated to form spheroids. On day 2 of culture, anti-PD-L1 (Biolegend) antibodies were injected into devices after a 1:100 dilution in culture media. EGFR-TM28-GITR-CD3z CAR-T cells (AMSBIO, AMS.PM-CAR1023-1M) were injected on day 3 at a concentration of 10×10^6/ml in a volume of 3μl and incubated for up to 72h with spheroids.

2.11 Immunofluorescence

2.11.1 EGFR Expression

Staining of cells to confirm EGFR expression levels was performed prior to CAR-T assays (**Section 5.2**). In a 24 well-plate, cells were seeded at a concentration of 0.05×10^6 in a volume of 0.5ml and cultured for 3 days with media changed after 24 hours. Cells were washed with room temperature PBS and fixed with 4% PFA for 10 minutes. The solution was removed and cells washed again with PBS before permeabilization with 0.1% Triton™ X-100 (ThermoFisher) for 10 minutes. The solution was removed and blocking solution containing 3% BSA added for 30 minutes. This was then removed and EGFR monoclonal antibody AlexaFluor 488 conjugate (ThermoFisher) at a dilution of 2 µg/mL in 0.1% BSA blocking buffer added and was stored overnight in the dark. Afterwards, the antibody was removed from cells which were washed twice with PBS. All staining steps performed were done so at room temperature. PBS was then added to each well prior to imaging.

2.11.2 Microfluidic Proliferation Assay

To establish changes in cell proliferation, cells were stained for a known proliferation marker, Ki-67. A chicken anti-Ki67 polyclonal antibody (ab254123, 1:200) was used in conjunction with a secondary goat anti-chicken antibody coupled to Alexa Fluor® 405 (ab175674, 1:200). Both antibodies were obtained from abcam and diluted in PBS containing 0.1% bovine serum albumin (BSA, Sigma-Aldrich), referred to as PBSB. Devices specified for proliferation analysis had media removed and were washed 3 times with PBSB. They were stored on ice for 30 minutes before another 30 minute on ice incubation with 4% paraformaldehyde (PFA, ThermoFisher) PFA was then removed and devices washed three times before blocking with PBS containing 0.5% Triton-X, 1% DMSO, 1% BSA and 1% FBS for 1 hour. Blocking solution was removed and devices washed again prior to the addition of the primary antibody. After 24 hours of storage at 4°C, the primary antibody was removed and devices washed three times. The secondary antibody could then be added for 2 hours with devices stored in the dark

at room temperature. Removal of the secondary antibody and washing was carried out immediately prior to imaging.

2.11.3 Microfluidic Viability Assay

Spheroid formation was monitored via bright-field microscopy and images collected every second day, as well as before and after drug treatment and nanoparticle exposure. To ascertain spheroid viability during the culture period, spheroids were stained with 8µg/mL fluorescein diacetate (FDA, Sigma-Aldrich), 20µg/mL propidium iodide (PI, Sigma-Aldrich) and 5µmol/L Hoechst33342 (Thermo Scientific) (**Figure 2.3**).
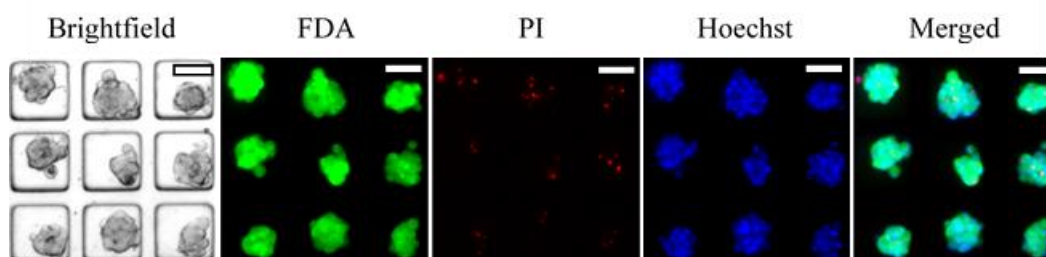
Figure 2.3 *Example of viability staining of spheroids with fluorescent dyes. FDA was used to stain live cells (green), PI was used to stain dead cells (red) and Hoechst33342 used to stain the nuclei of all cells (blue). Scale bar = 100µm.*

The staining solution was pipetted into the devices which were then incubated for 30 minutes. PBS was subsequently used to wash out excess staining solution and was refreshed prior to imaging. For nanoparticle experiments, staining of spheroids was performed at several time points which included immediately after nanoparticle exposure, 3 days after nanoparticle exposure and 6 days after nanoparticle exposure. Viability staining was carried out on day 5 for MIPs-treated spheroids and up to 72h after CAR-T exposure for combination immunotherapy experiments. For CAF co-culture experiments, fixing and staining of cells was carried out upon completion of inhibitor treatment of day 7 of culture. Viability staining was performed as previously described with the exclusion of FDA from the staining solution which was omitted due to the CAF transfection with GFP.

2.11.4 Microfluidic Collagen Deposition Assay

CNA35-mCherry staining solution was used to quantify collagen deposition in microfluidic devices, as previously described.[19] The staining solution was injected into both wells of each device channel simultaneously at a concentration of 1µM. Devices were then incubated for 2 hours before all liquid was removed from wells and PBS used to wash out residual staining solution. After washing twice with PBS, PBS was exchanged again prior to imaging of devices.

2.12 Microscopy

An inverted microscope (Observer A1, Zeiss) was used to observe spheroids at 5x and 10x magnification every 24–48 hours and brightfield images taken using an Orca Flash 4.0 camera (Hamamatsu). Epifluorescence microscopy was performed immediately after fixing and staining of the spheroids. Image analysis was performed using ZEN Blue 2.1, Fiji 1.53c and Matlab R2017b.

2.13 Image Analysis and Quantification

ImageJ was used to quantify EGFR expression, PD-L1 expression, proliferation, collagen deposition, CAR-T cell number and CAF and Cancer cell areas through normalization of minimum and maximum threshold values, conversion of images to 8-bit binary images and particle/analysis measurement. In house MATLAB routines were used to extract viable fraction, shape factor and area data from fluorescent and brightfield images. The viable fraction (V_f) of spheroids was established by calculating the ratio of FDA area on the day of staining ($Area_{FDA}$) over the brightfield area of the spheroid on the day prior to drug administration ($Area_{BF}$), as seen in the following equation:

$$V_f = \frac{Area_{FDA}}{Area_{BF}}$$

Brightfield and fluorescent spheroid areas and perimeters were obtained from images and processed using previously developed in-house Matlab routines.[15] Spheroids possessing a $V_f \geq 1$ were considered to have been unaltered by exposure to nanoparticles or fulvestrant treatment since they had either remained the same size or increased in size over the culture period. In contrast, spheroids with a $V_f < 1$ were regarded as unhealthy or as having been negatively affected due to administration of the nanoparticles or fulvestrant. The shape factor (S_f) of spheroids was also used as an assessment of its integrity, as previously described.[15]

2.14 Image Analysis of 3D CAF-Co-cultures

For CAF co-culture studies, czi files were separated into individual channels in Fiji and normalized to a given threshold range (**Figure 2.4**). The quantity of dead cells was established using signal from PI staining, through conversion of the TIFF file to an 8-bit binary image and then applying particle analysis. In parallel devices, this method was also used to quantify collagen deposition. This involved obtaining the CAF and collagen deposition areas, which could then be plotted as a ratio of collagen deposition/CAF area. The same method was applied for quantification of CAF proliferation. Owing to the well-defined dissociation of the CAF and cancer cells, it was possible to measure their separate spheroid areas by taking the signal

from the green channel, for CAF quantification, and using the brightfield channel image to trace around the spheroid to establish cancer spheroid area.
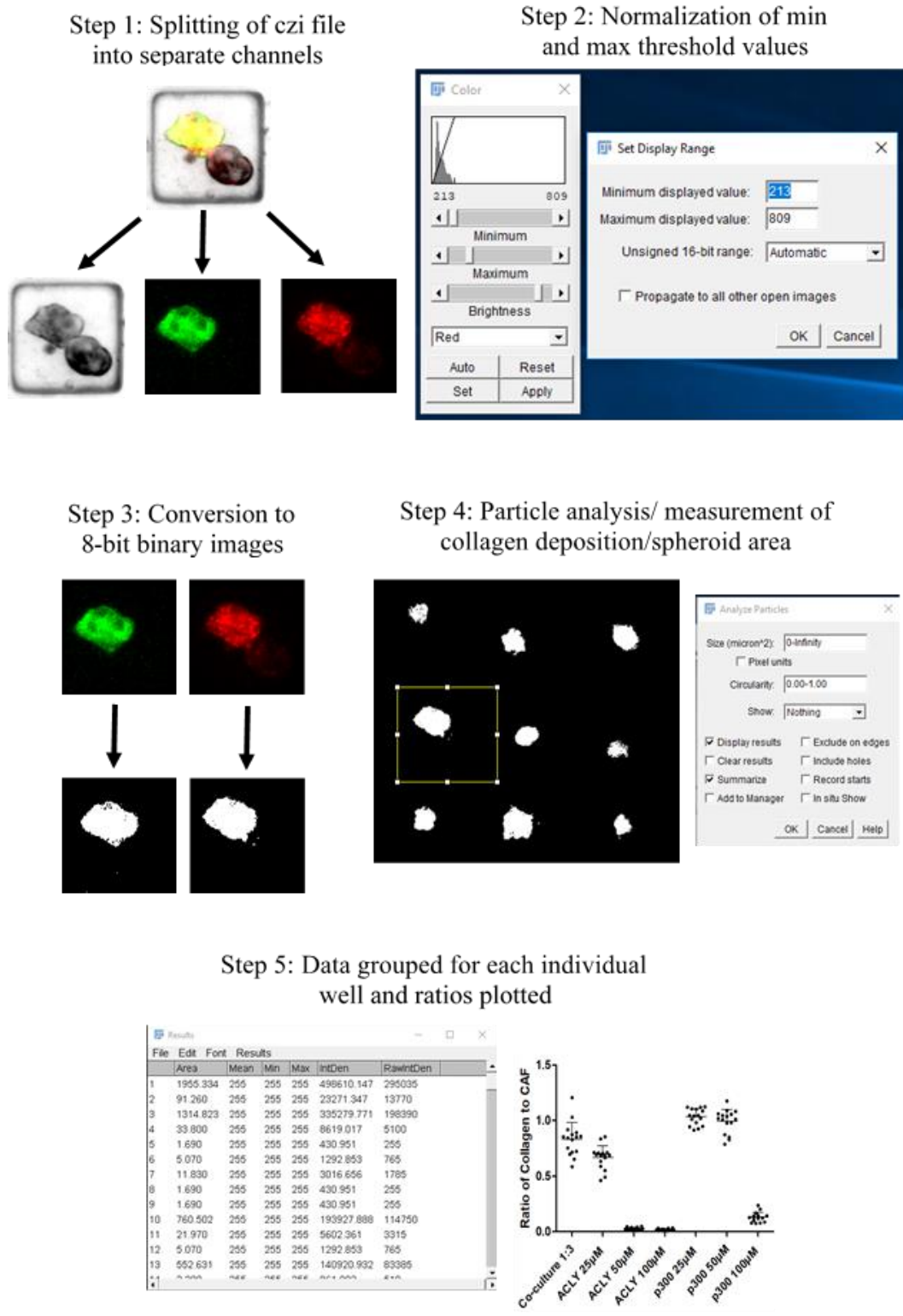
Figure 2.4 *Description of the method of data quantification for CAF co-culture studies. Fluorescent images show GFP transfected CAF (green) and staining of collagen deposition (red).*

2.15 Image Analysis of 3D CAR-T Assays

ZEN Blue and Fiji software were used to quantify spheroid area and the number of CAR-T cells present (**Figure 2.5**.). Co-localization of cancer cells and PI signal was performed by extracting separate TIFF files from each wavelength channel using Fiji and normalizing images to the same threshold range. TIFF images were then converted to an 8-bit binary image for analysis. CAF area was obtained from the GFP channel and CAR-T cell area obtained from the CellTrace Far Red channel. These were subsequently subtracted from the PI signal area which allowed estimation of co-localised area of PI signal with unlabelled cancer cells. Data was plotted as a percentage of the total PI area.
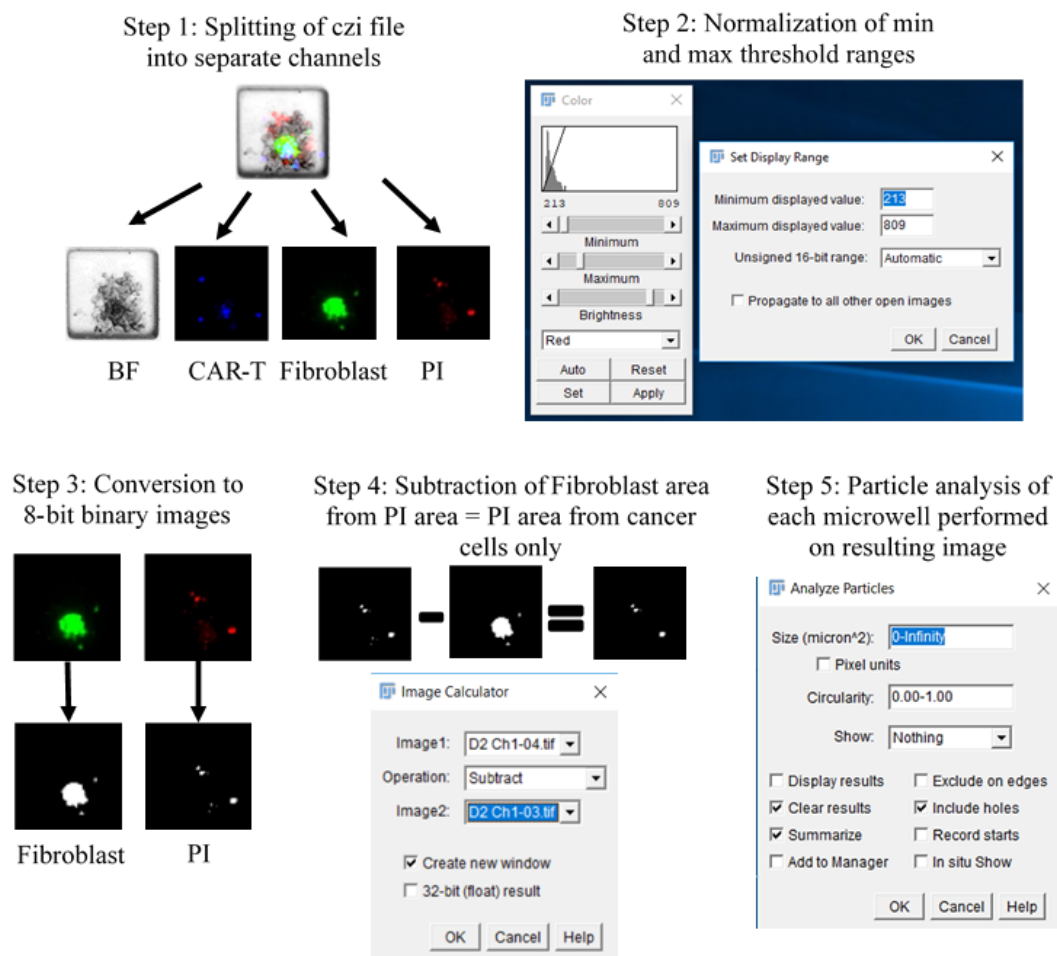
Figure 2.5 *Description of the method of data quantification for CAR-T studies. Fluorescent images show fluorescently labelled fibroblasts (green) and CAR-T (blue) and PI staining of dead cells (red).*

2.16 Statistical Analysis

Statistical analysis was performed using GraphPad Prism 8.1.2 (GraphPad Software, Inc., San Diego, CA). One- way analysis of variance was used for comparison of multiple independent groups. For comparison of multiple variables, two-way analysis of variance (ANOVA) with Bonferroni multiple comparison tests were conducted. All data is presented as mean $\pm$ standard deviation, unless otherwise stated, using bar graphs or scatter plots. T-tests were used for the comparison of two variables. Differences were considered significant at a P values < 0.05.

Chapter 3: Preliminary 3D Assay Development

The following chapter describes preliminary exploratory and collaborative work conducted at the beginning of this studentship. This included the use of microfluidic assays applied, for the first time, towards assessing the efficacy of targeted nanoparticles in a 3D microfluidic breast cancer model via surface enhanced Raman spectroscopy (SERS) and for the preliminary investigation into advancing current spheroid microfluidic models through the incorporation of a vascular network. These assays were developed at the beginning of the studentship and allowed expertise to be acquired creating various models and using the microfluidics for simpler monocultures prior to moving on to more advanced co-culture and immunotherapy models.

3.1 Drug Nanoparticle Studies

Collaboration with the Bionanotechnology and Analytical Chemistry group at the University of Strathclyde resulted in study of the specificity and toxicity of two different breast cancer receptors using a 7-channel spheroid forming device designed by T. Mulholland (ScreenIn3D Ltd, UK)[15] (**Figure 3.1**).
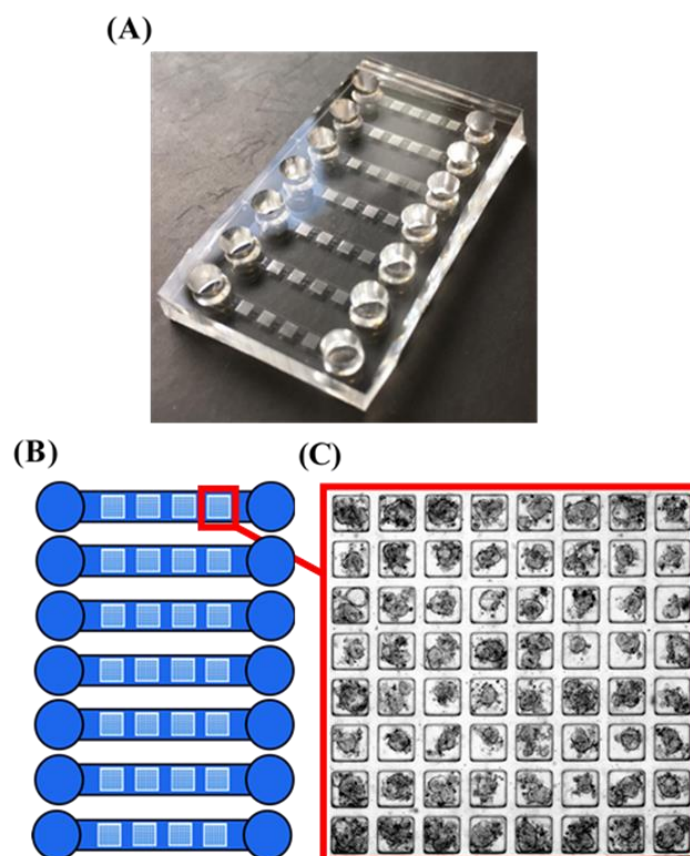
Figure 3.1 *7-channel spheroid forming device structure. (A) Image of 7-channel spheroid forming device. (B) Schematic of structure of 7-channel spheroid device with each channel containing 4 arrays of 8x8 150µm square traps (Channel length= 24.33mm, channel width= 3.58mm). (C) Brightfield image of array showing MCF-7 breast cancer spheroids on day 7 of culture. (5x magnification)*

The 7-channel spheroid device (**Figure 3.1**A) was used to carry out this testing in a 3D environment where each channel in the device consisted of 4 arrays of 64 150µm square traps per channel, allowing culture of up to 1792 spheroids per chip (**Figure 3.1**B and C). Devices were fabricated using previously described methods (**Section 2.1 and 2.2**). Endocrine therapy targeting the oestrogen receptor alpha (ERα) pathway has been employed to treat cancer patients suffering from ERα positive breast cancer. This treatment has been shown to cause less side effects than chemotherapy, without compromising on efficacy.[233] This form of therapy involves the use of compounds, known as selective oestrogen receptor down-regulators (SERDs). SERDs bind to ERα and consequentially degrade and downregulate the receptor, resulting in a loss of endocrine-dependent and endocrine-independent ER signalling.[234] The first SERD to receive approval for clinical use was the drug known as fulvestrant.[235] Achieving a more thorough understanding of the mechanism of action of this drug using 3D *in vitro* models could provide additional supporting data for its use clinically.[136,

[236, 237] As far as has been reported in the literature, this is the first recorded study of SERS used with microfluidic devices to detect ERα in breast cancer spheroids. The breast cancer cell line used for these studies was MCF-7 as it is positive for ERα and negative for human epidermal growth factor receptor 2 (HER2) expression (**Section 2.7**). MCF-7 spheroids were exposed to fulvestrant treatment for 24h on day 3 of culture prior to the addition of nanoparticles on day 4 for 2 hours and subsequent washing steps (**Section 2.9**). Functionalized nanoparticles were specific to either ERα or HER2 proteins. The cytotoxic effects of ERα were studied alone (ERα NPs) and in combination with HER2 specific nanoparticles (ERα/HER2 NPs). Fulvestrant treatment at 1 and 10μM concentrations was assessed as a monotherapy as well as in conjunction with nanoparticle exposure.

The effect of ERα NPs and ERα/HER2 NPs combination on MCF-7 spheroid integrity and viability was investigated over the 10 day culture period (**Figure 3.2**).
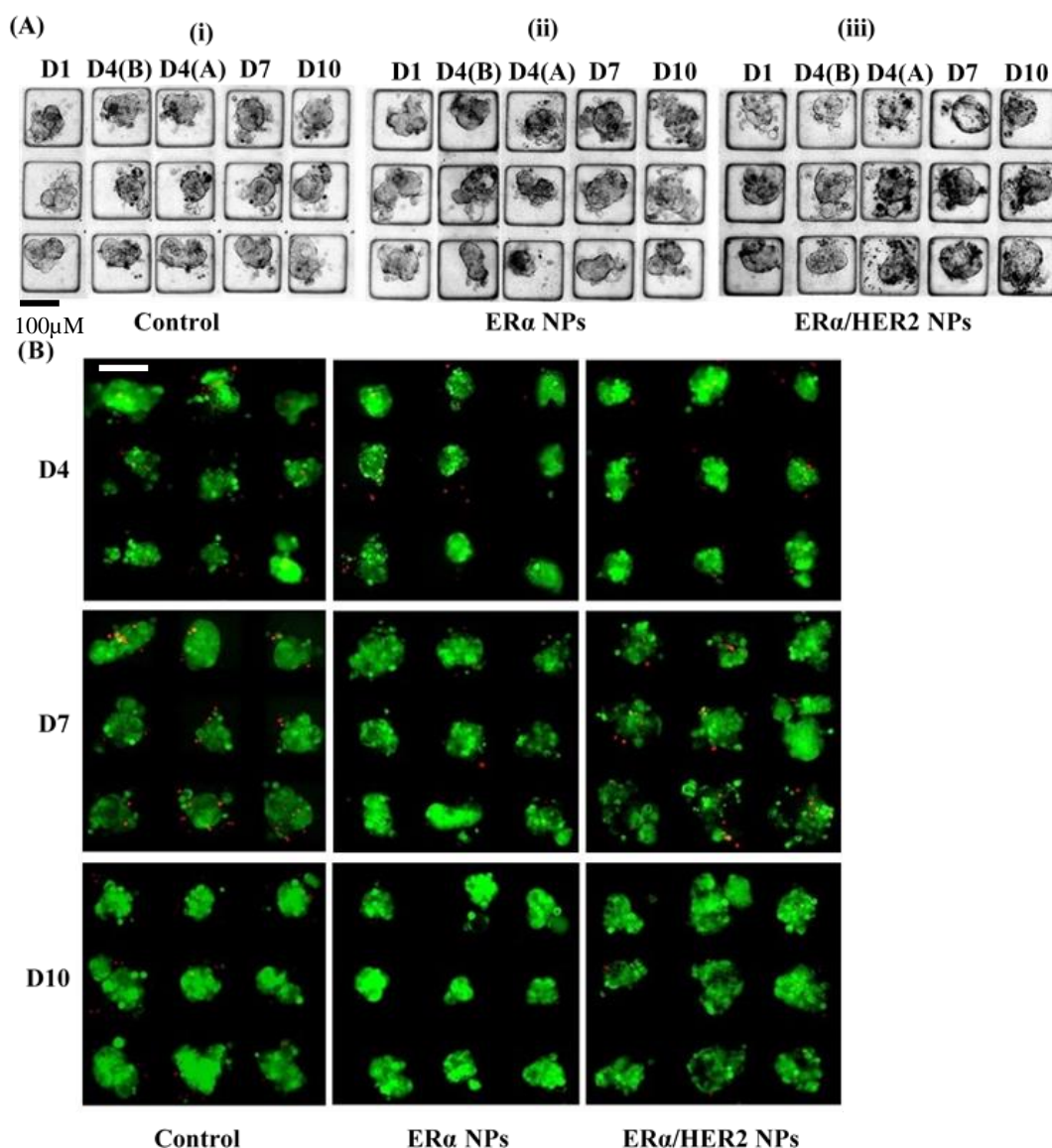
Figure 3.2 Effect of ERα NPs and ERα/HER2 NPs combination on spheroid formation and viability of MCF-7 spheroids. (A) Brightfield image timelines of MCF-7 spheroids culture in microfluidic devices over a period of ten days (i) without nanoparticles treatment (ii) with ERα NPs treatment and (iii) with ERα NPs and HER2 NPs. (D1 = day 1 (24h after MCF-7 cell seeding), D4 (B) = day 4 (before the addition of nanoparticles), D4 (A) = day 4 (after the addition of nanoparticles), D7 = day 7, D10 = day 10). (B) Fluorescence images of spheroid viability staining with FDA (green) and PI (red) at varying time points. (C) Plot of spheroid shape factor. n=32.(5x magnification) Scale bar = 100μm.

The MCF-7 cell line formed loosely aggregated spheroids (**Figure 3.2**A) which maintained good viability (**Section 2.11.3**) throughout their culture in microfluidic devices (**Figure 3.2**B). Due to seeding variations between central and exterior channel arrays, larger numbers of cells reached exterior microwells causing the formation of spheroids that were too large for analysis. As a result of this limitation, it was concluded that future immunotherapy studies should be performed in a device with shorter channel length, as is described in Chapter 5. Brightfield imaging was performed before and after nanoparticle administration to identify any induced

toxicity or structural changes in the spheroids. Quantification of spheroid shape factor, area growth and viable fraction was performed (**Figure 3.3**).
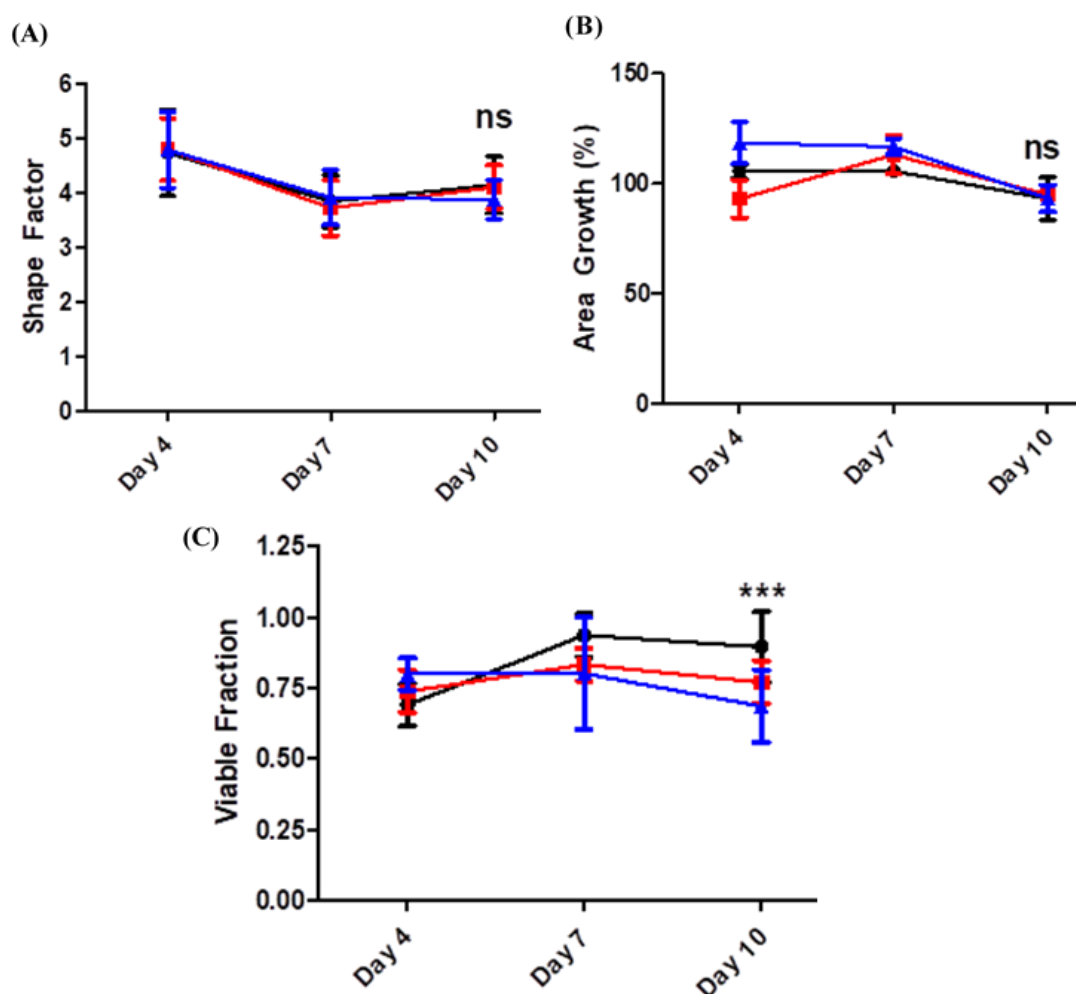
Figure 3.3: Quantification of shape factor, area growth and viable fraction of spheroids treated with ERα NPs and ERα/HER2 NPs. (A) Plot of shape factor. n=32. Data shows no significant differences in shape factor between control spheroids and nanoparticle treated spheroids on day 10. (B) Plot of the spheroid area growth taken from day 3 area (%). n=32. Data shows no significant differences in area growth between control spheroids and nanoparticle treated spheroids on day 10. (C) Plot of viable fraction of spheroids. n=32. Data shows a significant difference (***P ≤0.0001) between control spheroids on day 10 compared to control spheroids on day 4. For all plots, untreated cells are represented in black, cells exposed to ERα NPs are represented in red and cells exposed to ERα/HER2 NPs combination are represented in blue. 32 channels containing spheroids with a diameter of 50–100μm on day 3 of microfluidic culture were selected from the two middle arrays of each device channel for analysis. 3x3 tumour spheroid arrays are representative of those used for data analysis. Data shown as mean ± SD. ***P ≤0.0001, One-way ANOVA, Bonferroni's post-test.

Quantification of shape factor (**Section 2.13**) provided an assessment of spheroid disaggregation with more circular spheroids giving values close to 1 (**Figure 3.3**A). Nanoparticle administration did not elicit any significant impact on the structural integrity of the spheroids with respect to control spheroids throughout the culture period. By day 10, a

significant reduction in control spheroid size could be detected (**Section 2.13**) when compared to control spheroids on day 4 of culture (***P ≤0.0001), from one-way ANOVA analysis (**Figure 3.3**B). This suggested that spheroids become more compact with time in 3D culture. No significant differences in area growth between control and nanoparticle treated spheroids were detected by day 10. Viability staining was conducted using FDA which is only taken up by live cells that convert the non-fluorescent FDA into the green fluorescent metabolite fluorescein (Section 2.13). PI staining was also used for viability staining and is a red nuclei staining dye that is only able to pass through disordered areas of membranes of dead cells. Viability analysis of cells after exposure to nanoparticles was investigated on days 4, 7 and 10 and showed that, while nanoparticle treated spheroids did maintain strong viability, significantly greater viability (***P ≤0.0001) was detected for control spheroids on days 7 and 10 in comparison to nanoparticle treated spheroids. (**Figure 3.3**C). This could suggest that either nanoparticle binding to receptors or some component of the nanoparticle formulation could have elicited a degree of toxicity in cultures. Despite this, spheroids remained healthy.

Analysis of 1μM and 10μM fulvestrant treatment, administered after 3 days of microfluidic culture and incubated for 24h, was also performed (**Figure 3.4**).
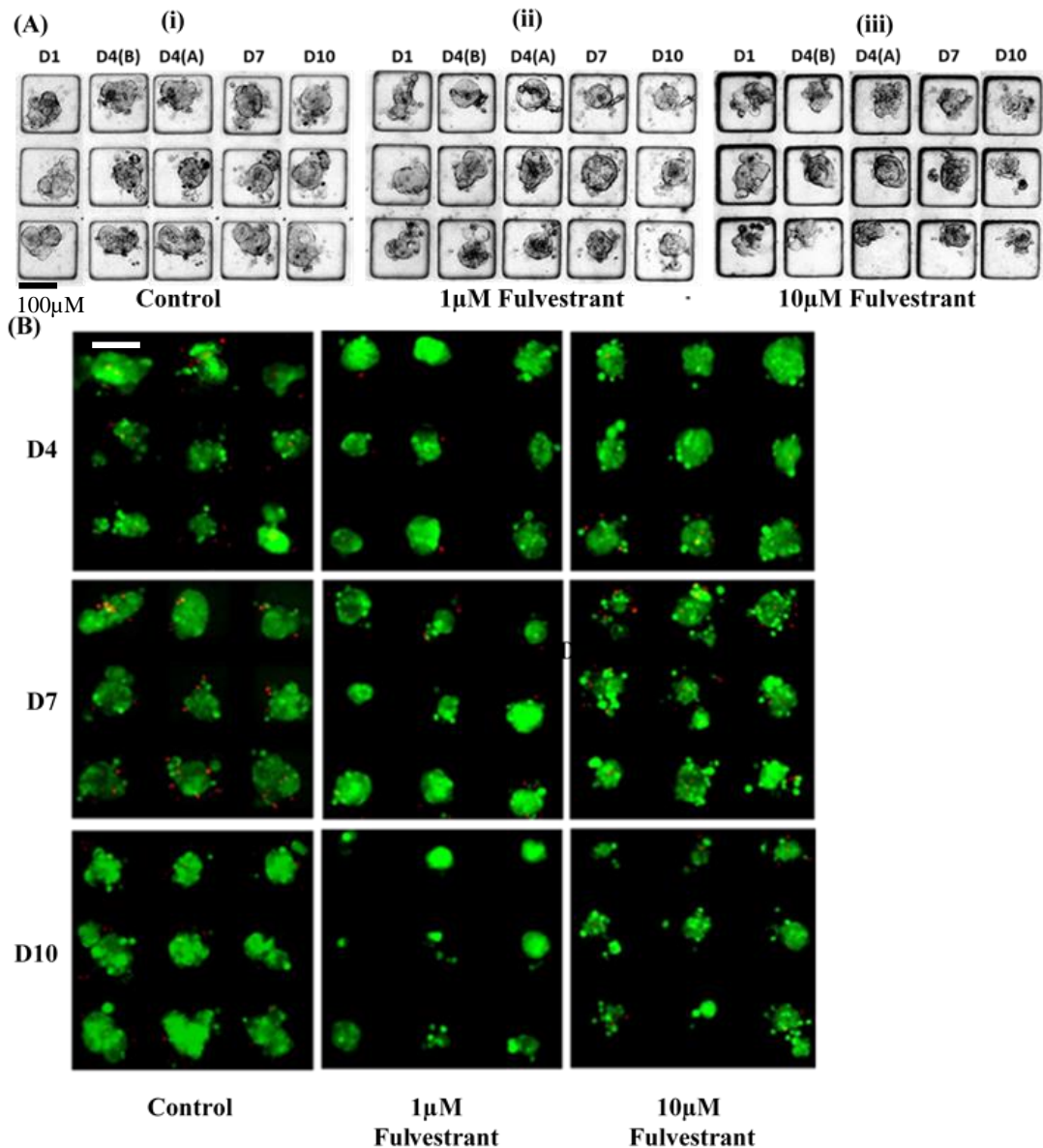
Figure 3.4 *Effect of fulvestrant on spheroid formation and viability of MCF-7 spheroids. (A) Brightfield image timelines of MCF-7 spheroids culture in a microfluidic device over a period of ten days (i) without drug treatment (ii) with 1µM fulvestrant treatment and (iii) with 10µM fulvestrant treatment. (D1 = day 1 (24h after MCF-7 cell seeding), D4 (B) = day 4 (before the addition of nanoparticles), D4 (A) = day 4 (after the addition of nanoparticles), D7 = day 7, D10 = day 10). (B) Fluorescence images of spheroid viability staining with FDA (green) and PI (red) at varying time points. (5x magnification)*

Brightfield image timelines showed spheroids became smaller and more disaggregated with fulvestrant treatment at both concentrations tested (**Figure 3.4**A). Fewer live cells were also visible in fluorescent images for drug treated spheroids in comparison to control spheroids

(**Figure 3.4**B). Quantification of spheroid shape factor, growth and viability was also performed (**Figure 3.5**).
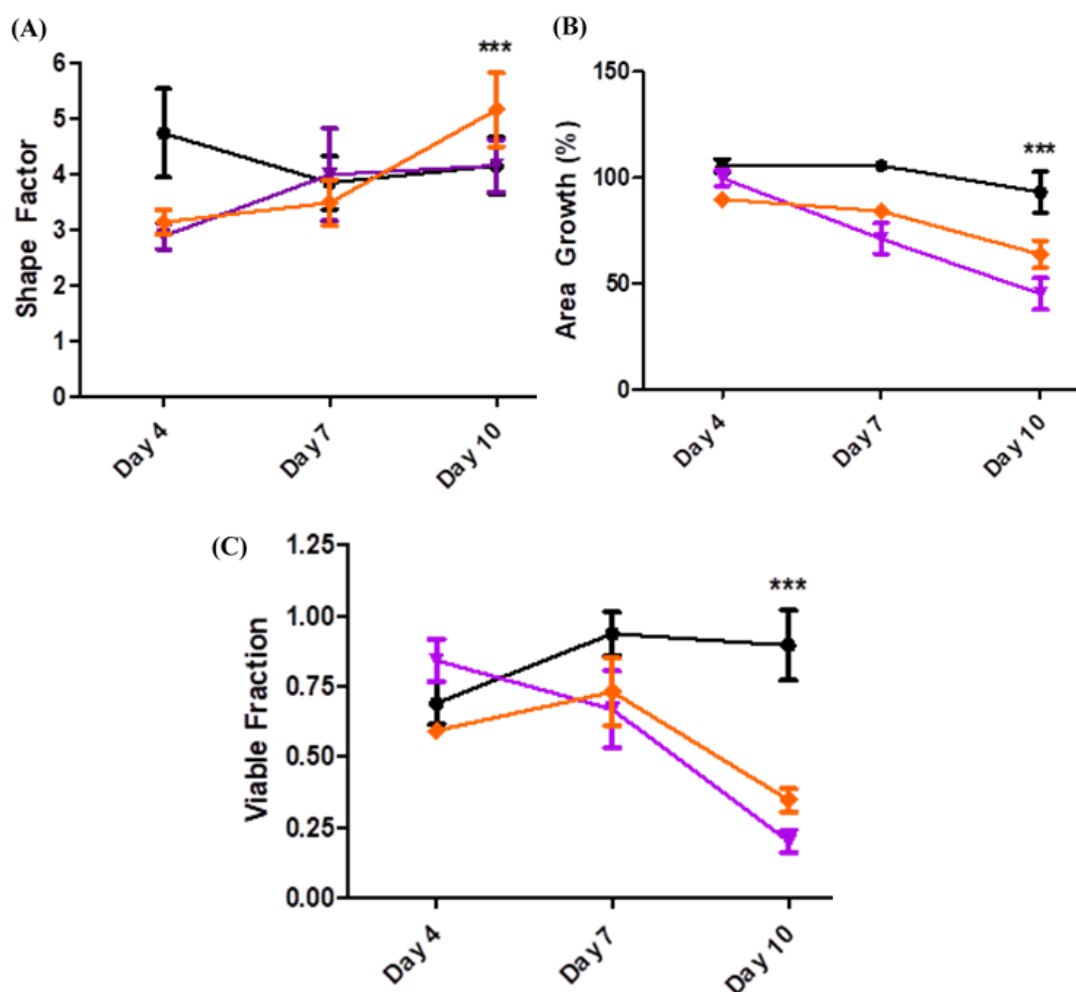
Figure 3.5: Quantification of shape factor, area growth and viable fraction of spheroids treated with fulvestrant. (A) Plot of spheroid shape factor. n=32. Data shows a significant difference in shape factor (***P ≤0.0001) between 10μM fulvestrant treated spheroids on day 10 compared to control spheroids. (B) Plot of the spheroid area growth taken from day 3 area prior to fulvestrant addition (%). n=32. Data shows a significant difference in area growth (***P ≤0.0001) between 1μM and 10μM fulvestrant treated spheroids on day 10 compared to control spheroids. (C) Plot of viable fraction of spheroids. n=32. Data shows a significant difference in the viable fraction (***P ≤0.0001) between 1μM and 10μM fulvestrant treated spheroids on day 10 compared to control spheroids. For all plots, untreated cells are represented in black, spheroids treated with 1μM fulvestrant are represented in purple and spheroids treated with 10μM fulvestrant are represented in orange. Data shown as mean ± SD. ***P ≤0.0001, One-way ANOVA, Bonferroni's post-test.

Significant differences (***P ≤0.0001) from one-way ANOVA analysis in shape factor were recorded between control spheroids and those treated with both drug concentrations on day 4, suggesting that fulvestrant addition on the day prior had resulted in some compaction of the spheroid (**Figure 3.5**A). By day 10, no significant differences in spheroid disaggregation were detected for control spheroids and those treated with 1μM fulvestrant. The 10μM fulvestrant concentration, however, resulted in significantly greater disaggregation of spheroids. Whilst no significant differences in spheroid growth were initially recorded at day 4 between

spheroids receiving the receptor targeting drug and control spheroids, fulvestrant treatment was shown to negatively impact growth (**Figure 3.5**B) and viability (**Figure 3.5**C) of MCF-7 spheroids by day 10 (***P $\leq$0.0001) from one-way ANOVA analysis. Consequently, day 4 was selected as the optimum stage for SERS analysis by collaborators. Data analysis could not be performed for spheroids treated with both fulvestrant and nanoparticles due to an insufficient quantity of spheroids remaining in traps after washing steps to remove nanoparticles. The combined treatment resulted in more loosely aggregated spheroids being flushed from traps leaving too few spheroids to perform robust analysis. These findings established that fulvestrant treatment increased the quantity of dead cancer cells over time, confirming its cytotoxic effect in 3D.

Assessment of the selectivity of these nanoparticles using 2D SERS was performed by A. Kapara (University of Strathclyde) from the collaborating group.[18] ERα nanoparticles and HER2 nanoparticles were labelled with two different Raman reporters, BPE and PPY respectively, for identification by SERS analysis. Analysis revealed significantly greater spheroid accumulation of ERα nanoparticles in comparison, HER2 nanoparticles. Low levels of untargeted HER2 nanoparticle accumulation in MCF-7 spheroids were detected, most likely due to non-specific binding as a result of the absence of HER2 receptors. 3D SERS mapping confirmed that nanoparticles were able to penetrate the spheroid. Results showed that while PDMS does produce a low intensity SERS spectrum, peaks do not intersect with those from nanoparticles. SERS mapping revealed less nanoparticle accumulation for spheroids treated with the higher fulvestrant concentration (10μM) in comparison to the lower concentration (1μM) and control spheroids.[18] This data suggested that fulvestrant had been successful in degrading ERα receptors, thus leaving less opportunity for ERα binding and accumulation in spheroids.

In conclusion, this work demonstrated the capacity of SERS and microfluidic technology to be combined as a means of *in vitro* tumour cell and nanoparticle characterization. Quantification of results revealed that spheroids were able to maintain their integrity and viability after incubation with nanoparticles, despite control spheroids exhibiting greater viability in comparison to nanoparticle treated spheroids after 10 days of microfluidic culture. Thus, providing a robust methodology for nanoparticle assessment in a miniaturized 3D tumour model. The negative impact of the anti-cancer drug, fulvestrant, on spheroid viability was established as well as its ability to disaggregate spheroids and limit their growth. SERS analysis performed by collaborators demonstrated the specificity and targeting ability of ERα nanoparticles against spheroids. These findings support the use of ERα NPs for monitoring

ERα expression levels after drug treatment and demonstrates the potential for combination of SERS with microfluidic 3D cultures as a means preclinical anti-cancer drug evaluation. This proof-of-concept assay has the potential to reduce the use of animals in the drug development process as only targets that had performed successfully would be selected for in vivo studies. This would provide enhanced knowledge when identifying the optimum treatment plan for a patient and increase the likelihood of successful outcomes. In future, this assay could be further increased in complexity with the addition of TME components and in combination with other therapeutic agents. Patient biopsy tissue could also be considered for spheroid formation to assess the response of expression levels of individuals to treatment.

3.2 Vascular Network

Of the various *in vitro* models that were researched, the prospect of combining a tumour spheroid model with a vascular network was of particular interest. This model would ideally allow investigation into the direction of network formation towards spheroids and create the potential for cells originating from spheroids to migrate out into an already developed vascular network, thereby mimicking intravasation. Various examples exist in the literature of microfluidic devices used in similar ways to study tumour vasculature, all using a range of gel formulations and collagen pH values, temperatures and incubation times.[41, 52, 176-180, 238, 239] Thus, various conditions were identified for testing in order to determine the optimum conditions for vascular network formation. A pre-existing vascular network device design was used for experiments that consisted of 3 parallel channels with interconnecting microposts (**Figure 3.6**).
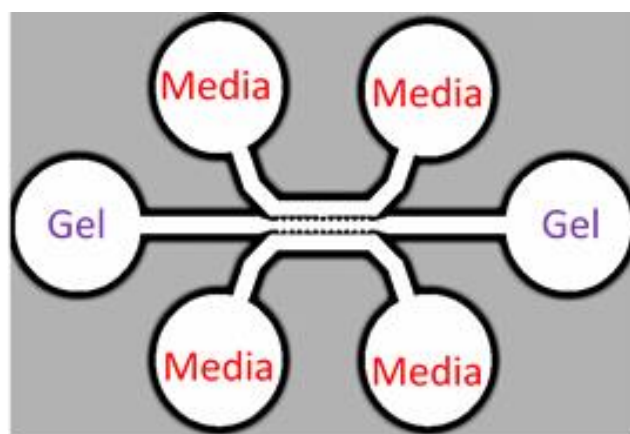
Figure 3.6 *Schematic of vascular network device. Structure (Central channel length= 11.69mm, central channel width= 0.85mm, central channel width at intersection= 0.45mm, length of intersection extrusions= 0.2mm, width of outer channels= 0.5mm, well diameter= 4mm).*

This design allowed for a fibrous gel to set in the central channel of the device without leakage into the two adjacent side channels or disruption by media injection (**Section 2.3**). Sterilisation

to prepare devices for cell culture was performed via oxygen plasma treatment (**Section 2.4**). This was followed by subsequent storage of devices overnight at 85°C in order to reinstate the hydrophobic conditions of the PDMS as it was noted that injecting the gel too soon after plasma treatment resulted in the gel being unable to be contained in the central device channel. HUVEC were chosen to be cultured in devices based on numerous previous successful reports of vascular network formation in the literature.[41, 176, 177, 179, 239, 240] Following gel injection, HUVEC were seeded into one of the side channels of the device and their growth monitored up to a maximum period of 9 days prior to viability staining (**Section 2.6**). From preliminary assays, it was noted that polymerisation was more successful after longer gel incubation periods of up to 60 minutes in comparison to 10 and 15 minute incubation periods. Enhanced polymerisation was also observed when collagen pH was higher, pH 9 in comparison to 7.4 and below. At lower pH values, small fibres were observed to form initially. However, media could not be contained within the side channels and leaked into the central channel. To prevent this, a higher collagen pH of 9 was used and devices stored at 4°C prior to injection of the gel. The gel administration was performed on ice to keep the hydrogel at as low a temperature as possible and to avoid premature collagen fibre formation (**Figure 3.7**).
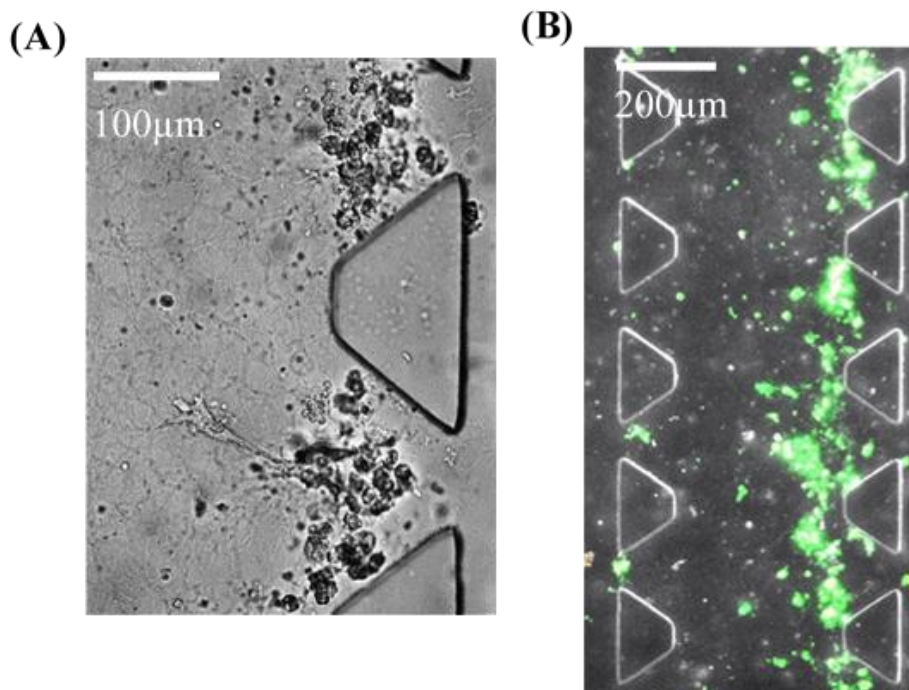
Figure 3.7 *Preliminary Vascular Network Device Cultures (A) Brightfield image of initial cell culture in vascular network devices on day 5. (B) Brightfield image with viability staining of initial cell culture in vascular network devices on day 5. (green = FDA, red = PI).*

Brightfield images showed the formation of vascular structures after 5 days of cell culture in devices (**Figure 3.7**A). Cells were stained with FDA and PI (**Section 2.11.3**) and were shown to be able to survive with minimal cell death in the device (**Figure 3.7**B). However, cells remained close to the injection site and were not able to penetrate through the gel to form a vascular network. While use of a higher collagen pH was shown to result in larger fibre formation, these fibres were inconsistently spread throughout the gel.

Subsequently, varying concentrations of thrombin, aprotinin and fibrinogen were added to the collagen to establish the composition that would produce gels with greater fibre formation and uniformity (**Figure 3.8**).
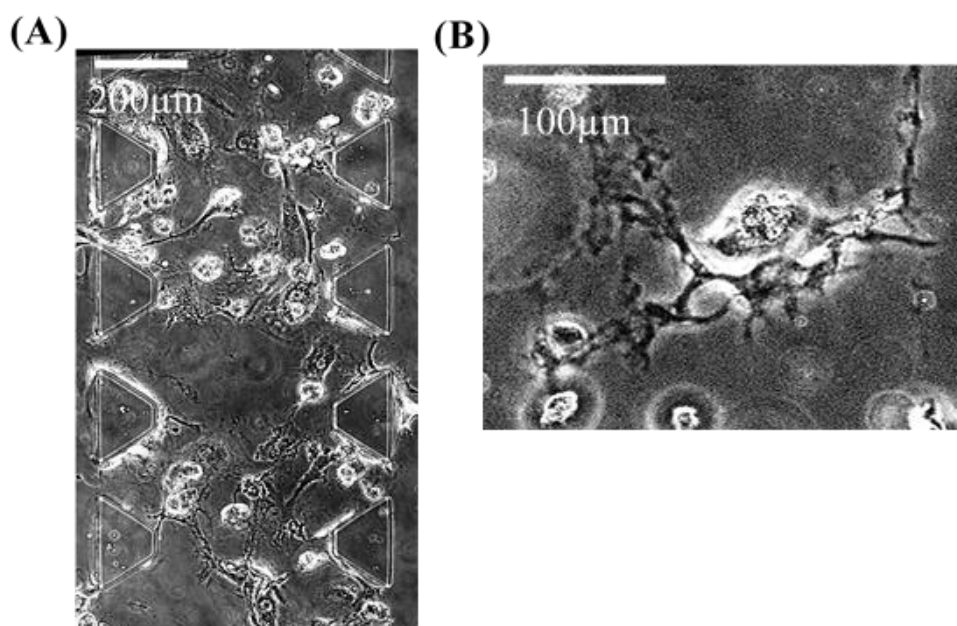
Figure 3.8 Optimization of gel composition. (A) Day 1 brightfield image of cell penetration into gel (B) Day 5 brightfield image of formation endothelial structures.

HUVEC were then seeded into devices and were able to penetrate further into the gel and form more aggregated structures by the fifth day of culture (**Figure 3.8**A and B). However, this modification to the protocol still failed to produce a confluent vascular network formation throughout the central channel and further optimization of protocols was required. It was concluded that to produce a combined tumour spheroid-vascular network device was out with the time-scale of this project but initial work conducted provides a foundation for future developments.

In summary, these initial collaborations and exploratory projects allowed experience to be gained in developing preliminary breast cancer models and protocols. Expertise acquired from

working with monoculture spheroids allowed aspects from these models to be further developed in later work. The microfluidic protocols developed were applied to the study of nanoparticles targeting specific receptors on breast cancer cells in collaboration with the Bionanotechnology and Analytical Chemistry group at the University of Strathclyde. This was the first report of microfluidic technology used in conjunction with SERS for the study of nanoparticle targeting efficacy in a 3D human breast cancer model. Miniaturization presents the advantage of allowing the formation of complex 3D models to enhance recapitulation of *in vivo* tumours with the aim of enhancing the predictive accuracy and reducing the cost of drug screening. In parallel, consideration was also given as to whether a vascular network should be incorporated into the spheroid devices to create a more complex and representative model. Many current methods of microfluidic vascular network formation involve the use of external actuation equipment which can be cumbersome and problematic to use. There exists the possibility to overcome these issues by developing an open well 3D tumour-vascular microfluidic model for studying the efficacy of novel anti-cancer drugs against cancer cells and their effects on tumour vasculature and intravasation. Vascular network culture conditions and gel formulation protocols were assessed using a pre-existing microfluidic device consisting of three parallel channels with interconnected microposts. However, this work was terminated as more novel opportunities arose involving immunotherapy studies. An important future consideration for such a 3D tumour-vascular model would be the consequences of the increased model complexity for increasing the throughput and automation. Automating the handling of current microfluidic devices would allow assays to be performed on a larger scale and would mean greater numbers of anti-cancer drugs could be assessed at a faster rate. Overall, valuable insight into creating tumour spheroid models was attained and which was the basis to develop subsequent TME relevant co-cultures that were ultimately used for immune-oncology assays.

Chapter 4: Recreating TME Characteristics with a CAF-Co-culture Model

In addition to representing the 3D tumour structure, it is also of great importance to consider the variety of cells present within the TME when designing *in vitro* models. The majority of anti-cancer agents are aimed towards the proliferating cancer cells without considering potential interactions with the surrounding stromal cells, which could affect treatment efficacy.[241] Targeting enzymes that encourage cancer progression has become a recent topic of interest in cancer treatment. If enzymes known to be overexpressed in the TME can be inhibited, this would allow enhancement of the effects of anti-tumour agents. Enzymes of significance and which have been considered in this work include ACLY, PDH, p300 and PYCR1. The purpose of this work, in collaboration with E. Kay and S. Zanivan (University of Glasgow, Cancer Research UK Beatson Institute) was to use an existing spheroid forming microfluidic platform, developed by T. Mulholland (ScreenIn3D Ltd, UK)[15], to establish a 3D breast cancer cell-stromal model and investigate the collagen production cycle of which the aforementioned enzymes are involved (**Figure 4.1**).[19]
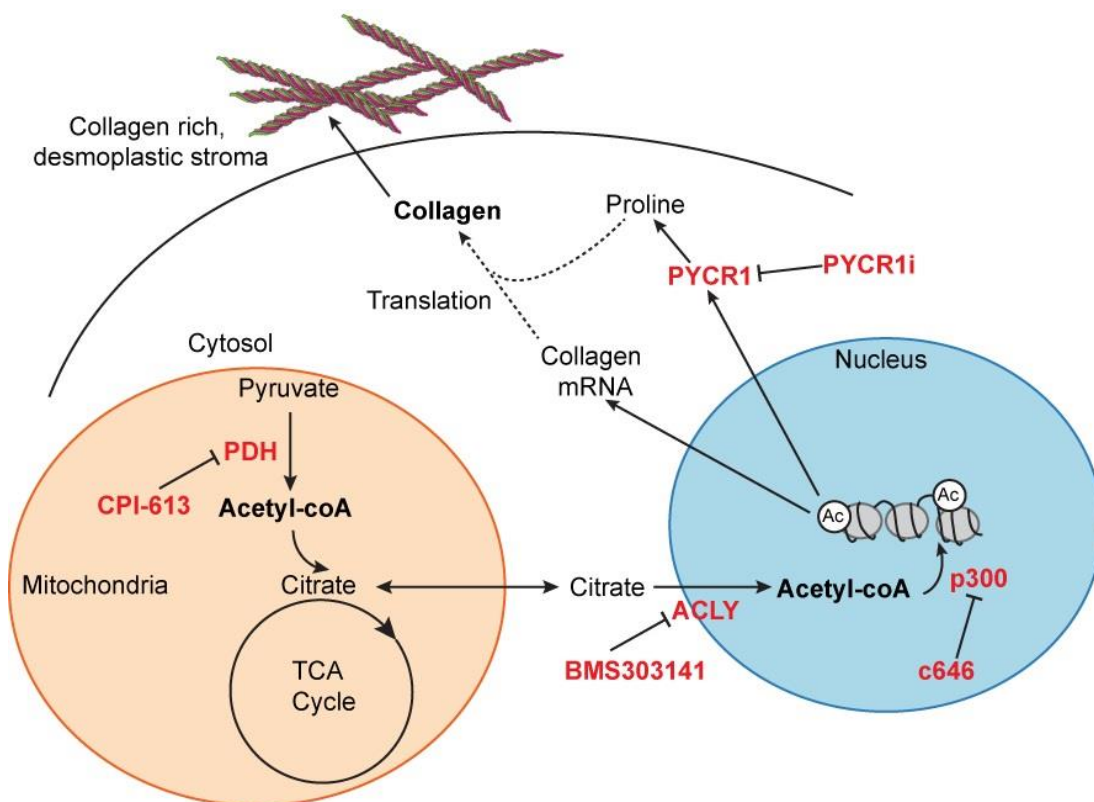
Figure 4.1*: Schematic diagram of the processes involved in collagen production by CAF. Adapted with permission from Kay et al., bioRxiv, 2021 https://creativecommons.org/licenses/by/4.0/. ACLY: ATP citrate synthase, PDH: pyruvate dehydrogenase, p300: histone acetyltransferase, PYCR1: pyrroline-5-carboxylate reductase 1, BMS303141: inhibitor of ACLY, c646: inhibitor of p300, CPI-613: inhibitor of PDH, PYCR1i: inhibitor of PYCR1, TCA: tricarboxylic acid.*

The collaborators had previously performed investigations into CAF in 2D and sought to further examine their influence on cancer cells in 3D co-cultures. The following chapter describes the development of a primary breast cancer cell-CAF spheroid co-culture and subsequent assessment of the effects of various enzyme inhibitors on viability, growth, collagen deposition and proliferation in a 3D microfluidic assay.

4.1 Formation of Co-Culture Spheroids

Using the 7-channel spheroid device (**Section 2.7**), described in chapter 3, a co-culture of two immortalized human cell types, the Cellaria Wood primary breast cancer cell line and immortalised CAF, was established (**Figure 4.2**).
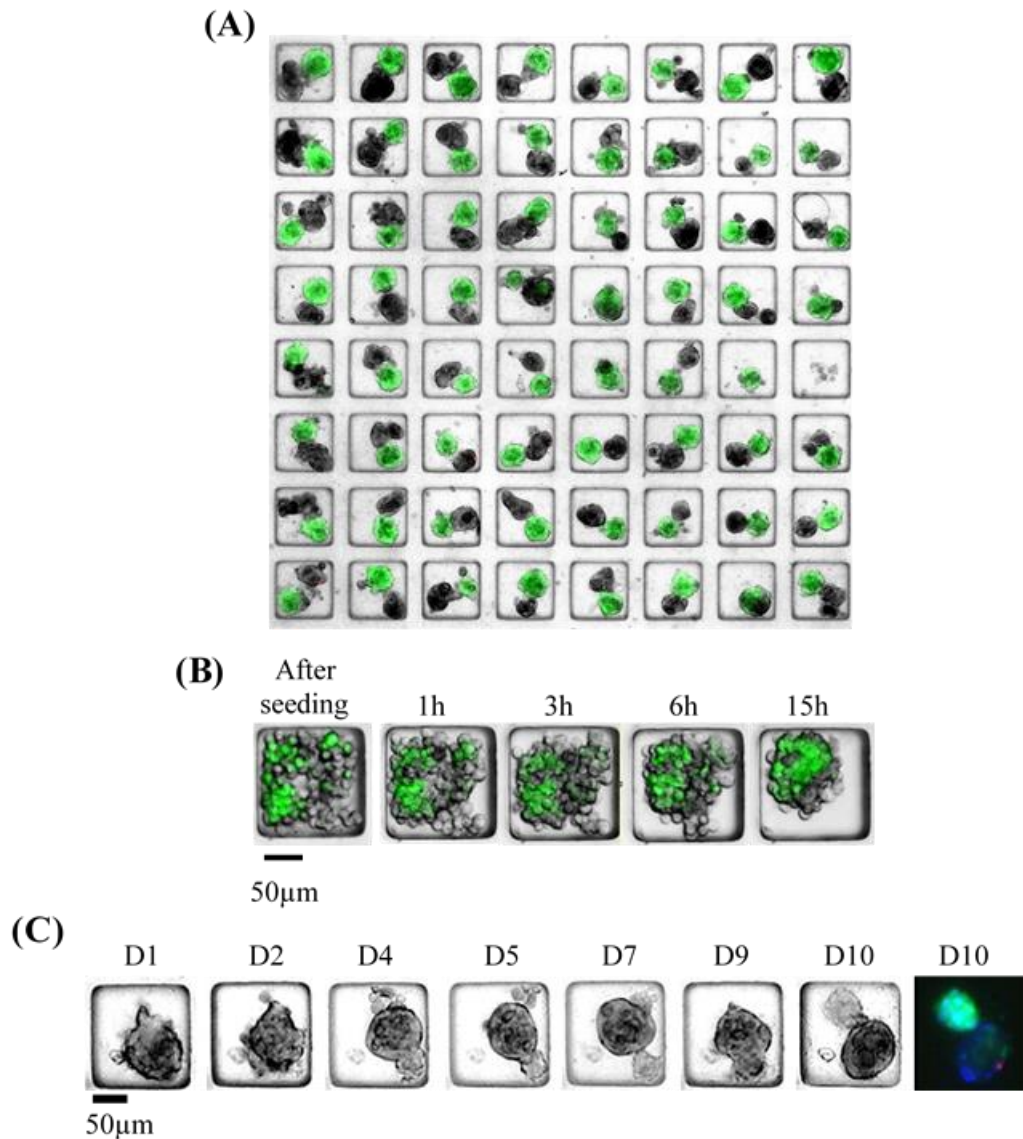
Figure 4.2 *Preliminary 1:1 Cancer cell: CAF Spheroid Co-cultures. (A) Brightfield image of array showing Cellaria Wood primary breast cancer cells in co-culture with CAF (green) on day 7 of culture.(5x magnification) (B) Still image sequence of co-cultured CAF and cancer cells taken from a time-lapse recording showing the dissociation of the two cells types over 15h after initial being seeded together simultaneously. (C) Brightfield image timeline of 1:1 primary breast cancer cell to CAF co-culture with fluorescent image from staining on day 10 showing GFP transfected CAF (green), PI (red) and Hoechst.(blue).*

The Cellaria Wood cell line was selected as Cellaria models are derived from patient tumours, the Cellaria Wood model originating from an infiltrating ductal and lobular breast carcinoma.[242] Cellaria cell lines possess a diverse cell population that has been characterized and compared to the original tumour.[242] Optimization of customary seeding protocols (**Section 2.7**) for CAF-cancer cell co-cultures was carried out as preliminary microfluidic cultures showed large differences between cells cultured in the external columns of the end arrays in comparison to spheroids in the central arrays. Additional flow was required to drive cells

further into the device to achieve an equal seeding pattern across the array of microwells (**Figure 4.2**A). The phenomena of CAF aggregating together is known to occur naturally in native tumours.[243] CAF-breast cancer cell dissociation was shown to begin soon after cell injection, with a large proportion of the two cell types already separated within the first three hours of co-culture (**Figure 4.2**B). The separation of cancer cells and CAF was maintained over a 10 day culture period (**Figure 4.2**C).

The CAF dissociation from cancer cells noted in microfluidic cultures was consistent with observations from equivalent 2D experiments from collaborators and with ovarian tumour histology sections (**Figure 4.3**).
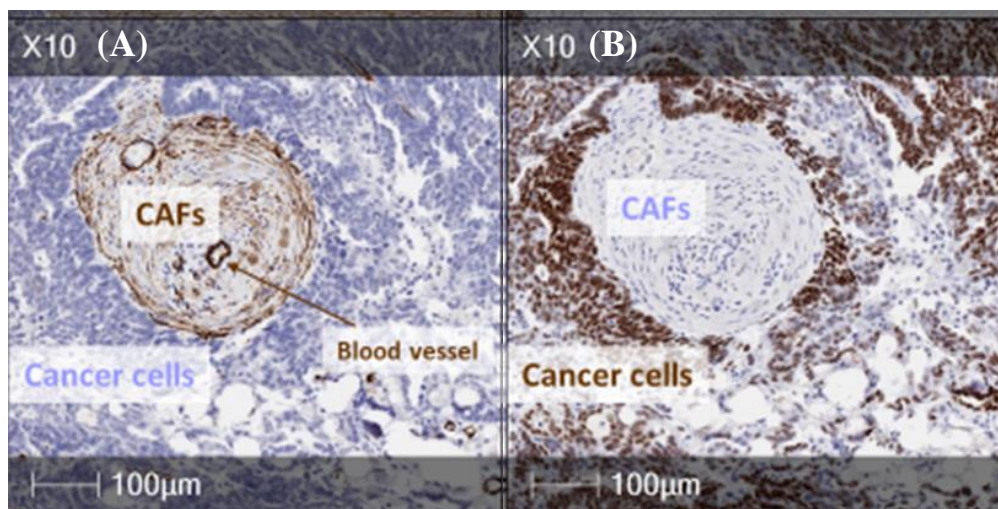
Figure 4.3 *Diaminobenzidine staining in Brightfield Microscopy Image (L. Neilson, Beatson Institute of Cancer Research, 2019). CAF histological sections of ovarian tumour where the (A) left hand side image shows staining for alpha-smooth muscle actin (SMA, CAF=brown, remaining tumour section=violet) and the (B) right hand side image shows staining for Wilms Tumour Protein (WT-1, Cancer cells=brown, remaining tumour section including CAF=violet).*

Images obtained by L. Neilson (Beatson Institute) using diaminobenzidine staining and brightfield microscopy show same region of tumour and stroma on consecutive sections. The left hand side image displays areas stained for alpha-SMA, a marker for fibroblasts (**Figure 4.3**A). Here, CAF are shown in brown and the remainder of the tumour, the majority of which is composed of cancer cells, in blue. The right hand side image shows the same areas but with staining for a marker of tumour cells, Wilms Tumour Protein (**Figure 4.3**B). In this image cancer cells are indicated in brown and the remaining tumour section, including CAF, in blue.

Quantification of collagen production (**Section 2.11.4**) was also performed for preliminary experiments (**Figure 4.4**).
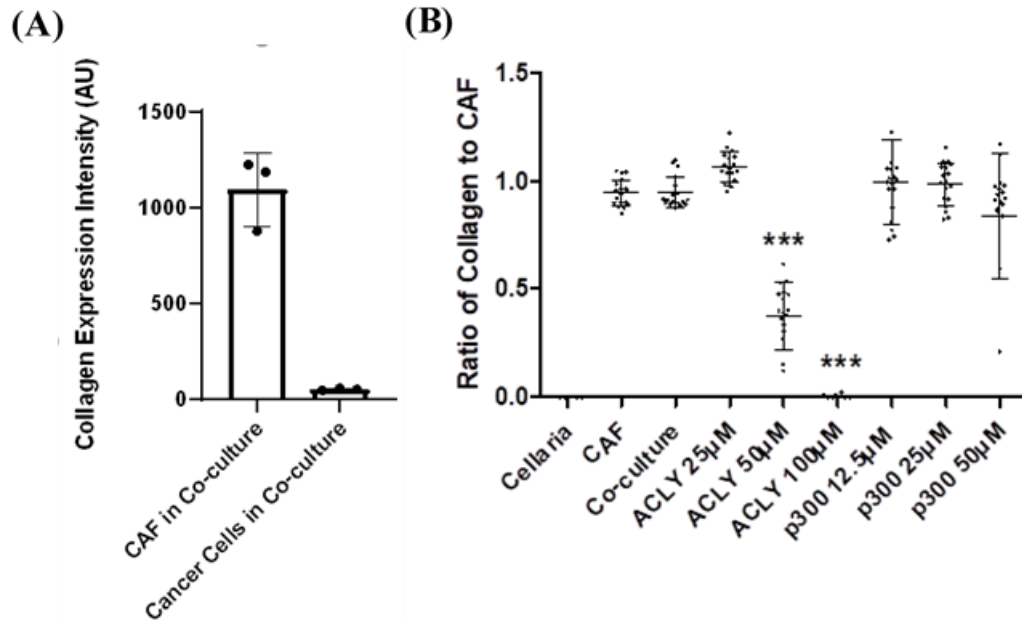
Figure 4.4 *Quantification of collagen production for preliminary experiments. (A) Plot of collagen deposition signal intensity for cancer cells and CAF in control co-culture conditions. n=3. Plot shows a significant difference. (***P ≤0.0001) between collagen deposition of CAF and cancer cell areas in co-cultures. Data shown as mean ± SD. ***P ≤0.0001, t-test. (B) Ratio of collagen to CAF areas after 10 days of culture. Inhibitor treatments were applied to co-cultures seeded in a 1:1 ratio of cancer cells to CAF. n=18. Data shows a significant difference in collagen: CAF ratio (***P ≤0.0001) between 50μM and 100μM ACLY inhibitor treated spheroids and control co-culture spheroids. Data shown as mean ± SD. ***P ≤0.0001, One-way ANOVA, Bonferroni's post-test.*

CAF and cancer cell collagen expression was quantified separately in co-culture control conditions (**Figure 4.4**A). A t-test was performed and showed that the majority of collagen produced in co-cultures (***P ≤0.0001) was shown to originate from CAF and not cancer cells. Thus, plotting the ratio of collagen area over CAF area to establish changes in collagen deposition was selected as an appropriate and robust method of data presentation for this model (**Section 2.14**). The mean ratio of collagen: CAF was found to be 1:1 for CAF and co-culture conditions with cancer cell monocultures producing negligible levels. Preliminary inhibitor testing showed that only the ACLY inhibitor triggered a significant reduction in collagen deposition at the higher levels when compared to a 1:1 control co-culture (**Section 2.8**). One-way ANOVA analysis showed the 50μM ACLY inhibitor concentration caused a reduction in collagen: CAF ratio to 1:3 (***P ≤0.0001) while the 100μM concentration resulted in a reduction in collagen: CAF ratio to 1:405 (***P ≤0.0001) (**Figure 4.4**B). There was no significant change in collagen production for cultures treated with the p300 inhibitor at concentrations ranging from 12.5-50μM. Thus, the decision was made to increase these values for subsequent experiments. This range was initially selected as a statistically significant effect was seen in 2D experiments from collaborators (Not shown) using lower concentrations of the

p300 than the ACLY. It was expected that p300 may be a more powerful inhibitor than ACLY 3D as it is in 2D. However, this was not the case for 3D spheroid assays.

For the second phase of experiments, viability and collagen expression analysis were perfomed for a range of ratios of cancer cells to CAF (1:1, 1:3, 1:5, 3:1 and 5:1) (**Figure 4.5**). Equivalent 2D experiments were also carried out by collaborators for comparison (Not shown).
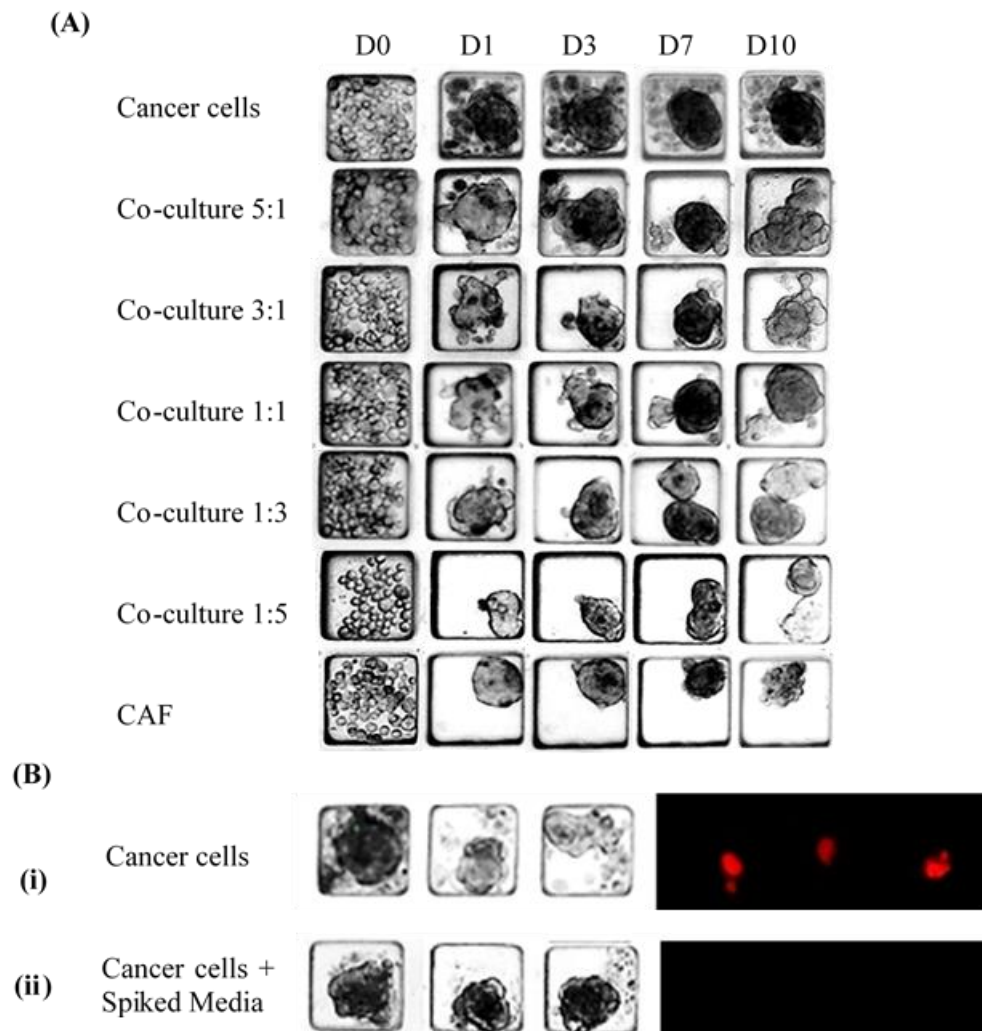
Figure 4.5 *Testing of cancer cell: CAF seeding ratios. (A) Brightfield image timelines of varying ratios of primary breast cancer cell-CAF spheroids. (B) Brightfield images with collagen fluorescent overlay (left) and fluorescent images of PI (right) staining (red) for (i) cancer spheroids cultured in regular RETM culture media and (ii) cancer spheroids cultured in RETM culture media spiked in a 1:1 ratio with CAF supernatant. (5x magnification)*

Over the 10 day culture period, cancer cells appeared less disaggregated when in co-culture with CAF in comparison to when cultured alone (**Figure 4.5**A). CAF monoculture spheroids were also observed to become more disaggregated and smaller in size as their time in culture progressed. However, this was not the case when in co-culture with cancer cells and suggests that both cell types are beneficial to the other's 3D culture. Brightfield image timelines of spheroids appeared to show a slight growth in co-cultures with a higher proportion of CAF

present. Therefore, the effect of cancer cell culture in CAF supernatant was also studied in devices (**Figure 4.5**B). Collagen signal was too weak to be detected and could not be observed when overlaid onto brightfield images for both cancer cell monocultures regardless of whether they were cultured in regular RETM media or with media that had been spiked with CAF supernatant. Fewer dead cancer cells were observed in cultures which had been exposed to CAF supernatant in a 1:1 mix with their customary RETM media. This demonstrated that CAF are not necessarily required to improve viability but that it is factors that they are able to secrete into the surrounding media which are beneficial to cancer cell survival. No change to collagen deposition was noted.

Viability staining on day 10 demonstrated the beneficial effect of the CAF on the cancer cells with fewer dead cancer cells in the co-culture than when in monoculture (**Section 2.11.3**). PI staining was performed for all cultures whilst FDA was administered only to cancer cell monoculture spheroids due to CAF being transfected with GFP (**Figure 4.6**).
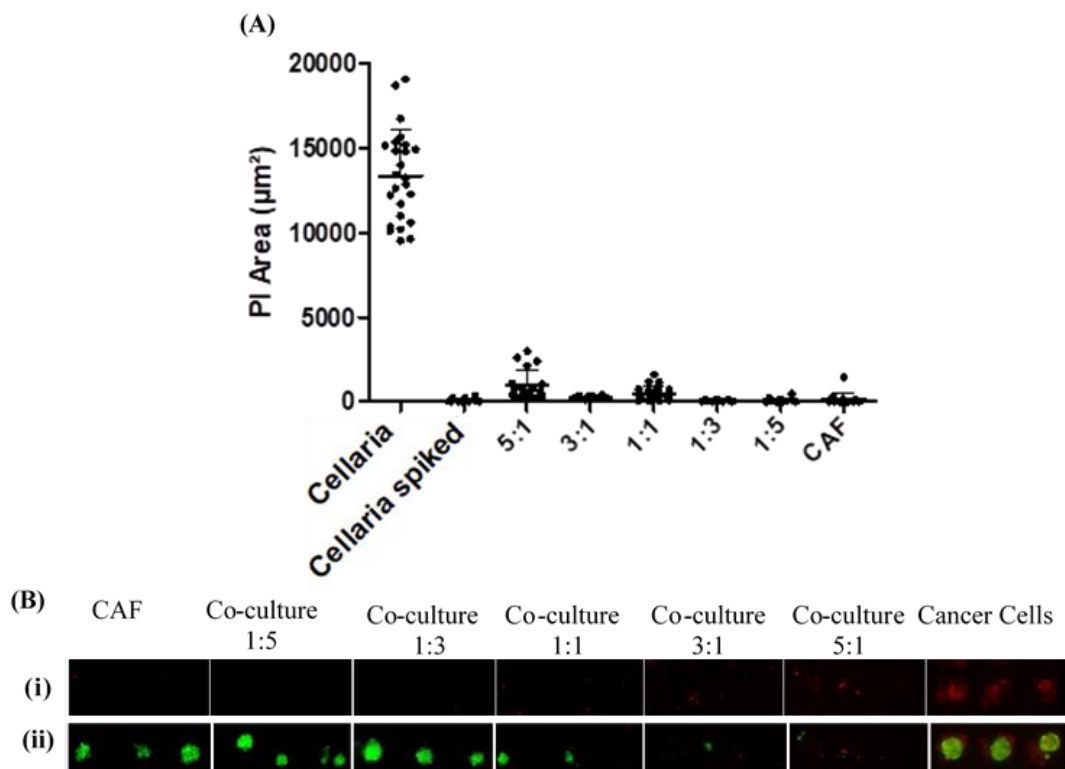
Figure 4.6: *Quantification of PI area and collagen staining of various cancer cell: CAF seeding ratios. (A) Plot of PI area. n=16. Cellaria spiked: cancer cell monocultures with media spiked with CAF supernatant in a 50:50 ratio. (B) Fluorescent images of spheroids after viability staining on day 10. (Green = CAF in co-cultures and FDA in primary breast cancer cell monocultures, red = PI). (i) PI (red) signal only. (ii) PI (red) signal for all culture conditions and FDA (green) for primary breast cancer cell monocultures only. Data shown as mean ± SD. ***P ≤0.0001, One-way ANOVA, Bonferroni's post-test.*

Less cell death in co-cultures with a higher CAF proportion was observed. However, this was minimal and non-significant (**Figure 4.6**A). Quantification of PI signal and one-way ANOVA analysis revealed a significant reduction (***P ≤0.0001) in all co-culture conditions in comparison to when cancer cells were cultured alone. It should also be noted that due to the CAF transfection with GFP, it was possible to differentiate between dead cancer cells (red), which make up the entirety of the dead cells in the co-culture, and CAF (yellow) (**Figure 4.6**B).

Quantification of cell areas and collagen deposition was also conducted for the various seeding ratios (**Figure 4.7**).
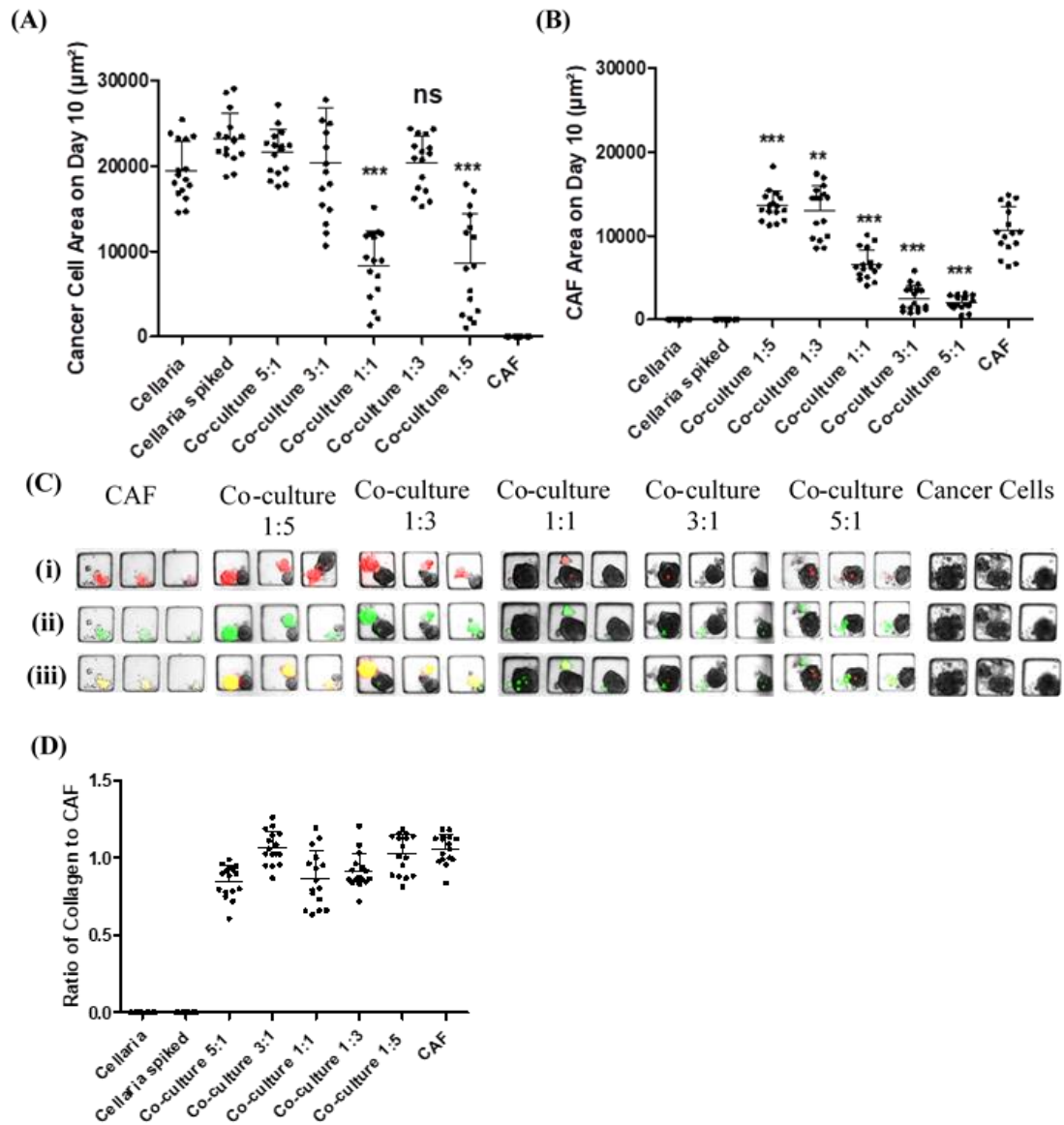
Figure 4.7 *Quantification of cell area and collagen deposition from testing of Cancer cell: CAF seeding ratios.*
(A) Plot of cancer cell area on day 10 of culture. n=16. Data shows a significant difference in cancer cell area
*(***P ≤0.0001) between control cancer cell monoculture spheroids and 1:1 and 1:5 co-cultures. (B) Plot of CAF*
spheroid area on day 10 of culture. n=16. Data shows a significant difference in CAF area between control CAF
*monoculture spheroids and 1:5, 1:1, 3:1 and 5:1 co-cultures (***P ≤0.0001) and 1:3 co-cultures (**P ≤ 0.01). (C)*
Brightfield images with (i) Collagen (red) overlay = first row (ii) CAF (green) overlay = second row (iii) Collagen
and CAF (yellow) overlay = third row. (D) Plot of ratio of collagen to CAF area. n=16. (5x magnification) Data
*shown as mean ± SD. ***P ≤0.0001, **P ≤ 0.01, One-way ANOVA, Bonferroni's post-test.*

By day 10 of culture no significant difference in cancer spheroid size between cells cultured
in RETM or spiked media was observed (**Figure 4.7**A). No significant difference between
cancer spheroid areas was recorded for the 1:3 ratio in comparison to cancer monoculture
spheroids. A significant difference (***P ≤0.0001) between the size of control CAF spheroids
and all of the variations of ratios tested was recorded using one-way ANOVA analysis, with

the 1:3 co-culture shown to produce the most similarly sized CAF spheroids to that of the monocultures (**Figure 4.7**B).

Subsequently, collagen deposition was also analysed for the range of cancer:CAF culture ratios (**Figure 4.7**C). Image analysis of the collagen deposition established that the amount of collagen signal detected was proportional to the amount of CAF present in the co-culture. Minimal collagen signal was detected from breast cancer cells when cultured alone (**Figure 4.7**D). Quantifying this data confirmed that independent of the co-culture ratio, a 1:1 ratio of CAF to collagen is always present. Since collagen expression levels in co-cultures were dependent upon the proportion of CAF present, collagen deposition was only considered in areas where CAF were present.

4.2 Cancer Cell:CAF Inhibitor Testing at 1:3 Seeding Ratio

The 1:3 cancer cell to CAF ratio was selected for inhibitor testing as this co-culture delivered a healthy phenotype with good viability, produced the same size of cancer spheroids in co-culture as when in monoculture. Inhibitor concentrations were initially selected based on 2D results from collaborators. However, subsequent experiments included a higher concentration of the p300 inhibitor in order to elicit detectable effects in 3D cultures (ACLY: 25µM, 50µM and 100µM, p300: 25µM,50µM and 100µM) (**Figure 4.8**).
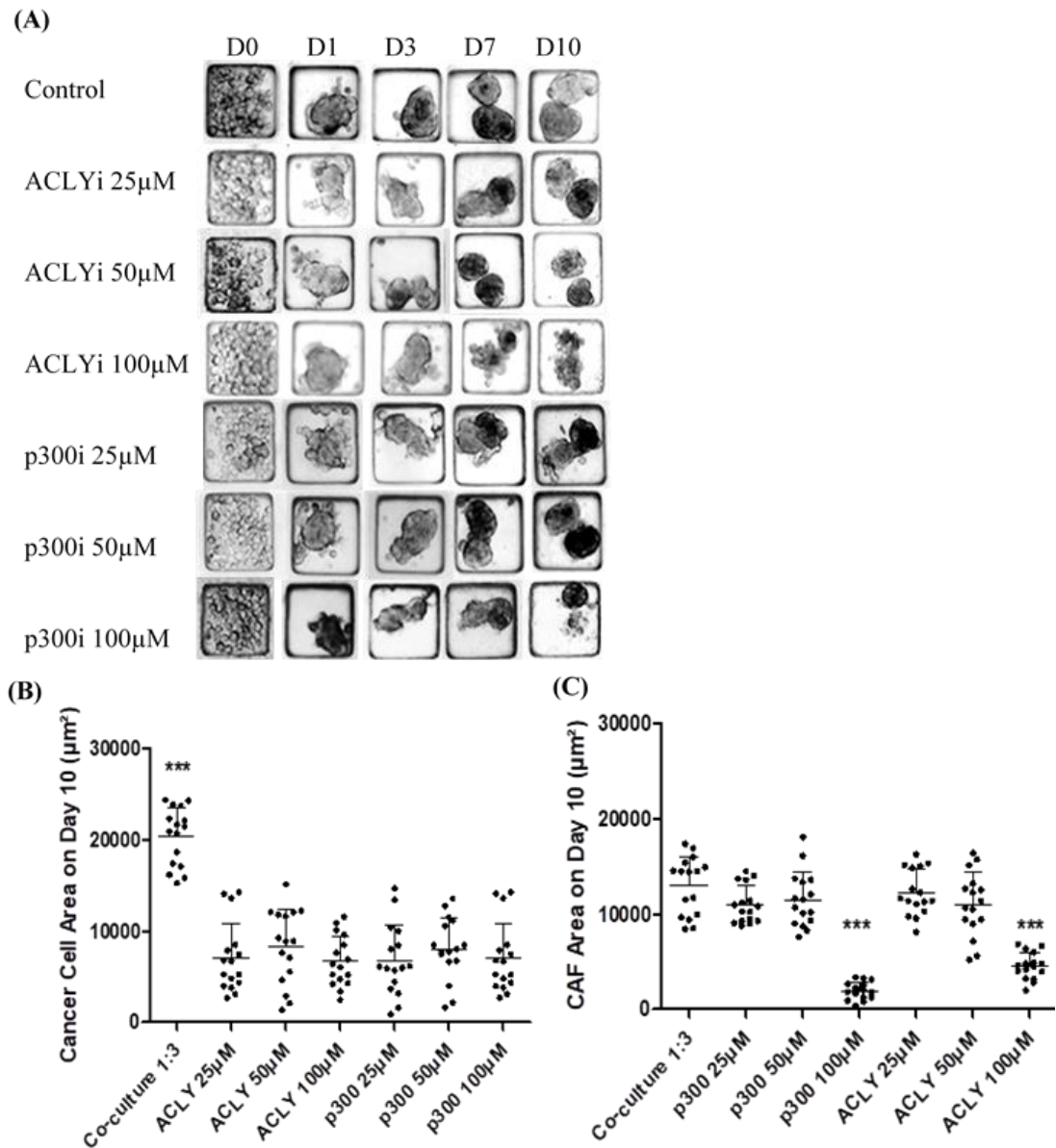
*Figure 4.8 Treatment of 1:3 Cancer cell: CAF Spheroids with ACLY and p300 inhibitor treatments. (A) Brightfield images of spheroid temporal evolution from days 0-10 (B) Plot of cancer spheroid areas on day 10. n=16. Data shows a significant difference in cancer cell area (***P ≤0.0001) between control 1:3 co-cultures and all inhibitor treated spheroids. (C) Plot of CAF spheroid areas on day 10. n=16. Data shows a significant difference in CAF area (***P ≤0.0001) between control 1:3 co-cultures and 100μM p300 inhibitor treated and 100μM p300 inhibitor treated co-cultures. (5x magnification) Data shown as mean ± SD. ***P ≤0.0001, One-way ANOVA, Bonferroni's post-test.*

Greater disaggregation at higher inhibitor concentrations was observed in spheroid timelines with reduced spheroid size in comparison to control and low inhibitor concentrations (**Figure 4.8**A). Once again, CAF can be seen to group together from early on in the culture period and remain clustered, even when treated with high inhibitor concentrations of up to 100μM. A significant difference (***P ≤0.0001) in cancer spheroid size between control and all inhibitor conditions was recorded via one-way ANOVA analysis (**Figure 4.8**B). Whereas, a significant

reduction (***P ≤0.0001) in CAF spheroid area was only seen with one-way ANOVA analysis between control and the highest concentration of ACLY and p300 inhibitor concentrations but not lower values (**Figure 4.8**C). Cell death and collagen deposition were also quantified (**Figure 4.9**).
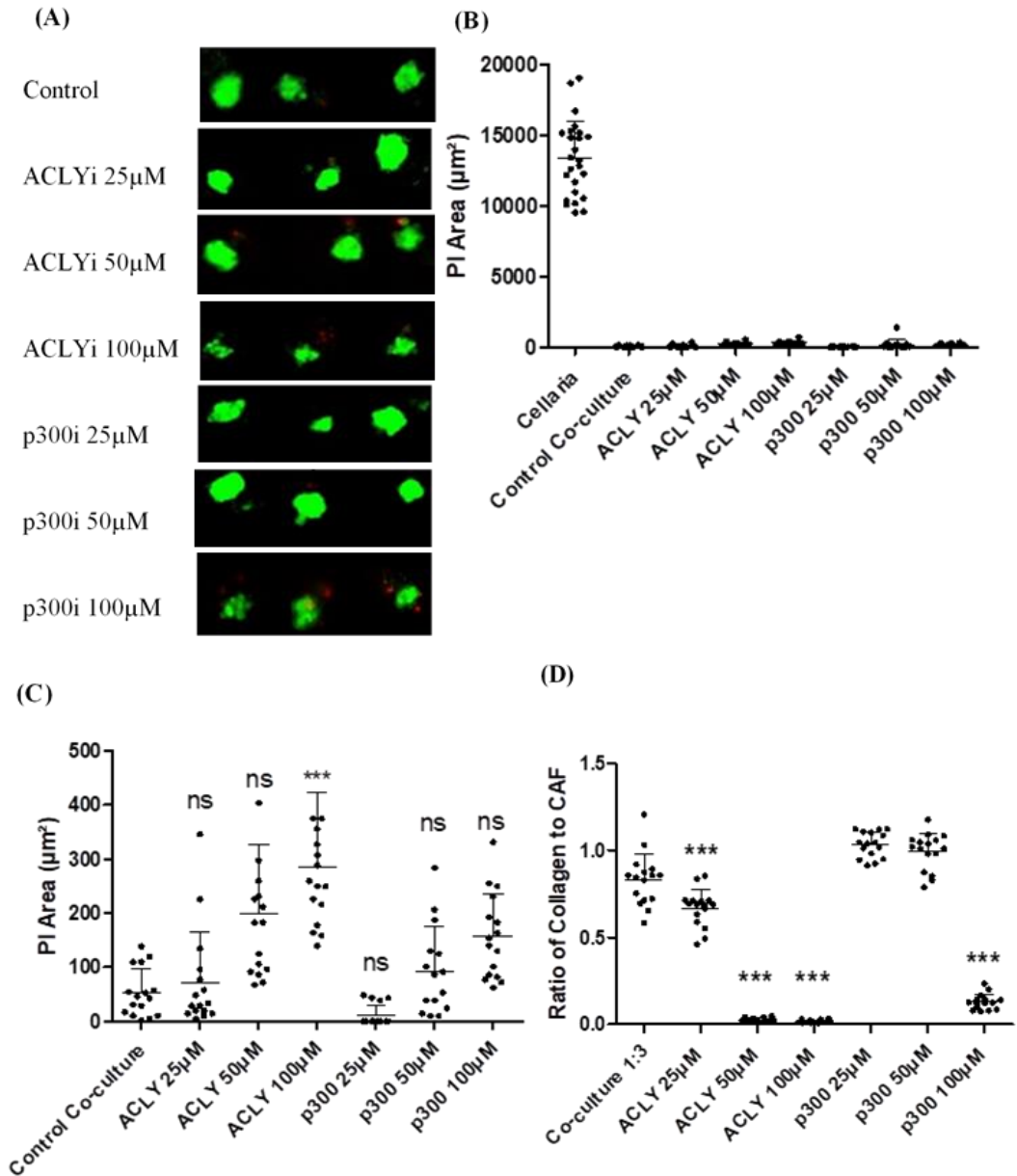
Figure 4.9: *Quantification of PI area and collagen deposition for 1:3 Cancer cell: CAF Spheroids treated with ACLY and p300 inhibitor treatments. (A) Fluorescent images of cancer cell and CAF (green) staining with PI (red) on day 10 of culture. Three spheroids were selected to include in the figure for each condition that were representative of those used for data analysis. (B) Plot of PI area. n=16. Data shows a significant difference in PI area (***P ≤0.0001) between cancer cell monocultures and all other co-culture conditions. (C) Plot of PI area with adjusted y-axis for visualisation of lower values. n=16. Data shows a significant difference in PI area (***P ≤0.0001) between control co-cultures and 100μM ACLY inhibitor treated spheroids. (D) Plot of collagen to CAF area ratio. n=16. Data shows a significant difference in collagen deposition (***P ≤0.0001) between control co-cultures and 50μM ACLY inhibitor, 100μM ACLY inhibitor and 100μM p300 treated spheroids. (5x magnification) Data shown as mean ± SD. ***P ≤0.0001, One-way ANOVA, Bonferroni's post-test.*

Viability analysis showed a negative effect of inhibitors could be seen on cancer cell viability but not CAF (**Figure 4.9**A). Interestingly, inhibitor treated spheroids were shown to be more viable (***P ≤0.0001) than cancer cells when cultured alone, without CAF using one-way ANOVA analysis (**Figure 4.9**B). Increasing PI area was recorded with increasing inhibitor concentrations for both ACLY and p300 (**Figure 4.9**C). However, only a statistically significant increase (***P ≤0.0001) in PI area was recorded with one-way ANOVA analysis for the 100μM ACLY inhibitor treatment. Quantification of collagen to CAF area ratios on day 10 of culture were consistent with preliminary data (**Figure 4.9**D). 1:3 cancer cell: CAF co-cultures again showed the greatest reduction in collagen production for the 100μM ACLY inhibitor, with a Collagen: CAF ratio of 1:56, followed by the 50μM concentration, with a collagen: CAF ratio of 1:37. Both control spheroids and those treated with lower doses of ACLY or p300 inhibitors recorded a mean Collagen: CAF ratio of 1:1. Treatment of spheroids with 100μM p300 inhibitor exhibited a reduction in collagen production to 1:8. The ACLY inhibitor decreased collagen deposition with increasing concentration while the p300 inhibitor was able to trigger a significant reduction (***P ≤0.0001) in collagen deposition at the highest concentration in comparison to control co-cultures, detected by one-way ANOVA analysis. Therefore, ACLY inhibitor was able to limit collagen expression to a much greater degree than p300 inhibitor in 3D culture.

In summary, the initial findings demonstrated cancer cells improved viability in 3D when in co-culture with CAFs and also when exposed to CAF conditioned media. Different ratios of cancer cells to CAF resulted in variation in collagen deposition which was found to be proportional to the number of CAF present in co-cultures. Increasing the concentration of both inhibitors triggered a reduction in collagen deposition with no substantial effect on the viability of the majority of cancer cells. However, higher inhibitor concentrations limited cancer cell and CAF spheroid growth. The need to use greater drug concentrations in 3D cultures to detect measurable cytotoxic effects is in agreement with reports from the literature and emphasizes the value of 3D *in vitro* assessment to provide drug testing information. It is known that 3D assays can commonly show increased resistance to anti-cancer drugs than comparative 2D cultures.[244] In addition, stromal cells can also offer protection to tumour cells against anti-cancer agents.[245]

4.3 Cancer Cell:CAF Inhibitor Testing at 1:1 Seeding Ratio

For this series of experiments, the seeding protocol was adapted using cancer cells and CAF in a 1:1 ratio to achieve a larger proportion of similarly sized spheroids throughout the array that would be suitable for analysis. This was as a result of cell seeding in devices proving more

challenging when higher numbers of fibroblasts were present in cell seeding suspension due to their tendency to aggregate in cell suspension and in channels when seeding. Inhibitors were added on the first day of culture and replenished every second day for one week prior to staining and imaging on day 7 (**Figure 4.10**).
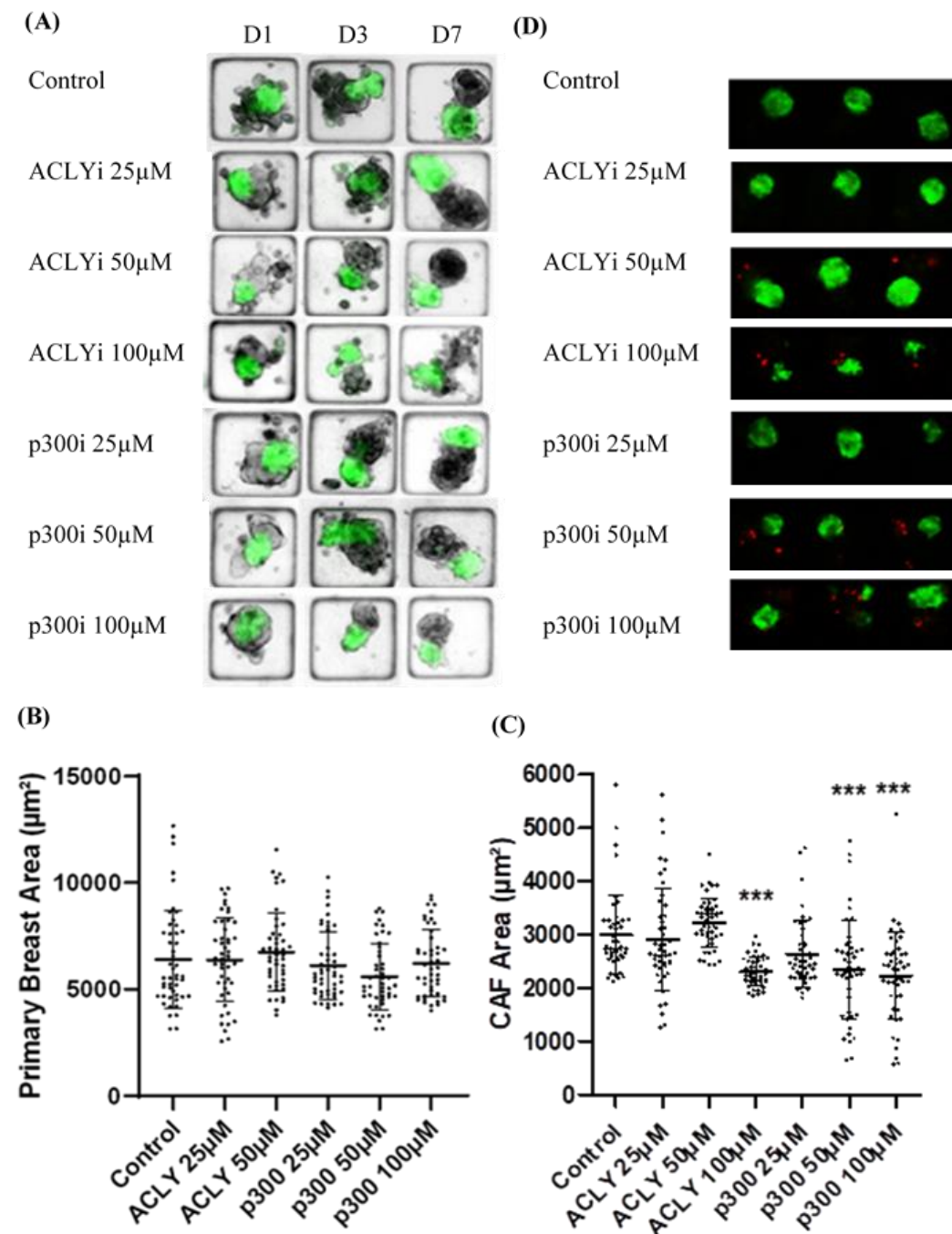
Figure 4.10 *Treatment of 1:1 Cancer cell: CAF Spheroids with ACLY and p300 inhibitor treatments. (A) Brightfield image timelines with CAF channel (green) overlay of spheroids from days 1-7. (B) Fluorescence images of viability staining of 1:1 cancer cell and CAF (green) co-cultures on day 7 with PI (red). (C) Cancer spheroid areas on day 7. n=48. (D) CAF spheroid areas on day 7. n=48. Data shows a significant difference (***P ≤0.0001) in CAF area between control co-cultures and 100μM ACLY inhibitor, 50μM p300 inhibitor and 100μM p300 inhibitor treated spheroids. (5x magnification) Data shown as mean ± SD. ***P ≤0.0001, One-way ANOVA, Bonferroni's post-test.*

Due to greater disaggregation at higher ACLY inhibitor concentrations, quantification of cancer and CAF areas was not obtainable for these spheroids (**Figure 4.10**A). A negative effect of inhibitors on cancer cell viability but not CAF could again be noted (**Figure 4.10**B). There was no significant difference in cancer spheroid size between control and all inhibitor conditions (**Figure 4.10**C). Variability in the size of spheroids occurs as a result of initial variation in seeding density across arrays, as discussed previously in Chapter 3. For analysis, spheroids from the two outer arrays were selected for analysis as those in central arrays were too small due to fewer cells traveling further through the channel during the seeding process. For future immunoassays in Chapter 5, a device with a shorter channel length was selected to provide more uniformly sized spheroid generation across arrays. CAF spheroid size was reduced for spheroids treated with the greater inhibitor concentrations in comparison to controls (**Figure 4.10**D). A significant difference (***P $\leq$0.0001) in CAF spheroid area between control and the highest inhibitor concentrations was detected by one-way ANOVA analysis. Thus, higher inhibitor concentrations were found to limit CAF but not cancer spheroid growth. Cell death and collagen deposition was quantified (**Figure 4.11**).
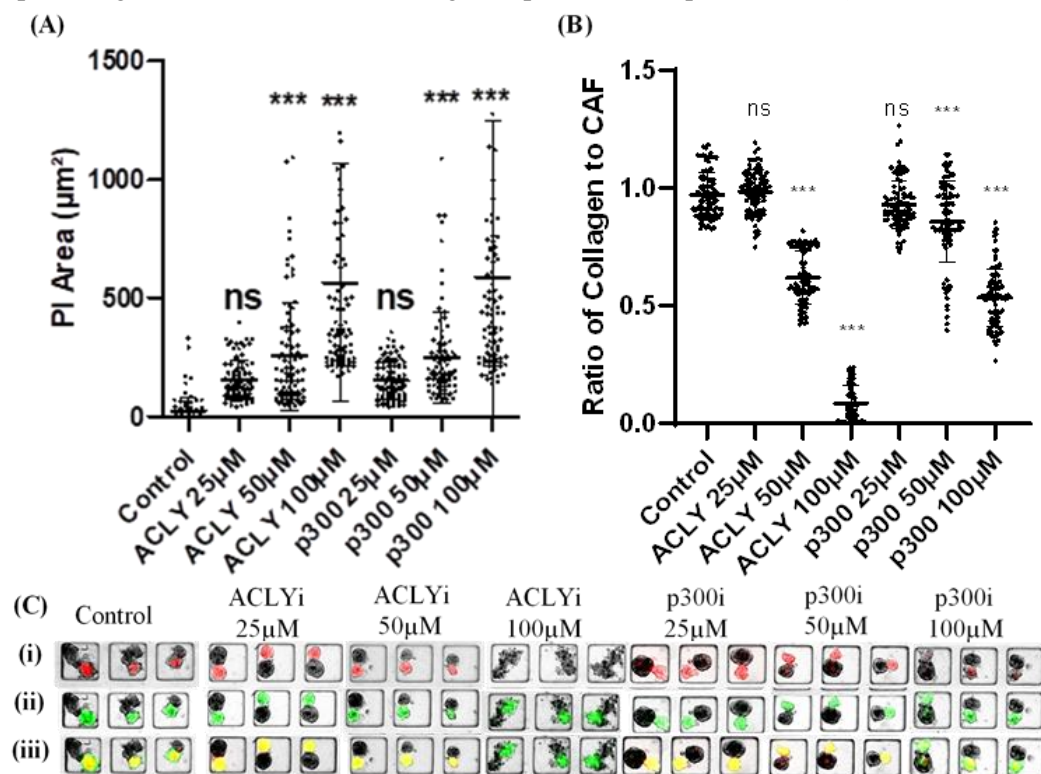
Figure 4.11: *Quantification of PI area and collagen deposition for 1:1 Cancer cell: CAF Spheroids treated with ACLY and p300 inhibitor treatments. (A) Plot of PI signal. n=90. Data shows a significant difference in PI area (***P $\leq$0.0001) between control spheroids and those treated with 50μM ACLY inhibitor, 100μM ACLY inhibitor, 50μM p300 inhibitor and 100μM inhibitor concentrations. (B) Quantification of collagen to CAF ratios with mean values. n=90. Data shows a significant difference in collagen deposition (***P $\leq$0.0001) between control spheroids and those treated with 50μM ACLY inhibitor, 100μM ACLY inhibitor, 50μM p300 inhibitor and 100μM inhibitor concentrations. (C) Brightfield images with (i) Collagen overlay (red) = first row (ii) CAF overlay (green) = second row (iii) Collagen and CAF overlay (yellow) = third row (5x magnification) Data shown as mean ± SD. ***P $\leq$0.0001, One-way ANOVA, Bonferroni's post-test.*

A significant increase in PI signal (***P ≤0.0001) for the highest inhibitor concentrations was detected with one-way ANOVA analysis in comparison to controls (**Figure 4.11**A). As seen in the previous experimental set-up, inhibitors decreased collagen expression with greater disaggregation of spheroids at higher concentrations (**Figure 4.11**B and C). The greatest reduction of collagen: CAF ratio was observed for the 100µM concentration (1:12 collagen: CAF ratio), followed by the 50µM concentration (1:2 collagen: CAF ratio). Treatment of spheroids with 100µM p300 inhibitor also triggered a reduction in collagen expression, giving a collagen: CAF ratio of 1:2. All other conditions maintained the same mean collagen: CAF ratio as that of control spheroids, 1:1.

In conclusion, a co-culture of two different tumour components was established and used to determine the toxicity and limitation to collagen deposition of two enzyme inhibitors. CAF were shown to have a beneficial effect on cancer cell survival, even when exposed to enzyme inhibitors treatment. This effect was seen not only from direct co-culture but also when cancer cells were cultured in media spiked with CAF supernatant. It was established that CAF produce collagen to a far greater extent than cancer cells and that varying the proportion of CAF in a co-culture proportionally varies the collagen deposition. It was observed that both inhibitors were able to limit collagen expression with a significant effect on cancer cell but not CAF viability at higher concentrations. At the greater concentrations, a significant reduction in CAF but not cancer cell area was observed, in concurrence with more pronounced disaggregation.

4.4 Spheroid Recovery with Rescue Agents: Proline Rescue of PYCR1 inhibitor Spheroids

The next enzyme inhibitor involved in the collagen deposition cycle to be investigated was against PYCR1. In addition to determining the effect of this inhibitor on collagen production and viability of the co-culture, the aim was also to establish the ability of using proline (500mM) as a rescue agent to recover treated cultures (**Figure 4.12**).
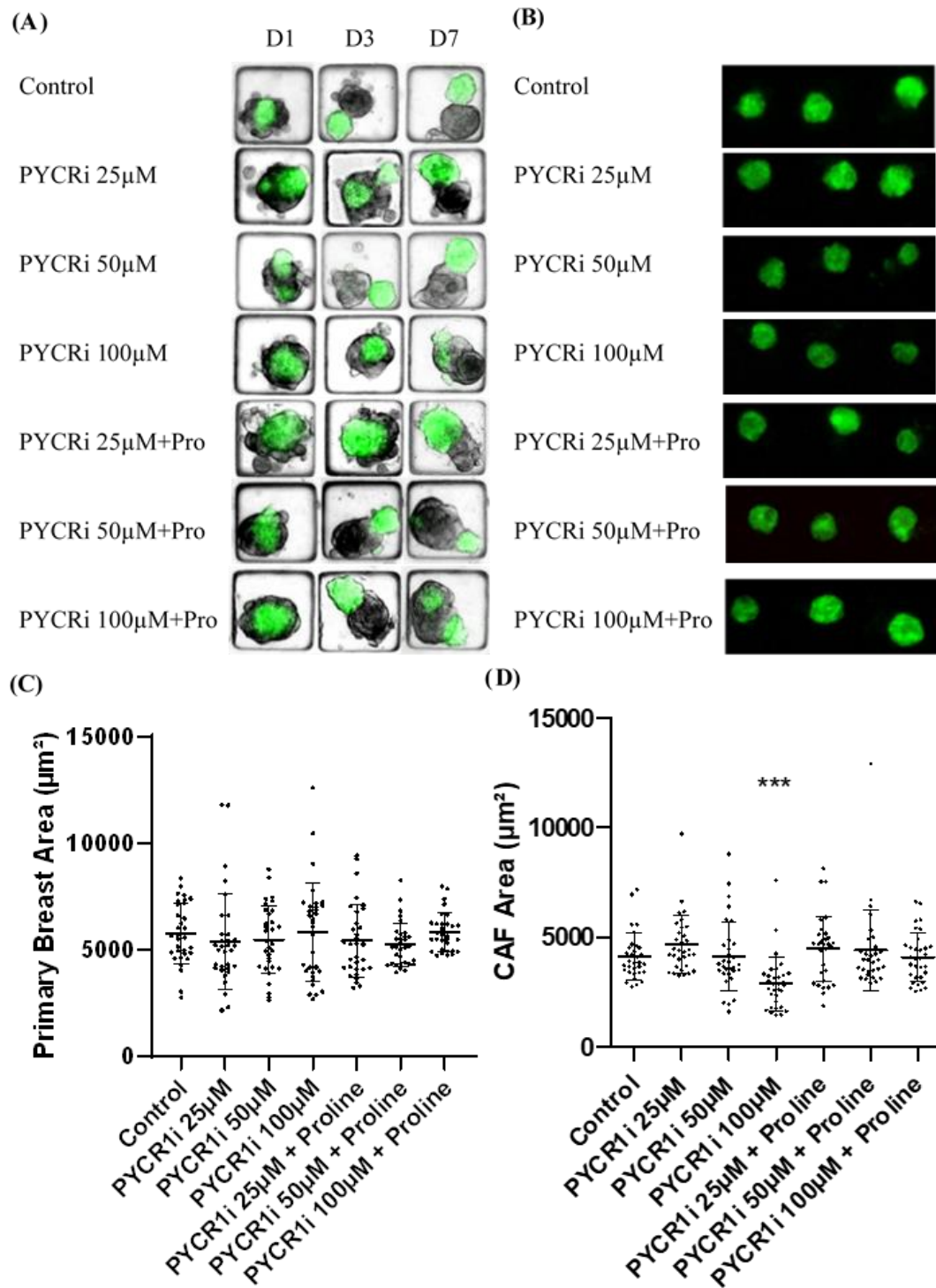
Figure 4.12 *Recovery of PYCR1 inhibitor treated spheroids with proline as a rescue agent. (A) Brightfield image timelines with CAF channel (green) overlay of spheroids from days 1-7. (B) Fluorescence images of viability staining with PI (red) of 1:1 cancer cell and CAF (green) co-cultures on day 7. (C) Cancer spheroid areas on day 7. n=32. (D) CAF spheroid areas on day 7. n=32. Data shows a significant difference (***P ≤0.0001) in CAF area between control co-cultures and those treated with the 100μM PYCR1 inhibitor concentration. (5x magnification) Data shown as mean ± SD. ***P ≤0.0001, One-way ANOVA, Bonferroni's post-test.*

PYCR1 inhibitor exposure did not cause disaggregation of either cell type (**Figure 4.12**A). Viability staining of cultures revealed no toxicity of this inhibitor towards either cell type (**Figure 4.12**B). There was no significant difference in cancer spheroid size with CAF remaining dissociated from the cancer spheroid in all conditions (**Figure 4.12**C). A statistically significant reduction (***P ≤0.0001) was detected with one-way ANOVA analysis for CAF spheroid size between spheroids treated with the highest inhibitor concentration and control co-cultures and was negated by proline administration (**Figure 4.12**D). Quantification of dead cell area and collagen deposition was carried out (**Figure 4.13**).
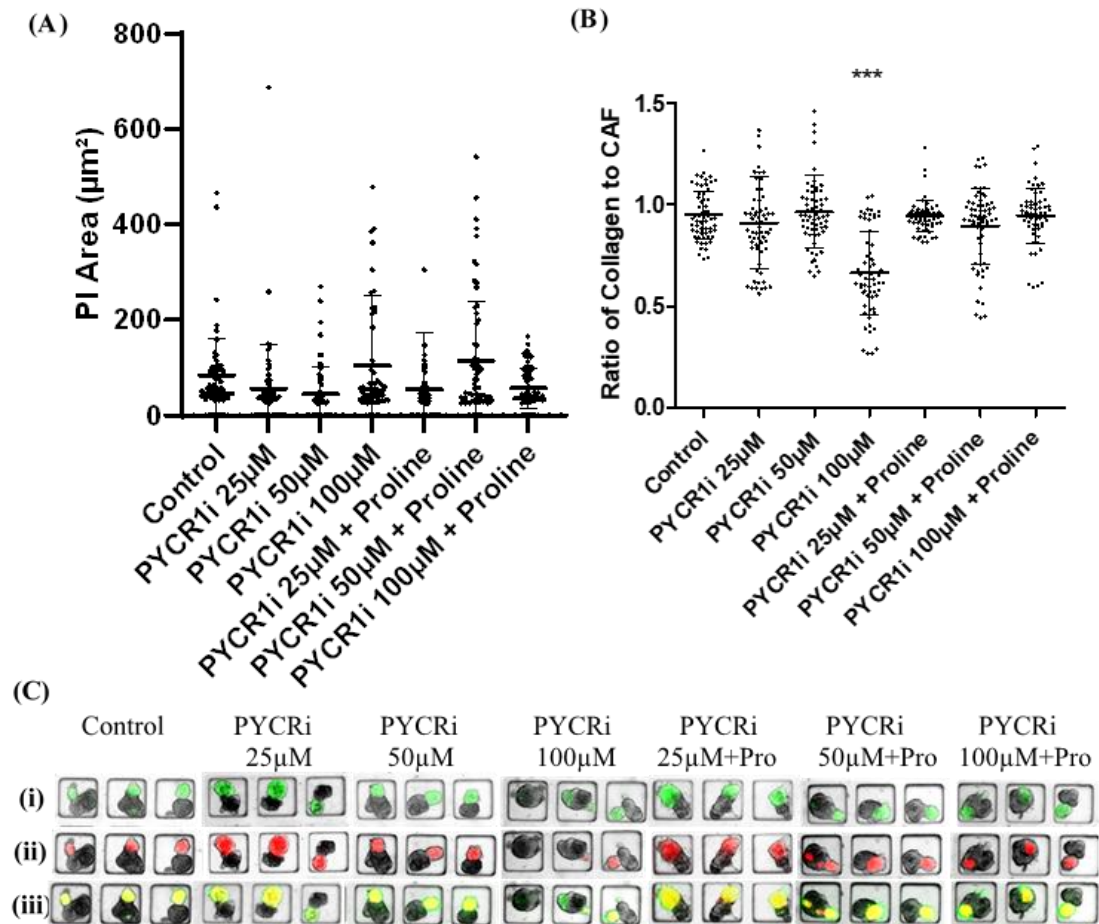
*Figure 4.13: Quantification of PI area and collagen deposition for PYCR1 inhibitor treated spheroids. (A) Plot of PI area. n=64. (B) Plot of collagen to CAF area ratios. n=64. Data shows a significant difference (***P ≤0.0001) in collagen deposition between control spheroids and those treated with the 100µM PYCR1 inhibitor concentration. (C) Brightfield images with (i) Collagen overlay (red) = first row (ii) CAF overlay (green) = second row (iii) Collagen and CAF overlay (yellow) = third row. (5x magnification) Data shown as mean ± SD. ***P ≤0.0001, One-way ANOVA, Bonferroni's post-test.*

No significant difference in PI signal for inhibitor treated spheroids in comparison to control spheroids was observed (**Figure 4.13**A). Furthermore, an effect of the PYCR1 inhibitor on collagen deposition was only detected at the highest concentration tested, 100µM, which produced spheroids with a collagen: CAF ratio of 1:2 (**Figure 4.13**B and C). This was rescued

with the addition of proline which returned the collagen to CAF ratio to 1:1. As was the case with the other enzyme inhibitors, PYCR1 inhibitor treatment reduced collagen deposition but this was shown to only occur at the highest concentration and was to a lesser extent when compared to that caused by the p300 and ACLY inhibitors.

Therefore, concentrations of PYCR1 inhibitor were increased with the aim of triggering a more pronounced effect from this treatment (**Figure 4.14**).
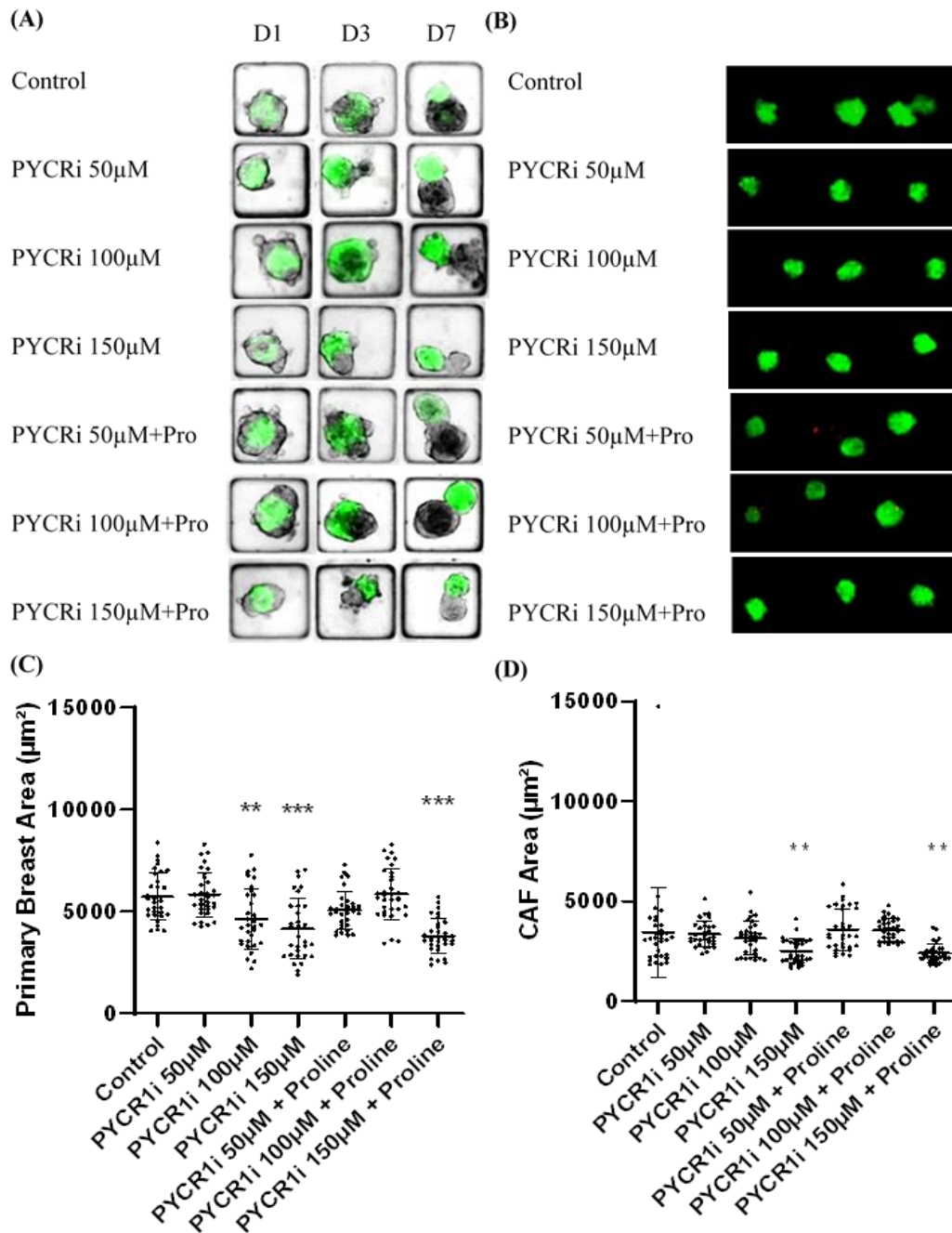
Figure 4.14 *Recovery of PYCR1 inhibitor treated spheroids with proline as a rescue agent at increased inhibitor concentrations. (A) Brightfield image timelines with CAF channel (green) overlay of spheroids from days 1-7. (B) Fluorescence images of viability staining with PI (red) of 1:1 cancer cell and CAF (green) co-cultures on day 7. (C) Cancer spheroid areas on day 7. n=32. Data shows a significant difference in cancer cell area between control spheroids and those treated with the 100μM PYCR1 inhibitor concentration (**P ≤ 0.01) and the 150μM PYCR1inhibitor concentration with and without the addition of proline (***P ≤0.0001). (D) CAF spheroid areas on day 7. n=32. Data shows a significant difference in CAF area between control spheroids and those treated with the 150μM PYCR1inhibitor concentration with and without the addition of proline (***P ≤0.0001). (5x magnification) Data shown as mean ± SD. ***P ≤0.0001, One-way ANOVA, Bonferroni's post-test.*

As seen previously, the PYCR1 inhibitor did not cause disaggregation of either cell type (**Figure 4.14**A). There was also no change in cell viability with the increased concentration (**Figure 4.14**B). However, the greater concentration of PYCR1 inhibitor did decrease cancer **Figure 4.14**C) and CAF (**Figure 4.14**D) spheroid size, of which the cancer spheroid size could be restored with proline administration for spheroids treated with PYCR1 inhibitor at 100µM. PI area and collagen deposition were quantified (**Figure 4.15**).
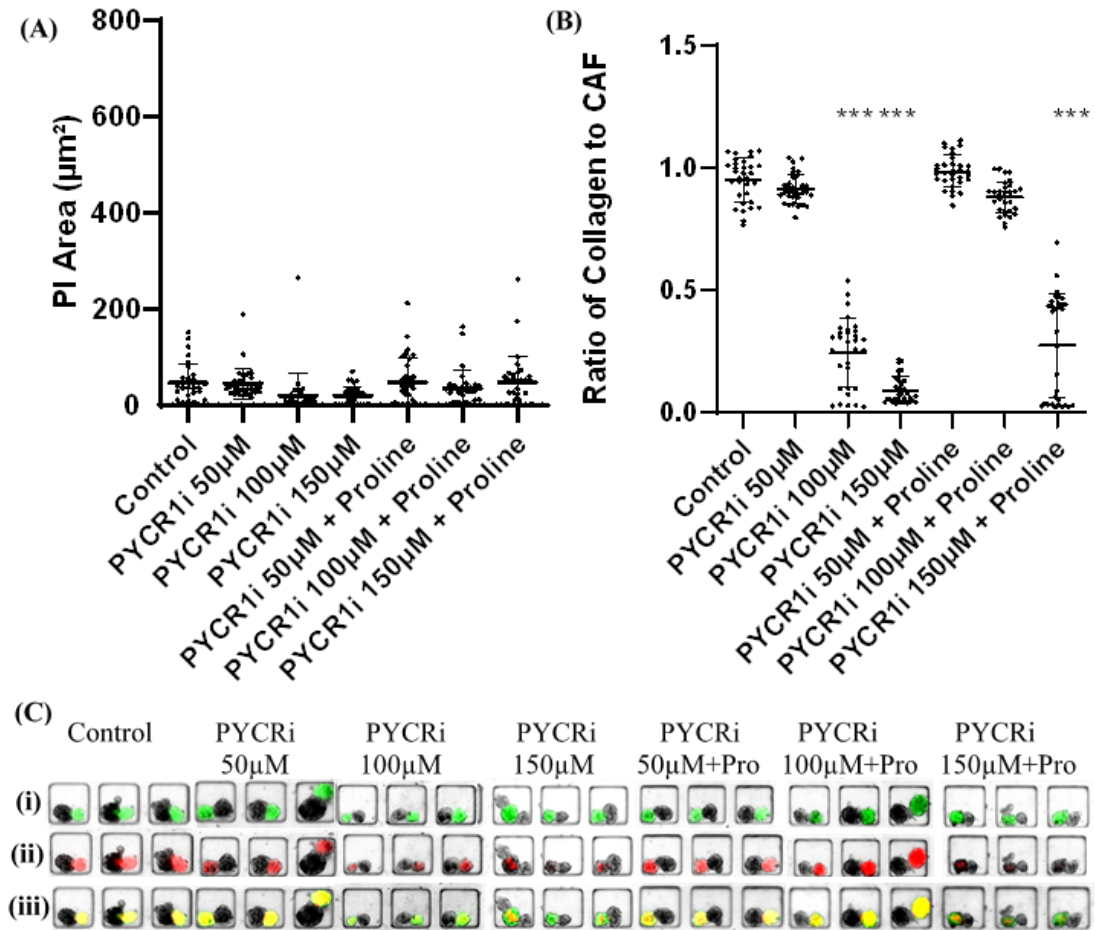
Figure 4.15: *Quantification of PI area and collagen deposition for PYCR1 inhibitor treated spheroids with proline as a rescue agent at increased inhibitor concentrations. (A) Plot of PI area. n=32. (B) Plot of collagen to CAF ratios. n=32. Data shows a significant difference in collagen deposition (***P ≤0.0001) between control co-cultures and those treated with the 100µM PYCR1 inhibitor concentration and the 150µM inhibitor concentration, with and without proline. (C) Brightfield images with (i) Collagen (red) overlay = first row (ii) CAF (green) overlay = second row (iii) Collagen and CAF (yellow) overlay = third row. (5x magnification) Data shown as mean ± SD. ***P ≤0.0001, One-way ANOVA, Bonferroni's post-test.*

PI area remained constant for all conditions (**Figure 4.15**A). The addition of proline was again proven to recover collagen deposition for the 100µM concentration back to a 1:1 collagen to CAF ratio (**Figure 4.15**B and C) and partially recover the collagen deposition for 150µM treated spheroids. For the 150µM concentration, collagen to CAF ratio was reduced to 1:11 which was partially recovered by proline administration to 1:4.

In summary, no negative effect of the PYCR1 inhibitor on cancer cell or CAF viability was observed. PYCR1 inhibitor treatment resulted in reduced CAF spheroid size with increasing inhibitor concentration. Proline was successful in negating the effect of reduced CAF spheroid size and collagen deposition in co-cultures treated with PYCR1 inhibitor. However, collagen production was not able to be fully recovered for spheroids treated with the 150μM PYCR1 inhibitor concentration tested. This is thought to be due to the inhibitor decreasing collagen deposition to such an extent that CAF were not able to fully recover their collagen producing function within the timescale of the assay.

4.5 Spheroid Recovery with Rescue Agents: Acetate Rescue of ACLY inhibitor Spheroids

Following on from previous work, ACLY inhibitor treatment was administered in combination with Acetate (2mM) to assess its ability to rescue inhibitor treated cultures (**Figure 4.16**).
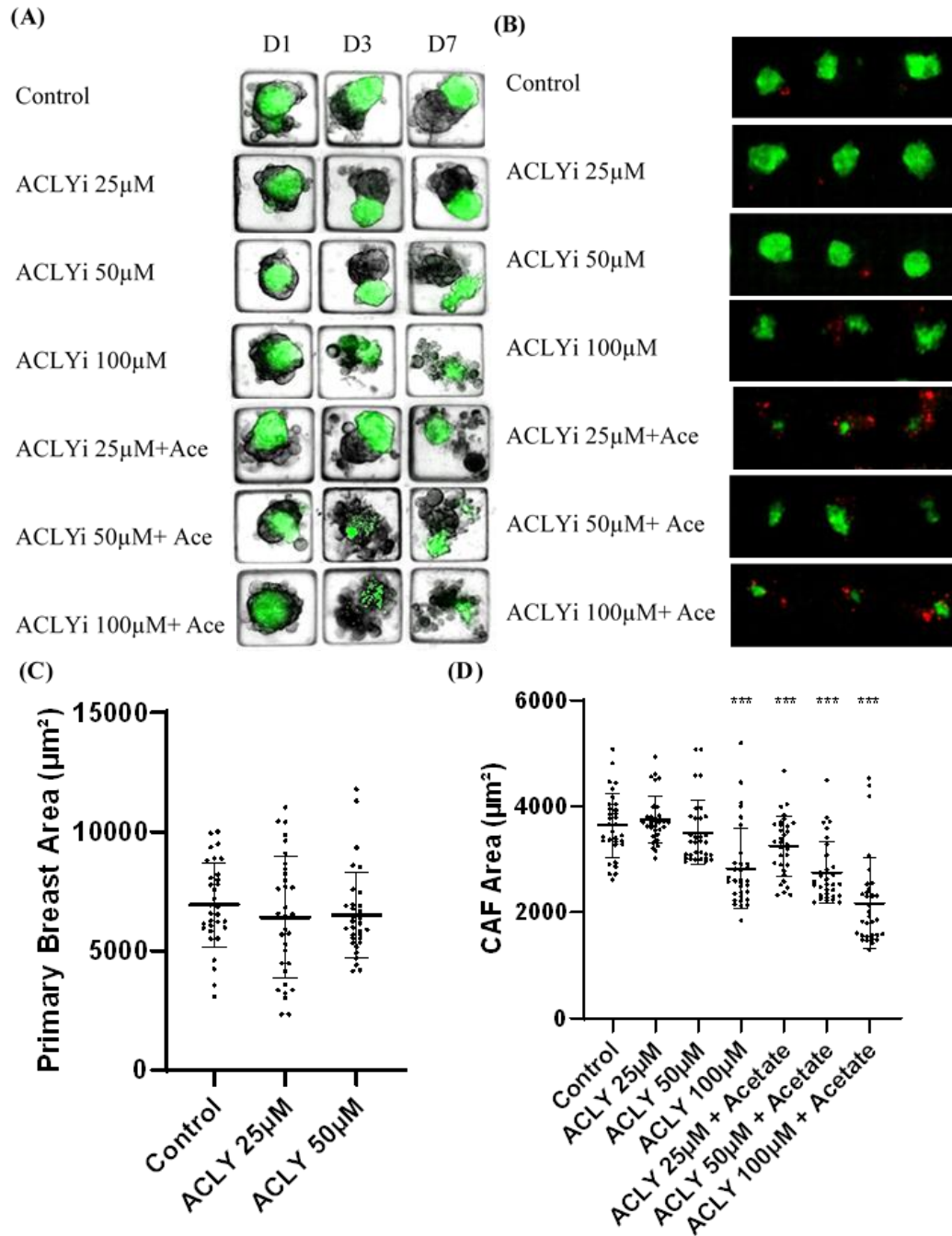
Figure 4.16 Recovery of ACLY inhibitor treated spheroids with acetate as a rescue agent. (A) Brightfield image timelines with CAF channel (green) overlay of spheroids from days 1-7. (B) Fluorescence images of viability staining with PI (red) of 1:1 cancer cell and CAF (green) co-cultures on day 7. (C) Cancer spheroid areas on day 7. n=32. (D) CAF spheroid areas on day 7. n=32. Data shows significant differences in CAF spheroid areas (***P ≤0.0001) between control co-cultures and those treated with the 100μM ACLY inhibitor concentration and all co-cultures treated with both ACLY inhibitors and acetate. (5x magnification) Data shown as mean ± SD. ***P ≤0.0001, One-way ANOVA, Bonferroni's post-test.

Greater disaggregation of cancer cell spheroids with increasing ACLY inhibitor concentration and, surprisingly, with acetate exposure was observed (**Figure 4.16**A). The reduction in cell viability was confirmed with PI staining (**Figure 4.16**B). Thus, cancer cell spheroid area was

only attainable for control spheroids and those treated with a low ACLY inhibitor concentrations (**Figure 4.16**C). Smaller CAF area (***P ≤0.0001) was present in co-cultures treated with the 100μM ACLY inhibitor concentration and when co-cultures were exposed to acetate in addition to ACLY inhibitor at the lower concentrations (**Figure 4.16**D), as determined by one-way ANOVA analysis. However, ACLY inhibitor administration alone at these levels did not trigger disaggregation of or a reduction in CAF area. Viability and collagen deposition were quantified (**Figure 4.17**).
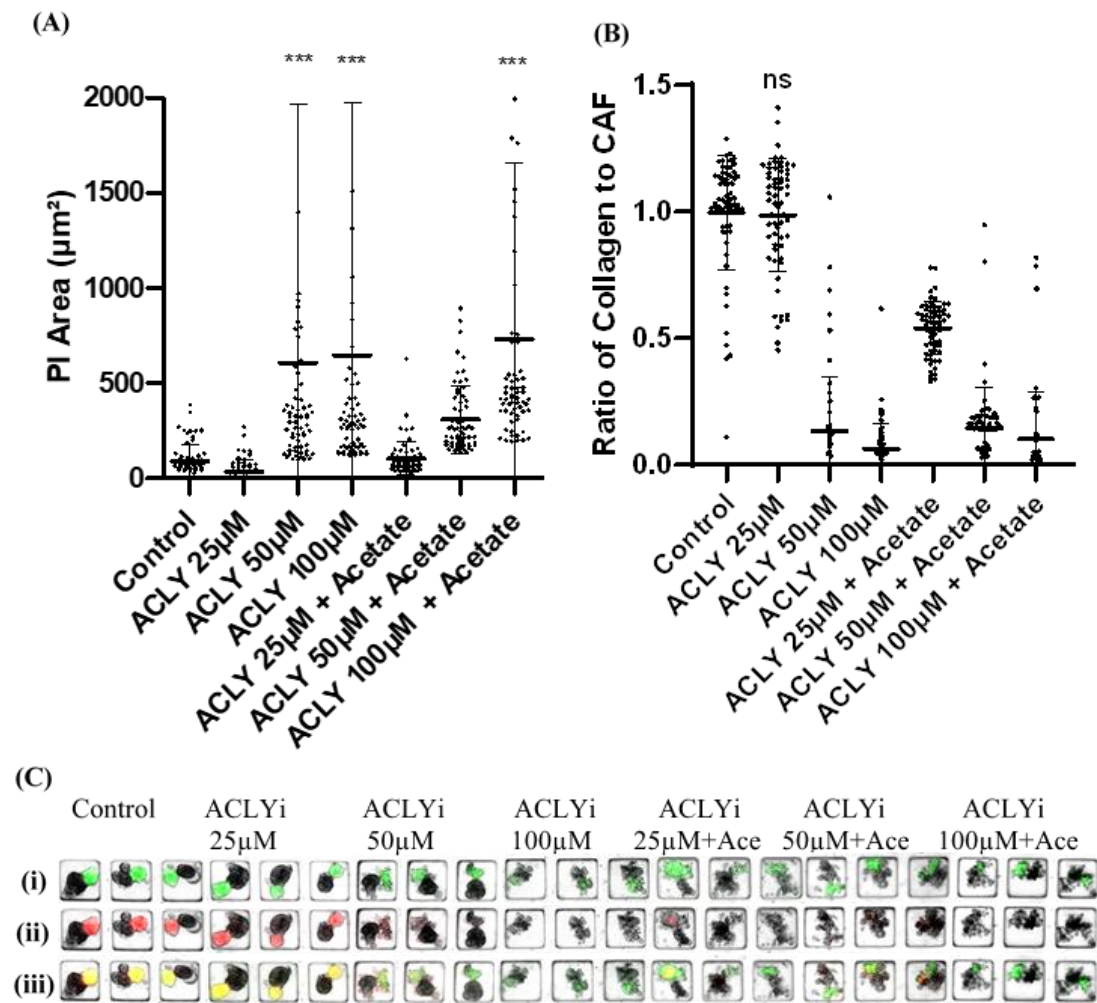
Figure 4.17: *Quantification of PI area and collagen deposition for ACLY inhibitor treated spheroids with acetate as a rescue agent. (A) Plot of PI area. n=64. Data shows a significant difference in PI area (***P ≤0.0001) between control spheroids and those treated with the 50μM ACLY inhibitor concentration and the 100μM ACLY inhibitor concentration, with and without acetate. (B)Plot of collagen to CAF ratios. n=64. Data shows significant differences in collagen deposition (***P ≤0.0001) between control co-cultures and all other conditions with exception for the 25μM ACLY inhibitor concentration. (C) Brightfield images with (i) Collagen (red) overlay = first row (ii) CAF (green) overlay = second row (iii) Collagen and CAF (yellow) overlay = third row.(5x magnification) Data shown as mean ± SD. ***P ≤0.0001, One-way ANOVA, Bonferroni's post-test.*

As was consistent with previous findings, a negative effect of the inhibitor on cancer cell viability but not CAF was observed via one-way ANOVA analysis with a significant increase

(***P ≤0.0001) in PI signal for high inhibitor concentrations which could not be recovered by the acetate administration (**Figure 4.17**A). Collagen deposition was decreased at higher ACLY inhibitor concentrations and at lower inhibitor concentrations when also exposed to acetate (**Figure 4.17**B and C). As in previous assays, collagen deposition was reduced for 50µM and 100µM to give collagen: CAF ratios of 1:8 and 1:16 respectively. Inhibitor-induced reduction of collagen deposition with increasing concentration was not recovered with acetate exposure in microfluidic devices. The reduction of collagen expression in spheroids treated with both ACLY inhibitor and acetate was more pronounced with increasing inhibitor concentration. Mean collagen: CAF ratios of 1:2, 1:7 and 1:10 were recorded for spheroids treated with 25µM, 50µM and 100µM, respectively. However, in equivalent 2D experiments conducted by collaborators the acetate was successful in restoring collagen deposition in ACLY inhibitor treated cultures. For the next phase of experiments, it was thought that the toxic effect of acetate could have potentially been due to its administration at too high a concentration and so its effect on the co-culture should be re-evaluated when in use at half of the original concentration, 1mM (**Figure 4.18**).
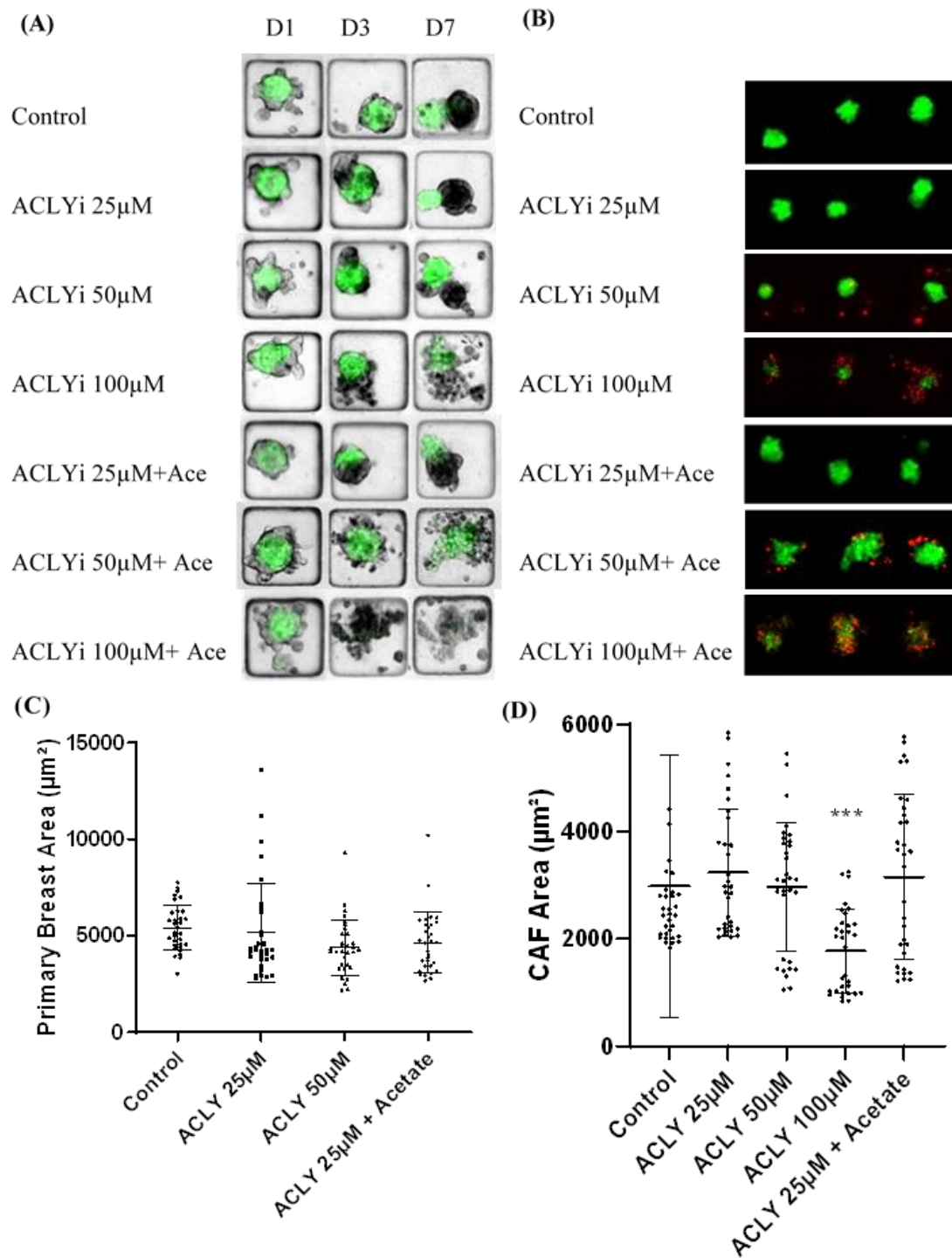
Figure 4.18 *Recovery of ACLY inhibitor treated spheroids with acetate, at reduced concentration, as a rescue agent. (A)Brightfield image timelines with CAF channel (green) overlay of spheroids from days 1-7. (B) Fluorescence images of viability staining with PI (red) of 1:1 cancer cell and CAF (green) co-cultures on day 7. (C) Cancer spheroid areas on day 7. n=32. (D) CAF spheroid areas on day 7. n=32. Data shows a significant difference in CAF area (***P ≤0.0001) between control co-cultures and those treated with the 100µM ACLY inhibitor concentration. (5x magnification) Data shown as mean ± SD. ***P ≤0.0001, One-way ANOVA, Bonferroni's post-test.*

Despite reducing the acetate concentration to the same level that had been successful in replenishing collagen in 2D cultures, greater disaggregation of cancer cells with increasing ACLY inhibitor concentration and with acetate exposure was again observed (**Figure 4.18**A). The reduced acetate concentration was again demonstrated to trigger cell death (***P in co-cultures, in addition to failing to restore collagen deposition in ACLY inhibitor treated co-cultures (**Figure 4.18**B). Once again, cancer spheroid areas were only attainable for control and co-cultures treated with low ACLY inhibitor concentrations due to disaggregation (**Figure 4.18**C). No significant difference in cancer spheroid size was recorded for 25µM and 50µM concentrations. A significant reduction (***P ≤0.0001) in CAF spheroid area was seen for the 100µM ACLY inhibitor concentration and those exposed to acetate in addition to ACLY inhibitor at the lower concentrations, as detected by one-way ANOVA analysis (**Figure 4.18**D). This was despite the ACLY inhibitor not resulting in disaggregation or a reduction in CAF area at these levels when administered alone. Quantification of PI area and collagen deposition was performed (**Figure 4.19**).
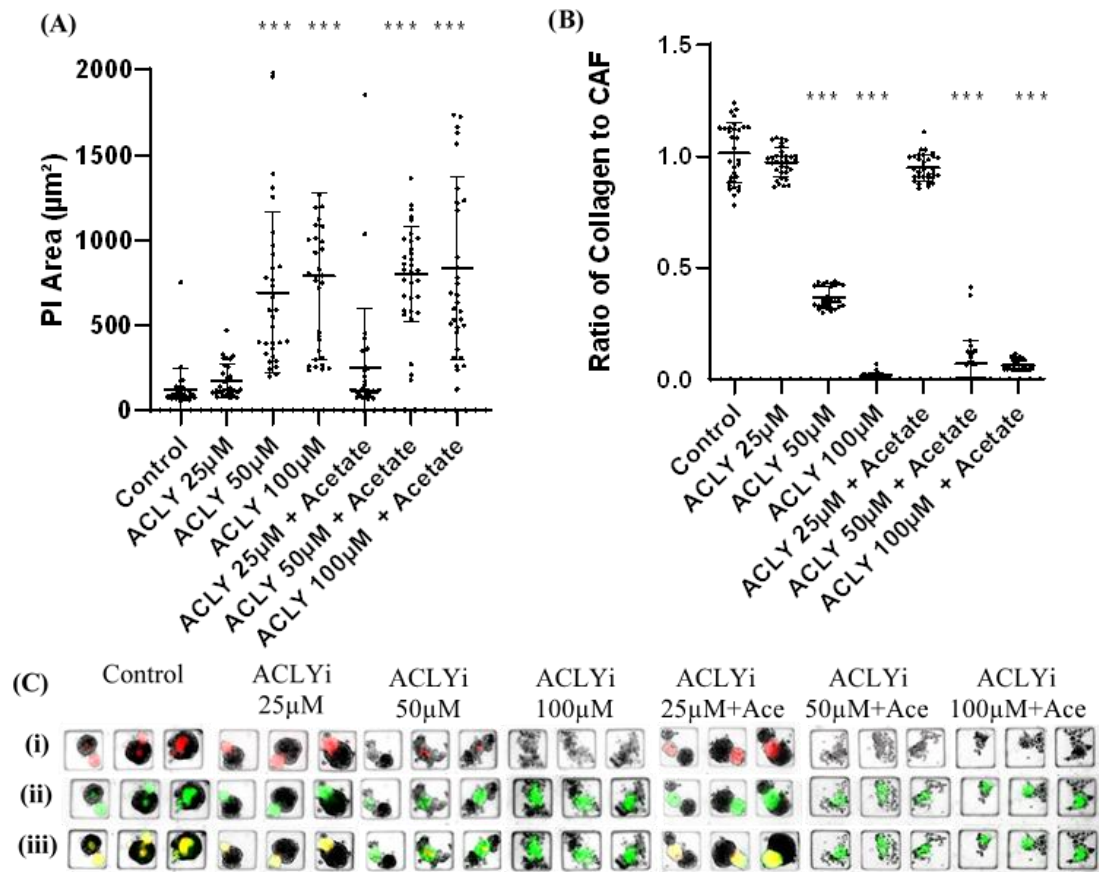
Figure 4.19: Quantification of PI area and collagen deposition for ACLY inhibitor treated spheroids with acetate, at reduced concentration, as a rescue agent. (A) Plot of PI area. n=32. Significant differences in PI area (***P ≤0.0001) were detected between control spheroids and those treated with the 50μM and 100μM ACLY inhibitor concentrations with and without acetate. (B) Plot of collagen to CAF ratios. n=32. Significant differences in collagen deposition (***P ≤0.0001) were detected between control spheroids and those treated with the 50μM and 100μM ACLY inhibitor concentrations with and without acetate. (C) Brightfield images with (i) Collagen (red) overlay = first row (ii) CAF (green) overlay = second row (iii) Collagen and CAF (yellow) overlay = third row. (5x magnification) Data shown as mean ± SD. ***P ≤0.0001, One-way ANOVA, Bonferroni's post-test.

A significant increase in PI signal (***P ≤0.0001) for high inhibitor concentrations with and without acetate was also noted as before using one-way ANOVA analysis (**Figure 4.19**A). Quantification of collagen production showed decreased collagen deposition at higher ACLY inhibitor concentrations and at lower inhibitor concentrations also when exposed to acetate (**Figure 4.19**B and C). Mean collagen: CAF ratios were consistent with previous findings showing a reduction for 50μM and 100μM ACLY inhibitor treated spheroids to 1:3 and 1:55 respectively. A reduction in collagen production for acetate treated spheroids which increased with increasing inhibitor concentration was also recorded as 1:4 for 25μM, 1:14 for 50μM and 1:16 for 100μM concentrations.

Thus, it can be concluded that acetate exposure does not recover collagen expression in 3D culture for ACLY inhibitor treated spheroids. In summary, from this phase of experiments investigating rescue agents, it was found that acetate increased disaggregation of both cell

types and failed to recover collagen deposition in ACLY inhibitor treated spheroids. Acetate also decreased CAF spheroid size and collagen deposition in low ACLY inhibitor concentration treated co-cultures which had been unaffected when treated with ACLY inhibitor alone. As collaborators did not observe a toxic effect of the acetate in 2D conditions, this could imply that a reaction between the inhibitor and the rescue agent in the 3D microfluidic environment creates an inhospitable environment for CAF survival. However, no reports of acetate toxicity in PDMS microfluidic devices could be identified in the literature.

4.6 Proliferation Analysis of CAF Monocultures

To further study the impact of acetate on CAF in 3D culture, ACLY inhibitor and acetate were administered to CAF monocultures (**Figure 4.20**).

(A)

	D1	D3	D7
Control			
ACLYi 25µM			
ACLYi 50µM			
ACLYi 100µM			
ACLYi 25µM+Ace			
ACLYi 50µM+ Ace			
ACLYi 100µM+ Ace			

(B)
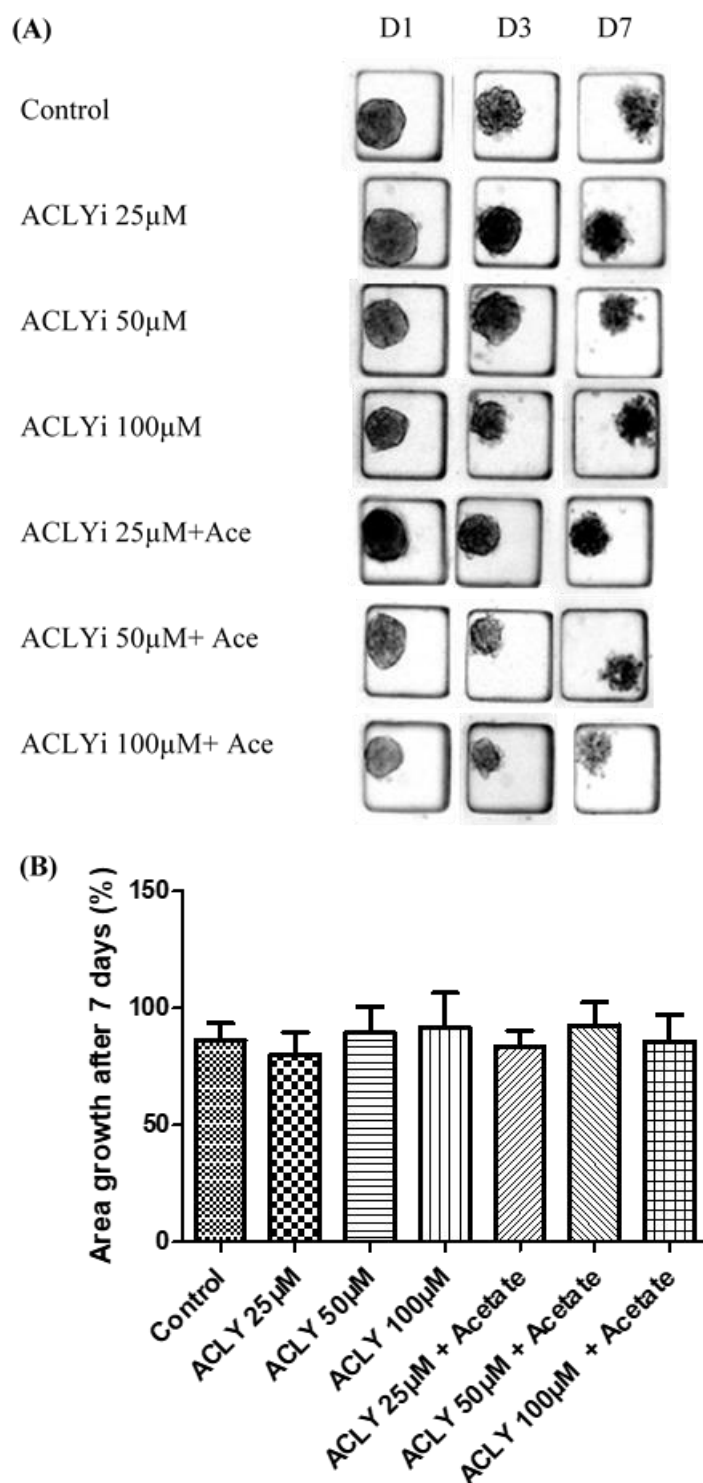
Figure 4.20 *Area growth of CAF monocultures (A) Brightfield timeline images. (B) Graph of area growth for CAF spheroids over a 7 day culture period. n=32. (5x magnification) Data shown as mean ± SD. ***P ≤0.0001, One-way ANOVA, Bonferroni's post-test.*

Proliferation of monoculture spheroids was quantified to determine if the reduction in CAF area was as a result of the inhibitors limiting CAF proliferation or was due to inhibitor killing of CAF (**Section 2.11.2**). Analysis was carried out using the Ki67 protein as a marker of

proliferation and plotted as a ratio against CAF area for each spheroid. As seen in preliminary experiments, CAF spheroids showed no growth over the seven day culture period when cultured alone while also becoming less compact over time (**Figure 4.20**A). No statistically significant differences in CAF size over the culture period was detected between conditions (**Figure 4.20**B). Proliferation of CAF monocultures was quantified (**Figure 4.21**).
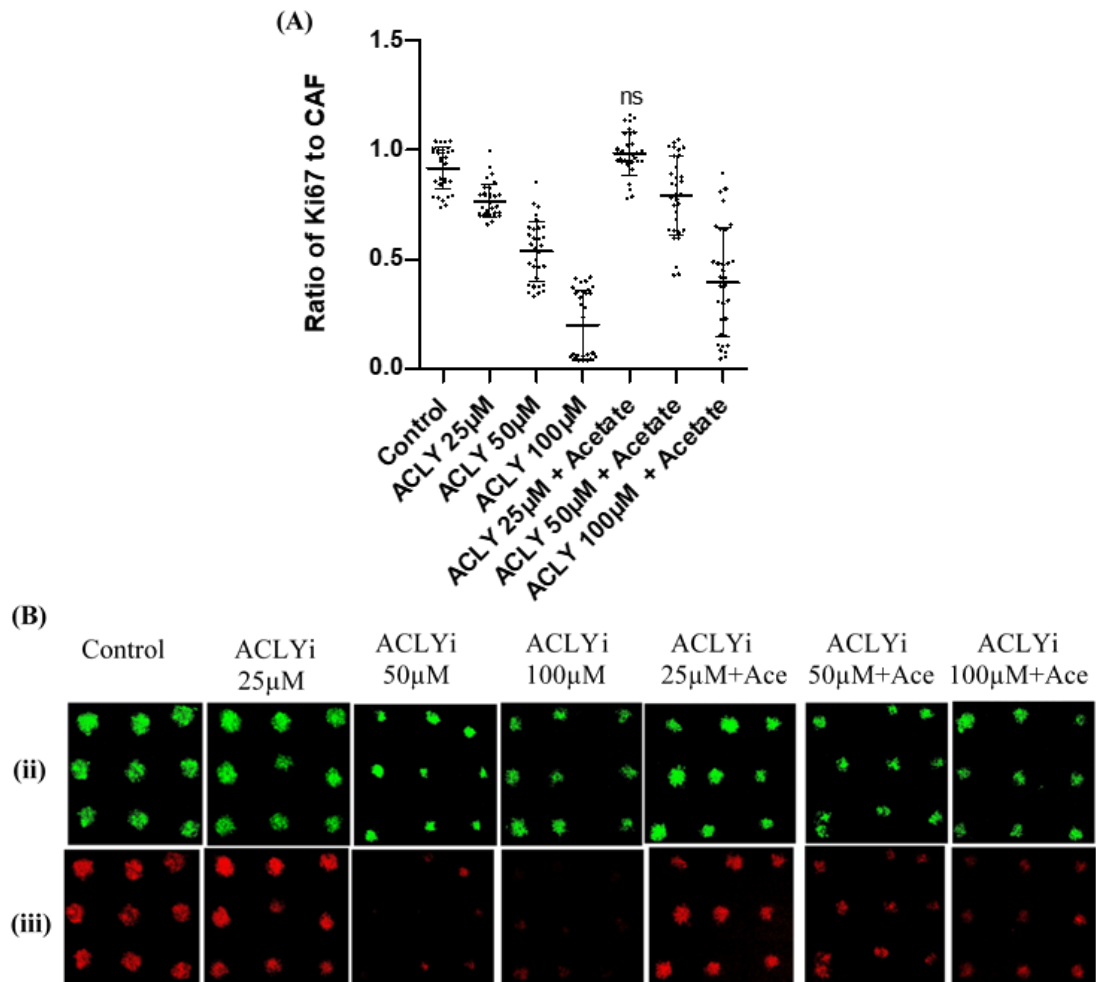
Figure 4.21: Quantification of proliferation for CAF monocultures (A) Plot of ratio of proliferative area over total CAF area. n=32. Data shows a significant difference in proliferation (***P ≤0.0001) between control spheroids and all conditions with exception for 25μM ACLY inhibitor and acetate treated spheroids. (B) Fluorescence images of (i) CAF (green) = first row (ii) Ki67 (red) = second row. (5x magnification) Data shown as mean ± SD. ***P ≤0.0001, One-way ANOVA, Bonferroni's post-test.

Control spheroids exhibited a mean Ki67: CAF ratio of 1:1 (**Figure 4.21**A). A reduction in proliferation was observed with the increasing inhibitor concentrations (**Figure 4.21**B). The statistically significant reduction in Ki67 expression in 25μM inhibitor treated spheroids (***P ≤0.0001) was entirely negated by acetate delivery as detected by one-way ANOVA analysis. Whilst the Ki67: CAF ratio for spheroids treated with 25μM and 50μM ACLY inhibitor was partially recovered. Therefore, the toxic effect seen with the acetate in the co-cultures was not

observed in CAF monocultures and, in fact, the acetate was able to have a beneficial effect in restoring CAF proliferation.

4.7 Proliferation Analysis of Co-cultures

To investigate whether the toxicity of acetate that occurs in co-cultures is as a direct result of the type of inhibitor used, co-cultures were treated with PDH inhibitor, where the effect of this inhibitor was expected to be negated by acetate. Proliferation analysis of CAF in co-cultures was carried out and results plotted as the ratio of CAF proliferative area over total CAF area (**Figure 4.22**). For comparison, proliferation of PYCR1 inhibitor treated co-cultures was also studied. PYCR1 inhibitor was previously shown to reduce collagen deposition in co-cultures and so proliferation measurements were taken to establish if the loss of collagen deposition coincided with a reduction in CAF proliferation.
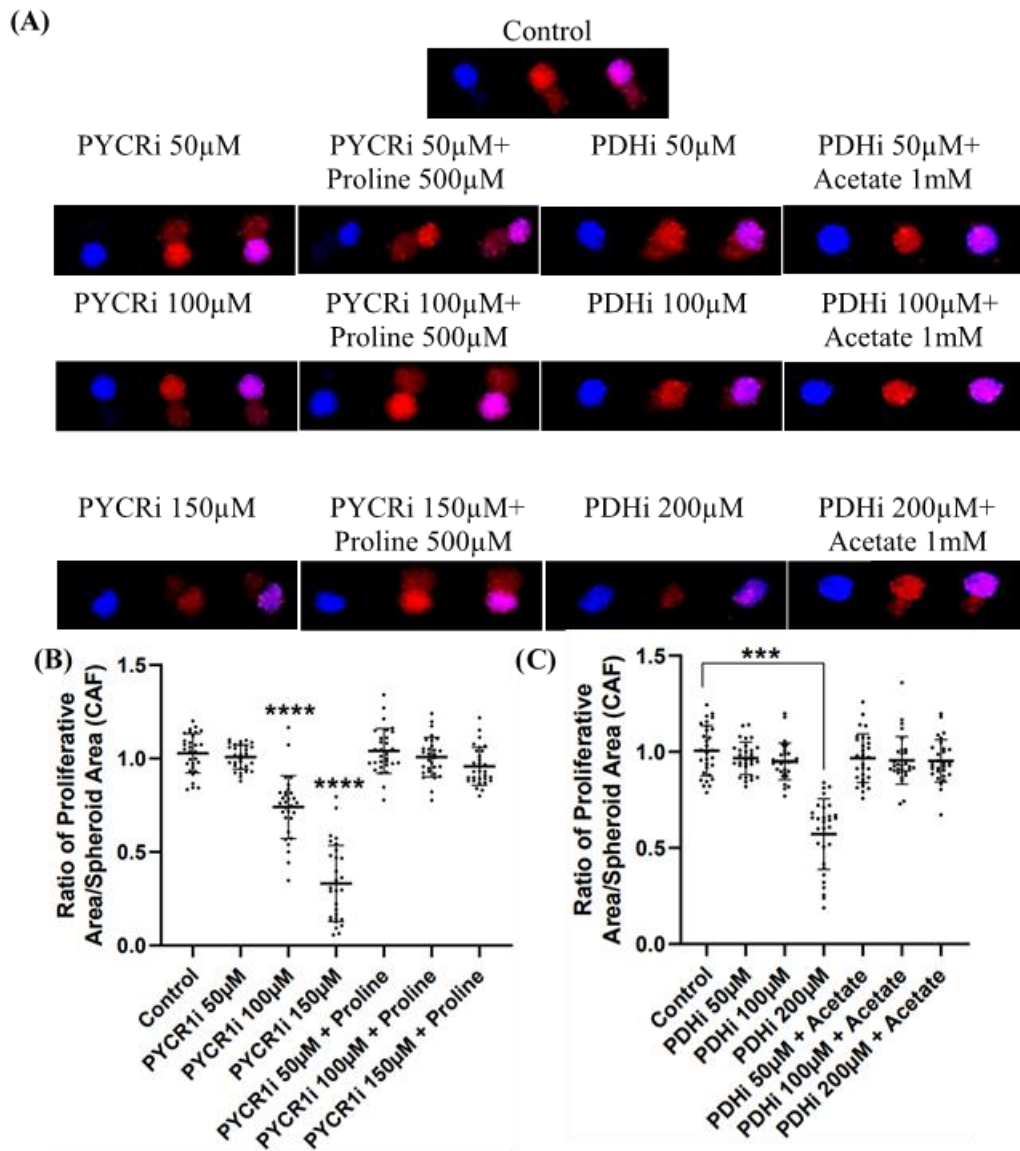
*Figure 4.22 Proliferation analysis of PYCR1 inhibitor and PDH inhibitor Treated CAF in co-cultures. (A) Representative fluorescent images of co-cultures after 7 Days (CAF = blue, Ki67= red and Overlap = purple) (B) Ratio of proliferative area to CAF area of PYCR1 inhibitor treated co-cultures after 7 days. n=30. Data shows significant differences in proliferation (***P ≤0.0001) between control spheroids and those treated with the 100μM and 150μM PYCR1 inhibitor concentrations. (C) Ratio of proliferative area to CAF area of PDH inhibitor treated co-cultures after 7 days. n=30. Data shows significant differences in proliferation (***P ≤0.0001) between control spheroids and those treated with the 200μM PDH inhibitor concentration. (5x magnification) Data shown as mean ± SD. ***P ≤0.0001, One-way ANOVA, Bonferroni's post-test.*

Due to the dissociation of the two cell types the proliferation of CAF and cancer cells could be clearly distinguished (**Figure 4.22**A). Quantifying these results showed a significant reduction in proliferation for treatment with both inhibitors which was shown to be to a greater extent for PYCR1 inhibitor treated spheroids (**Figure 4.22**B). The proliferation of all treated cultures was seen to be restored to levels not significantly different from control culture conditions. Therefore, both proline (**Figure 4.22**B) and acetate (**Figure 4.22**C) are able to rescue reduced proliferation in enzyme treated CAF-cancer co-culture spheroids.

In summary, all of the enzyme inhibitors involved in the collagen production cycle were shown to reduce collagen deposition from CAF with proline and acetate showing to recover deposition for PYCR1 inhibitor and PDH inhibitor treatments respectively (**Figure 4.23**).[19]
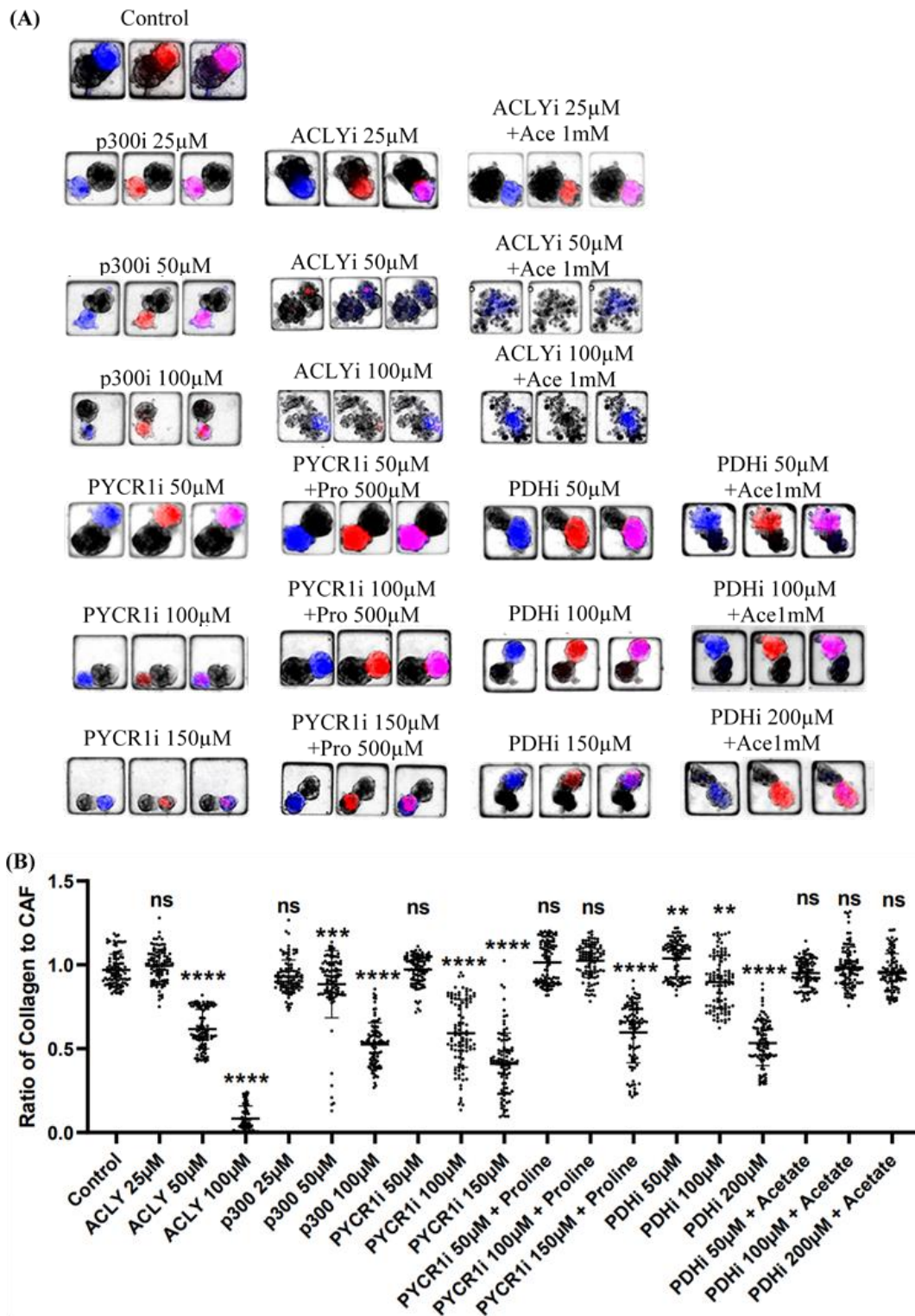
Figure 4.23 *Summarised proliferation analysis of inhibitor treated CAF in co-cultures. (A) Representative fluorescent images of co-cultures after 7 Days. Adapted with permission from Kay et al., bioRxiv, 2021 https://creativecommons.org/licenses/by/4.0/. (CAF = blue, Ki67= red and Overlap = purple) (B) Ratio of proliferative area to CAF area of inhibitor treated co-cultures after 7 days. n=30. Data shows significant differences in collagen deposition (***P ≤0.0001) between control co-cultures and those treated with the 50μM and 100μM ACLY inhibitor, 50μM and 100μM p300 inhibitor, 100μM, with and without proline, and the 150μM PYCR1 inhibitor and the 200μM PDH inhibitor concentrations. Data shows significant differences in collagen deposition (**P ≤0.01) between control co-cultures and those treated with the 50μM and 100μM PDH inhibitor concentrations. Data shown as mean ± SD. ***P ≤0.0001, One-way ANOVA, Bonferroni's post-test.*

In this chapter, protocols were developed to establish 3D co-cultures of CAF with a primary breast cancer cell line were performed in microfluidic devices to study the pathways involved in collagen production. The role of various enzyme inhibitors and their prevention of CAF collagen deposition was studied In parallel, separate co-cultures were exposed to both enzyme inhibitors and an additional supply of the required agent needed for collagen production. This microfluidic platform was able to provide real-time monitoring of cancer-CAF co-cultures and functional readouts, including fluorescence data on viability, collagen deposition and proliferation markers. Protocols were developed to analyse and quantify this data for robust comparison between conditions. Similarly to *in vivo* observations[19], CAF were found to dissociate from cancer cells soon after seeding in microfluidic devices and were found to be the primary source of collagen production. Collagen deposition by CAF could be attenuated using pharmacological agents, inhibitors of ACLY, p300, PDH and PYCR1, with dose-dependent effects. These inhibitors were also shown to negatively impact cancer cell viability and aggregation, as well as CAF proliferation (**Figure 4.23**A). Collagen production was restored for PYCR1 inhibitor treated co-culture spheroids with exogenous administration of proline and for PDH inhibitor treated spheroids with the addition of acetate (**Figure 4.23**B). In conclusion, these findings highlight the role of CAF in being a major producer of collagen in solid tumours. This platform and the developed protocols have been presented as a valuable tool for studying the metabolic processes involved in CAF production and potential methods for targeting these pathways to prevent CAF activation. These findings could be of benefit in the development of therapies to diminish ECM production in tumours and, thus, enhance the cytotoxic effects of anti-cancer agents. In future, patient biopsy tissue could be used in place of cancer cell lines to perform predictive studies and to provide valuable data on TME targeting agents. The experience gained whilst developing these CAF and cancer co-culture models was applied to subsequent immune assay development, described in the following chapter. These immunoassays included investigations into how the addition of the stromal component into the 3D tumour model influences CAR-T cell function.

Chapter 5: Solid Tumour Immunoassays

Knowledge gained from previous experience developing tumour-stromal models, as discussed in previous chapters, was subsequently applied to establishing a model that better reflects the native TME and that would be suitable for a variety of immunoassays. The TME is an imperative factor for the outcome of many cancer treatments, including immunotherapies.[84, 246-248] In particular, CAF are known to inhibit immune cell access to tumour cells *in vivo* and can lessen the effectiveness of immunotherapy treatment.[249] CAF are a major component of the TME and their collagen deposition provides protection to cancer cells against anti-cancer therapies and encourages tumour growth and metastasis through ECM remodelling.[19, 35] There is a lack of preclinical *in vitro* models for investigating the impact of the solid tumour on the efficacy of immunotherapies.[11] While *in vitro* models have largely been employed to study the effects of immunotherapies against liquid tumours, the solid tumour niche remains relatively unexplored with respect to immunotherapy.

CAR-T therapy is one of the most promising forms of immunotherapy and has been proven beneficial for haematological malignancies and melanoma.[111] [101] [82] However, CAR-T clinical success against the vast majority of solid tumour types has been limited thus far.[250] CAR-T cells are produced, firstly, by extraction of patient T cells from peripheral blood or tumour tissues.[15] This is followed by *ex vivo* genetic modification so cells specifically bind to tumour antigens.[251, 252] CAR-T cells are then expanded and activated prior to reinfusion into the patient.[15] Binding of tumour specific CAR-T cells to the target antigen induces cytokine secretion, T cell proliferation and cytotoxicity.[251] Furthermore, CAR-T therapy can be given in combination with other therapy types to enhance its effectiveness.[253] Thus, there exists a need for the development of new *in vitro* models that more faithfully represent the human solid TME for the assessment of these therapy combinations prior to *in vivo* studies. The high cost associated with CAR-T cell manufacture has hindered the widespread use of this therapy clinically.[117] Considering this, protocols for this work were optimized so as to minimize the number of CAR-T cells used in each experiment whilst still observing significant cytotoxic effects and extracting as much experimental data as possible. Based on previous experience with 3D CAF and cancer cell 3D culture, this knowledge could then be applied to the development of a novel microfluidic 3D immunoassay. This chapter presents, for the first time, immunoassays capable of the assessment of both treatment specificity and cytotoxicity of combination therapies *in vitro* with CAR-T cells.

5.1 Assay Development

The aim of this study was to create a 3D tumour-stromal co-culture model that could better represent *in vivo* TME structures whilst being suitable for the assessment of the performance of CAR-T cells (AMSBIO) specifically targeting cancer cells. To achieve this, the 24-channel *OC³D Single* microfluidic device (ScreenIn3D Ltd, UK) was selected for use in these assays (**Figure 5.1**).
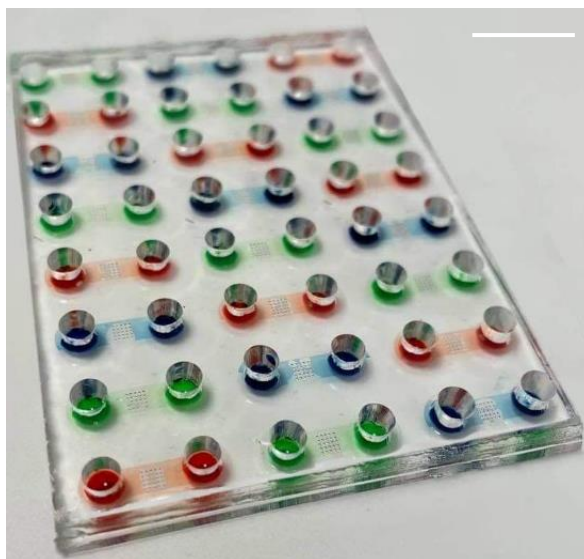
Figure 5.1 Image of the OC3D Single microfluidic device (ScreenIn3D Ltd, UK). Scale bar = 10mm.

The 24-channel *OC³D Single* microfluidic device was selected for use in CAR-T assays (**Section 2.7**), as opposed to the 7-channel spheroid device described in chapter 3, due to the shorter channel lengths of this platform, meaning that a lesser quantity of CAR-T cells would be required for seeding devices (**Figure 5.1**). Preliminary experiments were carried out to determine the optimal seeding concentrations and volumes using the smallest possible number of cells that would still allow a sufficient number of cells to enter microwells containing MDA-MB-468 and stromal co-culture spheroids. Assessment and optimization of the staining protocol for the 24-channel device was also performed to ensure CAR-T cells were not flushed from microwells during simultaneous culture media injection into both wells of each channel in devices (**Section 2.11.3**).

5.2 Target Selection

Once optimal seeding and staining protocols were established, a target for CAR-T cell targeting had to be selected (**Section 2.7**). As a proof of concept assay, the EGF receptor was chosen as a target as EGF is a common receptor that is overexpressed by many tumour cell types.[125] To demonstrate the selective cytotoxicity of the CAR-T cells, it was necessary to have

an EGFR overexpressing cell line and a low level EGFR expressing cell line cultured together. It was hypothesized that upon addition of the CAR-T cells, high level EGFR expressing cells would be killed whilst cells expressing EGFR at significantly lower levels would be spared. However, it was important to consider the extent of CAR-T cell exposure that could result in the killing of low level EGFR expressing cells, as well as high EGFR expressing tumour cells. This consideration was required in order to be able to demonstrate targeting specificity which is often a major challenge for CAR-T therapy. The aim of this work was to explore the efficacy of CAR-T cell target killing and to investigate off-target toxicity. CAR-T targeting when cancer cells were co-cultured with cancer associated cells in comparison to normal cells was also studied and, thus, two spheroid co-cultures were established. The MDA-MB-468 TNBC cell line was selected as the target EGFR expressing tumour cell line due to previous reports of EGFR overexpression.[254-257] For a control cell line, HUVEC were initially selected due to their low EGFR expression.[258, 259] However, whilst this cell line was relevant for depicting vasculature structures, they are not relevant to the TME. HUVEC spheroid cultures were ultimately not used in CAR-T cell assays as they were found to not culture well in spheroid devices and failed to form viable spheroids despite varying culture media and supplement conditions. Cells initially formed spheroids on the first day of culture but subsequently disaggregated in the days following. Several reports of HUVEC spheroid formation in collagen matrix exist.[260, 261] However, theses culture methods would not be suitable for the intended microfluidic assays to be carried out assessing CAR-T cell behaviour.

Subsequently, other alternatives were considered and the EGFR expression of CAF, normal human lung fibroblasts (NHLF) quantified against MDA-MB-468 expression in 2D (**Figure 5.2**).
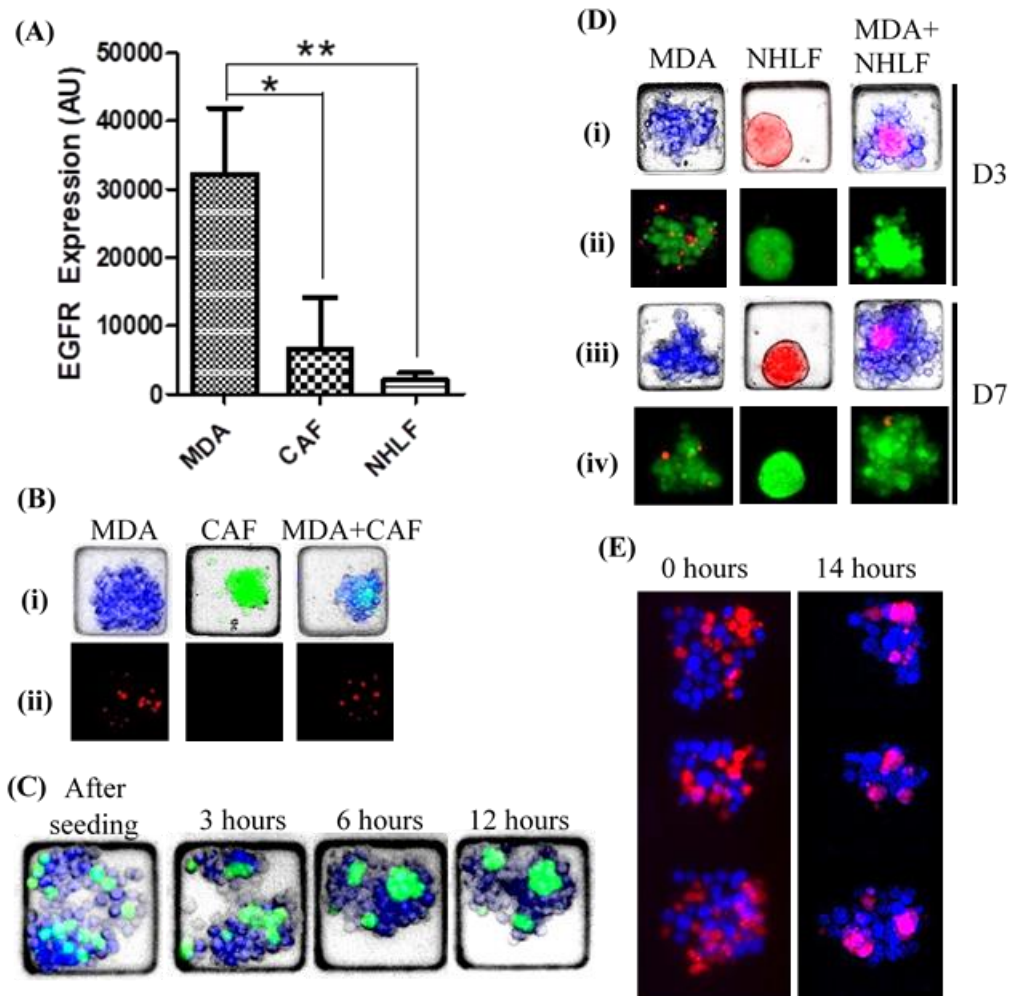
Figure 5.2 EGFR Target Selection. (A) Plot of normalized EGFR expression of MDA-MDB-468, CAF and NHLF cells in a 96-well plate after 3 days of culture. n=3. Data shows a significant difference in EGFR expression between MDA-MB-468 cells and CAF (*P ≤ 0.05) and between MDA-MB-468 cells and NHLF (**P ≤ 0.01). (B) Brightfield and fluorescent images of microfluidic monocultures and co-cultures of (i) MDA-MDB-468 (blue) and CAF (green) on day 3 of culture and of (ii) viability staining with PI (red) and FDA (green). (C) Brightfield and fluorescent images from time-lapse recording of MDA-MDB-468 (blue) and CAF (green) co-culture, beginning immediately after cell seeding. (D) Brightfield and fluorescent images of microfluidic monocultures and co-cultures of (i) MDA-MDB-468 (blue) and NHLF (red) on day 3 of culture, (ii) viability staining with PI (red) and FDA (green) on day 3 of culture, (iii) MDA-MDB-468 (blue) and NHLF (red) on day 7 of culture and (iv) viability staining with PI (red) and FDA (green) on day 7 of culture. (E) Fluorescent images from time-lapse recording of MDA-MDB-468 (blue) and NHLF (red) co-culture, beginning immediately after cell seeding. (MDA = MDA-MDB-468) (5x magnification) Data shown as mean ± SD. *P ≤ 0.05, **P ≤ 0.01, One-way ANOVA, Bonferroni's post-test.

MDA-MB-468 were shown, using t-test analysis, to have significantly greater EGFR expression (**Section 2.11.1**) than that of CAF (*P ≤ 0.05) and NHLF (**P ≤ 0.01) where minimal EGFR expression was detected for both cell types (**Figure 5.2**A). While slightly higher levels of EGFR expression were detected for CAF in comparison to NHLF, this was not statistically significant. Following on from these results, co-cultures of MDA-MB-468 with CAF were established in microfluidic devices and viability assessed (**Section 2.11.3**)

after 3 days of culture (**Figure 5.2**B). Cells were initially seeded into devices at a concentration of 5×10^6 cells/ml but this produced CAF spheroids that were too small for analysis and so the seeding concentration was increased to 7.5×10^6 cells/ml for subsequent experiments (**Section 2.7**). The two cell types could be distinguished due to CAF transfection with GFP and labelling of breast cancer cells with CellTrace Blue. PI staining of cultures showed minimal cell death in both mono- and co-cultures. CAF were anticipated to behave as previously seen (**Figure 4.2**) when co-cultured with the Cellaria Wood primary breast cancer cell line and form their own distinct spheroid within the co-culture aggregate. This would have allowed precise visualization of CAR-T homing to and killing of EGFR-expressing cells without detriment to cells with minimal EGFR expression. However, in this co-culture the CAF did not group together as seen with the Cellaria Wood primary breast cancer cell line and, instead, formed smaller clusters within the MDA-MB-468 aggregate within 12 hours from cell seeding (**Figure 5.2**C). This was also the case for MDA-MB-468 and NHLF co-cultures where NHLF also did not fully dissociate from cancer cells over the 14 hours after seeding (**Figure 5.2**D). NHLF did appear to group together within the loose MDA-MB-468 aggregate by day 3 but the two cell types did not dissociate from each other even after one week of co-culture (**Figure 5.2**E). All culture conditions were shown to be viable after 3 and 7 days with FDA signal more prominent for co-cultures in comparison to MDA-MB-468 monocultures. CAF and NHLF were not detrimental to cancer cells in microfluidic co-cultures and were selected for use in CAR-T assays.

5.3 2D Assessment of EGFR Specificity of CAR-T Cells

Once the EGFR target cell line was selected, the cytotoxic effect of CAR-T cells was first assessed in 2D before beginning 3D microfluidic experiments. MDA-MB-468 cells were seeded in 96-well plates and CAR-T cells added for 24 hours at an E:T ratio of 5:1. No statistically significant differences were observed for PI or FDA signal for MDA or NHLF signal when CAR-T added for 24h (Data not shown). CAR-T incubation time was subsequently increased to 48h and an E:T ratio of 2:1 was applied (**Figure 5.3**).
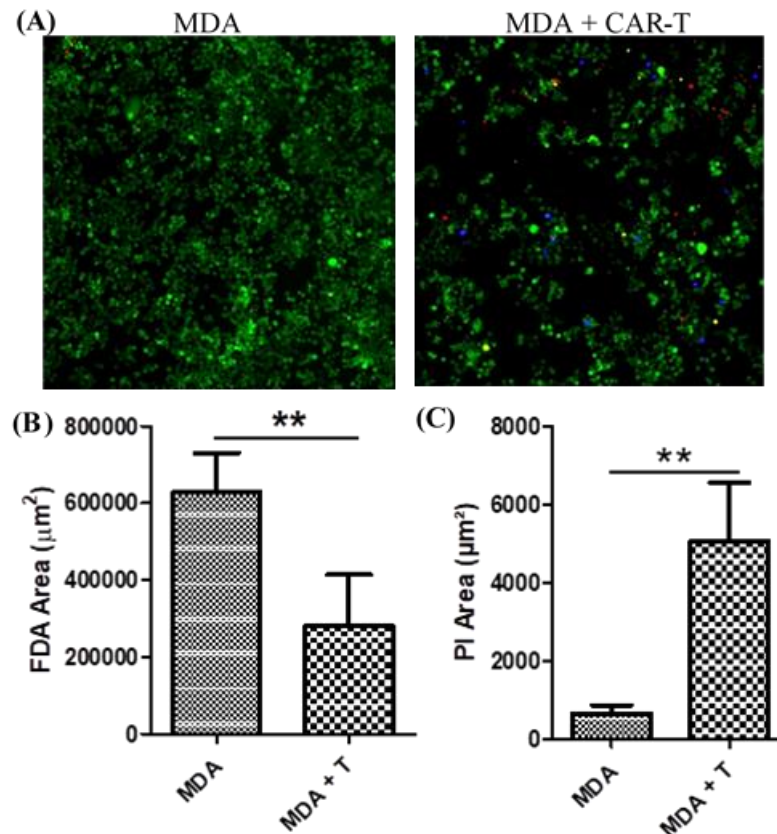
Figure 5.3 *2D assessment of CAR-T cytotoxicity after 48h incubation. (A) Day 4, 48h after adding CAR-T cells. Fluorescence images of viability staining with FDA (green) and PI (red) of MDA-MDB-468 in 96-well plates on day 4 of culture in control conditions and 48h after the addition of CAR-T cells (blue). Images acquired at 10x magnification. (B) Plot of FDA area. n=3. Data shows a significant difference (**P ≤ 0.01) in FDA area between control MDA-MB-468 cells and those treated with CAR-T cells. (C) Plot of PI area. n=3. Data shows a significant difference (**P ≤ 0.01) in PI area between control MDA-MB-468 cells and those treated with CAR-T cells. (MDA = MDA-MDB-468, T = CAR-T cells) Data shown as mean ± SD. **P ≤ 0.01, t-test.*

Few CAR-T cells remained bound to adherent cancer cells after washing steps and viability staining (**Figure 5.3**A).The longer CAR-T cell incubation time of 48h resulted in a statistically significant reduction in live cell area for CAR-T cell treated cultures in comparison to control cultures (**Figure 5.3**B). A significant increase in cell death was also recorded for cultures exposed to CAR-T cells with respect to control cultures (**Figure 5.3**C). Therefore, even at a low E:T ratio of 2:1, CAR-T cells were still able to produce a significant cytotoxic effect against tumour cells. Due to the high specificity of these CAR-T cells, lower E:T values were needed to produce cytotoxic effects than would typically be required for *in vitro* studies.

5.4 2D Optimization of Experimental Conditions

As a result of findings from preliminary 2D assays, further assessment of CAR-T killing was carried out in well plates prior to microfluidic studies. To observe an enhanced effect of CAR-T cell cytotoxicity, CAR-T incubation time was increased to 72 hours and the effects of a range of E:T ratios on CAR-T proliferation and killing of cancer cells investigated (**Figure 5.4**).[11]
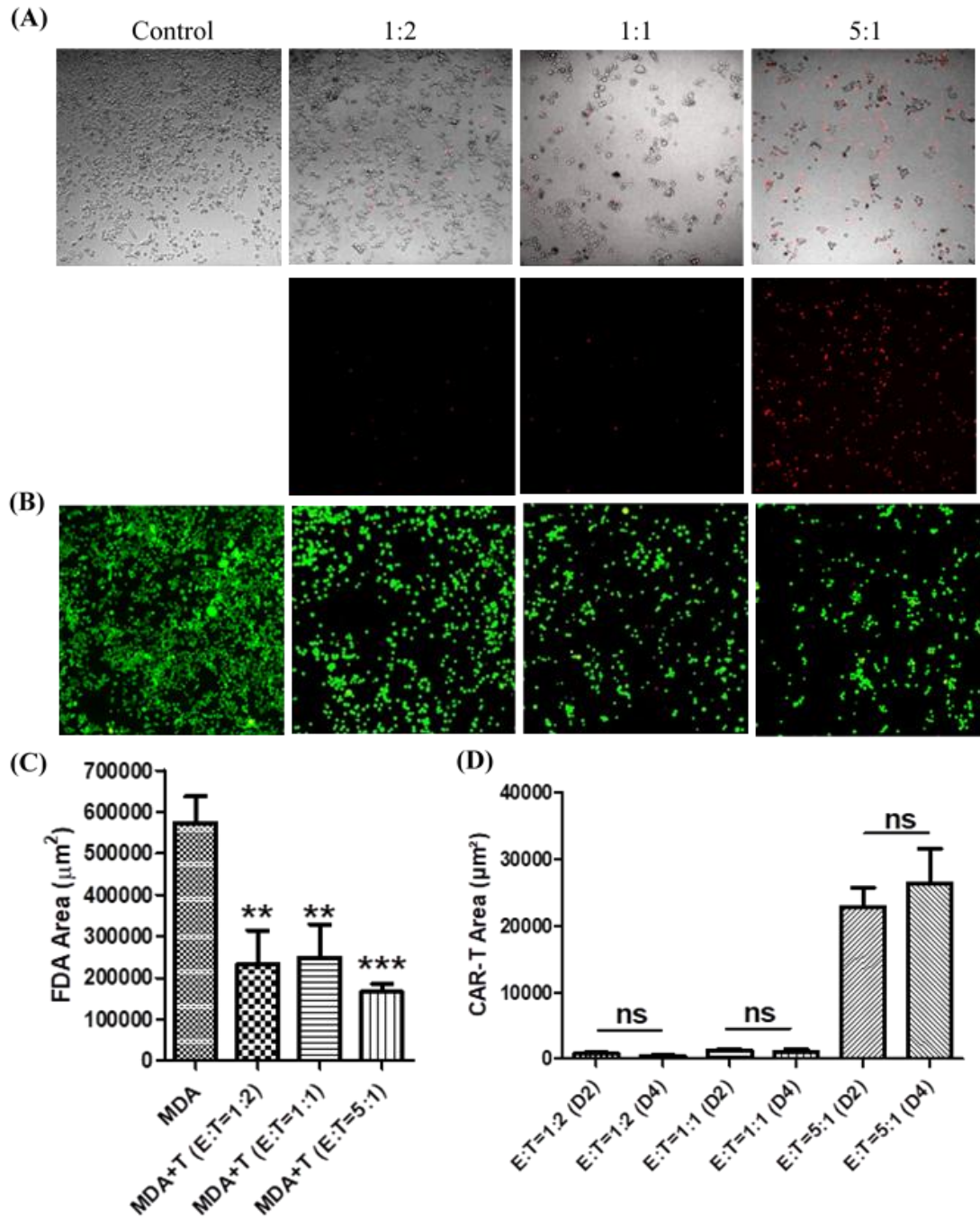
Figure 5.4 *2D Assessment of effect of E:T ratio on cancer cell viability with increased CAR-T incubation time. (A) Brightfield and fluorescence images of MDA-MB-468 in a 96-well plate on day 4 of culture. CAR-T cells (red) were added for 72h at 5:1, 1:2 and 1:1 E:T ratios. Images acquired at 10x magnification. (B) Viability staining with FDA (green) and PI (red) of MDA-MB-468 after 72h CAR-T incubation in a 96-well plate on day 5 of culture. (C) Plot of FDA area on day 5 of culture after 72h CAR-T incubation. n=3. Data shows a significant difference in FDA area between MDA-MB-468 control cultures and those treated with CAR-T cells at 1:2 and 1:1 E:T ratios(**P ≤ 0.01) and between MDA-MB-468 control cultures and those treated with CAR-T cells at a 5:1 E:T ratio (***P ≤0.0001). (D) Plot of CAR-T cell area 48h after addition to MDA-MB-468 cultures n=3. (MDA = MDA-MDB-468, T = CAR-T) Adapted with permission from Paterson et al., Lab on a chip, 2021, https://creativecommons.org/licenses/by/3.0/. (5x magnification) Data shown as mean ± SD. **P ≤ 0.01, ***P ≤0.0001, One-way ANOVA, Bonferroni's post-test.*

Brightfield imaging showed decreasing numbers of MDA-MB-468 cells present in 2D cultures after 48h incubation (**Figure 5.4**A). Live cancer cell area decreased with increasing E:T ratio in 2D cultures after 72h of CAR-T exposure (**Figure 5.4**B and C). CAR-T cells did not decrease in number over time, suggesting that their culture in microfluidic devices was not detrimental to their viability (**Figure 5.4**D). However, CAR-T cells also did not increase in number either, implying that the CAR-T cells would require additional supplementation and optimisation of their culture media for proliferation.

5.5 3D Co-culture Models

Having confirmed the high expression of EGFR by MDA-MB-468 tumour cells and the low EGFR expression of fibroblasts and considering the outcome of the 2D assays, the next stage was to validate cost effective 3D models that minimize the number of CAR-T cells required to elicit significant cytotoxic responses (**Figure 5.5**).[11]
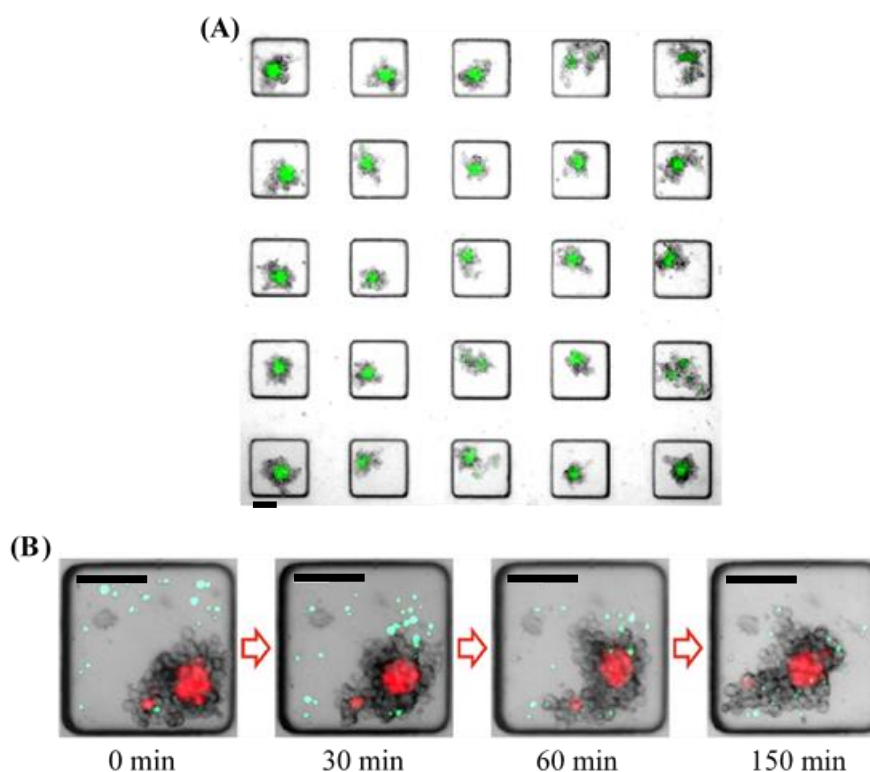
Figure 5.5 *Homing of CAR-T cells in 3D microfluidic cultures. (A) Brightfield and fluorescence image of a 25 spheroid microwell array. (5x magnification) (B) Time-lapse images co-culture of MDA-MDB-468 and NHLF (red) after CAR-T (green) exposure on day 6 of culture immediately after CAR-T cell injection into channel. Scale bar = 100µm. Adapted with permission from Paterson et al., Lab on a chip, 2021, https://creativecommons.org/licenses/by/3.0/.*

Thus, 2D CAR-T protocols were adapted for 3D microfluidic co-cultures (**Section 2.7**) of MDA-MB-468 and the two fibroblast cell lines seeded in a 1:1 ratio into devices (**Figure 5.5**A). To investigate CAR-T interaction with EGFR expressing cells, time-lapse experiments

were carried out with cells fluorescently labelled with CellTrace dyes (**Figure 5.5**B). Recordings showed rapid homing of CAR-T cells towards tumour cells soon after injection into devices (**Section 2.10**). Within three hours of CAR-T injection, each cell could be seen interacting with the spheroids mass.

5.6 Calcium Imaging of CAR-T and Cancer Cell Interaction

Calcium dyes were used to additionally study CAR-T cell interaction with tumour cells as these have been previously reported as a means of identification of CAR-T binding to target cells *in vivo*, using transgenic mouse models.[262] To perform this in 24 channel microfluidic devices, calcium loaded CAR-T cells were administered to microfluidic channels containing MDA-MB-468 and NHLF co-culture spheroids on day 2 of culture (**Figure 5.6**).
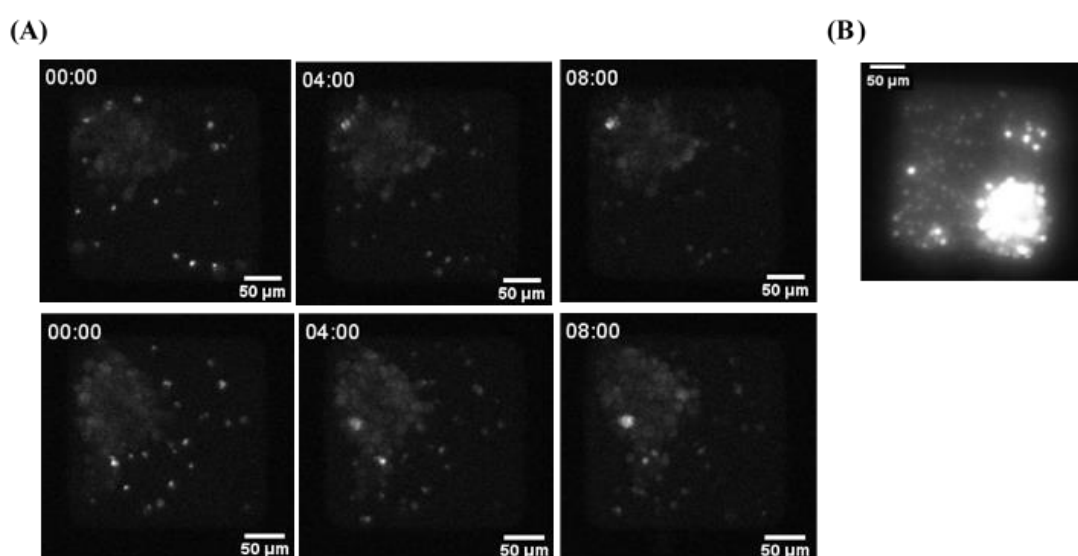
Figure 5.6 *Calcium imaging of CAR-T cell homing to cancer cells. (A) Time-lapse images of calcium-loaded CAR-T migrating towards a tumour spheroid. Scale bar = 50µm. (B) Calcium-loaded CAR-T surrounding a tumour spheroid. Scale bar = 50µm.*

Imaging was performed to show calcium release by CAR-T cells upon binding to cancer cell targets (**Figure 5.6**.A). Calcium-loaded CAR-T cells migrated towards target cells rapidly after injection into devices. Increased fluorescence in specific regions of the tumour mass was detected, indicative of CAR-T binding to EGFR receptors and subsequent calcium release. Images taken 30 minutes after initial CAR-T cell injection showed that a large proportion of CAR-T cells had bound to spheroids and increased calcium signal could be detected from the spheroid (**Figure 5.6**B).

5.7 3D Assessment of CAR-T Cell Targeting and Cytotoxicity

Having carried out time-lapse and calcium imaging to demonstrate CAR-T cell homing towards tumour spheroids, 3D cultures were established in microfluidic devices to assess both the specificity of CAR-T targeting and their mediated cytotoxicity on MDA-MB-468 tumour cells. Cancer cells and fibroblasts were cultured in devices as monoculture and co-culture spheroids (**Figure 5.7**).
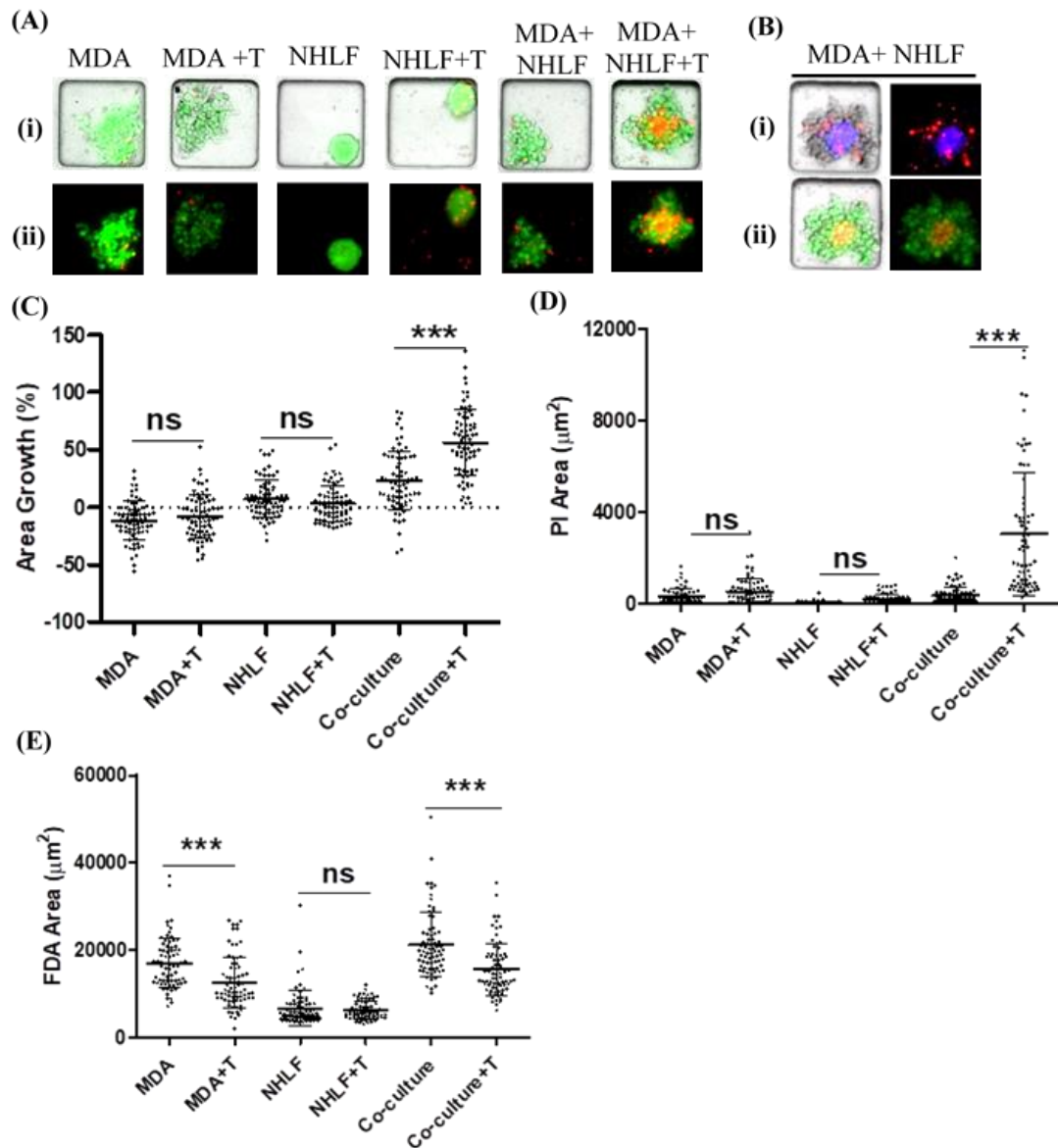
Figure 5.7 *Assessment of the cytotoxic effects of 24h CAR-T incubation in microfluidic devices. (A) Brightfield and fluorescence images of MDA-MDB-468 and NHLF mono- and co-culture spheroids on day 3 of culture after 24h of CAR-T incubation and viability staining with FDA (green) and PI (red). (B) Brightfield and fluorescence images of a representative MDA-MDB-468 and NHLF co-culture spheroid showing (i) dead MDA-MDB-468 (red), live NHLF (blue) and dead NHLF (purple) and (ii) live MDA-MDB-468 (green), live NHLF (yellow) and dead NHLF (red). (C) Percentage change in brightfield areas from day 2 to 3. n=74. Data shows a significant difference in area growth (***P ≤0.0001) between control co-cultures and those treated with CAR-T cells. (D) PI area on day 3 of culture. n=74. Data shows a significant difference in PI area (***P ≤0.0001) between control co-cultures and those treated with CAR-T cells. (E) FDA area on day 3 of culture. n=74. Data shows a significant difference in FDA area (***P ≤0.0001) between control co-cultures and those treated with CAR-T cells. (MDA = MDA-MDB-468, T = CAR-T cells) (5x magnification) Data shown as mean ± SD. ***P ≤0.0001, One-way ANOVA, Bonferroni's post-test.*

Cells were cultured in microfluidic devices for 48 hours prior to CAR-T cell injection on day 2 and incubated for 24 hours. Cancer cells and stromal cells could be differentiated from each other as stromal cells were fluorescently labelled with CellTrace Far Red (**Section 2.15**). This

meant that upon overlaying the FDA signal, live cancer cells would appear as green while live stromal cells would appear yellow. When the PI signal was overlaid, dead cancer cells would show as green while dead stromal cells would appear as purple. This was done by artificially altering the colour of the CellTrace Far Red signal in ImageJ to appear as blue, thus to allow for distinction between the CellTrace Far Red signal and that from the PI stain. Live/dead staining showed that the vast majority of cancer cells in monoculture spheroids remained viable after CAR-T cell treatment (**Figure 5.7**A). However, FDA signal was not as prominent when compared to control cancer cell monoculture spheroids. NHLF spheroids also maintained their integrity regardless of CAR-T incubation. Minimal PI overlap with NHLF co-culture spheroid areas was observed, indicating that the majority of dead cells are cancer cells and not the low EGFR expressing stromal cells (**Figure 5.7**B). All NHLF cell areas could be observed to overlap with the FDA signal, suggesting NHLF are alive and specificity of CAR-T killing of high EGFR expressing cells only. It was noted, however, that a large proportion of the cancer cell population was still present in in the culture after 24h CAR-T exposure. Thus, incubation time was increased for subsequent experiments, as was the case for the 2D experiments. For NHLF monoculture spheroids that had been exposed to CAR-T, dead cells floating in traps did not exhibit the NHLF CellTrace signal so could be identified as unlabelled CAR-T. This suggests that CAR-T cells may not be able to survive in cultures absent of their target antigen. Brightfield area measurements showed a significant increase in disaggregation (***P ≤0.0001), using one-way ANOVA analysis, for CAR-T treated co-cultures but not for either monoculture spheroids (**Figure 5.7**C). Brightfield area was quantified before and after viability staining to detect any changes to spheroid areas after washing steps. However, no significant differences between data sets were observed and, thus, area measurements from images acquired after viability staining were analysed for all subsequent data. Significantly greater cell death (***P ≤0.0001) was also detected, using one-way ANOVA analysis, for co-cultures only with CAR-T treatment. However, neither cancer cell nor fibroblast monoculture spheroids exhibited significantly greater cytotoxicity (**Figure 5.7**D). This can be explained due to the variation in effector to target cells between monocultures and co-cultures. While the customary seeding protocol ensured a constant number of cells in traps, this meant that in co-cultures, only half of the target cells (MDA-MB-468) were present in comparison to monocultures. This meant that there was a greater effector to target ratio in co-cultures in comparison to monocultures and is why greater cancer cell killing was observed. Despite this, a statistically significant reduction in FDA area (***P ≤0.0001) was detected from one-way ANOVA analysis for both MDA-MB-468 monocultures and co-cultures with no statistically significant difference to NHLF monocultures (**Figure

5.7E). This work provided initial evidence of specific CAR-T killing of cancer cells in 3D and demonstrated that for subsequent experiments, spheroids should be incubated with CAR-T cells for longer time periods to see a more pronounced disaggregation and killing of MDA-MB-468.

5.8 3D Optimization of Experimental Conditions

As a result of preliminary 2D and 3D CAR-T cell assays, the CAR-T incubation time for 3D experiments was also increased to 48 hours and 72 hours in accordance with 2D studies (**Figure 5.8**).[11]
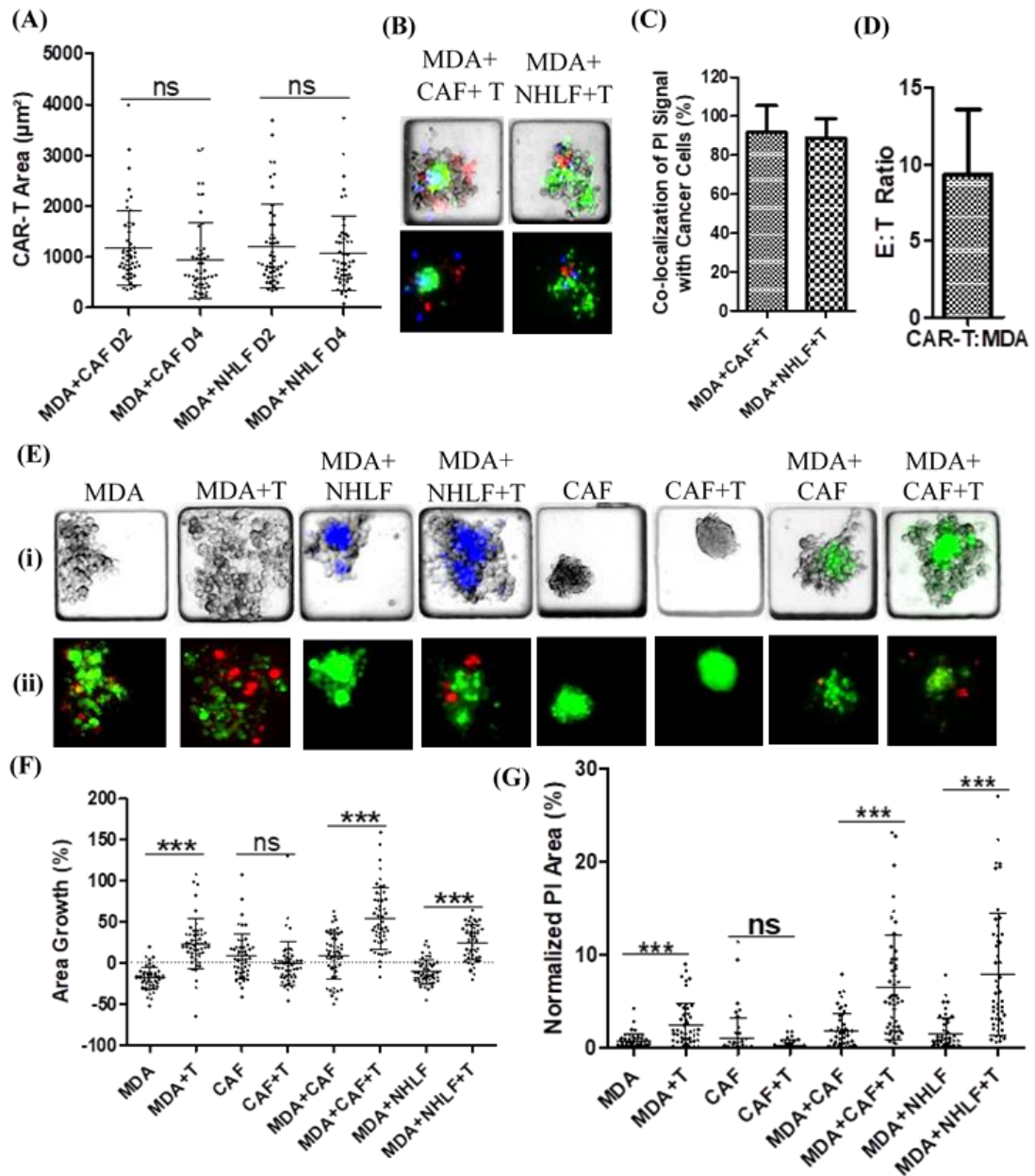
Figure 5.8 *3D Assessment of E:T ratios with increased CAR-T incubation time. (A) Plot of CAR-T area in devices immediately after CAR-T cell seeding (Day 2) and after 48h of incubation in devices (Day 4). (B) Brightfield and fluorescence images of MDA-MDB-468 co-cultures with fibroblasts (green) and CAR-T (blue), stained with PI (red) after 72h of CAR-T incubation in devices. Dead fibroblasts appear as yellow and dead CAR-T appear as purple. (C) Percentage of PI signal that does not overlap with fibroblast areas. n=50. (D) Plot of average ratio of CAR-T, seeded on day 2, to MDA-MDB-468, seeded on day 0, in microwells with 45±15 MDA cells on day 0. n=50. (E) Microfluidic device cultures on day 5 after 72h CAR-T incubation. (i) Brightfield and fluorescence images of MDA-MDB-468 (unlabeled), NHLF (blue) and CAF (green) mono- and co-cultures. (ii) Fluorescence images of viability staining with FDA (green) and PI (red) of MDA-MDB-468 monocultures and MDA-MDB-468 and NHLF co-cultures and staining with PI (red only) for CAF (green) monocultures and MDA-MDB-468 and CAF co-cultures. (F) Plot of the percentage change in brightfield area from day 2 to 5. n=50. Data shows a significant difference in area growth with CAR-T treatment (***P ≤0.0001) for cancer cell monocultures and CAF-cancer cell and NHLF-cancer cell co-cultures. (G) Plot of the percentage of brightfield area with PI signal. n=50. Data shows a significant difference in PI area with CAR-T treatment (***P ≤0.0001) for cancer cell monocultures and CAF-cancer cell and NHLF-cancer cell co-cultures. (MDA = MDA-MDB-468, T = CAR-T) Adapted with permission from Paterson et al., Lab on a chip, 2021, https://creativecommons.org/licenses/by/3.0/. (5x magnification) Data shown as mean ± SD. ***P ≤0.0001, One-way ANOVA, Bonferroni's post-test.*

No significant changes to CAR-T cell area were detected after 48h incubation with either co-culture of MDA-MB-468 and CAF or NHLF (**Figure 5.8**A). Brightfield and fluorescent images appeared to show PI signal was localized to cancer cell regions within co-culture spheroids (**Figure 5.8**B). To confirm this, image analysis protocols were developed that allowed quantification of the co-localisation of PI signal to cancer cells (**Figure 5.8**C). This analysis showed that the vast majority of PI signal, for both MDA-MB-468 and CAF co-cultures and for MDA-MB-468 and NHLF co-cultures originated from cancer cell regions of spheroids and not fibroblast areas. Mean and standard deviation values for both co-culture conditions were quantified as 91.68 ± 13.77% and 88.64 ± 10.05% respectively. An approximate E:T ratio was calculated to be 1:10 CAR-T cells to cancer cells (**Figure 5.8**D). This quantification was performed by taking the number of CAR-T cells, seeded on day 2, to MDA-MB-468, seeded on day 0, in microwells with an average of 45 ± 15 MDA-MB-468 cells per microwell present on day 0. Greater disaggregation of both mono- and co-cultures with MDA-MB-468 cells could be observed after 72h CAR-T exposure in comparison to control cultures (**Figure 5.8**E). This was confirmed with quantification of brightfield areas which showed statistically greater spheroid area (***$P \leq 0.0001$), with one-way ANOVA analysis, for MDA-MB-468 monocultures and co-cultures after CAR-T treatment (**Figure 5.8**F). In comparison, no increase in disaggregation was detected for stromal monoculture spheroids exposed to CAR-T. A statistically significant increase in cell death (***$P \leq 0.0001$) for mono- and co-cultures including cancer cells after 72h incubation with CAR-T was observed, with no statistically significant change in PI area for fibroblast monocultures using one-way ANOVA analysis, (**Figure 5.8**G). After 72h CAR-T exposure, MDA-MB-468 monocultures were expected to have only dead cells remaining and co-cultures to have only fibroblasts remaining. However, live cancer cells were still present in cultures even after the extended incubation period. It is likely that, similarly to 2D cultures, increasing E:T ratio for 3D assays would also result in greater cancer cell killing. However, increasing CAR-T cell dosage could also result in greater side effects for patients. The E:T ratios used in these assays provided the opportunity to investigate whether additional or synergistic effects could be produced by combining therapies. Therefore, it was considered that a combination of treatments should be introduced in order to establish their ability to enhance CAR-T cell killing.

5.9 Confirmation of CAR-T specific targeting through EGFR Recognition

Having established the ability of CAR-T cells to home towards and kill tumour cells targets, it was then important to verify the receptor targeting mechanism by which this occurs. To confirm CAR-T specific targeting of cancer cells through EGFR recognition, spheroids were

incubated with a blocking anti-EGFR antibody for 24h on day 1 of culture prior to 72h CAR-T incubation (**Figure 5.9**).[11]
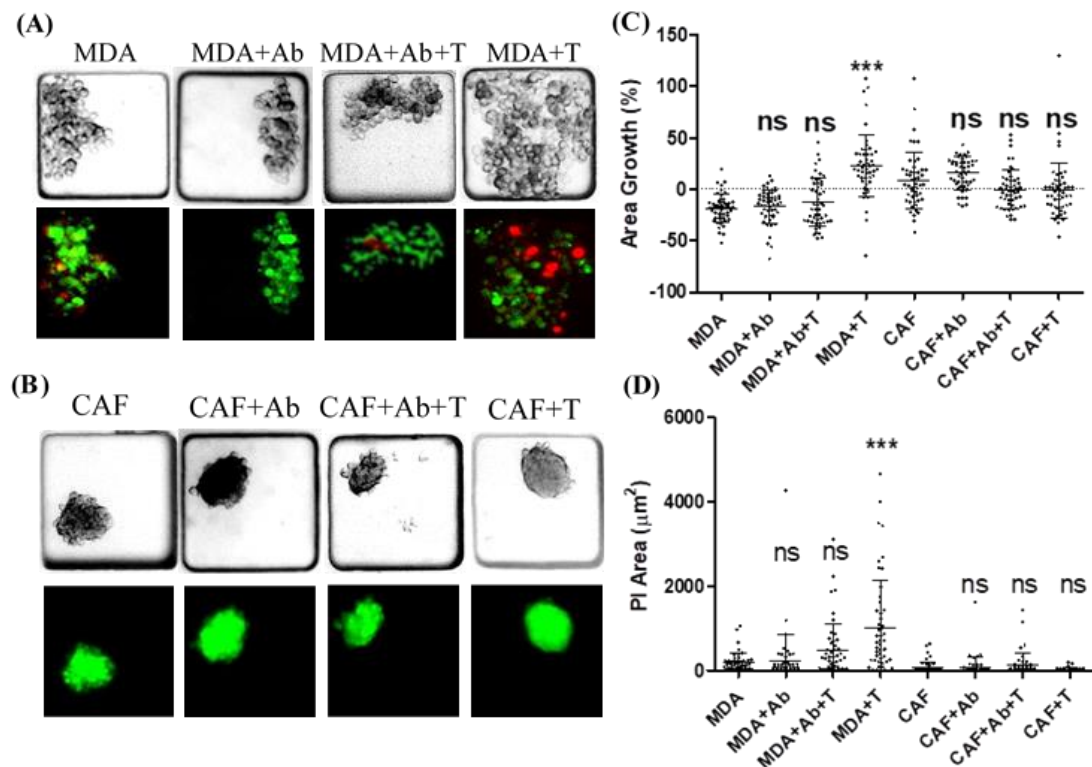
Figure 5.9 *CAR-T specific targeting through EGFR Recognition (A) Brightfield and fluorescent images of MDA-MDB-468 monocultures, stained with FDA (green) and PI (red). (B) Brightfield and fluorescent images of CAF (green) monocultures stained with PI (red). (C) Plot of the percentage change in brightfield area from day 2 to 5. n=50. Data shows a significant difference in area growth (***P ≤0.0001) for MDA-MB-468 monocultures treated with CAR-T cells in comparison to control MDA-MB-468 monocultures. (D) Plot of PI area on day 5. n=50. Data shows a significant difference in PI area (***P ≤0.0001) for MDA-MB-468 monocultures treated with CAR-T cells in comparison to control MDA-MB-468 monocultures. Adapted with permission from Paterson et al., Lab on a chip, 2021, https://creativecommons.org/licenses/by/3.0/. (5x magnification) Data shown as mean ± SD. ***P ≤0.0001, One-way ANOVA, Bonferroni's post-test.*

CAR-T treatment did not result in the disaggregation of cancer cell monocultures spheroids that had been previously incubated with anti-EGFR antibodies (**Figure 5.9**A). CAF spheroids maintained their compact spheroid formation and viability in all of the conditions tested (**Figure 5.9**B). Brightfield area was quantified to confirm that anti-EGFR antibodies were able to prevent CAR-T disaggregation of MDA-MB-468 spheroids (**Figure 5.9**C). A statistically significant increase in PI area (***P ≤0.0001) was detected using one-way ANOVA analysis for MDA-MB-468 spheroids with CAR-T treatment, as is consistent with previous results (**Figure 5.9**D). This effect was negated with anti-EGFR antibody exposure prior to CAR-T treatment. Therefore, CAR-T targeting and killing of cancer cells through EGFR recognition was confirmed.

5.10 Carboplatin Influence on Cancer Cell PD-L1 Expression

Once the selective killing by EGFR targeting CAR-T cells of EGFR expressing cancer cells had been validated in microfluidic devices, the aim of this next stage of work was to develop a novel immunoassay that, for the first time, would allow for the assessment of combination cancer therapies *in vitro* with CAR-T cells against 3D tumour-stromal co-cultures. To mimic clinical therapy regimes, carboplatin chemotherapy and anti-PD-L1 therapy were considered in various combinations for assessment with CAR-T therapy. PD-L1 expression on tumour cells is a powerful defence mechanism that tumour cells can employ to deactivate immune cells and prevent their attack.[263] The inhibitory effects of PD-L1 expression can be supressed through checkpoint blockade therapy using FDA approved PD-L1 inhibitors such as atezolizumab, durvalumab and avelumab.[264] It is known in the literature that chemotherapeutic agents can result in the upregulation of PD-L1 expression by cancer cells and could be an important contributing factor to the limited success of CAR-T therapy against solid tumours.[265] Therefore, in the initial stage of experiments, MDA-MB-468 expression of PD-L1 before and after chemotherapy treatment was assessed to determine if this would be a suitable choice of combination therapy treatment for this proof of concept assay. Carboplatin was selected as an appropriate chemotherapy to use in conjunction with CAR-T and anti-PD-L1 therapy as this drug is used clinically in breast cancer therapy regimes and in pre-clinical TNBC studies.[105, 266] Combination therapy using carboplatin pre-treatment followed by CAR-T therapy has been shown to elicit enhanced anti-tumour effects for *in vivo* mouse models.[267] It was hypothesized that applying initial chemotherapy would attack the tumour cells and TME. After which, anti-PD-L1 treatment could be administered and which would counteract any increase in PD-L1 expression caused by chemotherapy exposure. This sequence of treatment would prevent inhibition of CAR-T activation and, thus, provide a combination treatment regime that could lead to enhanced and specific tumour cell killing. A range of carboplatin concentrations were tested: 12.5µM, 25µM, 50µM, 100µM and 200µM. These were added on day 1 of culture for 24h before refreshment of cell culture media on days 2 and 3, which corresponded to the final experimental protocol timeline that would combine all three therapies (**Figure 5.10**).[11]
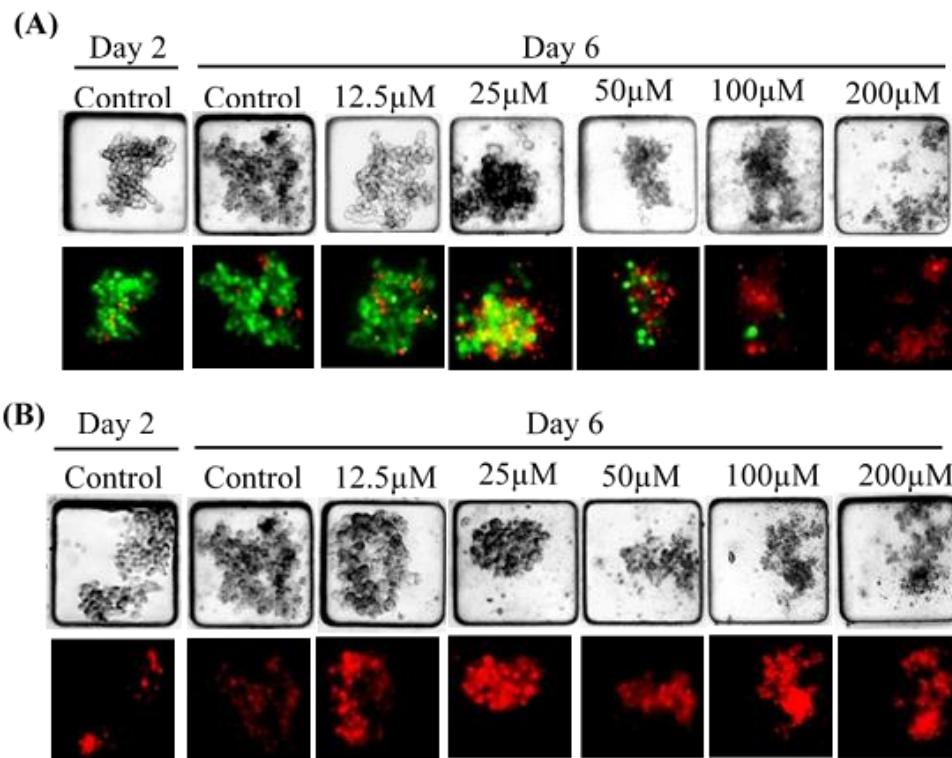
Figure 5.10 *Assessment of the effects of carboplatin on MDA-MDB-468 spheroid viability and protein expression. (A) Brightfield and fluorescent images after viability staining with FDA (green) and PI (red). (B) Brightfield and fluorescent images after staining with anti-PD-L1 antibodies (red). Adapted with permission from Paterson et al., Lab on a chip, 2021, https://creativecommons.org/licenses/by/3.0/. (5x magnification)*

Carboplatin treatment caused increasing cell death and disaggregation of spheroids with increasing concentrations (**Figure 5.10**A). PD-L1 expression of drug treated spheroids was also shown to be enhanced in comparison to control spheroids (**Figure 5.10**B). Quantification of viability and PD-L1 expression was performed (**Figure 5.11**).[11]
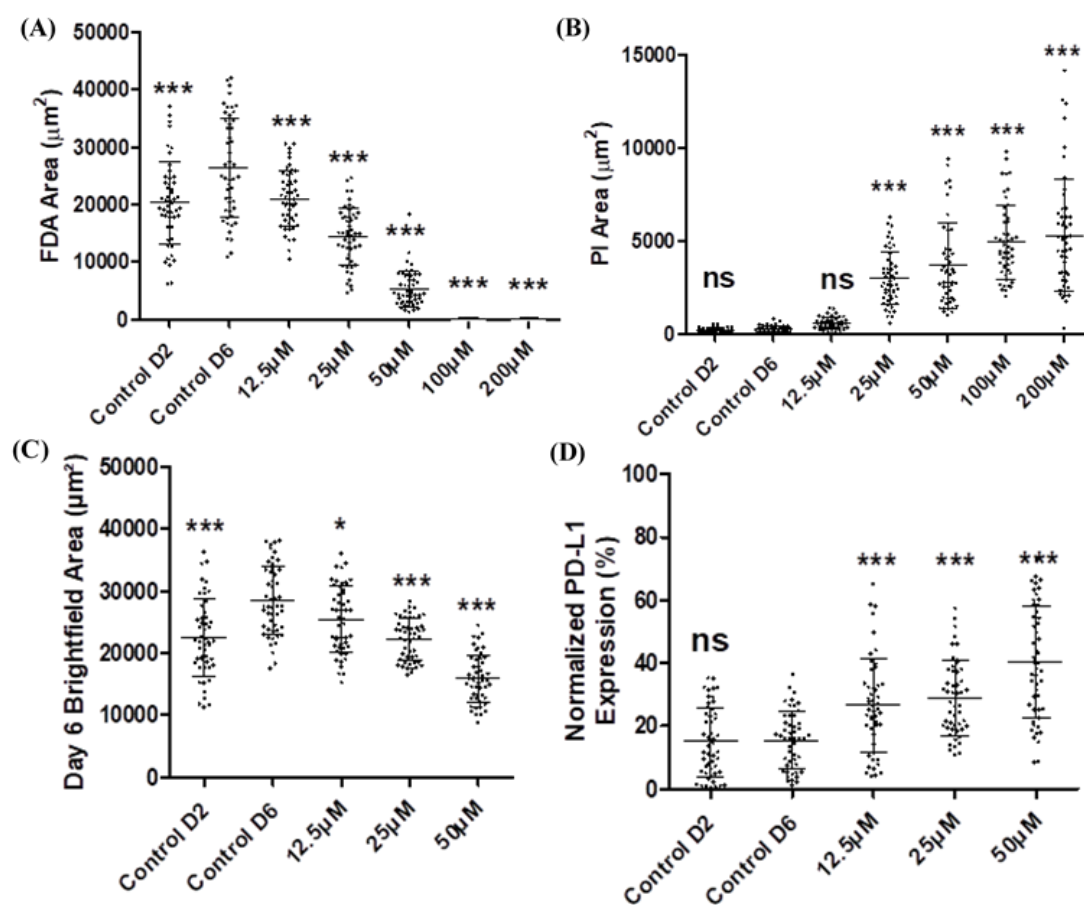
Figure 5.11: Quantification of viability and PD-L1 expression. (A) Plot of FDA area. n=50. Data shows a significant difference in FDA area (***P ≤0.0001) between control spheroids on day 6 and those treated with all carboplatin concentrations and control spheroids on day 2. (B) Plot of PI area. n=50. Data shows a significant difference in PI area (***P ≤0.0001) between control spheroids on day 6 and those treated with 25µM, 50µM, 100µM and 200µM carboplatin concentrations. (C) Plot of day 6 brightfield area. n=50. Data shows a significant difference in brightfield area (***P ≤0.0001) between control spheroids on day 6 and those treated with 12.5µM, 25µM and 50µM carboplatin concentrations and control spheroids on day 2. (D) Plot of the percentage of day 6 brightfield area with PD-L1 expression (%). n=50. Data shows a significant difference in PD-L1 expression (***P ≤0.0001) between control spheroids on day 6 and those treated with 12.5µM, 25µM and 50µM carboplatin concentrations. Adapted with permission from Paterson et al., Lab on a chip, 2021, https://creativecommons.org/licenses/by/3.0/. Data shown as mean ± SD. ***P ≤0.0001, One-way ANOVA, Bonferroni's post-test.

A statistically significant reduction in live spheroid area (***P ≤0.0001) with increasing concentration of carboplatin was detected by one-way ANOVA analysis (**Figure 5.11**A), as well as a statistically significant increase in cell death (***P ≤0.0001) (**Figure 5.11**B). The FDA area of control spheroids was also shown to increase from day 2 to day 6 with no significant changes in PI area, suggesting that cells are able to remain healthy and proliferate in microfluidic device cultures. Brightfield area was shown to decrease with increasing drug concentrations (**Figure 5.11**C). It should be noted that accurate area quantification was not attainable for spheroids treated with higher carboplatin concentrations due to disaggregation of spheroids. No statistically significant change in PD-L1 expression of control spheroids from

day 2 to 6 was observed (**Figure 5.11**D). A statistically significant increase in PD-L1 expression (***P ≤0.0001) by spheroids after 24h carboplatin exposure was recorded with one-way ANOVA analysis and which did not increase with increasing dose.

5.11 Combination Chemptherapy, Checkpoint Blockade and ACT

After analysis of the effects of a range of chemotherapy doses on MDA-MB-468 spheroid viability and PD-L1 expression, the next phase of experiments involved testing therapy combinations in monocultures and co-cultures of MDA-MB-468 cancer cells with CAF to establish an augmented cytotoxic effect in comparison to monotherapies (**Section 2.10**). The 12.5µM carboplatin concentration was selected for the next experimental phase with CAR-T cells. Administering this concentration resulted in a statistically significant increase in PD-L1 expression and reduction in FDA area without complete disaggregation of spheroids. Therefore, an enhanced cytotoxic effect with CAR-T added would be able to be seen in subsequent combination assays. For the combination treatment assays, carboplatin was introduced to cultures on day 1, followed by anti-PD-L1 antibodies on day 2 and 72h of CAR-T exposure beginning on day 3 (**Figure 5.12**).[11]
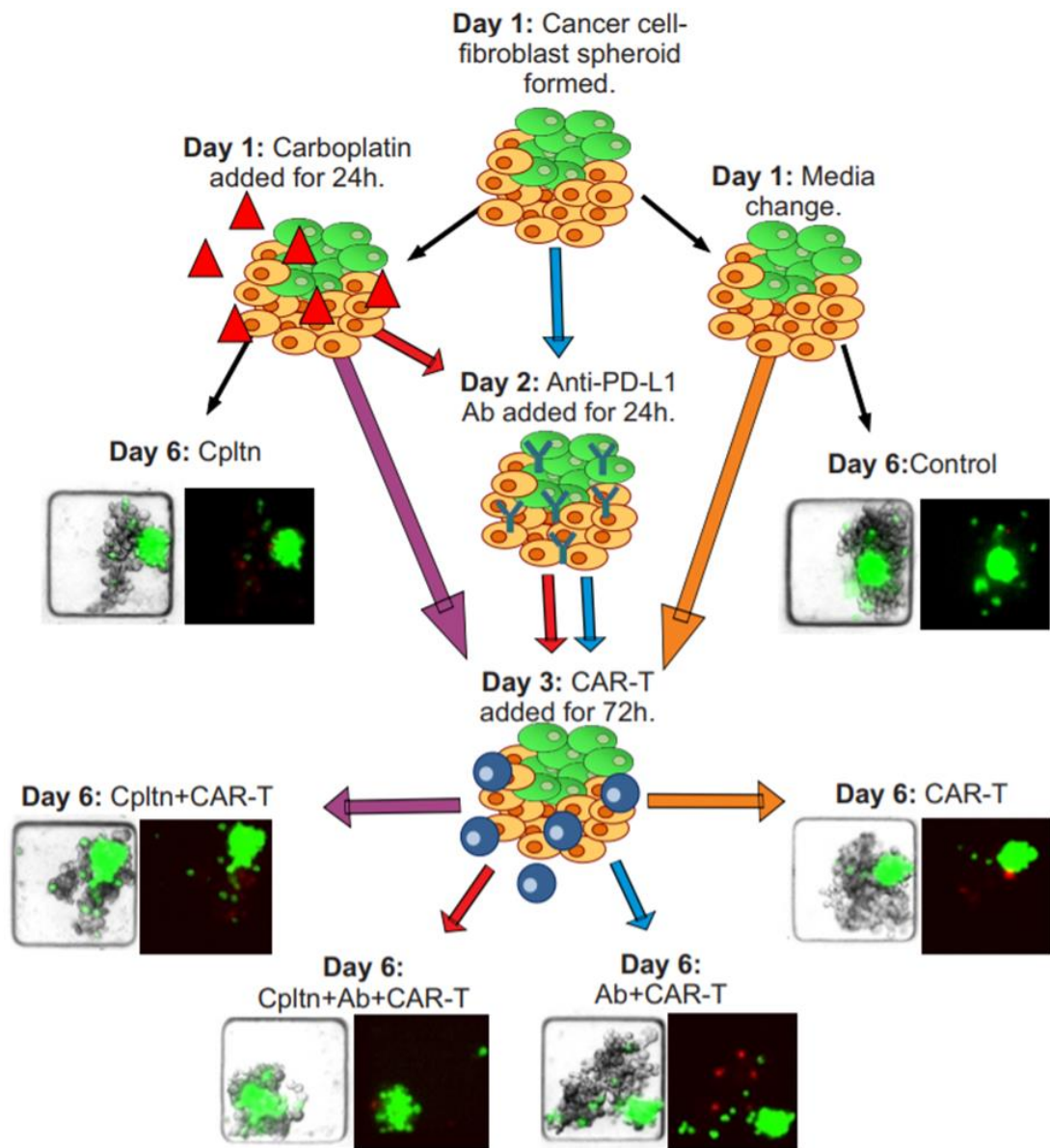
Figure 5.12 *Schematic drawing of combination therapy timeline for MDA-MDB-468 and CAF (green) co-culture spheroids with brightfield and fluorescent images acquired after staining with PI (red). (Cpltn = Carboplatin, Ab = anti-PD-L1 antibodies) Adapted with permission from Paterson et al., Lab on a chip, 2021,* *https://creativecommons.org/licenses/by/3.0/.*

Combination therapy was first studied in MDA-MB-468 monoculture spheroids prior to co-culture assays (**Figure 5.13**).[11]
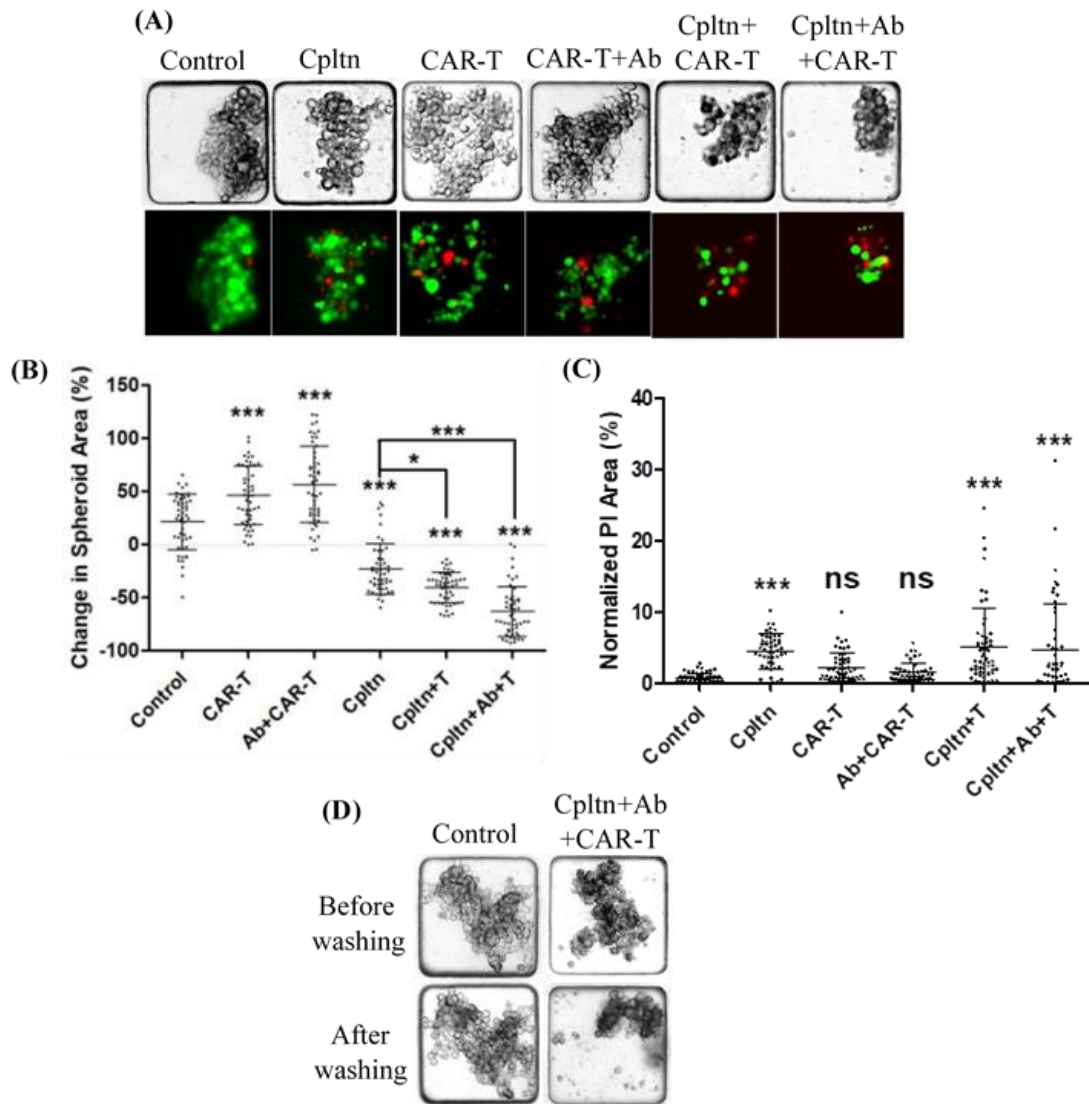
Figure 5.13: Combination therapy in cancer cell monoculture spheroids. (A) Brightfield and fluorescent images on day 6 with cells stained with PI (red) and FDA (green). (B) Plot of percentage change in brightfield area from day 1 to 6. (%) n=50. Data shows a significant difference in spheroid area (***P ≤0.0001) between control spheroids and those treated with all other therapy combinations. Data shows a significant difference in spheroid area between carboplatin monotherapy and with the addition of CAR-T therapy (*P ≤ 0.05) and with CAR-T therapy and anti-PD-L1 therapy in combination (***P ≤0.0001). (C) Plot of percentage of day 6 brightfield area with PI signal. n=50. Data shows a significant difference in PI area (***P ≤0.0001) between control spheroids and those treated with carboplatin monotherapy, carboplatin and CAR-T therapy and combination carboplatin, CAR-T and anti-PD-L1 therapy. (D) Brightfield images showing washing out of dead cells in treated monocultures but not control monocultures. (5x magnification) (Cpltn = Carboplatin chemotherapy, Ab = anti-PD-L1 antibodies, T = CAR-T cells) Adapted with permission from Paterson et al., Lab on a chip, 2021, https://creativecommons.org/licenses/by/3.0/. Data shown as mean ± SD. *P ≤ 0.05, ***P ≤0.0001, One-way ANOVA, Bonferroni's post-test.

For monocultures, a decrease in brightfield area when chemotherapy was applied alone and in combinations was observed (**Figure 5.13**A). The greatest decrease in brightfield area was detected with the chemotherapy, antibody and CAR-T cell combination (**Figure 5.13**B). Brightfield area was increased by CAR-T treatment as seen previously due to the breaking up of the spheroid structures by the CAR-T cells. A statistically significant increase in cell death

(***P ≤0.0001) with combination treatment was seen with on-way ANOVA analysis in all conditions including carboplatin (**Figure 5.13**C). Due to the washing steps involved in fixing and staining of the cells many of the dead cancer cells were detached from the tumour aggregate and were no longer present in microwells at the point of fluorescence imaging after carboplatin treatment in comparison to control cultures (**Figure 5.13**D). No statistically significant differences in brightfield or PI area were detected between CAR-T monotherapy and combined CAR-T and anti-PD-L1 therapy when chemotherapy was not included in treatment regimes. Thus, indicating that the inclusion of the checkpoint inhibitor in these therapy regimes offers a minor contribution to CAR-T performance.

Subsequently, the efficacy of the same therapeutic combinations was assessed in MDA-MB-468 and CAF spheroid co-cultures (**Figure 5.14**).[11]
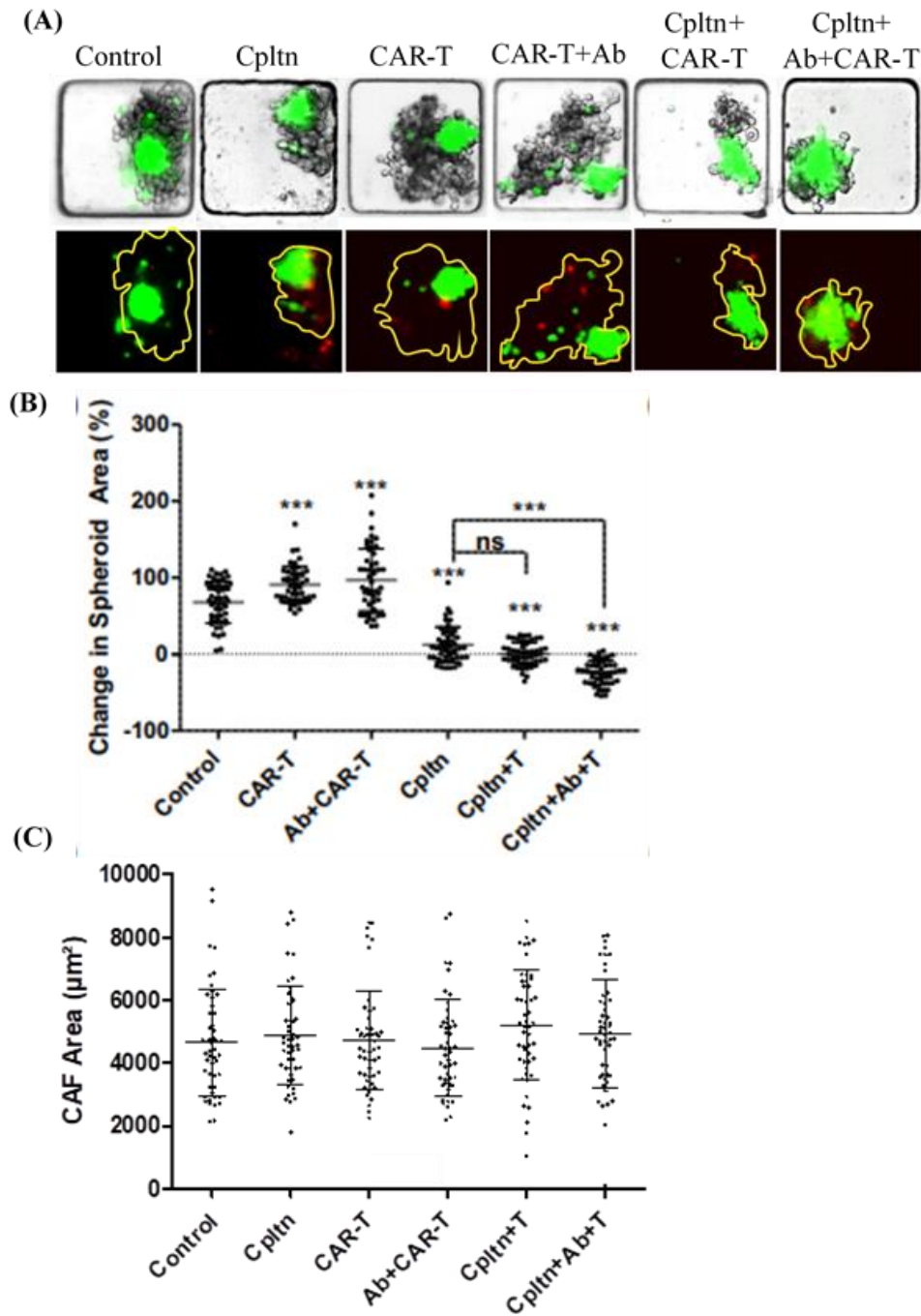
Figure 5.14 *Combination therapy in cancer cell-stromal co-culture spheroids. (A) Brightfield and fluorescent images on day 6 of MDA-MDB-468 and CAF (green) spheroids stained with PI (red). Outline of spheroid is shown in yellow for fluorescent images. (B) Plot of percentage change in brightfield area from day 1 to 6. n=50. Data shows a significant difference in percentage change in brightfield area (***P ≤0.0001) between control spheroids and all therapy combinations and between carboplatin monotherapy and with the addition of CAR-T therapy (***P ≤0.0001) and with CAR-T therapy and anti-PD-L1 therapy in combination (***P ≤0.0001) (C) Plot of CAF area on day 6 of culture. n=50. (Cpltn = Carboplatin chemotherapy, Ab = anti-PD-L1 antibodies, T = CAR-T cells) Adapted with permission from Paterson et al., Lab on a chip, 2021, https://creativecommons.org/licenses/by/3.0/. (5x magnification) Data shown as mean ± SD. ***P ≤0.0001, One-way ANOVA, Bonferroni's post-test.*

Results for co-culture assays were consistent with those obtained for MDA-MB-468 monocultures (**Figure 5.14**A). Spheroid area was analysed by one-way ANOVA and found to be significantly reduced (***P ≤0.0001) when chemotherapy was administered alone and in combinations with CAR-T and anti-PD-L1 treatment (**Figure 5.14**B). Once again, the greatest reduction in tumour spheroid mass was recorded where chemotherapy, anti-PD-L1 treatment and CAR-T cells were combined. Greater disaggregation of spheroids treated with CAR-T cells with and without checkpoint inhibitors was observed. As seen in monocultures, no significant differences between CAR-T treatment alone and combined CAR-T and anti-PD-L1 therapy were recorded for co-cultures in the absence of chemotherapy treatment. CAF area quantification for cancer-stromal co-cultures, showed no statistically significant differences between conditions (**Figure 5.14**C). This suggests that non-EGFR expressing cells are able to persist through combination non-specific low dose chemotherapy, checkpoint blockade therapy and EGFR specific CAR-T treatment. PI area and PI signal co-localization with cancer cells was quantified in co-cultures (**Figure 5.15**).[11]
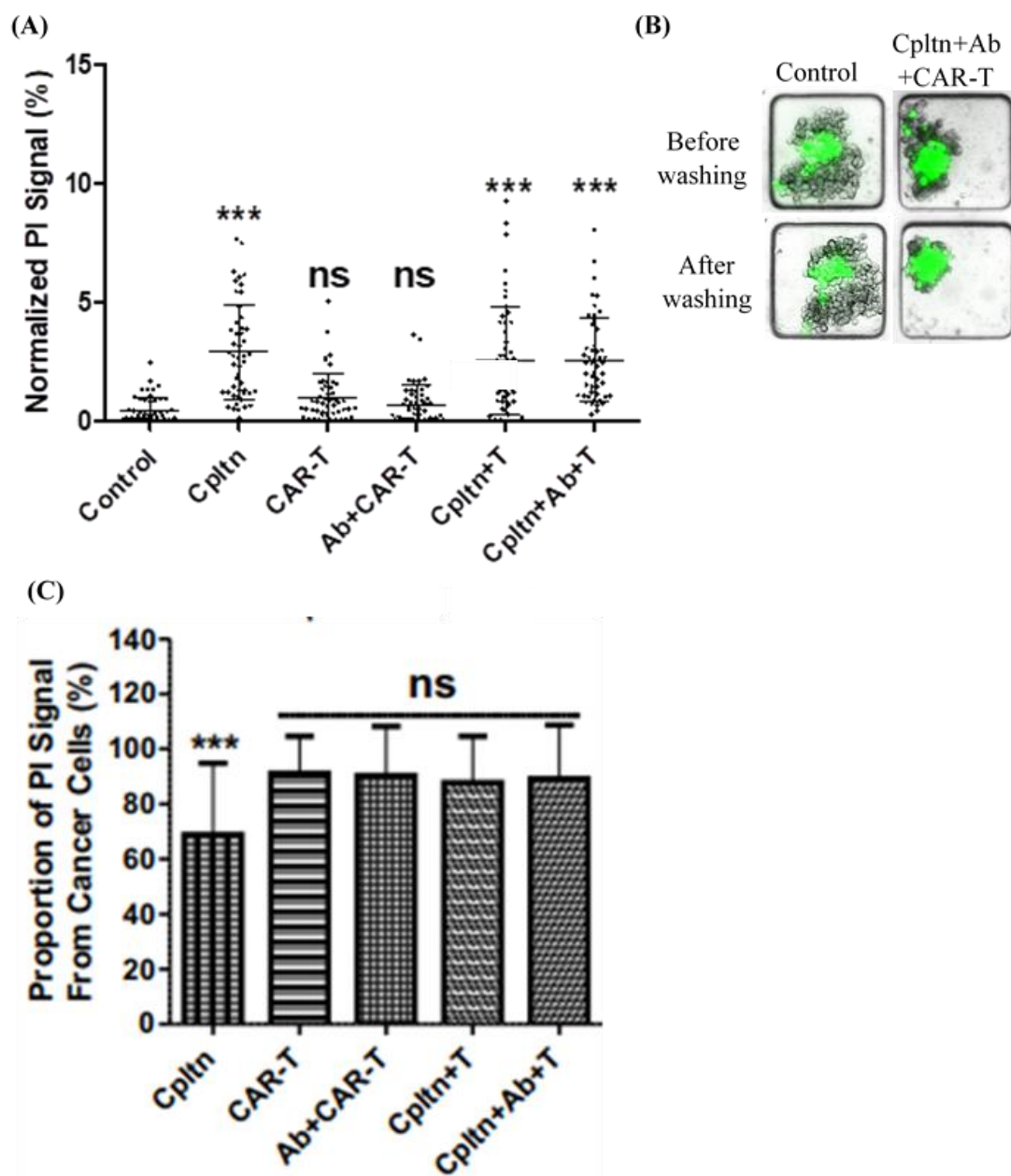
Figure 5.15*: Quantification of PI signal and co-localization in co-cultures. (A) Plot of percentage of brightfield area with PI signal. n=50. Data shows a significant difference in PI area (***P ≤0.0001) between control spheroids and those treated with carboplatin monotherapy, carboplatin and CAR-T therapy and combination carboplatin, CAR-T and anti-PD-L1 therapy. (E) Brightfield images showing washing out of dead cells in treated co-cultures but not control co-cultures. (F) Plot of percentage of MDA-MDB-468 area and PI area co-localization. n=30. Data shows a significant difference in PI co-localization with cancer cells (***P ≤0.0001) between carboplatin monotherapy treatment and all other therapy combinations. (Cpltn = Carboplatin chemotherapy, Ab = anti-PD-L1 antibodies, T = CAR-T cells) Adapted with permission from Paterson et al., Lab on a chip, 2021, https://creativecommons.org/licenses/by/3.0/. (5x magnification) Data shown as mean ± SD. ***P ≤0.0001, One-way ANOVA, Bonferroni's post-test.*

Significantly greater cell death (***P ≤0.0001) was only detected using one-way ANOVA for therapy regimes including carboplatin, for monotherapy and combination therapies (**Figure 5.15**A). As previously noted, many dead cells were removed from microwells during the staining process (**Figure 5.15**B). Combined checkpoint inhibitor and CAR-T therapy did not

induce a statistically significant increase in cell death and suggests that chemotherapy treatment is the primary influence for augmenting the cytotoxic effects of CAR-T cells. The percentage of PI signal and MDA-MB-468 co-localization was quantified and showed that the majority of PI signal originated from cancer cells and not CAF with CAR-T combination treatments (**Figure 5.15**C). Combination therapy incorporating chemotherapy, checkpoint blockade and CAR-T therapy gave an average and standard error value of 89.19 ± 3.30% co-localization of PI signal to cancer cells. This was in contrast to control co-cultures which showed 87.73 ± 4.73% co-localization and carboplatin treatment alone at 68.94 ± 4.37%. This demonstrates the on-target specificity of the EGFR targeting CAR-T cells used in these proof of concept assays.

5.12 Carboplatin Influence on Cancer Cell EGFR Expression

A review of the literature revealed that an increase in EGFR expression of cancer cells after chemotherapy exposure could potentially be the reason for the synergistic effects of chemotherapy and CAR-T cell therapy seen in combination studies. MDA-MB-468 monoculture EGFR expression was quantified (**Section 2.11.1**) using an anti-EGFR antibody to determine if the increase in MDA-MB-468 cell killing was due to increased EGFR expression after carboplatin exposure (**Figure 5.16**).[11]
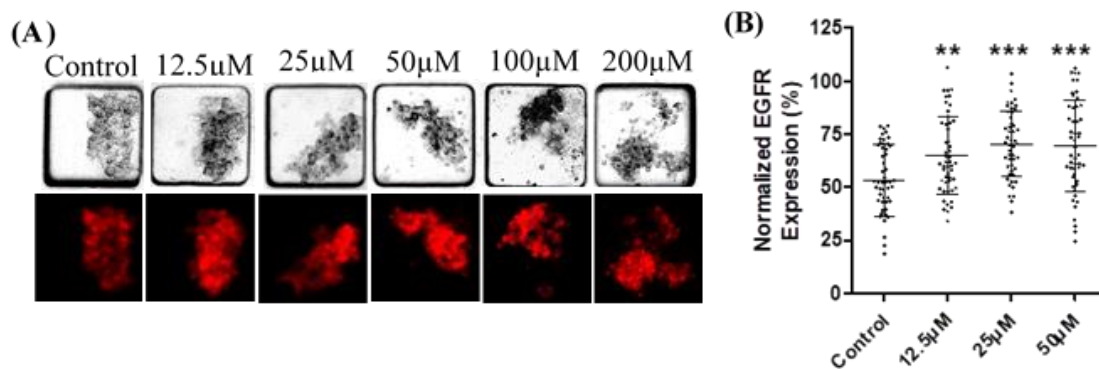
Figure 5.16** Assessment of the effects of carboplatin on MDA-MDB-468 spheroid EGFR expression. (A) Brightfield and fluorescent images after staining with anti-EGFR antibodies (red). (B) Plot of the percentage of day 5 brightfield area with EGFR expression after 24h of Carboplatin treatment beginning on day 1. n=50. Data shows a significant difference in EGFR expression between control spheroids and those treated with 12.5μM carboplatin (**P ≤ 0.01) and with 25μM and 50μM carboplatin (P ≤0.0001). Adapted with permission from Paterson et al., Lab on a chip, 2021, https://creativecommons.org/licenses/by/3.0/. (5x magnification) Data shown as mean ± SD. **P ≤ 0.01, ***P ≤0.0001, One-way ANOVA, Bonferroni's post-test.*

To be consistent with combination treatments, carboplatin was applied for 24h beginning on day 1 of culture. After 24h, media was refreshed and spheroids cultured for a further 24h. At this point CAR-T cells would be added in combination treatment experiments and so cells were fixed at this stage to establish the EGFR levels that would be present at the point at which CAR-T exposure would commence. EGFR expression as a function of brightfield area could

not be calculated for the 100μM and 200μM concentrations due to disaggregation after treatment (**Figure 5.16**A). Exposure of cancer cells to 12.5μM (**P ≤ 0.01) and to 25μM and 50μM (***P ≤0.0001) carboplatin concentrations resulted in a statistically significant increase in EGFR expression as detected by one-way ANOVA analysis (**Figure 5.16**B). Thus, the selected carboplatin concentration, 12.5μM, resulted in increased EGFR expression of cells without completely disrupting the spheroid structure. As a result of this increased EGFR expression, more binding sites would be available for CAR-T cells and provides reasoning for the enhanced cytotoxicity observed with combination chemotherapy and CAR-T cell therapy.

5.13 Consideration of Primary Cell Lines for EGFR Targeting Immunoassays

Having validated the platform for use in assessing the cytotoxicity and target specificity of CAR-T cells against a breast cancer cell line, the next aim was to demonstrate the application of this platform for primary cells. Primary breast and ovarian cancer cell lines, Cellaria Wood and Cellaria Powder respectively, were considered for combination immunotherapy treatment and their EGFR expression assessed in 2D using 24-well plates. The level of EGFR expressed by Cellaria Powder and Cellaria Wood in comparison to CAF and MDA-MB-468 cell lines was quantified after 3 days of 2D culture (**Figure 5.17**).
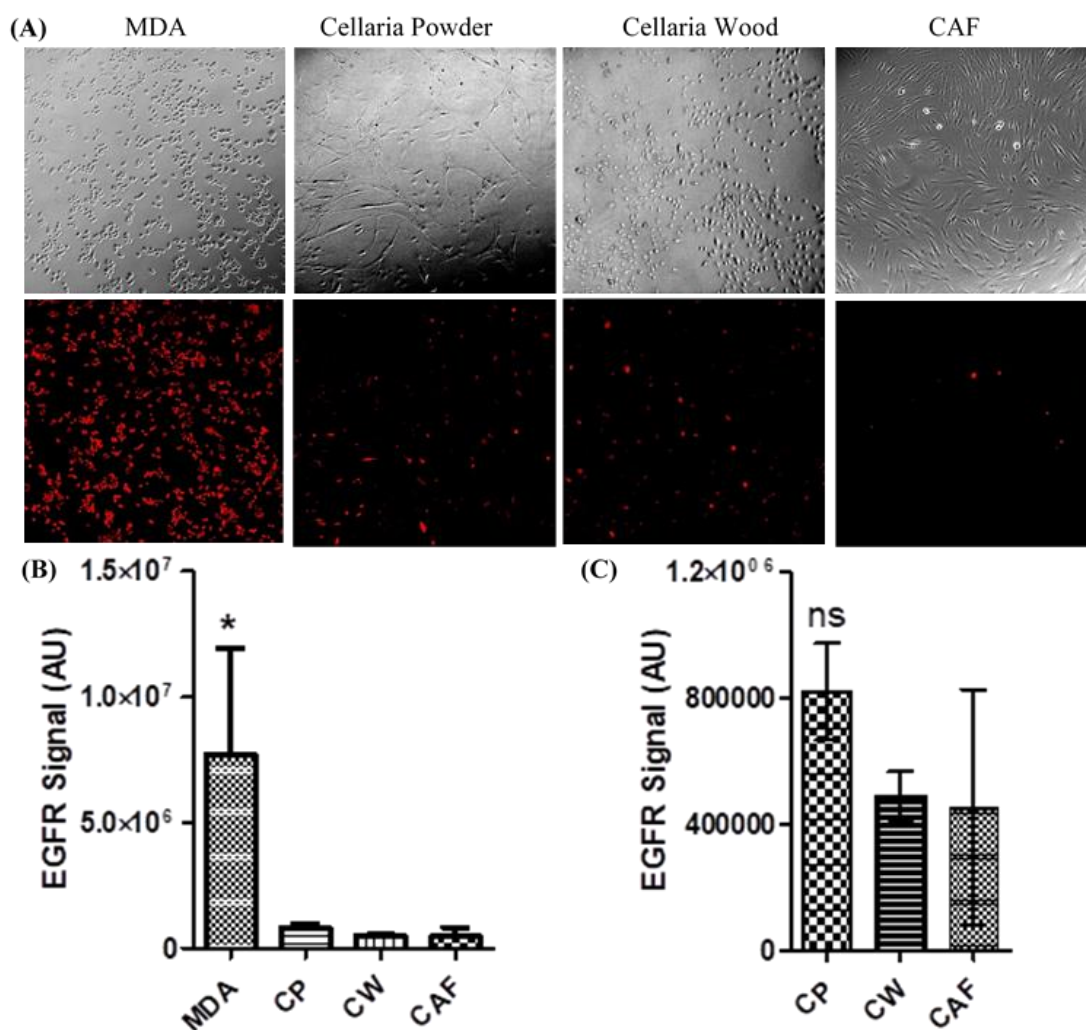
Figure 5.17 *Assessment of EGFR expression of primary cell lines. (A) Brightfield and fluorescent images of 24-well plate cultures fixed and stained on day 3 with anti-EGFR antibodies (red). Images acquired at 10x magnification. (B) Normalized EGFR signal. n=3. Data shows a significant difference in EGFR expression between MDA-MB-468 and all other cell lines assessed. (C) Normalized EGFR signal with adjusted y-axis for observation of lower expression levels. n=3. (MDA = MDA=MDB-468, CP = Cellaria Powder, CW = Cellaria Wood) (5x magnification) Data shown as mean ± SD. *P ≤ 0.05, One-way ANOVA, Bonferroni's post-test.*

Data analysis showed a statistically significant difference in EGFR expression (*P ≤ 0.05) between MDA-MB-468 and all other cell lines tested using one-way ANOVA analysis, Cellaria Powder, Cellaria Wood and CAF (**Figure 5.17**A and B). No statistically significant differences in EGFR expression between Cellaria Powder and Cellaria Wood or CAF were detected (**Figure 5.17**C). PD-L1 expression was also quantified for the primary cell lines (**Figure 5.18**).
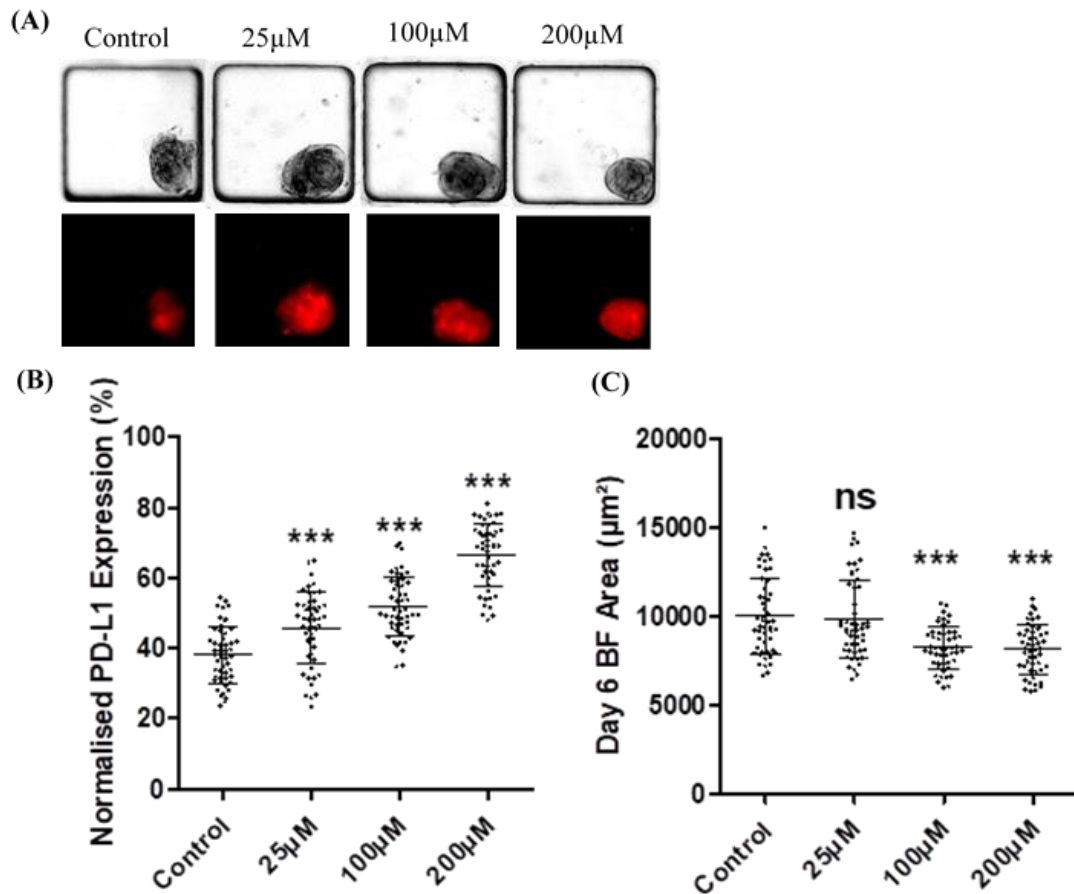
Figure 5.18: *Quantification of PD-L1 expression and brightfield area. (A) Brightfield and fluorescent images of Cellaria Wood monoculture spheroids stained for PD-L1 (red). (B) Percentage of day 6 area with PD-L1 expression. n=50. Data shows a significant difference in PD-L1 expression (***P ≤0.0001) between control spheroids and all carboplatin concentrations. (C) Day 6 brightfield area. n=50. Data shows a significant difference in brightfield area (***P ≤0.0001) between control spheroids and spheroids treated with 100µM and 200µM carboplatin concentrations. (MDA = MDA=MDB-468, CP = Cellaria Powder, CW = Cellaria Wood) Data shown as mean ± SD. ***P ≤0.0001, One-way ANOVA, Bonferroni's post-test. (5x magnification)*

PD-L1 expression of Cellaria Wood after carboplatin treatment was also assessed and showed a similar increase in expression to that seen in MDA-MB-468 cultures (**Figure 5.18**A and B). Cellaria Wood cancer cells appeared to form more compact spheroids in comparison to those formed using MDA-MB-468 cells. One-way ANOVA analysis was performed and showed that carboplatin only caused a statistically significant reduction in growth (***P ≤0.0001) at the higher 100µM and 200µM concentrations tested (**Figure 5.18C**). Due to neither Cellaria Wood nor Cellaria Powder cell lines demonstrating EGFR overexpression, EGFR specific CAR-T therapy would not be suitable in a model including these cell types. Future work would need to include the identification of a tumour cell specific target present on these cells for CAR-T therapy to be successful without presenting off-target toxicity. Due to laboratory closures as a result of the coronavirus pandemic, it was not possible to thoroughly investigate primary cancer cells or alternative cancer cell lines expressing lower EGFR levels than MDA-

MB-468 that were still greater than that of CAF. If more experimental time had been available, varying E:T ratios could also have been studied to more closely mimic real clinical values.

5.14 Primary Murine Immunoassay

In this chapter, the use of the microfluidic platform to perform solid tumour immunoassays for establishing the killing ability and target specificity of CAR-T cells was demonstrated. This work highlighted the potential of the device for providing physiologically relevant co-culture conditions in determining immunotherapeutic agent efficacy for patient-specific tissue and for gaining a better understanding of the immune mechanisms involved in treating solid tumours with immunotherapy. The protocols developed for previous immunoassays were applied to primary murine gamma delta T cell studies in collaboration with R. Weisheu (Cancer Research UK Beatson Institute, Glasgow, UK) and S. Coffelt (Institute of Cancer Sciences, University of Glasgow, Glasgow, UK, Cancer Research UK Beatson Institute, Glasgow, UK). 3D microfluidic models were established using KP and KB1P murine breast cancer cell lines to form tumour spheroids that were BRCA1-proficient and BRCA1-deficient respectively. Challenges for this project included the rapid growth and migratory phenotype seen for these cells when cultured in 3D. Thus, optimization of device preparation and cell seeding protocols was needed (**Section 2.7**). Gamma delta T cells were injected 24h after cell seeding to minimize the opportunity for spheroids to outgrow or migrate from microwells (**Figure 5.19**).
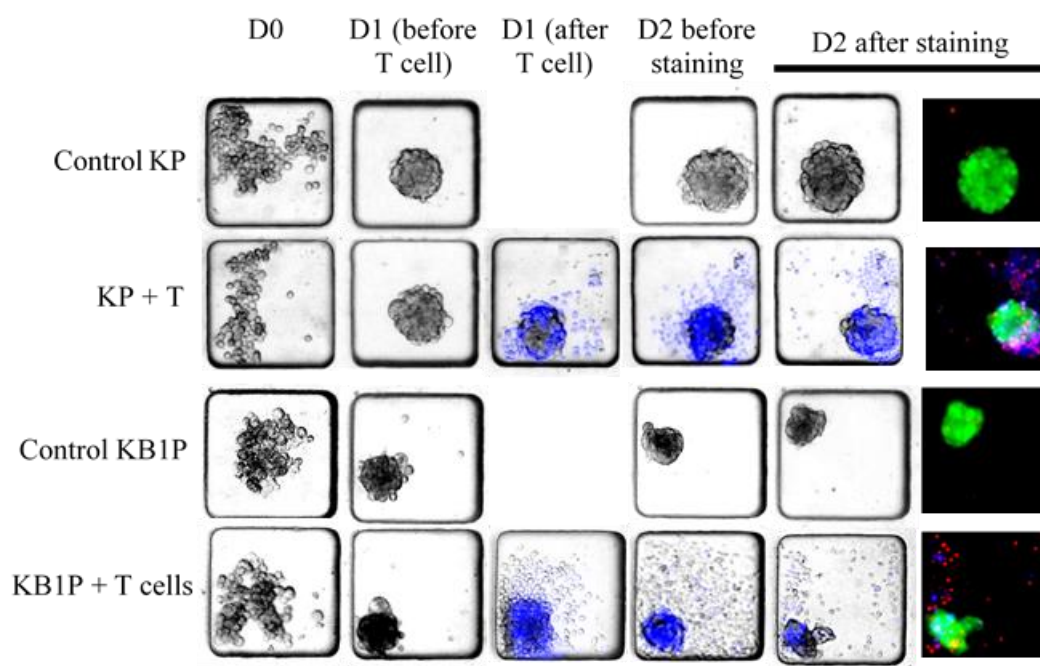
Figure 5.19 KP and KB1P spheroids cultured in microfluidic devices with 48h T cell exposure. Brightfield and fluorescence image timeline of KP and KB1P spheroids throughout 48h of T cell (blue) exposure stained with FDA (green) and PI (red) on day 2. (5x magnification).

Due to greater availability of these gamma delta T cells, in comparison to that from CAR-T assays, a higher estimated E:T ratio of up to 3:1 could be administered to spheroids. A limitation of this assay was that due to the rapid homing of T cells to the spheroid, 2D quantification of cell numbers to establish E:T ratio was not possible. However, this did suggest that T cells were activated in devices despite no obvious cytotoxic effect evident from viability staining with the vast majority of the tumour spheroid remaining viable after the 48h exposure period (**Section 2.11.3**). Thus, T cell exposure time was increased to 72h for subsequent experiments involving KP spheroids and two T cell groups with differing preparation methods (**Figure 5.20**).
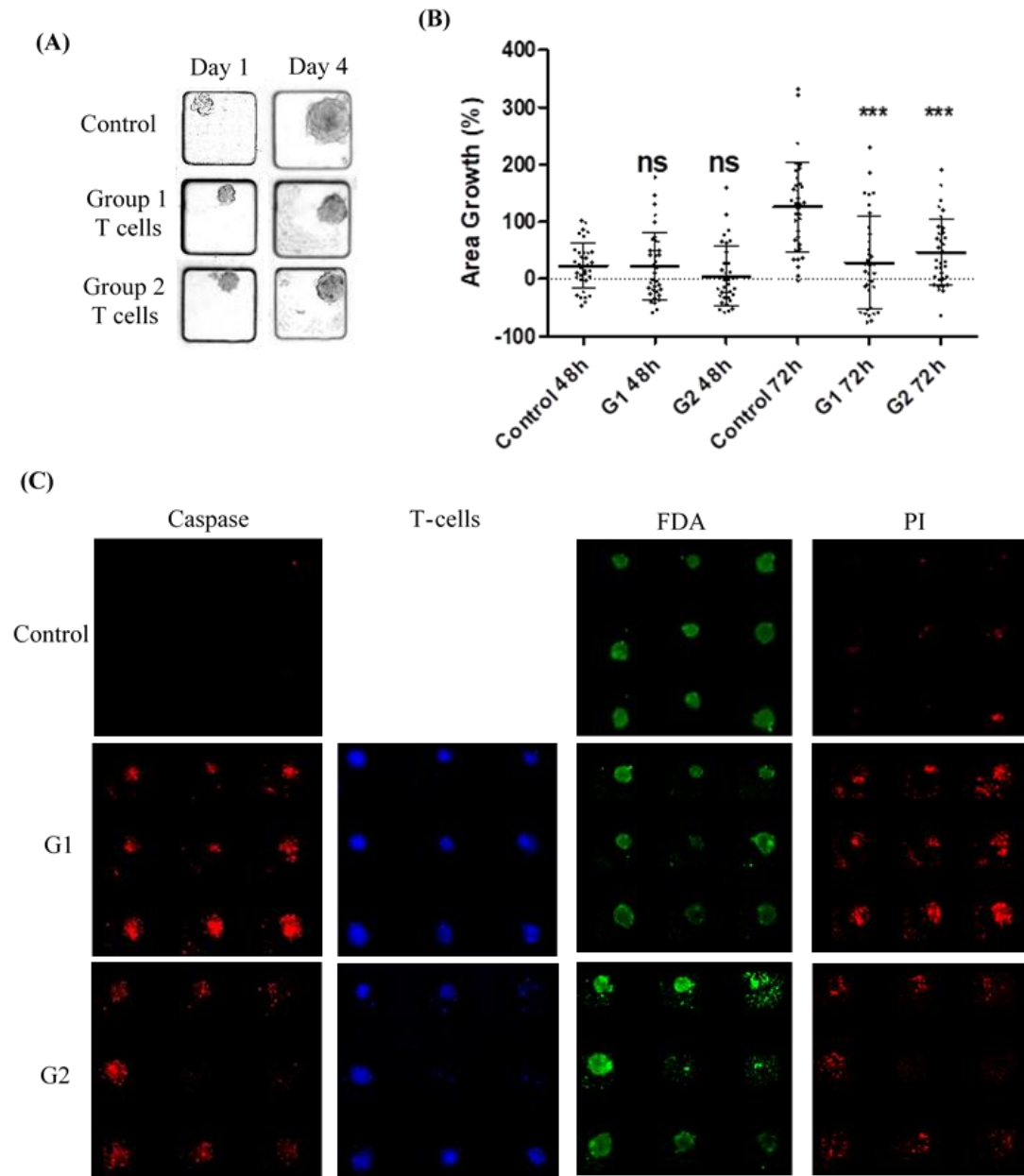
Figure 5.20 *KP spheroids cultured in microfluidic devices for 72h with two groups of T cells prepared under different conditions by collaborators. (A) Brightfield images of KP spheroids on day 1 and day 4 after 72h of T cell exposure. (B)Area growth (%). n=35. Data shows a significant difference in area growth (***P ≤0.0001) between control spheroids and those treated with both T cell groups after 72h of exposure. (C) Fluorescence images of day 4 staining of KP spheroids and labelled T cells (blue) with FDA (green), PI (red, right) and a far red Caspase apoptosis dye (red, left). G1 = Group 1 T cells, G2 = Group 2 T cells. (5x magnification). Data shown as mean ± SD. ***P ≤0.0001, One-way ANOVA, Bonferroni's post-test. (5x magnification)*

Whilst significant differences in spheroid growth could not be detected after 48h T cell treatment, by 72h control spheroids had grown to a significantly greater extent (***P ≤0.0001) than T cell treated spheroids (**Figure 5.20**A and B), as detected by one-way ANOVA analysis. Greater numbers of apoptotic and dead cancer cells could be observed in T cell treated cultures as opposed to control cultures after 72h (**Figure 5.20**C). However, as the majority of cells

comprising the tumour spheroid remained viable and T cells were not able to pull apart and disaggregate the tightly packed KP spheroids, this could present an opportunity to assess the effects of pre-treatment with other therapeutic agents to enhance the effects of the gamma delta T cells, as was seen in CAR-T investigations. Whilst additional therapies may be required to completely destroy KP spheroids in combination with gamma delta T cells, T cell monotherapy was shown to limit the growth of spheroids over a 72h period even at low E:T ratios. This work demonstrated the importance of primary immune cell incubation time with 3D tumour aggregates and the compactness of spheroid formation on the ability of immune cells to elicit a significant cytotoxic effect for future models. Optimization of T cell cytotoxicity is ongoing by collaborators prior to further microfluidic investigations.

In summary, the work completed in this chapter presented, for the first time, the use of microfluidic technology for the study of CAR-T therapy against 3D solid tumour co-cultures in combination with other anti-PD-L1 treatment and carboplatin chemotherapy. Microfluidic protocols were developed to establish this novel immunoassay and aimed to fill the gap in development of microfluidic models for solid tumour immune-oncology studies. Miniaturizing immunotherapy studies offers the advantages of being able to perform larger numbers of assays and obtain greater quantities of data than what would be possible with some conventional *in vitro* assays. Due to the small volumes required in these studies, the models developed are highly suited towards the use of CAR-T cells, which can be expensive to harvest and manufacture, as well as patient biopsy tissue. Protocols were optimized to use CAR-T cells as conservatively as possible and demonstrated the high specific toxicity of CAR-T cells in 3D. Furthermore, this novel TNBC immunoassay demonstrated the ability to study both CAR-T cell targeting specificity and cytotoxicity and is presented as a valuable means of augmenting output data from limited resources.

Chapter 6: Discussion and Conclusions

The aim of the work presented in this thesis was the development of novel protocols using microfluidic technology to establish miniaturised 3D solid tumour models that were representative of the TME and that could provide a suitable *in vitro* platform for the assessment of combination therapies and immunotherapies. This final chapter will discuss the main results and implications of this work, as well as potential future developments and applications.

6.1 Research Achievements

Analysis of the literature, reviewed in chapter 1, showed that current pre-clinical assays largely depend on 2D cancer cell lines and animal models, including patient-derived xenografts which are time and labour intensive. There exists a need for better *in vitro* models and protocols to efficiently and reliably predict therapy efficacy and side effects for pre-clinical drug trials and to provide precision medicine solutions. This thesis provided the development of a range of cell culture and image analysis protocols for assessing a range of anti-cancer therapies in 3D tumour-stromal microfluidic cultures. As a result of the protocols developed throughout this studentship, several collaboration projects have stemmed from this work. In chapter 3, the preliminary work carried out during this project was presented. Here, protocols were developed to establish the value of 3D culture using microfluidic devices and validate protocols. Nanoparticle based therapies were studied prior to advancing the 3D model with the addition of the stromal component to study the effects of inhibitor based therapy on CAF and collagen expression. Model complexity was further increased through the development of immunoassays for the assessment of T-cell therapies in combination with chemotherapeutics and checkpoint blockade therapy. Furthermore, initial work for incorporating a vascular network to advance current spheroid models was also conducted.

6.2 Microfluidic Platform

Following the validation of these microfluidic models, the technology could be utilised by R&D sectors, the pharmaceutical industry and in clinical settings. The devices used in these assays allowed the formation of a large number of spheroids from both tumour and stromal cells, a feature commonly lacking in traditional spheroid models. This platform also offers the advantage of more straightforward imaging methods in comparison to animal models. As these are open-well microfluidic systems, evaporation from device wells was closely monitored throughout experiments. However, incubating devices alongside PBS reservoirs was successful in preventing evaporation. The microfluidic technology used in this work provided both spatial and temporal control over the culture conditions without the requirement for external tubing or fluid actuation, as has been used in other microfluidic immune-oncology

studies.[198, 202, 212, 214, 219, 232] The majority of *in vitro* studies using microfluidic technology do not require the use of external actuation equipment, potentially due to the challenges of upscaling these types of assays for higher throughput applications.[268] Since the platforms used in this work do not require the use of syringe pumps or other external equipment, the cost, labour and complexity of performing these assays is reduced, as well as the required quantities of cells and reagents. Thus, these assays are ideally suited for the use of multi-channel pipettes and robotic dispensers for increased throughput applications in future. Increasing model complexity and data throughput could be achieved through combining microfluidic technology with automation of the microfluidic protocols and developing machine learning algorithms to interpret large amounts of data. Other aspects of the immune system and TME could be incorporated into assays to provide greater physiological representation, such as some of the microfluidic immunoassays discussed in Chapter 1.[192, 203, 269] However, if models are made more complex, such as those designs by Huh *et al.*[212], Charwat *et al.*[219] and Liu *et al.*[198], then this could have implications for increasing assay throughput. Furthermore, the use of concentration gradients could also be of use for future combination therapy testing and could increase the total number of conditions that could be tested simultaneously.

For future studies, drug absorption by PDMS has to be taken into account when considering relevant doses for patients, as well as factors such as human metabolism which are not accounted for in *in vitro* models. PDMS is commonly used in microfluidic applications due to its optical transparency, biocompatibility, low cost, ease of use and gas permeability. However, PDMS has been reported to leach uncured oligomers into cell culture chambers which could have implications for cell function and viability.[270, 271] Furthermore, PDMS can absorb proteins and other small hydrophobic molecules present in cell culture media which is of particular concern in regard to drug testing and could imply that the drug concentration injected into device wells is not the concentration that spheroids would, in fact, be exposed to.[270, 271] These are important considerations for future experiments and the extent of these effects could be assessed in devices to avoid data misinterpretation. If it was found that a particular drug compound to be tested was significantly absorbed by PDMS or that a certain cell type was sensitive to PDMS leaching, devices could instead be fabricated from alternative polymers, such as polystyrene which is produced by injection moulding and is known to have minimal absorption of molecules.[272-274] However, as polystyrene is a hard plastic, device designs may require alteration to allow sufficient gas exchange for cell culture.[275] Whilst PDMS is the predominant material used to create microfluidic devices for immunoassays,[268] several microfluidic immunotherapy studies described in this work have been conducted using alternative chip materials.[202, 206, 211, 227, 276]

Challenges potentially impacting the development of novel microfluidic assays include the difficulty in collection of patient samples and clinical data. The development of policies that would streamline access for researchers would accelerate the enhancement of microfluidic technology in this field, as well as the validation of new therapeutic agents. To realize the potential of microfluidics in this field, multi-disciplinary collaboration between academic groups, clinicians and the pharmaceutical industry is needed. Many autologous and allogenic cell therapies have been developed in recent years by companies including Novartis, Biotherapeutics, Adaptimmune and Immunocore. However, many biotechnology companies conduct *in vitro* assays in traditional 2D and well plate formats followed by animal studies. Filling the gap between these two assay types using microfluidic immunoassays is a field in development and collaboration between a range of disciplines is needed for progress in broadening the use of the technology and producing clinically relevant data.

6.3 Vascular Network

In this studentship, the development of miniaturised models of cancer was investigated and included consideration of various microfluidic designs from the literature. This thesis has presented the advantages of miniaturization and 3D *in vitro* assays for anticancer drug development, examined methods for the *in vitro* co-culture of multiple tumour and tumour associated cell types and demonstrated the potential for applications towards personalized medicine using human patient tumour tissue. The ultimate TME component absent from the models developed in this work is a vascular network. The complexities associated with current methods using external actuation equipment presents an opportunity to resolve these issues and develop an open well 3D tumour-vascular model for assessing novel immunotherapeutics in combination with other therapy types. Such a model would also enable investigations into tumour angiogenesis and intravasation. Using a pre-existing microfluidic device consisting of three parallel channels with interconnected microposts, various hydrogel conditions were assessed. These included optimization of gel formulation, pH, temperature and incubation time. Whilst this work showed the formation of viable vascular network structures in devices, further work would be needed to establish the necessary conditions for consistent 3D vascular network formation throughout the channel. Thus, the extensive work that would be required to achieve this fell out with the timescale of this project. However, initial assays have established protocols that could be of benefit for potential future study of vascular network-spheroid microfluidic devices and present a future avenue to explore in developing a more representative and complex *in vitro* model, such as that developed by Nashimoto *et al.*[186], Du *et al.*[187], and Lee *et al.*[231]. An important future consideration for such a model would be the impact on throughput and automation. As previously stated, automation of current platforms

would enable larger scale assays to be performed and would increase the quantity of therapeutic agents that could be tested simultaneously. However, it should be noted that increasing model complexity could hinder future automation of the technology for higher throughput applications.

6.4 3D Monoculture Spheroids for Anti-Cancer Nanoparticle Studies

Applications of the microfluidic platform and associated protocols were demonstrated with work regarding the assessment of nanoparticles, as well as the use of culturing primary tissue in devices. In parallel to the development of tumour-stromal and solid tumour immunotherapy models, microfluidic technology was, for the first time, combined with SERS for the assessment of targeted nanoparticles in a 3D human breast cancer model in collaboration with the Bionanotechnology and Analytical Chemistry group at the University of Strathclyde. 3D models are useful tools to aid the understanding of drug activity and transport, as well as cancer cell interactions, in contrast to commonly used 2D monolayer *in vitro* models of cancer. This is an important consideration for tumour models which have shown differences in cell behaviours, gene expression and drug sensitivity between 2D and 3D cultures.[3] These variations have had implications for clinical trials with multiple drugs shown to be beneficial in 2D assays, yet later being proven ineffective for patients.[3] Microfluidic technology can provide the opportunity to create complex 3D models to better recapitulate *in vivo* breast cancer for more predictive and cost-effective drug screening that can be combined with various imaging methods, such as fluorescence microscopy and SERS.

In this work, the ability of targeted and non-targeted nanoparticles functionalised with either ERα or HER2 antibodies to detect ERα expression in 3D using spheroids formed from the MCF-7 human breast cancer cell line which is positive for ERα and expresses non-detectable levels of HER2. Results from 2D and 3D SERS measurements demonstrated effective targeting of ERα nanoparticles but not HER2 which showed only minimal non-specific binding. 3D mapping allowed assessment of nanoparticle uptake, surface adherence and penetration. The PDMS devices used in these assays are well suited for SERS studies as the PDMS produced a low intensity SERS spectrum that did not interfere with those from nanoparticles allowing precise detection of nanoparticles. Results suggested that nanoparticles were able to infiltrate spheroids and not only adhere to the outer spheroid surface. If nanoparticles were able to selectively accumulate within MCF7 spheroids, this would provide evidence for their use in drug delivery and photothermal therapy for breast cancer. However, retention of nanoparticles within spheroids would require additional confirmation with other imaging techniques, such as transmission electron microscopy, and in co-cultures with non-

ERα expressing cells to confirm on-target binding. Spheroid shape factor, growth and viability were also assessed at various time points over the 10 day culture period. Quantification of data showed no statistically significant effect of nanoparticles on spheroid disaggregation or area growth after 10 days of culture. However, spheroids treated with nanoparticles showed significantly greater cell death than equivalent control spheroids with the vast majority of the spheroid mass remaining viable.

Also studied was the effect of the drug fulvestrant which degrades ERα present on cancer cells and has been proven beneficial as a treatment for ERα positive breast cancer patients.[234, 235] Fulvestrant treatment limited spheroid growth and resulted in increased disaggregation and cancer cell death by day 10, confirming its toxic effects against 3D cultures. Fulvestrant treatment also reduced ERα nanoparticle accumulation in comparison to control spheroids and confirmed specific nanoparticle targeting of ERα. Such nanoparticles would be of use in detecting cancer cell expression levels *in vivo* as a means of monitoring patient response to treatment. This model also has the potential for reducing animal studies in drug screening assays by first studying therapeutic effects in a more physiologically relevant *in vitro* environment before *in vivo* assessment.

This work presents the potential of combined SERS and microfluidic platforms in a miniaturized scalable 3D tumour model for assays involving nanoparticle characterization and target specificity, as well as for assessing responses to other pre-clinical compounds. This platform is presented as a useful tool in understanding the mechanism of action of such agents in a 3D environment and could be used to generate supporting data to accelerate the approval of compounds alone and in combination with other therapy types for clinical use. To increase the physiological relevance of this model, features of the TME, such as stromal and immune cells, could be readily incorporated for future studies. The system could be further developed by automating the system to permit higher throughput applications and with the use of patient biopsy tissue to be able to characterize individual patient tumours.

6.5 Tumour-Stromal Models for Inhibitor-Based Studies

From reviewing the relevant literature in chapter 1, the crucial role of the TME and ECM in cancer progression was discussed and the absence of TME representation in *in vitro* models identified as a major limitation for pre-clinical analysis of anti-cancer agents. In particular, CAF were identified as being a major producer of collagen-rich ECM in solid tumours which contributes to cancer invasion and progression and provides protection and resistance to cancer cells against anti-cancer therapies.[19, 277, 278] Collagen deposition can also impede therapeutic delivery to tumour cells, in addition to providing proline to cancer cells to metabolize due to

the nutrient scarcity that occurs in the TME.[19, 279] The metabolic processes involved in CAF production of ECM are not well understood and the development of models to better understand their role and potential ways to inhibit collagen production would be of benefit to cancer patients. Specifically, targeting enzymes involved in collagen synthesis is an area of importance. If ECM production could be inhibited, cancer cells would not receive protection from the ECM in their surrounding TME and, so, this would allow a greater enhancement of the cytotoxic effects of anti-cancer agents which could be delivered to the tumour cells more easily. To enhance our understanding of the influence of such enzyme inhibitors, it is important to consider the tumour and ECM in 3D. CAF can contribute significantly to total solid tumour mass, as much as 90% for carcinomas, and were highlighted as an important feature to be considered in *in vitro* models.[280]

In chapter 3, the value of 3D culture for improving the predictive value of *in vitro* assays and the potential for microfluidic technology to bridge the gap between traditional 2D cell monolayers and animal models was presented. In this chapter, protocols were developed to establish a 3D breast cancer cell-stromal model where spheroids were formed through co-culture of a primary breast cancer cell line and CAF, isolated by collaborators. The role of several enzyme inhibitors and their influence on CAF collagen production was explored through analysis of various readouts that included spheroid viability, size, proliferation and collagen deposition. 3D microfluidic assay results were compared with 2D experimental data from collaborators and presented at the BioMedEng 2019 conference, as well as being prepared for journal publication.[19]

This work focused on demonstrating the role of CAF in ECM production to encourage tumour progression and metastasis and the potential to use inhibiting agents of associated enzymes to limit this production. To confirm the mechanisms involved in collagen deposition, production of essential proteins required for collagen production was halted via enzyme inhibition and the effect on CAF collagen deposition assessed. Parallel co-cultures also exposed to enzyme inhibitors, additionally received an external supply of the required agent needed for collagen production. The device used in this work permitted real-time monitoring of spheroid co-cultures and functional readouts to be obtained, including fluorescence analysis of viability and proliferation marker staining. Image analysis protocols were developed to provide quantification of collagen deposition by CAF that could be normalized to CAF area for robust comparison between conditions and to control co-cultures. Briefly, all four enzyme inhibitors assessed in this work were proven to significantly reduce collagen production by CAF in co-cultures. Inhibitor concentrations were selected based on concentrations and exposure times

applied to 2D cultures that elicited a measurable effect on collagen production. Using the same enzyme inhibitor concentrations that had elicited a reduction in collagen production in 2D assays did not cause a significant change in 3D cultures, emphasizing the need for 3D *in vitro* assays to acquire relevant and valuable drug testing information. Doses were adapted to account for 3D cultures commonly being more resistant to anti-cancer drugs than equivalent monolayer cultures,[244] as well as for the inclusion of stromal cells in co-cultures which are known to provide protection to cancer cells.[245] ACLY inhibitor treatment caused cancer spheroid disaggregation and reduced CAF spheroid size in co-cultures, as well as decreased CAF proliferation in monocultures. In equivalent 2D assays performed by collaborators, acetate successfully restored collagen production for ACLY inhibitor treated co-cultures. However, in 3D microfluidic cultures, acetate increased disaggregation of both cell types for ACLY inhibitor treated spheroids and also did not recover collagen deposition. Furthermore, CAF spheroid size was reduced in acetate and low concentration ACLY inhibitor treated cultures, where no reduction in CAF spheroid size had been seen with ACLY inhibitor treatment only. In contrast, the extent of collagen reduction in CAF monocultures caused by ACLY inhibitor treatment was mitigated with additional exposure to acetate. This suggests that whilst acetate is unable to restore spheroid size and collagen deposition in co-cultures after ACLY inhibitor treatment, it is able to have a beneficial effect on CAF in monoculture conditions. Furthermore, acetate was shown to increase the proliferation of ACLY inhibitor treated CAF spheroids in monocultures and to recover collagen deposition and proliferation in PDH inhibitor treated co-culture spheroids. As the negative impact of acetate was only observed in 3D conditions with ACLY inhibitor treatment, this could suggest an interaction between the ACLY inhibitor and acetate that creates a toxic environment in 3D microfluidic culture that is not seen in 2D conditions. However the mechanisms behind these findings are unclear and no reports of acetate and ACLY toxicity in PDMS microfluidic devices could be found in the literature.

The PYCR1 inhibitor decreased both cancer and CAF spheroid size, as well as collagen expression, with increasing concentration. Proline negated the effects of reduced cancer spheroid size and collagen expression in co-cultures treated with 100μM of the PYCR1 inhibitor. However, co-cultures treated with higher inhibitor concentrations did not recover collagen deposition to control levels within the time-frame of the experiment. The PYCR1 inhibitor was not as potent an inhibitor in comparison to p300 and ACLY and had to be applied at greater concentrations in order to detect a reduction in collagen production. The PYCR1 inhibitor also did not result in significant toxicity to either cell type despite limiting CAF

spheroid growth. Therefore, this work demonstrates the benefit of analysing multiple experimental parameters to fully assess the efficacy of a stromal targeting agent.

The beneficial effects for cancer cells when co-cultured with CAF were also demonstrated. Increased cell death was observed in control cancer cell monocultures in comparison to, not only control tumour-stromal co-cultures, but also to co-cultures that had been exposed to inhibitors. In tumour-stromal co-cultures, CAF were the primary source of collagen production. This allowed quantification of the collagen ratio to CAF area to be established as a reliable method of data representation to demonstrate the effects of the selected enzyme inhibitors. As collagen production was directly proportional to CAF presence in co-cultures, any inhibitory effect from the agents being assessed could be detected if collagen: CAF ratios differed from the 1:1 control conditions. Dissociation of cancer cells and CAF began within the first couple of hours after cell injection into microfluidic devices and was shown to be maintained for up to 10 days. Fibroblast dissociation from cancer cells has also been reported in the literature, as well as the formation of tighter spheroids when cancer cells were co-cultured with fibroblasts in comparison to cancer cell monoculture spheroids.[241] This microfluidic work could be applied to future work exploring the symbiotic relationship between CAF and cancer cells further in a 3D environment.

Normalizing ECM production in tumours could be a useful therapeutic strategy in combination with other therapy types to delay tumour growth and impede its promotion and protection of tumour cells. For example, in 2020, an *in vitro* 3D model of neuroblastoma was developed using spheroids cultured in 96 well-plates that consisted of neuroblastoma tumour cells together with normal fibroblasts.[241] This study demonstrated that the anti-tumour effects of chemotherapeutics could be enhanced by inhibiting the tumour promoting function of the fibroblasts through mPGES-1 inhibitors. This thesis highlights the pathways involved in CAF activation and collagen production as a potential vulnerability of the TME and which has implications for the development of therapeutic agents inhibiting desmoplastic tumour growth. Several agents targeting the metabolic regulation of CAF collagen production are currently under clinical investigation and this assay could prove to be a useful tool for assessing the effects of such inhibitors on both cancerous and stromal cell types. Identifying treatments that target the tumour stroma would enhance drug delivery to the tumour site and, thus, the effectiveness of other anti-cancer therapies. In particular, collagen is known to limit the effectiveness of immunotherapies by hindering immune cell infiltration and promoting T cell exhaustion.[281] Many possibilities exist for combining the inhibitors discussed in this work with other therapy types whilst using this model to assess the best possible treatment regimens for

patients. An absence of appropriate pre-clinical models depicting heterogeneous solid tumours and their associated microenvironment is a significant challenge to discovering effective therapeutics. Looking ahead, this proof-of-concept model could be adapted for using patient-derived tissues to perform predictive studies to provide useful data on the potential efficacy of inhibiting collagen production in the TME *in vivo* and could enhance subsequent anti-cancer therapies. However, there is currently no universally accepted method of translation of *in vitro* data, taken from assays using patient tissue, into data relevant for clinical decision making regarding patient therapy regimes.

6.6 Solid Tumour Adoptive Cell Therapy Studies

Despite the promise of new microfluidic technologies, no robust, high-throughput platform currently exists for screening immunotherapies against the solid TME. Thus, this project has endeavoured to produce and validate microfluidic immunoassays that could contribute towards the filling of this technical gap. In chapter 5, the tumour-stromal co-culture protocols developed in chapter 4 were applied to the design and development of protocols for a novel immunoassay that for the first time can offer the potential for screening T cells in combination therapy regimes against 3D tumour spheroids in the context of the TME. Analysis of the literature discussed in chapter 1 demonstrated the need for more reliable *in vitro* preclinical tools that offer a more realistic recapitulation of solid human tumours to test novel immunotherapies. Chapter 1 considered the great potential of microfluidics for ACT efficacy studies. These miniaturised methods offer the potential to perform mechanistic studies to decipher the impact of the TME for immunotherapies and to use patient derived tissue at a higher throughput than would be possible with traditional *in vitro* methods. Microfluidics offers the advantages of being able to create complex *in vitro* assays with minimized costs and time to results in comparison to traditional T cell screening platforms. Such *in vitro* models can allow easier manipulation of experimental conditions in comparison to *in vivo* models depending on the specific variable to be investigated and can be imaged using a range of microscopy techniques.[95, 135]

6.6.1 CAR-T Immunoassays

CAR-T cell therapy has been demonstrated to be one of the most exciting advances in the field of immunotherapy and has been proven effective against a range of haematological malignancies and melanoma.[82, 101, 111] Yet, translating this success towards the majority of solid tumours has proven difficult.[250] As discussed in chapter 4, the TME and in particular CAF, is of paramount importance in dictating the success of many cancer therapies, including immunotherapies.[19, 35, 84, 246-249] Many *in vitro* assays assessing CAR-T efficacy do not consider

the 3D TME which can hinder CAR-T cell infiltration.[114] Furthermore the TME contains a range of cell types that release immunosuppressive molecules to protect cancer cells from CAR-T treatment.[114] Due to the significant role of CAF in the TME, T cell inhibition and therapy success, these were considered to be a critical feature of the assay design despite their absence from CAR-T *in vitro* assays prior.[11, 19, 35, 111, 245, 280] A review of the relevant literature showed that the application of CAR-T therapy towards solid tumours was limited in comparison to its use against haematological malignancies.[11] The high costs associated with CAR-T cell production have impaired the broader use of CAR-T therapy development.[117] Whilst a lack of suitable pre-clinical models has been identified as an obstruction to the study of CAR-T cell efficacy. Examples from the literature exist of CAR-T cell studies using microfluidics,[221, 225] as well as several other miniaturised immunoassays.[123, 219, 220, 224, 226, 229, 231] However microfluidic technology has not been widely utilized towards CAR-T investigations.[11] *In vitro* models offering more accurate depictions of the challenges of treating the solid TME are required to provide cost-effective solutions for quantifying CAR-T efficacy and off-target toxicity and screening possible therapy combinations prior to *in vivo* studies.

This thesis presents the first report of the use of a microfluidic TNBC immunoassay to study the effects of combination carboplatin chemotherapy, anti-PD-L1 therapy and CAR-T therapy on CAR-T killing efficacy in 3D and provides an opportunity for the shift of focus from tackling haematological tumours with CAR-T therapy to solid cancers using lab-on-chip technologies.[134, 188, 282] Furthermore, this is the first report of a microfluidic immunoassay capable of the assessment of both CAR-T cytotoxicity and targeting specificity in 3D *in vitro* conditions. The developed immunoassay is presented as a potential tool for the development of immunotherapeutics and medium throughput studies into 3D cancer cell-immune cell interactions. This novel combination tumour-stromal assay was developed in contrast to traditional CAR-T assays performed in 2D and those in 3D that are conducted in low-adhesion well-plates or that use hanging drop methods.[119-122, 124, 126-128] As well as for CAF and cancer cell co-culture models, the importance of 3D culture was also demonstrated for immunoassays. Greater cytotoxic effects were observed in 2D assays in comparison to 3D results. Furthermore, no physical barrier exists in 2D monolayer conditions between cancer cells and CAR-T cells as it would *in vivo*.

The development of this immunoassay was based on establishing a TNBC model. Epithelial malignancies are responsible for up to 90% of all cancer cases and have a wide range of escape mechanisms to avoid detection by immune surveillance.[111, 283] Specifically, TNBC accounts for up to 20% of breast cancers and is a highly aggressive form of cancer for which successful

therapeutic options are limited.[128, 284] Whilst TNBC lacks expression of ER, HER2 and progesterone receptor,[284] EGFR is expressed in many types of TNBC and is amongst some of the most targeted antigens for CAR-T cells used in clinical trials.[113, 121, 128, 285] As a proof of concept study, EGFR targeting CAR-T cells were assessed in 3D co-cultures of EGFR over-expressing cancer cells with either cancer associated or normal fibroblasts, both of which were low EGFR expressers. CAF and NHLF were identified as suitable targets based on quantification of their EGFR expression and represent different models for off-target toxicity studies and recreation of the TME, depending on the aim of investigation. For combination therapies, carboplatin chemotherapy was selected due to its regular incorporation into TNBC treatment regimes.[105] Anti-PD-L1 checkpoint blockade was also chosen due to animal and *ex vivo* studies showing better reduction in tumour mass and longer survival when carboplatin and anti-PD-L1 therapy are given in combination rather than as monotherapies.[104, 105]

All cell types were shown to culture well in devices for both mono- and co-cultures and were shown to be viable for up to 10 days in devices. 2D and 3D results were compared and showed that longer CAR-T incubation time was required in both cases with no significant cytotoxic effects seen after 24h but only with 72h of exposure. This effect was also neutralized with anti-EGFR antibody pre-treatment of spheroids, confirming CAR-T targeting and specificity of killing as a result of EGFR recognition. Both 2D and 3D assays also recorded no significant changes to CAR-T cell numbers after incubation with MDA-MBB-468. Furthermore, no statistically significant differences in cell death or brightfield area were detected for fibroblast monocultures after 72h incubation with CAR-T, demonstrating the selectivity of CAR-T cell killing. The image analysis protocols developed in this thesis allowed quantification of cell-mediated cytotoxicity, chemotherapy-induced cell expression changes, on-target specificity and CAR-T E:T ratio. Time-lapse imaging revealed rapid homing of EGFR specific CAR-T cells towards EGFR-expressing tumour cells to elicit a cytotoxic effect, without detriment to the viability of low EGFR-expressing fibroblasts. Data analysis showed enhanced CAR-T killing and targeting of cancer cells, in both monocultures and stromal co-cultures, for combination therapy with respect to control conditions. The cytotoxic effects from CAR-T cells were most pronounced with combination anti-PD-L1 therapy and carboplatin chemotherapy pre-treatment of spheroids in comparison to control spheroids and those treated with individual monotherapies. Image analysis of marker expression on cancer cells showed this effect was likely as a result of upregulation of EGFR expression induced by chemotherapy treatment. However, chemotherapy treatment also induced increased PD-L1 expression which could be accounted for through checkpoint blockade therapy prior to CAR-T cell exposure. This work highlights the potential benefits of testing multiple therapy combinations in parallel

to detect synergistic anti-cancer effects. In addition, this platform could be utilised for combining CAR-T therapy with other treatment types to identify any potential contraindications prior to *in vivo* assays. Furthermore, the majority of the PI signal detected was co-localized to cancer cell regions in microfluidic co-cultures, providing further quantitative data on CAR-T target specificity.

Due to the costly process of CAR-T cell harvesting and manufacture, there is a need for the development of miniaturised assays that will greatly reduce the required numbers of cells in comparison to traditional 2D *in vitro* models.[117] With this in mind, protocols were developed for as conservative use of CAR-T cells as possible whilst still demonstrating CAR-T cell efficacy in 3D. A change of device to the 24-channel OC^{3D} *Single* microfluidic devices (ScreenIn3D Ltd, UK) was needed to accommodate the smaller cell numbers used in these immunoassays and optimization experiments carried out to improve protocols for achieving larger numbers of cells in microwells during seeding even with low cell seeding volumes and densities. As a result of the miniaturized nature of this assay and high specific toxicity of the CAR-T cells used in this work, it was possible to use E:T ratios at much lower levels than is typically seen in *in vitro* assays that were nonetheless able to exert a significant cytotoxicity on cancer cells. Seeding experiments were conducted in microfluidic devices to determine the seeding conditions that would enable as high an E:T ratio as possible in order to see a cytotoxic effect of the CAR-T cells. Despite the low E:T ratios used in these conditions a statistically significant, yet specific, cytotoxic effect was still seen. This demonstrates the power of this therapy even at low E:T ratios and proves CAR-T therapy to be a promising anti-cancer treatment against solid tumours for future clinical use. In future, if protocols were developed to allow the expansion of these CAR-T cells, or if it became possible to produce CAR-T cells at lower costs, then these assays would be able to be performed at higher and more realistic E:T ratios. Seeding protocols have since been refined since the completion of this work and it is now possible to ascertain upwards of one hundred 3D CAR-T assays using a vial of only one million CAR-T cells. This work has demonstrated the microfluidic platform as a powerful tool for augmenting output data when resources are limited.

6.6.2 Future ACT Applications

The immunoassay developed in this work offers a flexible platform to better understand the impact of the TME on CAR-T cell performance, as well as for a range of other ACT therapies. This model would be useful in detecting potential off-target toxicity from CAR-T cells, which can lead to serious and potentially life-threatening responses to treatment,[111, 112, 115] and for better engineering of CAR-T cells. These immunoassays could be used to investigate the

longer term effects of immunotherapeutics on non-target expressing cells and could provide important biological data on immune cell interaction with cancerous and non-cancerous cells, as well as on the capability of these non-cancerous cells to survive in inflammatory conditions. This platform is able to provide statistically meaningful quantification of the assessment of novel immunotherapies in combination with numerous other therapy types to enhance and create a less hostile and immunosuppressive TME for CAR-T therapy. This model is particularly suited towards the establishment of mechanistic studies for assessing ACT efficacy and safety prior to pre-clinical animal studies and clinical trials. However, it could be also be used to assess other therapies in addition to ACT, such as to test the penetration and cytotoxicity of oncolytic viruses and antibody therapies. Furthermore, these assays could be used to minimize the use of animals when assessing the efficacy of novel immunotherapies by selecting only the most promising targets for *in vivo* assessment. Reducing the number of animals required for pre-clinical studies would also lessen the cost and labour associated with *in vivo* assays, such as patient derived xenografts.

This is a promising development for studying immunotherapies in the context of, not only the TNBC TME, but for a wide range of solid tumour environments expressing a range of markers. This immunoassay could be modified to recreate various aspects of the TME in 3D and would be a useful tool for real time investigation of cellular interactions between cancer and immune cells in a physiologically relevant solid TME. A more complex model could be established with the inclusion of hydrogels depending on the type of assay and cells involved. Furthermore, the development of hydrogels and supplements that are not derived from animals would increase the predictive value of such immunoassays by removing the potential for cross-species contamination. This microfluidic platform could be used to provide additional readouts for more in depth analysis of immune cell function, such as quantification of chemokine or cytokine secretions present in device culture media. Furthermore, the impact of oxygen availability on immune cell performance when targeting solid tumours could also be investigated using this platform. Many current microfluidic immunoassays are directed towards mechanistic and proof-of-concept studies. Thus, more examples of the application of these cost-effective lab-on-a-chip technologies for testing the efficacy of novel immunotherapies are required to drive the medical and biological investigations and further enhance the technology.

Critically, this model could be enhanced by using biologically-relevant biopsy tissue which could provide a more accurate prediction of therapy efficacy *in vivo* in comparison to previous assays using cell lines. Using primary cells would also be beneficial for translating results

towards *in vivo* studies. Several examples exist of the culture of primary tissue in microfluidic devices for immunotherapy investigations.[179, 214, 219, 221, 224] However, only a minority of these studies rely solely on primary tissue alone.[268] This is potentially as a result of most of these investigations being proof-of-concept studies and the use of immortalized cancer cell lines could reduce the cost and complexity of these studies in comparison to using primary cells.[268] Despite this, validation of microfluidic technology with clinically relevant samples would drive confidence in the technology and the potential of its use in future predictive studies for patient outcomes. Challenges facing the widespread implementation of microfluidic technology includes the gap in connection between laboratory research and the clinical applications. To enhance the feasibility of clinical implementation, clinically relevant human tissue needs to be made available during the development and optimization of microfluidic assays to accelerate development and avoid complete redesign of the platform at a later stage.[286]

Common 3D tumour models include ultra-low adhesion and hanging drop plates which necessitate a larger quantity of cancer cells to form tumour spheroids in comparison to what is required for the microfluidic assays performed in this work.[287, 288] Miniaturizing *in vitro* assays maximises the potential quantitative output data and potential therapy regimes that can be tested in parallel. The proof-of-concept immunoassays developed in this work are proposed as future preclinical screening tools for the discovery of novel immunotherapeutics and for use in personalized medicine using patient biopsy tissue to aid the selection of effective combination therapies to establish the optimum treatment plan for patients. Having demonstrated the use of so little cell numbers, the developed protocols could be adapted for biopsy tissue fragments, where the number of cells are often very limited. This miniaturised platform is ideally suited for personalized medicine as small pieces of biopsy tissue can be used to test multiple therapy types and combinations in parallel at a far higher throughput in comparison to what would be possible with traditional *in vitro* methods where much larger biopsy fragments would be required. This would avoid the long waiting periods for the expansion of patient-derived cells and allow for faster identification of efficacious treatments to aid clinical decision making. Using such tissue would also offer the advantage of possessing multiple TME cell types and would allow the formation of heterogeneous tumour organoids that could create a more physiologically relevant environment to increase the accuracy of predictions of treatment efficacy and resistance. However, it should be noted that the handling of clinical samples can be complex and particular design of microfluidic devices is required for the culture of biopsy tissue.[286]

However, even with the use of patient biopsy tissue, resident immune cells and native ECM would not be present in established 3D spheroid cultures which are particularly impactful to the efficacy of immunotherapies. Furthermore, primary tumour slices and fragments can maintain TME components but cannot be cultured for the prolonged periods of time required for some drug efficacy studies.[289, 290] Despite this, using human clinical samples, rather than relying on immortalised cell lines or animal models, is more likely to detect therapy resistance.[94] Retrospective assessment of clinical outcomes using patient biopsy tissue should be first demonstrated, prior to prospective assessment, to build confidence in the technology and to establish the reliability and predictive capabilities of new microfluidic immunoassays.

6.7 Conclusions

In conclusion, this thesis has described the development of cell culture and data analysis protocols for novel proof-of-concept 3D microfluidic assays. Specifically, microfluidic systems were utilized to demonstrate the value of establishing *in vitro* models that recreate the variety of cell types present in the TME of native tumours. In particular, the importance of CAF in supporting cancer cell survival as well as the mechanisms behind their collagen production and potential inhibition were investigated. This work successfully demonstrated the value of microfluidic systems for the 3D culture of cancer and cancer associated cells for assessing anti-cancer agents and their influence on cancer cell viability, protein expression, migration and growth. For the first time, microfluidic technology was combined with SERS to study targeted nanoparticle binding to and penetration of 3D tumour spheroids. The use of microfluidics to more accurately reproduce *in vivo* tumour physiology offers the potential for developing personalized therapies for individual cancer patients, in addition to permitting study of novel immunotherapies in combination with other anti-cancer agents and tumour-targeting nanoparticles. The first report of the assessment of EGFR specific CAR-T cell efficacy and specificity in 3D tumour-stromal co-cultures and in combination with carboplatin chemotherapy and anti-PD-L1 therapy was presented. Preliminary work using primary murine gamma delta T cells demonstrated the potential for human primary tissue to be used in microfluidic immunoassays and presents possible avenues for the future of ACT therapy development.

References

1.   Krzyszczyk P, Acevedo A, Davidoff EJ, Timmins LM, Marrero-Berrios I, Patel M, White C, Lowe C, Sherba JJ, Hartmanshenn C, O'Neill KM, Balter ML, Fritz ZR, Androulakis IP, Schloss RS, Yarmush ML. The growing role of precision and personalized medicine for cancer treatment. Technology (Singap World Sci). 2018;6(3-4):79-100.

2.   Fetah KL, DiPardo BJ, Kongadzem E-M, Tomlinson JS, Elzagheid A, Elmusrati M, Khademhosseini A, Ashammakhi N. Cancer Modeling-on-a-Chip with Future Artificial Intelligence Integration. Small. 2019;15(50):1901985.

3.   Edmondson R, Broglie JJ, Adcock AF, Yang L. Three-dimensional cell culture systems and their applications in drug discovery and cell-based biosensors. Assay and drug development technologies. 2014;12(4):207-18.

4.   Bregenzer ME, Horst EN, Mehta P, Novak CM, Raghavan S, Snyder CS, Mehta G. Integrated cancer tissue engineering models for precision medicine. PLoS One. 2019;14(5):e0216564.

5.   Seyfoori A, Samiei E, Jalili N, Godau B, Rahmanian M, Farahmand L, Majidzadeh-A K, Akbari M. Self-filling microwell arrays (SFMAs) for tumor spheroid formation. Lab on a Chip. 2018;18(22):3516-28.

6.   Goto T. Patient-Derived Tumor Xenograft Models: Toward the Establishment of Precision Cancer Medicine. Journal of Personalized Medicine 2020;10(3):64.

7.   Hegde PS, Chen DS. Top 10 Challenges in Cancer Immunotherapy. Immunity. 2020;52(1):17-35.

8.   Williams JA. Using PDX for Preclinical Cancer Drug Discovery: The Evolving Field. Journal of Clinical Medicine. 2018;7(3).

9.   Mak IW, Evaniew N, Ghert M. Lost in translation: animal models and clinical trials in cancer treatment. American journal of translational research. 2014;6(2):114-8.

10.   Borenstein JT. Microfluidic techniques for cancer therapies. European Pharmaceutical Review. 2017;22(3):50-3.

11.   Paterson K, Zanivan S, Glasspool R, Coffelt SB, Zagnoni M. Microfluidic technologies for immunotherapy studies on solid tumours. Lab on a Chip. 2021;21(12):2306-29.

12.   Soler M, Lechuga L. Boosting Cancer Immunotherapies with Optical Biosensor Nanotechnologies. European Medical Journal. 2019.

13.   Adriani G, Pavesi A, Tan AT, Bertoletti A, Thiery JP, Kamm RD. Microfluidic models for adoptive cell-mediated cancer immunotherapies. Drug Discov Today. 2016;21(9):1472-8.

14.   Moshksayan K, Kashaninejad N, Saidi M, Moshksayan K, Kashaninejad N, Saidi MS. Inventions and Innovations in Preclinical Platforms for Cancer Research. Inventions. 2018;3(3):43.

15.   Mulholland T, McAllister M, Patek S, Flint D, Underwood M, Sim A, Edwards J, Zagnoni M. Drug screening of biopsy-derived spheroids using a self-generated microfluidic concentration gradient. Scientific Reports. 2018;8(1):1-17.

16.   Ventola CL. Cancer Immunotherapy, Part 3: Challenges and Future Trends. Pharmacy and Therapeutics. 2017.

17.   Liu Y, Yang Q, Cao L, Xu F. Analysis of Leukocyte Behaviors on Microfluidic Chips. Adv Healthc Mater. 2019;8(4):1801406.

18.   Kapara A, Findlay Paterson KA, Brunton VG, Graham D, Zagnoni M, Faulds K. Detection of Estrogen Receptor Alpha and Assessment of Fulvestrant Activity in MCF-7 Tumor Spheroids Using Microfluidics and SERS. Analytical Chemistry. 2021;93(14):5862-71.

19.   Kay EJ, Paterson K, Domingo CR, Sumpton D, Daebritz H, Tardito S, Boldrini C, Hernandez-Fernaud JR, Athineos D, Dhayade S, Stepanova E, Gjerga E, Neilson LJ, Lilla S, Hedley A, Koulouras G, McGregor G, Jamieson C, Johnson RM, Park M, Kirschner K, Miller C, Kamphorst JJ, Loayza-Puch F, Saez-Rodriguez J, Mazzone M, Blyth K, Zagnoni M, Zanivan S. PYCR1-dependent proline synthesis in cancer-associated fibroblasts is required for the deposition of pro-tumorigenic extracellular matrix. bioRxiv. 2021:2020.05.30.125237.
20.   Paterson K, Paterson S, Mulholland T, Coffelt SB, Zagnoni M. Assessment of CAR-T mediated and targeted cytotoxicity in 3D microfluidic TBNC co-culture models for combination therapy. bioRxiv. 2021:2021.09.14.458168.
21.   Ray S. Cancer Survival Rates Are Improving With Advances In Treatment Options. 2017.
22.   Latosińska M, Latosińska JN. Introductory Chapter: Having a Brain is Not Necessary to Get Cancer… but Indispensable to Fight It. Unique Aspects of Anti-cancer Drug Development 2017.
23.   Cancer in the UK 2019. Cancer, Intelligence Team, Cancer Research UK. 2019.
24.   Schüz J, Espina C, Wild CP. Primary prevention: a need for concerted action. Mol Oncol. 2019;13(3):567-78.
25.   Plummer M, de Martel C, Vignat J, Ferlay J, Bray F, Franceschi S. Global burden of cancers attributable to infections in 2012: a synthetic analysis. The Lancet Global Health. 2016;4(9):e609-e16.
26.   Hanahan D, Weinberg RA. The hallmarks of cancer. Cell. 2000;100(1):57-70.
27.   Hanahan D, Weinberg RA. Hallmarks of cancer: the next generation. Cell. 2011;144(5):646-74.
28.   Sevic I, Spinelli FM, Cantero MJ, Reszegi A, Kovalszky I, Garcia MG, Alaniz L. The Role of the Tumor Microenvironment in the Development and Progression of Hepatocellular Carcinoma. In: Tirnitz-Parker JEE, editor. Hepatocellular Carcinoma. Brisbane (AU): Hepatocellular Carcinoma; 2019.
29.   Wang M, Zhao J, Zhang L, Wei F, Lian Y, Wu Y, Gong Z, Zhang S, Zhou J, Cao K, Li X, Xiong W, Li G, Zeng Z, Guo C. Role of tumor microenvironment in tumorigenesis. Journal of Cancer. 2017;8(5):761-73.
30.   Zhong S, Jeong J-H, Chen Z, Chen Z, Luo J-L. Targeting Tumor Microenvironment by Small-Molecule Inhibitors. Translational Oncology. 2020;13(1):57-69.
31.   Fang H, DeClerck YA. Targeting the Tumor Microenvironment: From Understanding Pathways to Effective Clinical Trials. Cancer Research. 2013;73:4965-77.
32.   Tang T, Huang X, Zhang G, Hong Z, Bai X, Liang T. Advantages of targeting the tumor immune microenvironment over blocking immune checkpoint in cancer immunotherapy. Signal Transduction and Targeted Therapy. 2021;6(1):72.
33.   Pitt JM, Marabelle A, Eggermont A, Soria JC, Kroemer G, Zitvogel L. Targeting the tumor microenvironment: removing obstruction to anticancer immune responses and immunotherapy. Annals of Oncology. 2016;27(8):1482-92.
34.   Nishida N, Yano H, Nishida T, Kamura T, Kojiro M. Angiogenesis in cancer. 2006.
35.   Santi A, Kugeratski FG, Zanivan S. Cancer Associated Fibroblasts: The Architects of Stroma Remodeling. PROTEOMICS. 2018;18(5-6):1700167.
36.   Laitala A, Erler JT. Hypoxic Signalling in Tumour Stroma. Frontiers in Oncology. 2018;8:189.
37.   Däster S, Amatruda N, Calabrese D, Ivanek R, Turrini E, Droeser RA, Zajac P, Fimognari C, Spagnoli GC, Iezzi G, Mele V, Muraro MG. Induction of hypoxia and necrosis in multicellular tumor spheroids is associated with resistance to chemotherapy treatment. Oncotarget. 2017;8(1):1725-36.
38.   Teicher BA. Hypoxia and drug resistance. Cancer and Metastasis Reviews. 1994;13(2):139-68.

39.   Minassian LM, Cotechini T, Huitema E, Graham CH. Hypoxia-Induced Resistance to Chemotherapy in Cancer. In: Gilkes DM, editor. Hypoxia and Cancer Metastasis. Cham: Springer International Publishing; 2019. p. 123-39.
40.   Siemann DW. The unique characteristics of tumor vasculature and preclinical evidence for its selective disruption by Tumor-Vascular Disrupting Agents. Cancer treatment reviews. 2011;37(1):63-74.
41.   Kim S, Lee H, Chung M, Jeon NL. Engineering of functional, perfusable 3D microvascular networks on a chip. Lab on a Chip. 2013;13(8):1489.
42.   Lugano R, Ramachandran M, Dimberg A. Tumor angiogenesis: causes, consequences, challenges and opportunities. Cellular and Molecular Life Sciences. 2020;77(9):1745-70.
43.   Baish JW, Stylianopoulos T, Lanning RM, Kamoun WS, Fukumura D, Munn LL, Jain RK. Scaling rules for diffusive drug delivery in tumor and normal tissues. Proceedings of the National Academy of Sciences of the United States of America. 2011;108(5):1799-803.
44.   Caballero D, Blackburn SM, De Pablo M, Samitier J, Albertazzi L. Tumour-vessel-on-a-chip models for drug delivery. Lab on a Chip. 2017;17:3760.
45.   Huang R, Zheng W, Liu W, Zhang W, Long Y, Jiang X. Investigation of Tumor Cell Behaviors on a Vascular Microenvironment-Mimicking Microfluidic Chip. Scientific Reports. 2016;5(1):17768.
46.   Chiang SPH, Cabrera RM, Segall JE. Tumor cell intravasation. American journal of physiology Cell physiology 2016;311(1):C1-C14.
47.   Cai J, Ma H, Huang F, Zhu D, Bi J, Ke Y, Zhang T. Correlation of bevacizumab-induced hypertension and outcomes of metastatic colorectal cancer patients treated with bevacizumab: a systematic review and meta-analysis. World Journal of Surgical Oncology. 2013;11(1):306.
48.   Rini BI, Cohen DP, Lu DR, Chen I, Hariharan S, Gore ME, Figlin RA, Baum MS, Motzer RJ. Hypertension as a Biomarker of Efficacy in Patients With Metastatic Renal Cell Carcinoma Treated With Sunitinib. JNCI: Journal of the National Cancer Institute. 2011;103(9):763-73.
49.   Lu P, Weaver VM, Werb Z. The extracellular matrix: a dynamic niche in cancer progression. The Journal of cell biology. 2012;196(4):395-406.
50.   Li Y, Kumacheva E. Hydrogel microenvironments for cancer spheroid growth and drug screening. Science Advances. 2018;4(4):eaas8998-eaas.
51.   Xiong G-F, Xu R. Function of cancer cell-derived extracellular matrix in tumor progression. Journal of Cancer Metastasis and Treatment. 2016;2:357-64.
52.   Lee SW, Kwak HS, Kang M-H, Park Y-Y, Jeong GS. Fibroblast-associated tumour microenvironment induces vascular structure-networked tumouroid. Scientific Reports. 2018;8(1):2365.
53.   Gascard P, Tlsty TD. Carcinoma-associated fibroblasts: orchestrating the composition of malignancy. Genes & development. 2016;30(9):1002-19.
54.   Fang M, Yuan J, Peng C, Li Y. Collagen as a double-edged sword in tumor progression. Tumour biology : the journal of the International Society for Oncodevelopmental Biology and Medicine. 2014;35(4):2871-82.
55.   Granchi C. ATP citrate lyase (ACLY) inhibitors: An anti-cancer strategy at the crossroads of glucose and lipid metabolism. European Journal of Medicinal Chemistry. 2018;157:1276-91.
56.   Koukourakis MI, Giatromanolaki A, Sivridis E, Gatter KC, Harris AL, Tumor, Angiogenesis Research G. Pyruvate dehydrogenase and pyruvate dehydrogenase kinase expression in non small cell lung cancer and tumor-associated stroma. Neoplasia. 2005;7(1):1-6.
57.   Heemers HV, Debes JD, Tindall DJ. The role of the transcriptional coactivator p300 in prostate cancer progression. Adv Exp Med Biol. 2008;617:535-40.

58. Xiao S, Li S, Yuan Z, Zhou L. Pyrroline-5-carboxylate reductase 1 (PYCR1) upregulation contributes to gastric cancer progression and indicates poor survival outcome. Ann Transl Med. 2020;8(15):937.

59. Abbott M, Ustoyev Y. Cancer and the Immune System: The History and Background of Immunotherapy. Semin Oncol Nurs. 2019;35(5):150923.

60. Zhang C, Yang M, Ericsson AC. Function of Macrophages in Disease: Current Understanding on Molecular Mechanisms. Frontiers in Immunology. 2021;12.

61. Hu W, Wang G, Huang D, Sui M, Xu Y. Cancer Immunotherapy Based on Natural Killer Cells: Current Progress and New Opportunities. Frontiers in Immunology. 2019;10.

62. Martin-Gayo E, Yu XG. Role of Dendritic Cells in Natural Immune Control of HIV-1 Infection. Frontiers in Immunology. 2019;10.

63. Zamarron BF, Chen W. Dual roles of immune cells and their factors in cancer development and progression. (1449-2288 (Electronic)).

64. Giannios JN. Immunoediting, Immunosurveillance, Tumor-induced Immunosuppression and Immunoresistance, Immunomodulation, Immunotherapy, and Immunonutrition in Personalized and Precision Cancer Medicine. Immunopathology and Immunomodulation2015.

65. Arruebo M, Vilaboa N, Saez-Gutierrez B, Lambea J, Tres A, Valladares M, Gonzalez-Fernandez A. Assessment of the evolution of cancer treatment therapies. Cancers (Basel). 2011;3(3):3279-330.

66. Moding EJ, Kastan MB, Kirsch DG. Strategies for optimizing the response of cancer and normal tissues to radiation. Nat Rev Drug Discov. 2013;12(7):526-42.

67. Jaffray D, Gospodarowicz M. Radiation Therapy for Cancer. Disease Control Priorities: Cancer. 32015.

68. Carter S, Thurston D. Immuno-oncology agents for cancer therapy. The Pharmaceutical Journal. 2020.

69. Ramlaul A, Vosper M. Cancer Chemotherapy Drugs. Patient Centered Care in Medical Imaging and Radiotherapy. 12013. p. 107-8.

70. Verma RS, Adachi M, Barth S, Benhar I, Bette M, Brinkmann U, Carloni P, Cremer C, Dergachev V, Devilakshmi S, Gadadhar S, Hehmann-Titt G, Karande AA, Madhumathi J, Bonavida B, Melmer G, Mueller F, Nachreiner T, Pastan I, Robak P, Robak T, Schiffer S, Stahl S, Takeshita A, Walter R. Targeted Cancer Therapy: History and Development of Immunotoxins. Resistance to immunotoxins in cancer therapy /. 2015;6:1-31.

71. Gao Y, Tang M, Leung E, Svirskis D, Shelling A, Wu Z. Dual or multiple drug loaded nanoparticles to target breast cancer stem cells. RSC Advances. 2020;10(32):19089-105.

72. Boussommier-Calleja A, Li R, Chen MB, Wong SC, Kamm RD. Microfluidics: A new tool for modeling cancer-immune interactions. Trends Cancer. 2016;2(1):6-19.

73. Herter-Sprie GS, Kung AL, Wong K-K. New cast for a new era: preclinical cancer drug development revisited. The Journal of clinical investigation 2013;123(9):3639-45.

74. Matthews H, Hanison J, Nirmalan N. "Omics"-Informed Drug and Biomarker Discovery: Opportunities, Challenges and Future Perspectives. Proteomes. 2016;4:28.

75. Low LA, Mummery C, Berridge BR, Austin CP, Tagle DA. Organs-on-chips: into the next decade. Nat Rev Drug Discov. 2020.

76. Pan E, Bogumil D, Cortessis V, Yu S, Nieva J. A Systematic Review of the Efficacy of Preclinical Models of Lung Cancer Drugs. Front Oncol. 2020;10:591.

77. Dhandapani M, Goldman A. Preclinical Cancer Models and Biomarkers for Drug Development: New Technologies and Emerging Tools. Journal of Molecular Biomarkers & Diagnosis 2017;8(5):356.

78. Dobosz P, Dzieciatkowski T. The Intriguing History of Cancer Immunotherapy. Front Immunol. 2019;10:2965.

79. Newman JH, Zloza A. Infection: a Cause of and Cure for Cancer. Curr Pharmacol Rep. 2017;3(6):315-20.

80. Lee Ventola C. Cancer immunotherapy, part 3: Challenges and future trends. P and T. 2017;42(8):514-21.

81. Nixon NA, Blais N, Ernst S, Kollmannsberger C, Bebb G, Butler M, Smylie M, Verma S. Current landscape of immunotherapy in the treatment of solid tumours, with future opportunities and challenges. Current Oncology. 2018;25(5):E373-E84.

82. Kruger S, Ilmer M, Kobold S, Cadilha BL, Endres S, Ormanns S, Schuebbe G, Renz BW, D'Haese JG, Schloesser H, Heinemann V, Subklewe M, Boeck S, Werner J, von Bergwelt-Baildon M. Advances in cancer immunotherapy 2019 - latest trends. Journal of Experimental & Clinical Cancer Research 2019;38(1):268.

83. Liu TY, Han CC, Wang SW, Fang PQ, Ma ZF, Xu L, Yin R. Cancer-associated fibroblasts: an emerging target of anti-cancer immunotherapy. Journal of Hematology & Oncology. 2019;12(1).

84. Marayati R, Quinn CH, Beierle EA. Immunotherapy in Pediatric Solid Tumors-A Systematic Review. Cancers (Basel). 2019;11(12).

85. Martinez M, Moon EK. CAR T Cells for Solid Tumors: New Strategies for Finding, Infiltrating, and Surviving in the Tumor Microenvironment. Frontiers in Immunology. 2019;10:128-.

86. Di Tucci C, Schiavi MC, Faiano P, D'Oria O, Prata G, Sciuga V, Giannini A, Palaia I, Muzii L, Benedetti Panici P. Therapeutic vaccines and immune checkpoints inhibition options for gynecological cancers. Crit Rev Oncol Hematol. 2018;128:30-42.

87. Hong WX, Haebe S, Lee AS, Westphalen B, Norton JA, Jiang W, Levy R. Intratumoral immunotherapy for early stage solid tumors. Clinical Cancer Research 2020.

88. Zhao Z, Zheng L, Chen W, Weng W, Song J, Ji J. Delivery strategies of cancer immunotherapy: recent advances and future perspectives. Journal of Hematology & Oncology. 2019;12(1):126.

89. Sanmamed MF, Chen L. A Paradigm Shift in Cancer Immunotherapy: From Enhancement to Normalization. Cell. 2018;175(2):313-26.

90. Irimia D, Wang X. Inflammation-on-a-Chip: Probing the Immune System Ex Vivo. Elsevier Ltd; 2018. p. 923-37.

91. Li Z, Qiu Y, Lu W, Jiang Y, Wang J. Immunotherapeutic interventions of Triple Negative Breast Cancer. Journal of Translational Medicine. 2018;16(1):147.

92. Toulouie S, Johanning G, Shi Y. Chimeric antigen receptor T-cell immunotherapy in breast cancer: development and challenges. Journal of Cancer. 2021;12(4):1212-9.

93. Mediratta K, El-Sahli S, D'Costa V, Wang L. Current Progresses and Challenges of Immunotherapy in Triple-Negative Breast Cancer. Cancers (Basel). 2020;12(12).

94. Kumar V, Varghese S. Ex Vivo Tumor-on-a-Chip Platforms to Study Intercellular Interactions within the Tumor Microenvironment. Adv Healthc Mater. 2019;8(4):e1801198.

95. Polini A, del Mercato LL, Barra A, Zhang YS, Calabi F, Gigli G. Towards the development of human immune-system-on-a-chip platforms. Elsevier Ltd; 2019. p. 517-25.

96. Lee S, Margolin K. Cytokines in cancer immunotherapy. Cancers (Basel). 2011;3(4):3856-93.

97. van der Zanden SY, Luimstra JJ, Neefjes J, Borst J, Ovaa H. Opportunities for Small Molecules in Cancer Immunotherapy. Trends Immunol. 2020;41(6):493-511.

98. Schlom J, Hodge JW, Palena C, Tsang KY, Jochems C, Greiner JW, Farsaci B, Madan RA, Heery CR, Gulley JL. Therapeutic cancer vaccines. Adv Cancer Res. 2014;121:67-124.

99. Hollingsworth RE, Jansen K. Turning the corner on therapeutic cancer vaccines. npj Vaccines. 2019;4(1):7.

100. Mougel A, Terme M, Tanchot C. Therapeutic Cancer Vaccine and Combinations With Antiangiogenic Therapies and Immune Checkpoint Blockade. Frontiers in Immunology. 2019;10.

101.	Pham T, Roth S, Kong J, Guerra G, Narasimhan V, Pereira L, Desai J, Heriot A, Ramsay R. An Update on Immunotherapy for Solid Tumors: A Review. Annals of Surgical Oncology. 2018;25(11):3404-12.

102.	Alhunaidi O, Zlotta AR. The use of intravesical BCG in urothelial carcinoma of the bladder. Ecancermedicalscience. 2019;13:905.

103.	Pardoll DM. The blockade of immune checkpoints in cancer immunotherapy. Nat Rev Cancer. 2012;12(4):252-64.

104.	Bassez A, Vos H, Van Dyck L, Floris G, Arijs I, Desmedt C, Boeckx B, Vanden Bempt M, Nevelsteen I, Lambein K, Punie K, Neven P, Garg AD, Wildiers H, Qian J, Smeets A, Lambrechts D. A single-cell map of intratumoral changes during anti-PD1 treatment of patients with breast cancer. Nature Medicine. 2021;27(5):820-32.

105.	Gao M, Wang T, Ji L, Bai S, Tian L, Song H. Therapy With Carboplatin and Anti-PD-1 Antibodies Before Surgery Demonstrates Sustainable Anti-Tumor Effects for Secondary Cancers in Mice With Triple-Negative Breast Cancer. Frontiers in Immunology. 2020;11(366).

106.	Kim I, Sanchez K, McArthur HL, Page D. Immunotherapy in Triple-Negative Breast Cancer: Present and Future. Current Breast Cancer Reports. 2019;11(4):259-71.

107.	Oualla K, Kassem L, Nouiakh L, Amaadour L, Benbrahim Z, Arifi S, Mellas N. Immunotherapeutic Approaches in Triple-Negative Breast Cancer: State of the Art and Future Perspectives. International journal of breast cancer 2020;2020:8209173.

108.	Guan M, Zhou YP, Sun JL, Chen SC. Adverse events of monoclonal antibodies used for cancer therapy. Biomed Res Int. 2015;2015:428169.

109.	O'Donnell JS, Teng MWL, Smyth MJ. Cancer immunoediting and resistance to T cell-based immunotherapy. Nature reviews. 2019;16(3):151-67.

110.	Jacobson CA, Ritz J. Time to put the CAR-T before the horse. Blood. 2011;118(18):4761-2.

111.	Srivastava S, Riddell SR. Chimeric Antigen Receptor T Cell Therapy: Challenges to Bench-to-Bedside Efficacy. Journal of immunology (Baltimore, Md : 1950). 2018;200(2):459-68.

112.	Abreu TR, Fonseca NA, Gonçalves N, Moreira JN. Current challenges and emerging opportunities of CAR-T cell therapies. Journal of Controlled Release. 2020;319:246-61.

113.	Schaft N. The Landscape of CAR-T Cell Clinical Trials against Solid Tumors—A Comprehensive Overview. Cancers. 2020;12(9):2567.

114.	Marofi F, Motavalli R, Safonov VA, Thangavelu L, Yumashev AV, Alexander M, Shomali N, Chartrand MS, Pathak Y, Jarahian M, Izadi S, Hassanzadeh A, Shirafkan N, Tahmasebi S, Khiavi FM. CAR T cells in solid tumors: challenges and opportunities. Stem Cell Research & Therapy. 2021;12(1):81.

115.	Titov A, Petukhov A, Staliarova A, Motorin D, Bulatov E, Shuvalov O, Soond SM, Piacentini M, Melino G, Zaritskey A, Barlev NA. The biological basis and clinical symptoms of CAR-T therapy-associated toxicites. Cell Death Dis. 2018;9(9):897.

116.	Titov A, Valiullina A, Zmievskaya E, Zaikova E, Petukhov A, Miftakhova R, Bulatov E, Rizvanov A. Advancing CAR T-cell therapy for solid tumors: Lessons learned from lymphoma treatment. Cancers. 2020;12(1):1-22.

117.	Harrison RP, Zylberberg E, Ellison S, Levine BL. Chimeric antigen receptor–T cell therapy manufacturing: modelling the effect of offshore production on aggregate cost of goods. Cytotherapy. 2019;21(2):224-33.

118.	Eyles JE, Vessillier S, Jones A, Stacey G, Schneider CK, Price J. Cell therapy products: focus on issues with manufacturing and quality control of chimeric antigen receptor T-cell therapies. Journal of Chemical Technology & Biotechnology. 2019;94(4):1008-16.

119.	Zhou R, Yazdanifar M, Roy LD, Whilding LM, Gavrill A, Maher J, Mukherjee P. CAR T Cells Targeting the Tumor MUC1 Glycoprotein Reduce Triple-Negative Breast Cancer Growth. Frontiers in Immunology. 2019;10(1149).

120.   Dillard P, Köksal H, Inderberg E-M, Wälchli S. Killing Assay by CAR T Cells. Journal of Visualized Experiments : JoVE 2018(142):58785.

121.   Li Y, Gao Q, Liu H, Lin S, Chen H, Ding R, Gu Y, Chao C-c, Dong X. The Targeting Effect of Cetuximab Combined with PD-L1 Blockade against EGFR-Expressing Tumors in a Tailored CD16-CAR T-Cell Reporter System. Cancer Investigation. 2021;39(4):285-96.

122.   Liu G, Rui W, Zheng H, Huang D, Yu F, Zhang Y, Dong J, Zhao X, Lin X. CXCR2-modified CAR-T cells have enhanced trafficking ability that improves treatment of hepatocellular carcinoma. European Journal of Immunology. 2020:eji.201948457-eji.

123.   Ronteix G, Jain S, Angely C, Cazaux M, Khazen R, Bousso P, Baroud CN. A Multiscale Immuno-Oncology on-Chip System (MIOCS) establishes that collective T cell behaviors govern tumor regression. bioRxiv. 2021:2021.03.23.435334.

124.   Herter S, Morra L, Schlenker R, Sulcova J, Fahrni L, Waldhauer I, Lehmann S, Reisländer T, Agarkova I, Kelm JM, Klein C, Umana P, Bacac M. A novel three-dimensional heterotypic spheroid model for the assessment of the activity of cancer immunotherapy agents. Cancer Immunology, Immunotherapy. 2017;66(1):129-40.

125.   Wykosky J, Fenton T Fau - Furnari F, Furnari F Fau - Cavenee WK, Cavenee WK. Therapeutic targeting of epidermal growth factor receptor in human cancer: successes and limitations. Chinese Journal of Cancer 2011(1000-467X (Print)).

126.   Bergeron AB, Gitschier HJ. CAR-T Cell Screening in Tumor Spheroids using Corning ® Spheroid Microplates and the KILR ® Cytotoxicity Assay Application Note.

127.   Wallstabe L, Göttlich C, Nelke LC, Kühnemundt J, Schwarz T, Nerreter T, Einsele H, Walles H, Dandekar G, Nietzer SL, Hudecek M. ROR1-CAR T cells are effective against lung and breast cancer in advanced microphysiologic 3D tumor models. JCI Insight. 2019;4(18).

128.   Liu Y, Zhou Y, Huang K-H, Li Y, Fang X, An L, Wang F, Chen Q, Zhang Y, Shi A, Yu S, Zhang J. EGFR-specific CAR-T cells trigger cell lysis in EGFR-positive TNBC. Aging. 2019;11.

129.   Riley RS, June CH, Langer R, Mitchell MJ. Delivery technologies for cancer immunotherapy. Nat Rev Drug Discov. 2019;18(3):175-96.

130.   Reidy E, Leonard NA, Treacy O, Ryan AE. A 3D View of Colorectal Cancer Models in Predicting Therapeutic Responses and Resistance. Cancers. 2021;13(2).

131.   Chulpanova DS, Kitaeva KV, Rutland CS, Rizvanov AA, Solovyeva VV. Mouse Tumor Models for Advanced Cancer Immunotherapy. International journal of molecular sciences. 2020;21(11):4118.

132.   Zhong W, Myers JS, Wang F, Wang K, Lucas J, Rosfjord E, Lucas J, Hooper AT, Yang S, Lemon LA, Guffroy M, May C, Bienkowska JR, Rejto PA. Comparison of the molecular and cellular phenotypes of common mouse syngeneic models with human tumors. BMC Genomics. 2020;21(1):2.

133.   Doke SK, Dhawale SC. Alternatives to animal testing: A review. Saudi Pharmaceutical Journal. 2015;23(3):223-9.

134.   Mengus C, Muraro MG, Mele V, Amicarella F, Manfredonia C, Foglietta F, Muenst S, Soysal SD, Iezzi G, Spagnoli GC. In Vitro Modeling of Tumor–Immune System Interaction. ACS Biomaterials Science & Engineering. 2017;4(2):314-23.

135.   Tsai HF, Trubelja A, Shen AQ, Bao G. Tumour-on-a-chip: microfluidic models of tumour morphology, growth and microenvironment. Journal of The Royal Society Interface 2017;14(131).

136.   Rodrigues J, Heinrich MA, Teixeira LM, Prakash J. 3D In Vitro Model (R)evolution: Unveiling Tumor-Stroma Interactions. Trends Cancer. 2021;7(3):249-64.

137.   Chen Q, Wang Y. The application of three-dimensional cell culture in clinical medicine. Biotechnology Letters. 2020;42(11):2071-82.

138.   Bray LJ, Hutmacher DW, Bock N. Addressing Patient Specificity in the Engineering of Tumor Models. Front Bioeng Biotechnol. 2019;7:217.

139.   Yang H, Sun L, Liu M, Mao Y. Patient-derived organoids: a promising model for personalized cancer treatment. Gastroenterol Rep (Oxf). 2018;6(4):243-5.
140.   Fan H, Demirci U, Chen P. Emerging organoid models: leaping forward in cancer research. Journal of Hematology & Oncology. 2019;12(1):142.
141.   Velasco V, Shariati SA, Esfandyarpour R. Microtechnology-based methods for organoid models. Microsystems & Nanoengineering. 2020;6(1):76.
142.   Kim J, Koo B-K, Knoblich JA. Human organoids: model systems for human biology and medicine. Nature Reviews Molecular Cell Biology. 2020;21(10):571-84.
143.   Xu H, Lyu X, Yi M, Zhao W, Song Y, Wu K. Organoid technology and applications in cancer research. Journal of Hematology & Oncology. 2018;11(1):116.
144.   Barisam M, Saidi MS, Kashaninejad N, Nguyen N-T. Prediction of Necrotic Core and Hypoxic Zone of Multicellular Spheroids in a Microbioreactor with a U-Shaped Barrier. Micromachines. 2018;9(3).
145.   Katt ME, Placone AL, Wong AD, Xu ZS, Searson PC. In Vitro Tumor Models: Advantages, Disadvantages, Variables, and Selecting the Right Platform. Frontiers in Bioengineering and Biotechnology. 2016;4(12).
146.   Lazzari G, Nicolas V, Matsusaki M, Akashi M, Couvreur P, Mura S. Multicellular spheroid based on a triple co-culture: A novel 3D model to mimic pancreatic tumor complexity. Acta Biomaterialia. 2018;78:296-307.
147.   Mirab F, Kang YJ, Majd S. Preparation and characterization of size-controlled glioma spheroids using agarose hydrogel microwells. PLoS One. 2019;14(1):e0211078.
148.   Weydert Z, Lal-Nag M, Mathews-Greiner L, Thiel C, Cordes H, Küpfer L, Guye P, Kelm JM, Ferrer M. A 3D Heterotypic Multicellular Tumor Spheroid Assay Platform to Discriminate Drug Effects on Stroma versus Cancer Cells. SLAS DISCOVERY: Advancing Life Sciences R&D. 2019:2472555521988019.
149.   Wu C-G, Chiovaro F, Curioni-Fontecedro A, Casanova R, Soltermann A. In vitro cell culture of patient derived malignant pleural and peritoneal effusions for personalised drug screening. Journal of Translational Medicine. 2020;18(1):163.
150.   Geng Y. 3D101 Part 2: Keep Calm and Culture On; InSphero's easy to use GravityPLUS™ Hanging Drop System and GravityTRAP™ ULA Plate.
151.   Ausländer D, Ausländer S, Pierrat X, Hellmann L, Rachid L, Fussenegger M. Programmable full-adder computations in communicating three-dimensional cell cultures. Nature Methods. 2018;15(1):57-60.
152.   Raghavan S, Mehta P, Horst EN, Ward MR, Rowley KR, Mehta G. Comparative analysis of tumor spheroid generation techniques for differential in vitro drug toxicity. Oncotarget. 2016;7(13):16948-61.
153.   Campos DM, Soares GA, Anselme K. Role of culture conditions on in vitro transformation and cellular colonization of biomimetic HA-Col scaffolds. Biomatter. 2013;3(2).
154.   Wong CH, Siah KW, Lo AW. Estimation of clinical trial success rates and related parameters. Biostatistics. 2019;20(2):273-86.
155.   Tehranirokh M, Kouzani AZ, Francis PS, Kanwar JR. Microfluidic devices for cell cultivation and proliferation. Biomicrofluidics. 2013;7(5):51502.
156.   Convery N, Gadegaard N. 30 years of microfluidics. Micro and Nano Engineering. 2019;2:76-91.
157.   Paguirigan AL, Beebe DJ. Microfluidics meet cell biology: bridging the gap by validation and application of microscale techniques for cell biological assays. Bioessays. 2008;30(9):811-21.
158.   Sohrabi Kashani A, Packirisamy M. Efficient Low Shear Flow-based Trapping of Biological Entities. Sci Rep. 2019;9(1):5511.
159.   Velve-Casquillas G, Le Berre M, Piel M, Tran PT. Microfluidic tools for cell biological research. Nano Today. 2010;5(1):28-47.

160.   Nielsen JB, Hanson RL, Almughamsi HM, Pang C, Fish TR, Woolley AT. Microfluidics: Innovations in Materials and Their Fabrication and Functionalization. Analytical Chemistry. 2020;92(1):150-68.

161.   Wang Z, Volinsky AA, Gallant ND. Crosslinking effect on polydimethylsiloxane elastic modulus measured by custom-built compression instrument. Journal of Applied Polymer Science. 2014;131(22).

162.   Annabestani M, Esmaeili-Dokht P, Fardmanesh M. A novel, low cost, and accessible method for rapid fabrication of the modifiable microfluidic devices. Scientific Reports. 2020;10(1):16513.

163.   Cui P, Wang S. Application of microfluidic chip technology in pharmaceutical analysis: A review. Journal of Pharmaceutical Analysis. 2019;9(4):238-47.

164.   Byun CK, Abi-Samra K, Cho YK, Takayama S. Pumps for microfluidic cell culture. Electrophoresis. 2014;35(2-3):245-57.

165.   Gupta N, Liu JR, Patel B, Solomon DE, Vaidya B, Gupta V. Microfluidics-based 3D cell culture models: Utility in novel drug discovery and delivery research. Bioeng Transl Med. 2016;1(1):63-81.

166.   Trujillo-de Santiago G, Flores-Garza BG, Tavares-Negrete JA, Lara-Mayorga IM, González-Gamboa I, Zhang YS, Rojas-Martínez A, Ortiz-López R, Álvarez MM. The tumor-on-chip: Recent advances in the development of microfluidic systems to recapitulate the physiology of solid tumors. MDPI AG; 2019.

167.   Horowitz LF, Rodriguez AD, Dereli-Korkut Z, Lin R, Castro K, Mikheev AM, Monnat RJ, Jr., Folch A, Rostomily RC. Multiplexed drug testing of tumor slices using a microfluidic platform. NPJ Precis Oncol. 2020;4:12.

168.   Patra B, Lafontaine J, Bavoux M, Zerouali K, Glory A, Ahanj M, Carrier JF, Gervais T, Wong P. On-chip combined radiotherapy and chemotherapy testing on soft-tissue sarcoma spheroids to study cell death using flow cytometry and clonogenic assay. Sci Rep. 2019;9(1):2214.

169.   Cheah R, Srivastava R, Stafford ND, Beavis AW, Green V, Greenman J. Measuring the response of human head and neck squamous cell carcinoma to irradiation in a microfluidic model allowing customized therapy. International Journal of Oncology 2017(1791-2423 (Electronic)).

170.   Chen Y, Gao D, Liu H, Lin S, Jiang Y. Drug cytotoxicity and signaling pathway analysis with three-dimensional tumor spheroids in a microwell-based microfluidic chip for drug screening. Analytica Chimica Acta. 2015;898:85-92.

171.   Oyama TG, Oyama K, Taguchi M. A simple method for production of hydrophilic, rigid, and sterilized multi-layer 3D integrated polydimethylsiloxane microfluidic chips. Lab on a Chip. 2020;20(13):2354-63.

172.   Ko J, Ahn J, Kim S, Lee Y, Lee J, Park D, Li Jeon N. Tumor spheroid-on-a-chip: a standardized microfluidic culture platform for investigating tumor angiogenesis. Lab on a Chip. 2019.

173.   Patra B, Chen Y-H, Peng C-C, Lin S-C, Lee C-H, Tung Y-C. A microfluidic device for uniform-sized cell spheroids formation, culture, harvesting and flow cytometry analysis. Biomicrofluidics. 2013;7(5):54114.

174.   Patra B, Peng C-C, Liao W-H, Lee C-H, Tung Y-C. Drug testing and flow cytometry analysis on a large number of uniform sized tumor spheroids using a microfluidic device. Scientific reports. 2016;6:21061.

175.   Berger Fridman I, Ugolini GS, VanDelinder V, Cohen S, Konry T. High throughput microfluidic system with multiple oxygen levels for the study of hypoxia in tumor spheroids. Biofabrication. 2021;13(3).

176.   Chrobak KM, Potter DR, Tien J. Formation of perfused, functional microvascular tubes in vitro. Microvascular Research. 2006;71(3):185-96.

177.   Lee H, Park W, Ryu H, Jeon NL. A microfluidic platform for quantitative analysis of cancer angiogenesis and intravasation. Biomicrofluidics. 2014;8(5):054102-.

178.   Oh S, Ryu H, Tahk D, Ko J, Chung Y, Lee HK, Lee TR, Jeon NL. "Open-Top" Microfluidic Device for in Vitro Three-Dimensional Capillary Beds. Lab on a Chip. 2017;17(20):3405-14.

179.   Zervantonakis IK, Hughes-Alford SK, Charest JL, Condeelis JS, Gertler FB, Kamm RD. Three-dimensional microfluidic model for tumor cell intravasation and endothelial barrier function. Proc Natl Acad Sci U S A. 2012;109(34):13515-20.

180.   Phan DTT, Wang X, Craver BM, Sobrino A, Zhao D, Chen JC, Lee LYN, George SC, Lee AP, Hughes CCW. A vascularized and perfused organ-on-a-chip platform for large-scale drug screening applications. Lab on a Chip. 2017;17(3):511-20.

181.   Sobrino A, Phan DTT, Datta R, Wang X, Hachey SJ, Romero-López M, Gratton E, Lee AP, George SC, Hughes CCW. 3D microtumors in vitro supported by perfused vascular networks. Scientific Reports. 2016;6(1):31589.

182.   Abe Y, Watanabe M, Chung S, Kamm RD, Tanishita K, Sudo R. Balance of interstitial flow magnitude and vascular endothelial growth factor concentration modulates three-dimensional microvascular network formation. APL Bioengineering. 2019;3(3):036102.

183.   van Zijl F, Krupitza G, Mikulits W. Initial steps of metastasis: cell invasion and endothelial transmigration. Mutat Res. 2011;728(1-2):23-34.

184.   Supriya N. Three-Dimensional Microfluidic Based Tumor-Vascular Model to Study Cancer Cell Invasion and Intravasation 2017.

185.   Jeon JS, Bersini S, Gilardi M, Dubini G, Charest JL, Moretti M, Kamm RD. Human 3D vascularized organotypic microfluidic assays to study breast cancer cell extravasation. Proceedings of the National Academy of Sciences. 2015;112(1):214-9.

186.   Nashimoto Y, Hayashi T, Kunita I, Nakamasu A, Torisawa Y-S, Nakayama M, Takigawa-Imamura H, Kotera H, Nishiyama K, Miura T, Yokokawa R. Integrative Biology Interdisciplinary approaches for molecular and cellular life sciences rsc.li/integrative-biology Integrating perfusable vascular networks with a three-dimensional tissue in a microfluidic device. Integrative Biology. 2017;9:506.

187.   Du Z, Mi S, Yi X, Xu Y, Sun W. Microfluidic system for modelling 3D tumour invasion into surrounding stroma and drug screening. Biofabrication. 2018;10(3):034102-.

188.   Sun W, Luo Z, Lee J, Kim HJ, Lee K, Tebon P, Feng Y, Dokmeci MR, Sengupta S, Khademhosseini A. Organ-on-a-Chip for Cancer and Immune Organs Modeling. Adv Healthc Mater. 2019;8(4):e1801363.

189.   Chowdury MA, Heileman KL, Moore TA, Young EWK. Biomicrofluidic Systems for Hematologic Cancer Research and Clinical Applications. SLAS Technol. 2019;24(5):457-76.

190.   Sun Y, Haglund TA, Rogers AJ, Ghanim AF, Sethu P. Review: Microfluidics technologies for blood-based cancer liquid biopsies. Analytica Chimica Acta. 2018;1012:10-29.

191.   Aboulkheyr Es H, Montazeri L, Aref AR, Vosough M, Baharvand H. Personalized Cancer Medicine: An Organoid Approach. Elsevier Ltd; 2018. p. 358-71.

192.   Hsu TH, Kao YL, Lin WL, Xiao JL, Kuo PL, Wu CW, Liao WY, Lee CH. The migration speed of cancer cells influenced by macrophages and myofibroblasts co-cultured in a microfluidic chip. Integr Biol (Camb). 2012;4(2):177-82.

193.   Businaro L, De Ninno A, Schiavoni G, Lucarini V, Ciasca G, Gerardino A, Belardelli F, Gabriele L, Mattei F. Cross talk between cancer and immune cells: exploring complex dynamics in a microfluidic environment. Lab on a Chip 2013;13(2):229-39.

194.   Agliari E, Biselli E, De Ninno A, Schiavoni G, Gabriele L, Gerardino A, Mattei F, Barra A, Businaro L. Cancer-driven dynamics of immune cells in a microfluidic environment. Sci Rep. 2014;4:6639.

195.   Mattei F, Schiavoni G, De Ninno A, Lucarini V, Sestili P, Sistigu A, Fragale A, Sanchez M, Spada M, Gerardino A, Belardelli F, Businaro L, Gabriele L. A multidisciplinary study using in vivo tumor models and microfluidic cell-on-chip approach

to explore the cross-talk between cancer and immune cells. Journal of Immunotoxicology 2014;11(4):337-46.

196.   Bai J, Adriani G, Dang TM, Tu TY, Penny HX, Wong SC, Kamm RD, Thiery JP. Contact-dependent carcinoma aggregate dispersion by M2a macrophages via ICAM-1 and β2 integrin interactions. Oncotarget. 2015;6(28):25295-307.

197.   Zhao Y, Wang D, Xu T, Liu P, Cao Y, Wang Y, Yang X, Xu X, Wang X, Niu H. Bladder cancer cells re-educate TAMs through lactate shuttling in the microfluidic cancer microenvironment. Oncotarget. 2015;6(36):39196-210.

198.   Liu PF, Cao YW, Zhang SD, Zhao Y, Liu XG, Shi HQ, Hu KY, Zhu GQ, Ma B, Niu HT. A bladder cancer microenvironment simulation system based on a microfluidic co-culture model. Oncotarget. 2015;6(35):37695-705.

199.   Vacchelli E, Ma Y, Baracco EE, Sistigu A, Enot DP, Pietrocola F, Yang H, Adjemian S, Chaba K, Semeraro M, Signore M, De Ninno A, Lucarini V, Peschiaroli F, Businaro L, Gerardino A, Manic G, Ulas T, Günther P, Schultze JL, Kepp O, Stoll G, Lefebvre C, Mulot C, Castoldi F, Rusakiewicz S, Ladoire S, Apetoh L, Bravo-San Pedro JM, Lucattelli M, Delarasse C, Boige V, Ducreux M, Delaloge S, Borg C, André F, Schiavoni G, Vitale I, Laurent-Puig P, Mattei F, Zitvogel L, Kroemer G. Chemotherapy-induced antitumor immunity requires formyl peptide receptor 1. Science. 2015;350(6263):972-8.

200.   Biselli E, Agliari E, Barra A, Bertani FR, Gerardino A, De Ninno A, Mencattini A, Di Giuseppe D, Mattei F, Schiavoni G, Lucarini V, Vacchelli E, Kroemer G, Di Natale C, Martinelli E, Businaro L. Organs on chip approach: a tool to evaluate cancer -immune cells interactions. Sci Rep. 2017;7(1):12737.

201.   Lucarini V, Buccione C, Ziccheddu G, Peschiaroli F, Sestili P, Puglisi R, Mattia G, Zanetti C, Parolini I, Bracci L, Macchia I, Rossi A, D'Urso MT, Macchia D, Spada M, De Ninno A, Gerardino A, Mozetic P, Trombetta M, Rainer A, Businaro L, Schiavoni G, Mattei F. Combining Type I Interferons and 5-Aza-2'-Deoxycitidine to Improve Anti-Tumor Response against Melanoma. Journal of Investigative Dermatology 2017;137(1):159-69.

202.   Chen MB, Hajal C, Benjamin DC, Yu C, Azizgolshani H, Hynes RO, Kamm RD. Inflamed neutrophils sequestered at entrapped tumor cells via chemotactic confinement promote tumor cell extravasation. Proc Natl Acad Sci U S A. 2018;115(27):7022-7.

203.   Boussommier-Calleja A, Atiyas Y, Haase K, Headley M, Lewis C, Kamm RD. The effects of monocytes on tumor cell extravasation in a 3D vascularized microfluidic model. Biomaterials. 2019;198:180-93.

204.   Lei X, Lei Y, Li J-K, Du W-X, Li R-G, Yang J, Li J, Li F, Tan H-B. Immune cells within the tumor microenvironment: Biological functions and roles in cancer immunotherapy. Cancer Letters. 2020;470:126-33.

205.   Wimalachandra DC, Li Y, Liu J, Shikha S, Zhang J, Lim Y-C, Zhang Y. Microfluidic-Based Immunomodulation of Immune Cells Using Upconversion Nanoparticles in Simulated Blood Vessel–Tumor System. ACS Applied Materials & Interfaces. 2019;11(41):37513-23.

206.   Lei KF, Chang C-H, Chen M-J. Paper/PMMA Hybrid 3D Cell Culture Microfluidic Platform for the Study of Cellular Crosstalk. ACS Applied Materials & Interfaces. 2017;9(15):13092-101.

207.   Lu YT, Pendharkar GP, Lu CH, Chang CM, Liu CH. A microfluidic approach towards hybridoma generation for cancer immunotherapy. Oncotarget. 2015;6(36):38764-76.

208.   Jenkins RW, Aref AR, Lizotte PH, Ivanova E, Stinson S, Zhou CW, Bowden M, Deng J, Liu H, Miao D, He MX, Walker W, Zhang G, Tian T, Cheng C, Wei Z, Palakurthi S, Bittinger M, Vitzthum H, Kim JW, Merlino A, Quinn M, Venkataramani C, Kaplan JA, Portell A, Gokhale PC, Phillips B, Smart A, Rotem A, Jones RE, Keogh L, Anguiano M, Stapleton L, Jia Z, Barzily-Rokni M, Cañadas I, Thai TC, Hammond MR, Vlahos R, Wang ES, Zhang H, Li S, Hanna GJ, Huang W, Hoang MP, Piris A, Eliane J-P, Stemmer-Rachamimov AO, Cameron L, Su M-J, Shah P, Izar B, Thakuria M, Leboeuf NR, Rabinowits G, Gunda V, Parangi S, Cleary JM, Miller BC, Kitajima S, Thummalapalli R,

Miao B, Barbie TU, Sivathanu V, Wong J, Richards WG, Bueno R, Yoon CH, Miret J, Herlyn M, Garraway LA, Van Allen EM, Freeman GJ, Kirschmeier PT, Lorch JH, Ott PA, Hodi FS, Flaherty KT, Kamm RD, Boland GM, Wong K-K, Dornan D, Paweletz CP, Barbie DA. Ex Vivo Profi ling of PD-1 Blockade Using Organotypic Tumor Spheroids. 2017.

209.   Kulasinghe A, Perry C, Kenny L, Warkiani ME, Nelson C, Punyadeera C. PD-L1 expressing circulating tumour cells in head and neck cancers. BMC Cancer. 2017;17(1):333.

210.   Parlato S, De Ninno A, Molfetta R, Toschi E, Salerno D, Mencattini A, Romagnoli G, Fragale A, Roccazzello L, Buoncervello M, Canini I, Bentivegna E, Falchi M, Bertani FR, Gerardino A, Martinelli E, Natale C, Paolini R, Businaro L, Gabriele L. 3D Microfluidic model for evaluating immunotherapy efficacy by tracking dendritic cell behaviour toward tumor cells. Sci Rep. 2017;7(1):1093.

211.   Aref AR, Campisi M, Ivanova E, Portell A, Larios D, Piel BP, Mathur N, Zhou C, Coakley RV, Bartels A, Bowden M, Herbert Z, Hill S, Gilhooley S, Carter J, Canadas I, Thai TC, Kitajima S, Chiono V, Paweletz CP, Barbie DA, Kamm RD, Jenkins RW. 3D microfluidic ex vivo culture of organotypic tumor spheroids to model immune checkpoint blockade. Lab on a Chip 2018;18(20):3129-43.

212.   Huh D, Leslie DC, Matthews BD, Fraser JP, Jurek S, Hamilton GA, Thorneloe KS, McAlexander MA, Ingber DE, Di Mascolo D, Varesano S, Benelli R, Mollica H, Salis A, Zocchi MR, Decuzzi P, Poggi A, Zhao Y, Wang D, Xu T, Liu P, Cao Y, Wang YY, Yang X, Xu X, Wang X, Niu H, Charwat V, Rothbauer M, Tedde SF, Hayden O, Bosch JJ, Muellner P, Hainberger R, Ertl P, Ke LY, Kuo ZK, Chen YS, Yeh TY, Dong M, Tseng HW, Liu CH, Kulasinghe A, Perry C, Kenny L, Warkiani ME, Nelson C, Punyadeera C, Layer JP, Kronmüller MT, Quast T, Boorn-Konijnenberg Dvd, Effern M, Hinze D, Althoff K, Schramm A, Westermann F, Peifer M, Hartmann G, Tüting T, Kolanus W, Fischer M, Schulte J, Hölzel M, Lei KF, Chang CHCM, Chen MJ, Lu YT, Pendharkar GP, Lu CH, Chang CHCM, Liu CH, Lucarini V, Buccione C, Ziccheddu G, Peschiaroli F, Sestili P, Puglisi R, Mattia G, Zanetti C, Parolini I, Bracci L, Macchia I, Rossi A, D'Urso MT, Macchia D, Spada M, De Ninno A, Gerardino A, Mozetic P, Trombetta M, Rainer A, Businaro L, Schiavoni G, Mattei F, Martin M, Kaplan H, Gurven M, Jolles AE, Mpairwe H, Elliott AM, Yazdanbakhsh M, Joseph A, McFalls MH, Gurven M, Kaplan H, Stieglitz J, Blackwell AD, Gurven M, Kaplan H, Brinkworth J, Pechenkina K, Guilbert LJ, Wegmann TG, Belosevic M, Mosmann TR, Yirmiya R, Hooper PL, Stieglitz J, Gurven M, Kreager P, Winne B, Ulijaszek S, Capelli C, Loukas A, Muehlenbein MP, Maldonado I, Cortez E, Zabala N, Wimalachandra DC, Li Y, Liu J, Shikha S, Zhang J, Lim YC, Zhang Y, Yin C, Wang YY, Ji J, Cai B, Chen H, Yang Z, Wang K, Luo C, Zhang W, Yuan C, Wang F, Diering. A human disease model of drug toxicity-Induced pulmonary edema in a lung-on-a-chip microdevice Oncotarget. 2018;6(1):139-48.

213.   Moore N, Doty D, Zielstorff M, Kariv I, Moy LY, Gimbel A, Chevillet JR, Lowry N, Santos J, Mott V, Kratchman L, Lau T, Addona G, Chen H, Borenstein JT. A multiplexed microfluidic system for evaluation of dynamics of immune-tumor interactions. Lab on a Chip 2018;18(13):1844-58.

214.   Nguyen M, De Ninno A, Mencattini A, Mermet-Meillon F, Fornabaio G, Evans SS, Cossutta M, Khira Y, Han W, Sirven P, Pelon F, Di Giuseppe D, Bertani FR, Gerardino A, Yamada A, Descroix S, Soumelis V, Mechta-Grigoriou F, Zalcman G, Camonis J, Martinelli E, Businaro L, Parrini MC. Dissecting Effects of Anti-cancer Drugs and Cancer-Associated Fibroblasts by On-Chip Reconstitution of Immunocompetent Tumor Microenvironments. Cell Rep. 2018;25(13):3884-93 e3.

215.   Yin C, Wang Y, Ji J, Cai B, Chen H, Yang Z, Wang K, Luo C, Zhang W, Yuan C, Wang F. Molecular Profiling of Pooled Circulating Tumor Cells from Prostate Cancer Patients Using a Dual-Antibody-Functionalized Microfluidic Device. Anal Chem. 2018;90(6):3744-51.

216.   Zervantonakis IK, Hughes-Alford SK, Charest JL, Condeelis JS, Gertler FB, Kamm RD. Three-dimensional microfluidic model for tumor cell intravasation and endothelial

barrier function. Proceedings of the National Academy of Sciences of the United States of America. 2012;109(34):13515-20.

217.	Jenkins RW, Aref AR, Lizotte PH, Ivanova E, Stinson S, Zhou CW, Bowden M, Deng J, Liu H, Miao D, He MX, Walker W, Zhang G, Tian T, Cheng C, Wei Z, Palakurthi S, Bittinger M, Vitzthum H, Kim JW, Merlino A, Quinn M, Venkataramani C, Kaplan JA, Portell A, Gokhale PC, Phillips B, Smart A, Rotem A, Jones RE, Keogh L, Anguiano M, Stapleton L, Jia Z, Barzily-Rokni M, Canadas I, Thai TC, Hammond MR, Vlahos R, Wang ES, Zhang H, Li S, Hanna GJ, Huang W, Hoang MP, Piris A, Eliane JP, Stemmer-Rachamimov AO, Cameron L, Su MJ, Shah P, Izar B, Thakuria M, LeBoeuf NR, Rabinowits G, Gunda V, Parangi S, Cleary JM, Miller BC, Kitajima S, Thummalapalli R, Miao B, Barbie TU, Sivathanu V, Wong J, Richards WG, Bueno R, Yoon CH, Miret J, Herlyn M, Garraway LA, Van Allen EM, Freeman GJ, Kirschmeier PT, Lorch JH, Ott PA, Hodi FS, Flaherty KT, Kamm RD, Boland GM, Wong KK, Dornan D, Paweletz CP, Barbie DA. Ex Vivo Profiling of PD-1 Blockade Using Organotypic Tumor Spheroids. Cancer Discov. 2018;8(2):196-215.

218.	van Meer BJ, de Vries H, Firth KSA, van Weerd J, Tertoolen LGJ, Karperien HBJ, Jonkheijm P, Denning C, Ijzerman AP, Mummery CL. Small molecule absorption by PDMS in the context of drug response bioassays. Biochemical and Biophysical Research Communications. 2017;482(2):323-8.

219.	Charwat V, Rothbauer M, Tedde SF, Hayden O, Bosch JJ, Muellner P, Hainberger R, Ertl P. Monitoring Dynamic Interactions of Tumor Cells with Tissue and Immune Cells in a Lab-on-a-Chip. Analytical Chemistry. 2013;85(23):11471-8.

220.	Layer JP, Kronmuller MT, Quast T, van den Boorn-Konijnenberg D, Effern M, Hinze D, Althoff K, Schramm A, Westermann F, Peifer M, Hartmann G, Tuting T, Kolanus W, Fischer M, Schulte J, Holzel M. Amplification of N-Myc is associated with a T-cell-poor microenvironment in metastatic neuroblastoma restraining interferon pathway activity and chemokine expression. Oncoimmunology. 2017;6(6):e1320626.

221.	Pavesi A, Tan AT, Koh S, Chia A, Colombo M, Antonecchia E, Miccolis C, Ceccarello E, Adriani G, Raimondi MT, Kamm RD, Bertoletti A. A 3D microfluidic model for preclinical evaluation of TCR-engineered T cells against solid tumors. JCI Insight. 2017;2(12).

222.	Ayuso JM, Truttschel R, Gong MM, Humayun M, Virumbrales-Munoz M, Vitek R, Felder M, Gillies SD, Sondel P, Wisinski KB, Patankar M, Beebe DJ, Skala MC. Evaluating natural killer cell cytotoxicity against solid tumors using a microfluidic model. 2018.

223.	Ke LY, Kuo ZK, Chen YS, Yeh TY, Dong M, Tseng HW, Liu CH. Cancer immunotherapy µ-environment LabChip: taking advantage of optoelectronic tweezers. Lab on a Chip 2017;18(1):106-14.

224.	Lee SWL, Adriani G, Ceccarello E, Pavesi A, Tan AT, Bertoletti A, Kamm RD, Wong SC. Characterizing the Role of Monocytes in T Cell Cancer Immunotherapy Using a 3D Microfluidic Model. Front Immunol. 2018;9:416.

225.	Ando Y, Siegler EL, Ta HP, Cinay GE, Zhou H, Gorrell KA, Au H, Jarvis BM, Wang P, Shen K. Evaluating CAR-T Cell Therapy in a Hypoxic 3D Tumor Model. Advanced Healthcare Materials. 2019;8(5):1900001.

226.	Di Mascolo D, Varesano S, Benelli R, Mollica H, Salis A, Zocchi MR, Decuzzi P, Poggi A. Nanoformulated Zoledronic Acid Boosts the Vdelta2 T Cell Immunotherapeutic Potential in Colorectal Cancer. Cancers (Basel). 2019;12(1).

227.	Park D, Son K, Hwang Y, Ko J, Lee Y, Doh J, Jeon NL. High-Throughput Microfluidic 3D Cytotoxicity Assay for Cancer Immunotherapy (CACI-IMPACT Platform). Front Immunol. 2019;10:1133.

228.	Wu D, Yu Y, Zhao C, Shou X, Piao Y, Zhao X, Zhao Y, Wang S. NK-Cell-Encapsulated Porous Microspheres via Microfluidic Electrospray for Tumor Immunotherapy. ACS Appl Mater Interfaces. 2019;11(37):33716-24.

229.	Chen SC, Wu PC, Wang CY, Kuo PL. Evaluation of cytotoxic T lymphocyte-mediated anticancer response against tumor interstitium-simulating physical barriers. Sci Rep. 2020;10(1):13662.

230.	Ayuso JM, Rehman S, Virumbrales-Munoz M, McMinn PH, Geiger P, Fitzgerald C, Heaster T, Skala MC, Beebe DJ. Microfluidic tumor-on-a-chip model to evaluate the role of tumor environmental stress on NK cell exhaustion. Science Advances. 2021;7.

231.	Lee J, Kim SE, Moon D, Doh J. A multilayered blood vessel/tumor tissue chip to investigate T cell infiltration into solid tumor tissues. Lab on a Chip 2021.

232.	Ayuso JM, Truttschel R, Gong MM, Humayun M, Virumbrales-Munoz M, Vitek R, Felder M, Gillies SD, Sondel P, Wisinski KB, Patankar M, Beebe DJ, Skala MC. Evaluating natural killer cell cytotoxicity against solid tumors using a microfluidic model. Oncoimmunology. 2019;8(3):1553477.

233.	Bonotto M, Gerratana L, Di Maio M, De Angelis C, Cinausero M, Moroso S, Milano M, Stanzione B, Gargiulo P, Iacono D, Minisini AM, Mansutti M, Fasola G, De Placido S, Arpino G, Puglisi F. Chemotherapy versus endocrine therapy as first-line treatment in patients with luminal-like HER2-negative metastatic breast cancer: A propensity score analysis. Breast (Edinburgh, Scotland). 2017;31:114-20.

234.	Shagufta, Ahmad I, Mathew S, Rahman S. Recent progress in selective estrogen receptor downregulators (SERDs) for the treatment of breast cancer. RSC Medicinal Chemistry. 2020;11(4):438-54.

235.	Rocca A, Maltoni R, Bravaccini S, Donati C, Andreis D. Clinical utility of fulvestrant in the treatment of breast cancer: a report on the emerging clinical evidence. Cancer Management and Research. 2018;Volume 10:3083-99.

236.	Jensen C, Teng Y. Is It Time to Start Transitioning From 2D to 3D Cell Culture? Front Mol Biosci. 2020;7:33.

237.	Kapałczyńska M, Kolenda T, Przybyła W, Zajączkowska M, Teresiak A, Filas V, Ibbs M, Bliźniak R, Łuczewski Ł, Lamperska K. 2D and 3D cell cultures - a comparison of different types of cancer cell cultures. Arch Med Sci. 2018;14(4):910-9.

238.	Nagaraju S, Truong D, Mouneimne G, Nikkhah M. Microfluidic Tumor–Vascular Model to Study Breast Cancer Cell Invasion and Intravasation. Advanced Healthcare Materials. 2018;7(9).

239.	Han W, Chen S, Yuan W, Fan Q, Tian J, Wang X, Chen L, Zhang X, Wei W, Liu R, Qu J, Jiao Y, Austin RH, Liu L. Oriented collagen fibers direct tumor cell intravasation. Proceedings of the National Academy of Sciences of the United States of America. 2016;113(40):11208-13.

240.	Xu Z, Li E, Guo Z, Yu R, Hao H, Xu Y, Sun Z, Li X, Lyu J, Wang Q. Design and Construction of a Multi-Organ Microfluidic Chip Mimicking the in vivo Microenvironment of Lung Cancer Metastasis. ACS Applied Materials & Interfaces. 2016;8(39):25840-7.

241.	Kock A, Bergqvist F, Steinmetz J, Elfman LHM, Korotkova M, Johnsen JI, Jakobsson PJ, Kogner P, Larsson K. Establishment of an in vitro 3D model for neuroblastoma enables preclinical investigation of combined tumor-stroma drug targeting. FASEB J. 2020.

242.	Cellaria Cancer Cell Models & Media: AMSBIO; [12th March 2022]. Available from: https://www.amsbio.com/cellaria-cancer-cell-models-media/.

243.	Kubo N, Araki K, Kuwano H, Shirabe K. Cancer-associated fibroblasts in hepatocellular carcinoma. World Journal of Gastroenterology. 2016;22(30):6841.

244.	Mei N, Zhao N, Tian T, Jiao M, Li C. Biological features, gene expression profile, and mechanisms of drug resistance of two- and three-dimensional hepatocellular carcinoma cell cultures. Pharmacology Research & Perspectives. 2021;9(1):e00715.

245.	Ping Q, Yan R, Cheng X, Wang W, Zhong Y, Hou Z, Shi Y, Wang C, Li R. Cancer-associated fibroblasts: overview, progress, challenges, and directions. Cancer Gene Therapy. 2021.

246.   Gasser S, Lim LHK, Cheung FSG. The role of the tumour microenvironment in immunotherapy. Endocr Relat Cancer. 2017;24(12):T283-T95.

247.   Roma-Rodrigues C, Mendes R, Baptista PV, Fernandes AR. Targeting Tumor Microenvironment for Cancer Therapy. International journal of molecular sciences. 2019;20(4):840.

248.   Jin MZ, Jin WL. The updated landscape of tumor microenvironment and drug repurposing. Signal Transduct Target Ther. 2020;5(1):166.

249.   Ford K, Hanley CJ, Mellone M, Szyndralewiez C, Heitz F, Wiesel P, Wood O, Machado M, Lopez M-A, Ganesan A-P, Wang C, Chakravarthy A, Fenton TR, King EV, Vijayanand P, Ottensmeier CH, Al-Shamkhani A, Savelyeva N, Thomas GJ. NOX4 Inhibition Potentiates Immunotherapy by Overcoming Cancer-Associated Fibroblast-Mediated CD8 T-cell Exclusion from Tumors. Cancer research. 2020;80(9):1846-60.

250.   Hou AJ, Chen LC, Chen YY. Navigating CAR-T cells through the solid-tumour microenvironment. Nat Rev Drug Discov. 2021;20(7):531-50.

251.   Yu S, Li A, Liu Q, Li T, Yuan X, Han X, Wu K. Chimeric antigen receptor T cells: a novel therapy for solid tumors. Journal of Hematology & Oncology. 2017;10(1):78.

252.   Castella M, Caballero-Baños M, Ortiz-Maldonado V, González-Navarro EA, Suñé G, Antoñana-Vidósola A, Boronat A, Marzal B, Millán L, Martín-Antonio B, Cid J, Lozano M, García E, Tabera J, Trias E, Perpiña U, Canals JM, Baumann T, Benítez-Ribas D, Campo E, Yagüe J, Urbano-Ispizua Á, Rives S, Delgado J, Juan M. Point-Of-Care CAR T-Cell Production (ARI-0001) Using a Closed Semi-automatic Bioreactor: Experience From an Academic Phase I Clinical Trial. Frontiers in Immunology. 2020;11(482).

253.   Maggs L, Cattaneo G, Dal AE, Moghaddam AS, Ferrone S. CAR T Cell-Based Immunotherapy for the Treatment of Glioblastoma. Frontiers in Neuroscience. 2021;15.

254.   El Guerrab A, Bamdad M, Kwiatkowski F, Bignon Y-J, Penault-Llorca F, Aubel C. Anti-EGFR monoclonal antibodies and EGFR tyrosine kinase inhibitors as combination therapy for triple-negative breast cancer. Oncotarget. 2016;7(45):73618-37.

255.   Hossein-Nejad-Ariani H, Althagafi E, Kaur K. Small Peptide Ligands for Targeting EGFR in Triple Negative Breast Cancer Cells. Scientific Reports. 2019;9(1):2723.

256.   Jackson NM, Ceresa BP. Protein Kinase G facilitates EGFR-mediated cell death in MDA-MB-468 cells. Experimental cell research. 2016;346(2):224-32.

257.   Wendt MK, Williams WK, Pascuzzi PE, Balanis NG, Schiemann BJ, Carlin CR, Schiemann WP. The Antitumorigenic Function of EGFR in Metastatic Breast Cancer is Regulated by Expression of Mig6. Neoplasia. 2015;17(1):124-33.

258.   EGFR The Human Protein Atlas; [RNA Expression Overview]. Available from: https://www.proteinatlas.org/ENSG00000146648-EGFR/cell.

259.   Amin DN, Hida K, Bielenberg DR, Klagsbrun M. Tumor Endothelial Cells Express Epidermal Growth Factor Receptor (EGFR) but not ErbB3 and Are Responsive to EGF and to EGFR Kinase Inhibitors. Cancer Research. 2006;66(4):2173-80.

260.   Heiss M, Hellström M, Kalén M, May T, Weber H, Hecker M, Augustin HG, Korff T. Endothelial cell spheroids as a versatile tool to study angiogenesis in vitro. FASEB Journal. 2015;29(7):3076-84.

261.   Stahl A, Wu X, Wenger A, Klagsbrun M, Kurschat P. Endothelial progenitor cell sprouting in spheroid cultures is resistant to inhibition by osteoblasts: A model for bone replacement grafts. FEBS Letters. 2005;579(24):5338-42.

262.   Cazaux M, Grandjean CL, Lemaître F, Garcia Z, Beck RJ, Milo I, Postat J, Beltman JB, Cheadle EJ, Bousso P. Single-cell imaging of CAR T cell activity in vivo reveals extensive functional and anatomical heterogeneity. The Journal of Experimental Medicine 2019;216(5):1038-49.

263.   Han Y, Liu D, Li L. PD-1/PD-L1 pathway: current researches in cancer. American Journal of Cancer Research 2020;10(3):727-42.

264.   Akinleye A, Rasool Z. Immune checkpoint inhibitors of PD-L1 as cancer therapeutics. Journal of Hematology & Oncology. 2019;12(1):92.

265.   Ng HY, Li J, Tao L, Lam AK-Y, Chan KW, Ko JMY, Yu VZ, Wong M, Li B, Lung ML. Chemotherapeutic Treatments Increase PD-L1 Expression in Esophageal Squamous Cell Carcinoma through EGFR/ERK Activation. Translational oncology. 2018;11(6):1323-33.

266.   Hollern DP, Contreras CM, Dance-Barnes S, Silva GO, Pfefferle AD, Xiong J, Darr DB, Usary J, Mott KR, Perou CM. A mouse model featuring tissue-specific deletion of p53 and Brca1 gives rise to mammary tumors with genomic and transcriptomic similarities to human basal-like breast cancer. Breast Cancer Res Treat. 2019;174(1):143-55.

267.   Parente-Pereira AC, Whilding LM, Brewig N, van der Stegen SJC, Davies DM, Wilkie S, van Schalkwyk MCI, Ghaem-Maghami S, Maher J. Synergistic Chemoimmunotherapy of Epithelial Ovarian Cancer Using ErbB-Retargeted T Cells Combined with Carboplatin. The Journal of Immunology. 2013;191(5):2437.

268.   Paterson K, Zanivan S, Glasspool R, Coffelt SB, Zagnoni M. Microfluidic technologies for immunotherapy studies on solid tumours. Lab on a Chip. 2021.

269.   Aref AR, Huang RYJ, Yu W, Chua KN, Sun W, Tu TY, Bai J, Sim WJ, Zervantonakis IK, Thiery JP, Kamm RD. Screening therapeutic EMT blocking agents in a three-dimensional microenvironment. Integrative Biology (United Kingdom). 2013;5(2):381-9.

270.   Regehr KJ, Domenech M, Koepsel JT, Carver KC, Ellison-Zelski SJ, Murphy WL, Schuler LA, Alarid ET, Beebe DJ. Biological implications of polydimethylsiloxane-based microfluidic cell culture. Lab on a chip. 2009;9(15):2132-9.

271.   Carter S-SD, Atif A-R, Kadekar S, Lanekoff I, Engqvist H, Varghese OP, Tenje M, Mestres G. PDMS leaching and its implications for on-chip studies focusing on bone regeneration applications. Organs-on-a-Chip. 2020;2:100004.

272.   Gencturk E, Mutlu S, Ulgen KO. Advances in microfluidic devices made from thermoplastics used in cell biology and analyses. Biomicrofluidics. 2017;11(5):051502-.

273.   Chan CY, Goral VN, DeRosa ME, Huang TJ, Yuen PK. A polystyrene-based microfluidic device with three-dimensional interconnected microporous walls for perfusion cell culture. Biomicrofluidics. 2014;8(4):046505-.

274.   Pentecost AM, Martin RS. Fabrication and characterization of all-polystyrene microfluidic devices with integrated electrodes and tubing. Analytical Methods. 2015;7(7):2968-76.

275.   Ochs CJ, Kasuya J, Pavesi A, Kamm RD. Oxygen levels in thermoplastic microfluidic devices during cell culture. Lab on a chip. 2014;14(3):459-62.

276.   Ando Y, Siegler EL, Ta HP, Cinay GE, Zhou H, Gorrell KA, Au H, Jarvis BM, Wang P, Shen K. Evaluating CAR-T Cell Therapy in a Hypoxic 3D Tumor Model. Adv Healthc Mater. 2019;8(5):1900001.

277.   Minchinton AI, Tannock IF. Drug penetration in solid tumours. Nature reviews Cancer. 2006;6(8):583-92.

278.   Gill JK, Maskarinec G, Pagano I, Kolonel LN. The association of mammographic density with ductal carcinoma in situ of the breast: the Multiethnic Cohort. Breast Cancer Res. 2006;8(3):R30.

279.   Olivares O, Mayers JR, Gouirand V, Torrence ME, Gicquel T, Borge L, Lac S, Roques J, Lavaut MN, Berthezene P, Rubis M, Secq V, Garcia S, Moutardier V, Lombardo D, Iovanna JL, Tomasini R, Guillaumond F, Vander Heiden MG, Vasseur S. Collagen-derived proline promotes pancreatic ductal adenocarcinoma cell survival under nutrient limited conditions. Nature communications. 2017;8:16031.

280.   Rodriguez-Garcia A, Palazon A, Noguera-Ortega E, Powell DJ, Jr., Guedan S. CAR-T Cells Hit the Tumor Microenvironment: Strategies to Overcome Tumor Escape. Front Immunol. 2020;11:1109.

281.   Kay EJ, Koulouras G, Zanivan S. Regulation of Extracellular Matrix Production in Activated Fibroblasts: Roles of Amino Acid Metabolism in Collagen Synthesis. Front Oncol. 2021;11:719922.

282.   Shelton SE, Nguyen HT, Barbie DA, Kamm RD. Engineering approaches for studying immune-tumor cell interactions and immunotherapy. iScience. 2020;24(1):101985-.

283.   Hinck L, Näthke I. Changes in cell and tissue organization in cancer of the breast and colon. Curr Opin Cell Biol. 2014;26:87-95.

284.   Jung KH, Lee JH, Park JW, Kim DH, Moon SH, Cho YS, Lee KH. Targeted therapy of triple negative MDA-MB-468 breast cancer with curcumin delivered by epidermal growth factor-conjugated phospholipid nanoparticles. Oncol Lett. 2018;15(6):9093-100.

285.   Wykosky J, Fenton T, Furnari F, Cavenee WK. Therapeutic targeting of epidermal growth factor receptor in human cancer: successes and limitations. Chinese journal of cancer. 2011;30(1):5-12.

286.   Zhang Z, Nagrath S. Microfluidics and cancer: are we there yet? Biomedical microdevices. 2013;15(4):595-609.

287.   Zhao L, Xiu J, Liu Y, Zhang T, Pan W, Zheng X, Zhang X. A 3D Printed Hanging Drop Dripper for Tumor Spheroids Analysis Without Recovery. Scientific Reports. 2019;9(1):19717.

288.   Stadler M, Scherzer M, Walter S, Holzner S, Pudelko K, Riedl A, Unger C, Kramer N, Weil B, Neesen J, Hengstschläger M, Dolznig H. Exclusion from spheroid formation identifies loss of essential cell-cell adhesion molecules in colon cancer cells. Scientific Reports. 2018;8(1).

289.   Naipal KAT, Verkaik NS, Sánchez H, van Deurzen CHM, den Bakker MA, Hoeijmakers JHJ, Kanaar R, Vreeswijk MPG, Jager A, van Gent DC. Tumor slice culture system to assess drug response of primary breast cancer. BMC Cancer. 2016;16(1):78.

290.   Roelants C, Pillet C, Franquet Q, Sarrazin C, Peilleron N, Giacosa S, Guyon L, Fontanell A, Fiard G, Long JA, Descotes JL, Cochet C, Filhol O. Ex-Vivo Treatment of Tumor Tissue Slices as a Predictive Preclinical Method to Evaluate Targeted Therapies for Patients with Renal Carcinoma. Cancers (Basel). 2020;12(1).